Université de Toulouse

THESE

En vue de l'obtention du

DOCTORAT DE L'UNIVERSITÉ DE TOULOUSE

Délivré par *l'Institut National des Sciences Appliquées de Toulouse*
Discipline ou spécialité : *Systèmes Automatiques*

Présentée et soutenue par *Yanjun XU*
Le *10 Juillet 2009*

Titre : *Modulation and detection schemes based on chaotic attractors properties: Application to wideband transmissions*

JURY

Géza Kolumbán: Rapporteur, Professeur à l'Université de Technologie et d'Economie de Budapest
Jean-Pierre Cances: Rapporteur, Professeur à l'Université de Limoges
Daniel Roviras: Examinateur, Professeur à CNAM Paris
Danièle Fournier-Prunaret: Directrice de Thèse, Professeure à l'INSA de Toulouse
Pascal Chargé: Directeur de Thèse, Maître de conférences à l'INSA de Toulouse

---

Ecole doctorale : *Ecole Doctorale Systèmes*
Unité de recherche : *LAboratoire Toulousain de Technologie et d'Ingénierie des Systèmes*
Directeur(s) de Thèse : *Danièle Fournier-Prunaret, Pascal Chargé*
Rapporteurs : *(s'ils ne font pas partie des membres du jury)*

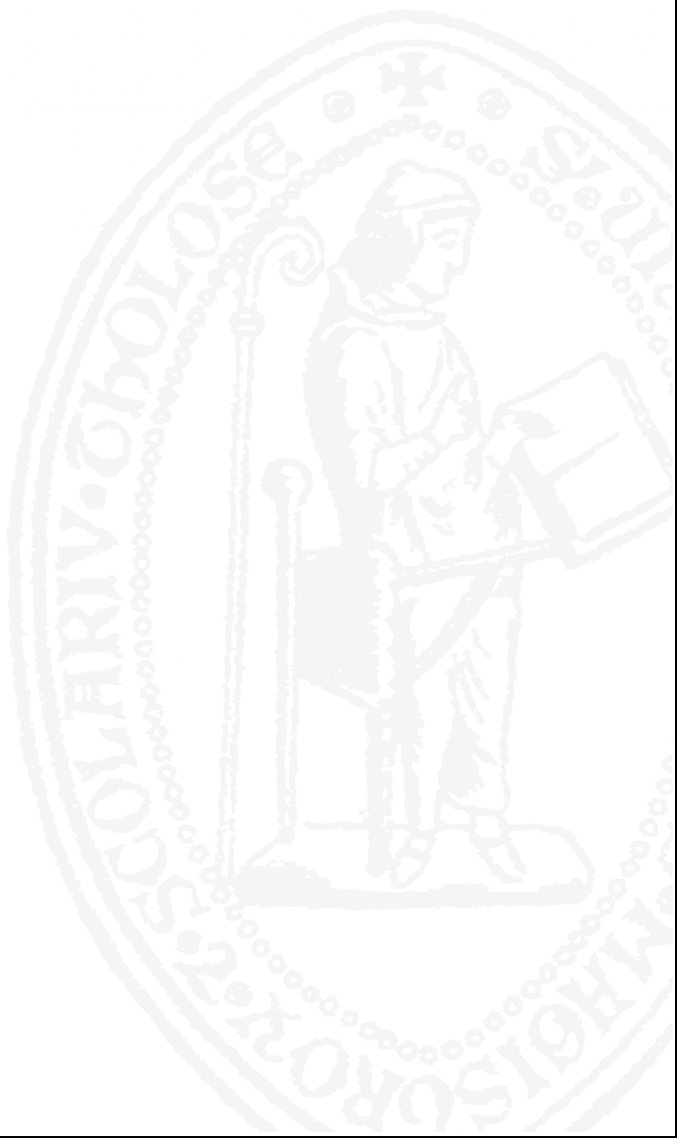

Remerciements

Ce fut un privilège pour moi d'effectuer mes études sous la direction de Danièle Fournier-Prunaret et de Pascal Chargé. C'est donc à eux que je dédie mes remerciements les plus sincères.

Merci Danièle pour avoir encadré cette thèse. Merci de m'avoir mis le pied à l'étrier avec ta profonde connaissance du domaine de systèmes dynamiques. Dans ce domaine nouveau pour moi, j'ai pu bénéficier de tes conseils et commentaires toujours constructifs. Tout cela avec une gentillesse et un humour sans pareil !

Merci Pascal pour avoir co-encadré ma thèse. Merci de m'avoir guidée pour touver le sujet final ainsi que pour toutes les discussions sur les télécommunications au cours desquelles j'ai pu profiter de tes vastes compétences. Tes conseils et commentaires toujours constructifs ont permis de faire avancer les résultats plus loin que je ne l'imaginais. Ta patience, ta disponibilité et ta gentillesse ont largement contribué à me laisser un excellent souvenir de mon passage à Toulouse.

Daniel Roviras m'a fait l'honneur et le plaisir d'accepter de présider le jury et je vous en suis très reconnaissante. Je remercie sincèrement Géza Kolumbán et Jean-Pierre Cances pour avoir accepté la laborieuse tâche de rapporteur, et j'ai beaucoup apprécié pour l'attention que vous avez consacrée à la lecture de ce manuscrit.

Lors des trois ans de ma thèse, j'ai eu des discussions intéressantes et enrichissantes avec Abdel-Kaddous Taha. Tu as agrandie champ de mes connaissance en mathématiques. J'ai eu aussi des discussions intéressantes avec Med Lamine Sahari, Jie Xu, Georges Kaddoum et Pierre Pinel. J'ai largement profité de vos échanges et je vous en remercie.

Je remercie les organisateurs du programme CSC/UT-INSA qui m'ont permis de venir en France et d'effectuer ma thèse sans aucun souci de financement. Je suis reconnaissante envers le laboratoire de m'avoir donné l'occasion de participer à différentes conférences. Cela m'a permis de nombreuses discussions intéressantes. Je remercie les

secrétaires de notre laboratoire et de l'école doctorale, Rosa, Estelle, Joëlle, Karima, Sophie, qui m'ont beaucoup aidé pour les dossiers administratifs et les procedures de soutenance.

Je tiens aussi à remercier Jacques Erschler et Ruijin Zhang pour votre soutien lors de mes premiers mois sur Toulouse. J'aimerais remercier beaucoup Susu, avec qui je suis venue en France et avec qui j'ai passé beaucoup de temps. Lors de mon séjour à Toulouse, j'ai fait la connaissance de nombreuses personnes que j'ai beaucoup appréciées: Anne, Ghada, Guillaume A., Guillaume F., Hugues, Jean-Pierre, Karim, Mihai, Mousa, Nada, Pascal, Samuel A.B., Samuel R. Je remercie également Minh, Etienne et Eléna, Yiqian et Florent, Mike et Pauline, Sylvain, David et Nina.

Je remercie tous les membres du programme CSC/UT-INSA à Toulouse: Ruijin, Yanwen, Junfeng, Susu, Hongwei, Xiaoxiao, Yanping, Fan, Letian, Zhe, Xinwei, Dongdong, Haojun.

Je remercie ma famille: Yanni et Haifeng, Miaobin, et en particulier mes parents. Mes études se sont toujours fondées sur votre soutien. Je remercie également Michael et Magali, Oma, Fritz et Karin.

Merci à Andreas qui m'a supportée, soutenue et éclairée lors de la rédaction et au-delà.

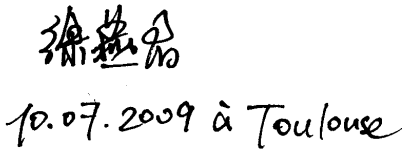

Contents

List of Abbreviations

ASK	amplitude-shift keying
AWGN	additive white Gaussian noise
BER	bit error ratio
BPSK	binary phase-shift keying
CCA	chaotic cyclic attractor
CCAFSK	chaotic cyclic attractors frequency-shift keying
CCASK	chaotic cyclic attractors shift keying
CDMA	code-division multiple access
COOK	chaotic on-off keying
CPM	chaotic parameter modulation
CSK	chaos shift keying
DAB	digital audio broadcasting
DC	direct current
DCSK	differential chaos shift keying
DFT	discrete Fourier transform
DMV	downsampled mean variance
DS	direct-sequence
DS-CDMA	direct-sequence code-division multiple access
DSSS	direct-sequence spread spectrum
DTFT	discrete-time Fourier transform
DVB	digital video broadcasting
ECPM	ergodic chaotic parameter modulation
FFT	fast Fourier transform
FH	Frequency hopping
FHSS	requency-hopping spread spectrum

FM ..... Frequency Modulation
FPGA ..... field programmable gate arrays
FSK ..... frequency-shift keying
i.i.d. ..... independent and identically-distributed
IDFT ..... inverse discrete Fourier transform
IFFT ..... inverse fast Fourier transform
ISM ..... industrial, scientific and medical
LPF ..... lowpass filter
LPI ..... low probability of intercept
OFDM ..... orthogonal frequency-division multiplexing
PCS ..... personal communication services
PN ..... pseudorandom noise
PSD ..... power spectral density
PSK ..... phase-shift keying
QoS ..... quality of service
TR ..... transmitted reference
UWB ..... ultra-wideband
WLAN ..... wireless local area networks
WLL ..... wireless local loop
WPAN ..... wireless personal area networks
WWAN ..... wireless wide-area networks

General Introduction

Over the past decade, wireless technologies have undergone significant changes; new and innovative techniques have been introduced, the focus of wireless communications is increasingly changing from mobile voice applications to wireless data (including multimedia) applications [1]. In this context, not only the content of transmitted information is changed, but also the scale of networks. In other words, the mobile voice applications usually locate in *wireless wide-area networks* (WWAN), i.e., cellular networks [1]; while the wireless data applications consist of the communications not only in WWAN, but also in *wireless local area networks* (WLAN) [2], such as IEEE 802.11a/b/g/n, as well as in *wireless personal area networks* (WPAN) [3], e.g., Bluetooth, *ultra-wideband* (UWB), wireless ad hoc networks, etc. The expanding wireless networks allow secure, reliable wireless communications among all possible hand-held devices [1]. Variety of communication systems have been proposed and selected for the applications in different networks, and more systems are being studied, pursuing better *quality of service* (QoS), higher transmission rate, or less complexity in transceiver, hence low-cost device.

On the other side, telecommunication is the transmission of signals over a distance for the purpose of communication, in which the signals are typically generated by electronic devices. Furthermore, the synchronization between the transmitted signals and the received ones is indispensable for a successful communication. Hence, no matter a signal is periodic, chaotic or random, it can be used as the information carrier if it can be generated and synchronized.

In the beginning of 1980s, the generation of chaotic signals by simple electronic circuits was found possible [4], and the research on the synchronization of the generated chaotic signals have been carried out [5]. In the following two decades, the application of chaos in the field of communications has attracted lots of attentions, which formed a research domain called chaos-based communications. Depending on which step the

chaos is applied in the communication systems, different chaotic applications can be obtained, i.e., chaotic masking, chaotic spreading sequence, chaotic modulation, etc.

Because of the wideband nature of chaotic signals which can be possibly generated by simple electronic circuits, chaotic modulation is considered potentially more resistant to multipath propagation then a modulation based on the periodic basis functions without spectrum spreading [6], and has less complexity in transceiver to the conventional spread spectrum systems.

However, although chaotic signals are deterministic, they are very sensible to the initial conditions. This sensibility can cause the difficulty (or impossibility) to the synchronization, especially when the wireless propagation channel is concerned, so that the interference (including additive noise and interference from other applications) and distortion are unavoidable. Hence, if the chaotic modulation is applied in the wireless communications, two solutions are more robust: a chaotic modulation with noncoherent detection, or a *transmitted reference* (TR) chaotic modulation with differentially coherent detection, since the synchronization is not required in both of them. However, as long as the additive noise performance is concerned, the communication systems with coherent receivers offer the best performance if the synchronization can be achieved, or, the optimal noise performance of the 'robust' chaotic modulation systems are always behind the one of the conventional narrowband modulation systems.

Hence, if a potential application is searched for the chaotic modulations, such application should be found where the performance limit is less important [7][8], and in contrary, the realization of wideband transmissions with simple (low-cost) transceiver is the main deciding factor. The short range transmissions usually take place in complicated environments, such as houses and offices, where the signals are transmitted not only by the direct path, but by the reflections of lots of furniture and bureaus [9], hence, the multipath attenuation is the determinative factor rather than the additive noise. In this context, wideband systems can be used. The applications in such environments which require numerous devices for simple functions may need low-cost transceivers.

The motivation of this thesis is to study a dynamical system, in order to determine some properties of chaotic signals, and to propose a chaotic modulation system utilizing these properties in the noncoherent detection. Our system should be different to the existing chaotic modulation systems, and should outperform them under certain conditions. The application of our system will be the general short range wideband

transmissions, without entering into the particular networks, hence no consideration on the power control or frequency band allocation.

As a study in the cross domains, the outline of thesis is organized as follows:

Chapter 1 presents firstly the basic fundamental theories of both dynamical systems and wideband communications, and then the state of the art in the field of chaos-based communications. The introduction on dynamical systems and chaos gives the necessary definitions of the basic terms, as well as the mathematical methods for analyzing the simplest behaviors of a dynamical system. The part of wideband communications introduces the advantages compared to the narrowband communications, and the popular conventional wideband communication systems realized by different spectrum spreading techniques.

To a certain extent, the spectrum spreading belongs to the modulation step of the communication systems. Furthermore, both techniques of chaotic spectrum spreading and chaotic modulation can be applied in the wideband communications. In order to avoid the confusion on the terms, the application of chaos in the modulations of wideband communication systems will be called generally the chaos-based wideband communications in the context of this thesis, and the two implementations are treated as two branches of the research, respectively called: the chaotic spreading sequence modulations, and the direct chaotic signals modulations. The state of the art of both research branches is presented. Among the mentioned systems, *differential chaos shift keying* (DCSK) has been widely studied in the past decade, and considered to be the most practical chaos-based modulation scheme when the radio propagation environment is concerned.

In Chapter 2, a sinusoidal two-dimensional discrete-time dynamical system is selected, and its periodic behaviors are studied, using the mathematical tool of bifurcation analysis defined in Chapter 1, as well as the numerical method for the higher periods. Variety of attractors can be derived by the analysis, including the *chaotic cyclic attractor* (CCA). Further studies on CCAs show their specific properties, which are found being parametrized by the periods.

Chapter 3 concentrates on the application of CCA properties in the wideband communications. Two CCA-based modulation schemes are proposed, with the simple noncoherent detections realized by observing the specific properties of received signals.

The performance evaluation of each CCA-based modulation system using different detection schemes in the *additive white Gaussian noise* (AWGN) channel is theoretically analyzed and simulated. Furthermore, the performance of CCA-based modulation systems in the basic multipath channel model are discussed, as well as a simple case of multi-user application for the second system, hence the possibility of multiple-access.

Finally, the conclusion and perspective of the thesis are given.

1

Chaos-based Communications

1.1 Introduction

Although the dynamical systems and chaos theory have been deeply studied and developed by the mathematicians for longtime, it is only until recent decades that chaos theory became a very active area in the communication engineering domain, when the generation of chaotic signals by simple electronic circuits was found possible [4][10][11], and the synchronization of the generated chaotic signals can be realized [5][12][13]. In the signal level, the most important characteristics of the chaotic signals compared to the periodic signals are that, the former has a nature wideband spectrum.

Meanwhile, as a quickly expanding domain, communication engineering has encountered lots of developments, innovations as well as challenges, which will doubtlessly continue in the predictable future. In the recent twenty years, the combination of chaos theory and the communications has formed a special research topic named chaos-based communications, which has attracted considerable attentions. One part of chaos-based communications is focused on the wideband applications, utilizing the natural wideband of the chaotic signals. We define this research branch as chaos-based wideband communications in the context of this thesis.

Our research is based on the study of chaotic attractor properties and the application of these properties in the wideband communication systems. For this object, this chapter presents the general introduction of chaos theory and conventional wideband communications, as well as the state of the art in the chaos-based wideband communications, with a purpose to firstly introduce the principles of both systems, and then

the motivation of our research works.

1.2 Dynamical Systems and Chaos

Around 1975, a large number of scientists around the world became aware that there exists a third kind of motion, which differs from steady state and either periodic or quasi-periodic oscillation, which is now called 'chaos' [14]. This motion looks erratic, is not simply quasi-periodic with a large number of periods, and is not necessarily due to a large number of interacting particles.

Chaos describes the behavior of these dynamical systems that may exhibit non-periodicity and highly sensitive dependence on initial conditions. As a result of this sensitivity, which manifests itself as an exponential growth of perturbations in the initial conditions, the behavior of chaotic systems appears to be random, though actually they are deterministic with no random elements involved, i.e., the future dynamics of these systems are uniquely defined by their initial conditions. Figure 1.1 uses a schematic diagram to show the sensitivity of a chaotic system $\mathbf{x}_k = \mathbf{f}(\mathbf{x}_{k-1})$, where $\mathbf{x}_0$ and $\mathbf{x}_0^{'}$ are two different initial conditions with a very close Euclidean distance.

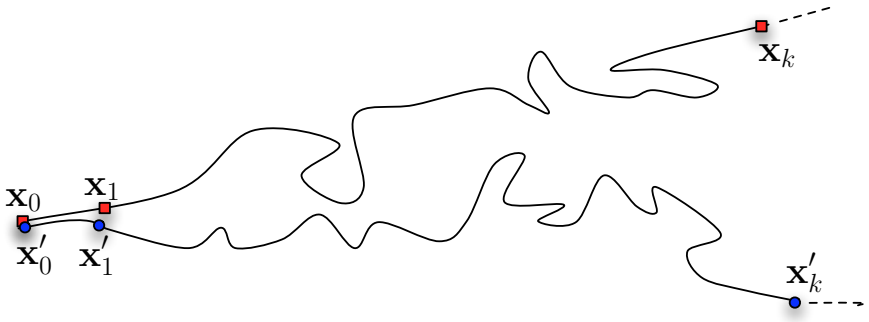

Figure 1.1: Schematic diagram of the sensitivity of a chaotic system $\mathbf{x}_k = \mathbf{f}(\mathbf{x}_{k-1})$ under different but very close initial conditions $\mathbf{x}_0$ and $\mathbf{x}_0'$.

The system in Figure 1.1 is given in a discrete-time domain, which is one of the following two types of dynamical systems [15][16]:

- (**Discrete-time dynamical system**) *A* discrete-time dynamical system *takes the current state as input and updates the situation by producing a new state as output. Such a system is usually modeled by a map.*

- (**Continuous-time dynamical system**) *A* continuous-time dynamical system *can be considered as the limit of discrete system with smaller and smaller updating time. Such a system is otherwise modeled by a differential equation.*

1.2.1 Discrete-Time Dynamical System

The discrete-time dynamical system can be represented in the form of map as [15]

$$\mathbf{x} \mapsto \mathbf{g}(\mathbf{x}; \mu) \tag{1.1}$$

or in a difference equation of the following form

$$\mathbf{x}_k = \mathbf{g}(\mathbf{x}_{k-1}; \mu) \tag{1.2}$$

where $\mathbf{g} : \mathbb{R}^m \times \mathbb{R}^p \mapsto \mathbb{R}^m$ is at least a continuous or piecewise continuous function with m the dimension of the map, and $\mu \in \mathbb{R}^p$ stands for the internal parameters of the systems with p the number of parameters. $\mathbf{x}_k \in \mathbb{R}^m$ is a m-dimensional vector in state k. The set of vectors $\{\mathbf{x}_0,\ \mathbf{g}(\mathbf{x}_0; \mu),\ \mathbf{g}^2(\mathbf{x}_0; \mu),\ ...\}$ is called the trajectory through the initial point $\mathbf{x}_0 \in \mathbb{R}^m$.

The periodic behavior of the trajectories of the m-dimensional map $\mathbf{g}(\mathbf{x}; \mu)$ can be defined as follow [14][16]:

- (**Periodic Point and Fixed Point**) *A point* $\mathbf{x}^* \in \mathbb{R}^m$ *is a* periodic point of period q (*also called* period-q point) *of the map* $\mathbf{g}(\mathbf{x}; \mu)$ *with* μ *fixed, if* $\mathbf{g}^q(\mathbf{x}^*; \mu) = \mathbf{x}^*$*, meanwhile if* q *is the smallest such positive integer. Especially, the periodic point* $\mathbf{x}^*$ *is a* fixed point *of the map* $\mathbf{g}(\mathbf{x}; \mu)$ *with* μ *fixed if the period is* 1*, i.e.,* $\mathbf{g}(\mathbf{x}^*; \mu) = \mathbf{x}^*$.

- (**Periodic Orbit**) *The orbit with the initial point being the periodic point of period* q *is called a* periodic orbit of period q (*also called* period-q orbit, *or* order q cycle).

and the periodic behavior can be characterized by their stability, which is defined as [16][14]:

- (**Asymptotically Stable and Unstable**) *The periodic point* $\mathbf{x}^* \in \mathbb{R}^m$ *is called* **attractive** *or* asymptotically stable, *if for every initial condition* $\mathbf{x}_0$ *belonging to a sufficiently small neighborhood* $\mathbf{U}$ *of* $\mathbf{x}^*$*, we have* $\lim_{k\to\infty} \mathbf{x}_k = \mathbf{x}^*$*. In contrary,*

$\mathbf{x}^*$ *is called or* unstable *if for an initial condition* $\mathbf{x}_0 \in \mathbf{U}$*, we get at least one* $\mathbf{x}_k \notin \mathbf{U}$.

- (**Hyperbolic Fixed Point**) *The fixed point* $\mathbf{x}^* \in \mathbb{R}^m$ *is called a* hyperbolic fixed point *if none of the eigenvalues of* $D\mathbf{g}(\mathbf{x}^*)$ *have unit modulus, where* $D\mathbf{g}$ *is the derivative of* $\mathbf{g}$.

- (**Basin of Attraction**) *The* basin of attraction *of the fixed point (or period-q point)* $\mathbf{x}^*$ *is the set of points* $\mathbf{x}$ *such that* $\lim_{k\to\infty} \mathbf{g}^k(\mathbf{x}) = \mathbf{x}^*$.

Hence, the iteration in the phase plane $\mathbb{R}^m$ with the initial point $\mathbf{x}_0$ belonging to the basin of attraction of a periodic point goes ultimately to the periodic point.

Besides the periodic behavior, dynamical systems can have a more complex asymptotic behavior. The asymptotic behavior of the trajectories of the m-dimensional map $\mathbf{g}$ can give rise to more complex attractive sets, with the following necessary definitions [14][16]:

- (**Invariant Set**) *A set* $\Lambda \subset \mathbb{R}^m$ *is called an* invariant set *of* $\mathbf{g}$ *if* $\mathbf{g}(\Lambda) \subset \Lambda$.

- (**Attracting Set and Repelling Set**) *A closed invariant set* $\Lambda \subset \mathbb{R}^m$ *is called an* attracting set *if there is some neighborhood* U *of* Λ *such that:* $\forall k \geq 0$, $\mathbf{g}^k(U) \subset U$ *and* $\cap_{k>0}\mathbf{g}^k(U) = \Lambda$. *A* repelling set *is defined by replacing* k *by* $-k$.

- (**Basin of Attraction**) *The* basin of attraction *of an attracting set* Λ *is given by* $\bigcup_{k\leq 0} \mathbf{g}^k(U)$*, where* U *is any open set satisfying the definition of the attracting set.*

- (**Attractor**) *An* attractor *is a topologically transitive attracting set, with the topological transitivity defined as: a closed invariant set* Λ *is said to be topologically transitive if, for any two open sets* $U, V \subset \Lambda$, $\exists k \in \mathbb{Z}$*, so that* $\mathbf{g}^k(U) \cap V \neq \emptyset$.

Therefore, the iteration in the phase plane $\mathbb{R}^m$ with the initial point $\mathbf{x}_0$ belonging to the basin of attraction of an attracting set goes ultimately to the attractor.

Among the attractors, one can focus on
- invariant closed curve
- chaotic attractor
with the characteristics related to the term 'chaos' defined as follow [15]:

- (**Sensitive Dependence on Initial Conditions**) *The map* $\mathbf{g}(\mathbf{x};\mu)$ *with* μ *fixed is said to have* sensitive dependence on initial conditions on Λ *if there exists* $\epsilon > 0$ *such that, for any* $\mathbf{x} \in \Lambda$ *and any neighborhood* U *of* $\mathbf{x}$*, there exists* $\mathbf{x}' \in U$ *and* $k > 0$ *such that* $\|\mathbf{g}^k(\mathbf{x};\mu) - \mathbf{g}^k(\mathbf{x}';\mu)\| > \epsilon$.

- (**Chaotic**) Λ *is said to be* chaotic *if*

  1. $\mathbf{g}(\mathbf{x};\mu)$ *has sensitive dependence on initial conditions on* Λ.
  2. $\mathbf{g}(\mathbf{x};\mu)$ *is topologically transitive on* Λ.
  3. *The periodic orbits of* $\mathbf{g}(\mathbf{x};\mu)$ *are dense in* Λ.

All the above mentioned definitions are done under the condition that the parameter μ is fixed. Then, how is the stability or instability affected as μ is varied? For a hyperbolic fixed point, varying μ slightly doesn't change the stability of the fixed point [15]. However, when the fixed point $(\mathbf{x}^*;\mu^*)$ is not hyperbolic, for μ very close to μ^*, radically new dynamical behaviors can occur, e.g., fixed points can be created or destroyed, and periodic or even chaotic dynamics can be created [15]. The phenomena is called **bifurcation** of fixed points. In dynamical systems, a bifurcation occurs when a small smooth change made to the parameter values of a system causes a sudden 'qualitative' or topological change in its behavior.

Since the dynamics of the discrete-time dynamical system depend on the dimension, let's talk about the simplest one-dimensional maps and two-dimensional maps separately.

1.2.1.1 One-Dimensional Maps

As a one-dimensional map, the logistic map is given by:

$$x \mapsto g(x;a) = ax(1-x) \tag{1.3}$$

where $x \in \mathbb{R}$, and $a \in \mathbb{R}$ is the parameter.

Let $a = 2$, so that the corresponding difference equation is $x_k = 2x_{k-1}(1 - x_{k-1})$, with initial condition $x_0 \in (0, 1)$. The trajectories through the initial points $x_0 = 0.1$, $x_0 = 0.2$ and $x_0 = 0.75$ are illustrated in Figure 1.2, which shows that the three different initial conditions lead the trajectories to approach the same attractive fixed point $x = 0.5$ quickly.

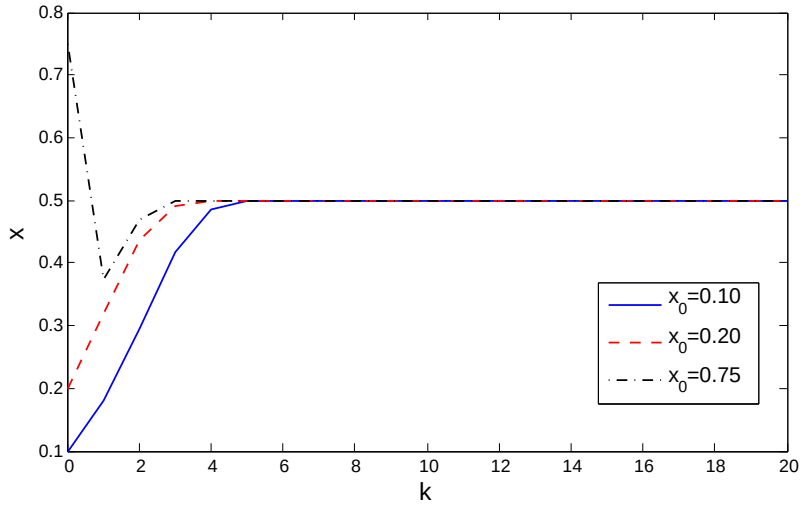

Figure 1.2: Trajectories of $x_k = 2x_{k-1}(1 - x_{k-1})$ through the initial points $x_0 = 0.1$, $x_0 = 0.2$ and $x_0 = 0.75$, with the first 21 states ($k \in [0, 20]$).

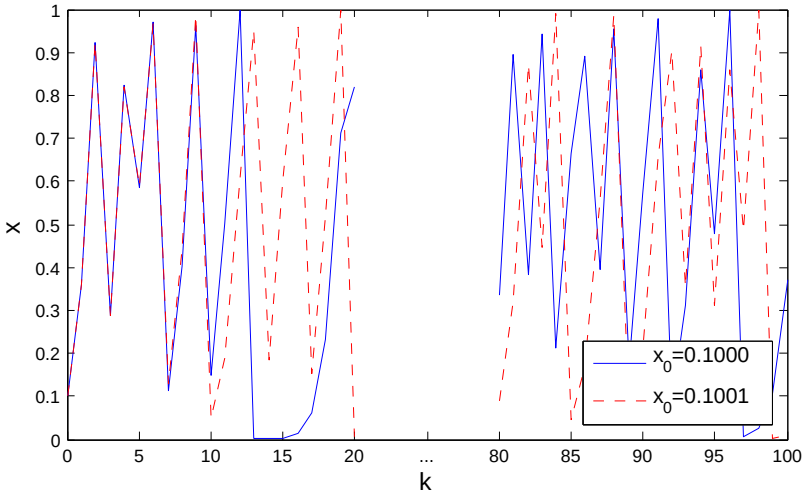

Figure 1.3: Trajectories of $x_k = 4x_{k-1}(1 - x_{k-1})$ through the initial points $x_0 = 0.1$ and $x_0 = 0.1001$, with the states $k \in [0, 20]$ and $k \in [80, 100]$.

In contrast, when $a = 4$, another difference equation $x_k = 4x_{k-1}(1 - x_{k-1})$, $x_0 \in (0, 1)$ shows a different behavior. As illustrated in Figure 1.3, the trajectories through the slightly different initial points, i.e., $x_0 = 0.1$ and $x_0 = 0.1001$, come to two completely separate orbits. It shows the sensitive dependence of the map $g(x; 4)$ on initial conditions, which gives rise to a chaotic attractor.

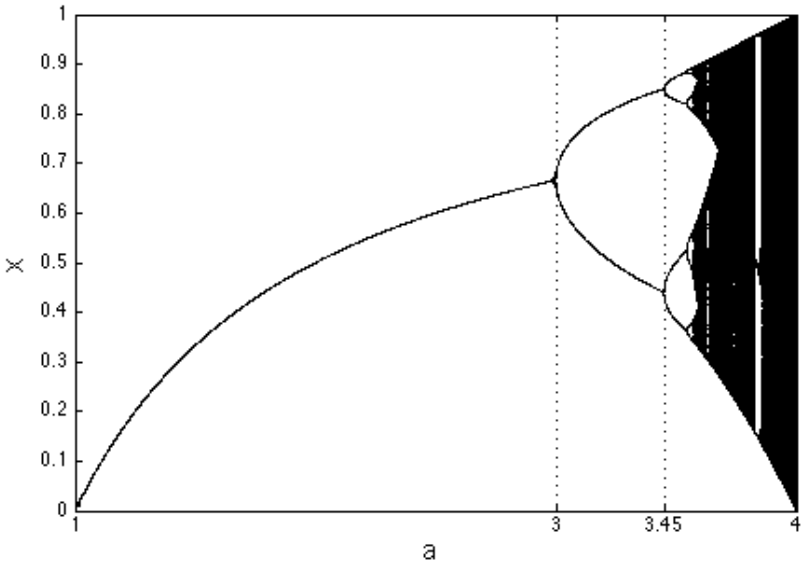

Figure 1.4: Bifurcation diagram of $g(x; a) = ax(1 - x)$.

From the above two examples, we can see that the behavior of a map can be completely different under different parameter values. For analyzing the stability of fixed points, there are two basic bifurcations for the one-dimensional map $g(x; \mu)$ [15]:

- (**Tangent bifurcation**) *A* tangent bifurcation (*or a* fold bifurcation) *is a bifurcation in which a birth of two fixed points arrives, who collide and annihilate each other. A tangent bifurcation occurs to the fixed point* $(x^*; \mu)$ *when* $D_g(x^*; \mu)$ *has the eigenvalue equal to* 1.

- (**Period-doubling bifurcation**) *A* period-doubling bifurcation (*or a* flip bifurcation) *is a bifurcation in which the system switches to a new behavior with twice the period of the original system. A period-doubling bifurcation occurs to the fixed point* $(x^*; \mu)$ *when* $D_g(x^*; \mu)$ *has the eigenvalue equal to* -1.

A **bifurcation diagram** is often taken to show the birth, evolution, and death of attracting sets. The bifurcation diagram of the logistic map is illustrated in Figure 1.4, which shows that fixed point exists for $0 \leq a < 3$, while it turns to a period-2 orbit at the 'bifurcation point' $a = 3$, and then a period-4 orbit arrives at $a \approx 3.45$. This is a standard period-doubling bifurcation. Furthermore, the increase of value of a leads to more complicated orbits, such as period-q^n ($q = 1, 2, ...$; $n = 1, 2, ...$) orbits, as well as chaotic orbits .

1.2.1.2 Two-Dimensional Maps

A two-dimensional map can be presented as

$$\mathbf{x} = (x, y) \mapsto \mathbf{g}(\mathbf{x}; \mu) = \Big(g_1(x, y; \mu), g_2(x, y; \mu)\Big) \tag{1.4}$$

where $g_1, g_2 : \mathbb{R} \mapsto \mathbb{R}$ are smooth maps, $x, y \in \mathbb{R}$, and $\mu \in \mathbb{R}^p$ is the parameter.

The fixed points for a two-dimensional map includes three types: an attracting fixed point is also called a **sink**; a repelling fixed point is called **source**; and a new type of fixed points called **saddle**, which has one attracting direction and one repelling direction.

As long as the stability of a two-dimensional map is concerned, three types of bifurcations can be observed [15]:

- *A* tangent bifurcation *as defined for the one-dimensional maps, which occurs to the fixed point* $(x^*, y^*; \mu)$*, when* $D_{\mathbf{g}}(x^*, y^*; \mu)$ *has one real eigenvalue be equal to* 1.

- *A* period-doubling bifurcation *as defined for the one-dimensional maps, which occurs to the fixed point* $(x^*, y^*; \mu)$*, when* $D_{\mathbf{g}}(x^*, y^*; \mu)$ *has one real eigenvalue be equal to* -1.

- (**Neimark-Sacker bifurcation**) *A* Neimark-Sacker bifurcation *is the birth of a* **closed invariant curve** *from a fixed point, when the fixed point changes stability. It occurs to the fixed point* $(x^*, y^*; \mu)$*, when* $D_{\mathbf{g}}(x^*, y^*; \mu)$ *has two complex conjugate eigenvalues having modulus 1.*

The derivative of $\mathbf{g}$ mentioned above can be given by

$$D_{\mathbf{g}}(x^*, y^*; \mu) = \left[\begin{array}{cc} \frac{\partial g_1(x,y;\mu)}{\partial x} & \frac{\partial g_1(x,y;\mu)}{\partial y} \\ \frac{\partial g_2(x,y;\mu)}{\partial x} & \frac{\partial g_2(x,y;\mu)}{\partial y} \end{array} \right] \Bigg|_{(x,y)=(x^*,\ y^*)} \tag{1.5}$$

1.2.2 Continuous-Time Dynamical System

A discrete-time dynamical system describes the time evolution of a dynamical system by expressing its present state as a function of its previous states, so that the system motion through time corresponds to the iteration of the map. A continuous-time dynamical system can be given in the form of differential equations, by expressing the change rate of the present state as a function of the state itself, as:

$$\dot{\mathbf{x}} = \mathbf{f}(\mathbf{x}, t; \mu) \tag{1.6}$$

$$\dot{\mathbf{x}} = \mathbf{f}(\mathbf{x}; \mu) \tag{1.7}$$

where $\mathbf{f} : \mathbb{R}^m \times \mathbb{R}^p \mapsto \mathbb{R}^m$ is a continuous function, m is the dimension of the system, $\mathbf{x}$ is a m-dimensional vector, and $\mu \in \mathbb{R}^p$ is the parameter. Remind that the first differential equation stands for **nonautonomous** type of systems, where the time variable $t \in \mathbb{R}$ explicitly appears in the differential equation, while the second one stands for **autonomous** type of systems [14][15].

The fixed point of a continuous-time dynamical system is defined as the solution of $\mathbf{f}(\mathbf{x}, t; \mu) = 0$, and the solution of equation (1.6) or equation (1.7) forms the trajectory of the system. Based on the reason that the continuous-time dynamical systems have not been particularly studied during our research, we won't give the other definitions of periodic or dynamical behaviors in this section. Reference [15] is recommended for further interests.

The Lorenz dynamical system could be given as an example of continuous-time dynamical system, which is three-dimensional with the following differential equation:

$$\begin{cases} \dot{x} &= -\sigma x + \sigma y \\ \dot{y} &= -xz + rx - y \\ \dot{z} &= xy - bz \end{cases} \tag{1.8}$$

where $\mathbf{x} = [x\ y\ z]$ is the state vector, and σ, r, b are three real valued parameters. The Lorenz system belongs to the autonomous type of dynamical systems.

As a three-dimensional system with three parameters, the Lorenz system can lead to very complicated behavior on changing the parameter values. Here we choose the standard parameter values $\sigma = 10$, $r = 28$, and $b = \frac{8}{3}$, under which the well-known 'butterfly' attractor exists, as shown in Figure 1.5.

Till now, we have given the definitions of the most basic terms of the dynamical systems, as well as several familiar examples. These definitions are necessary for us to

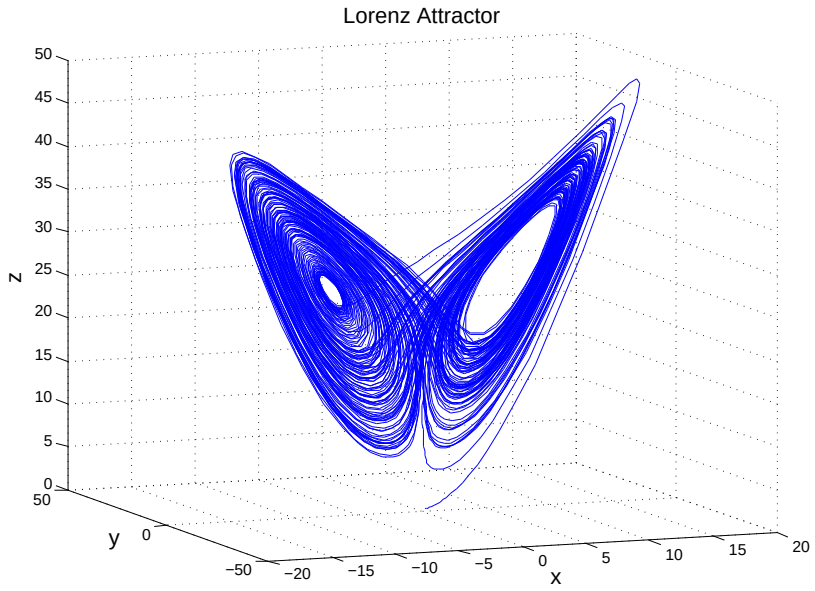

Figure 1.5: Lorenz attractor with parameters values $\sigma = 10$, $r = 28$, and $b = \frac{8}{3}$ initial conditions $[x(0)\ y(0)\ z(0)] = [0.3\ 0.3\ 0.3]$.

study the properties of chaotic attractor in the second chapter. On the other side, our further study in the third chapter is concentrated on the application of these properties in the wideband communication systems. Therefore, the fundamental concepts of conventional wideband communications are necessary, as well as the state of art of the existing chaos-based wideband communications.

1.3 Wideband Communications

During the past 50 years, the communication domain has experienced a lot of developments, from wired to wireless, from voice communication to data transmission, from narrowband to wideband, recently even *ultra-wideband* (UWB), etc. Intuitively speaking, if the requirement of wireless communications can trace its roots to the migration/moving nature of human beings and the pursuit of convenient facilities, and if the data transmission is caused by the computer development and information digitalization, then how to explain the development from narrowband to wideband commu-

nications? In fact, it's more than a single question.

Firstly, what is wideband?

In communications, wideband is a relative term (to narrowband) used to describe a wide range of frequencies in a spectrum. Generally, a wideband system uses many times larger than the bandwidth required to transmit information. It's often known as a **spread spectrum system**.

It seems that a spread spectrum signal could be counterproductive, as the receive filter will require an increased bandwidth and, hence, will pass more noise power to the demodulator. However, a matched filter [17] is often used in the receiver of a spread spectrum system. Since the filter is matched to the signal, it's mismatched to the noise. The remarkable aspect of this result is that the filter bandwidth and the output noise power are irrelevant. Thus, there is no fundamental barrier to the use of spread-spectrum communications.

Secondly, what advantages can spread spectrum gain?

Spread-spectrum communication systems are useful for suppressing **interference**, making **interception** difficult, accommodating **fading**, and providing a **multiple-access** capability. Here we take interference suppressing and fading accommodating for example.

In communications, interference is anything which alters, modifies, or disrupts a signal as it travels along a channel between a source and a receiver. Interference may be broadly categorized into two types: broadband interference and narrowband interference. **Narrowband interference** usually arises from intentional transmissions such as radio and TV stations, pager transmitters, cell phones, etc.; while **broadband interference** usually comes from incidental radio frequency emitters. Figure 1.6 shows how a signal uses the spread spectrum to resist the narrowband interference [18]: *The narrowband signal is firstly spread onto a large frequency band with a much lower power level, and then transmitted into the channel, where both narrowband and broadband interferences are added to it. In the receiver, despreading the spread signal is meanwhile spreading to the narrowband interference, which consequently makes the power lever of narrowband interference much lower. In this way, the receiver can reconstruct the original data because the power level of user signal is much stronger than the remaining interference.*

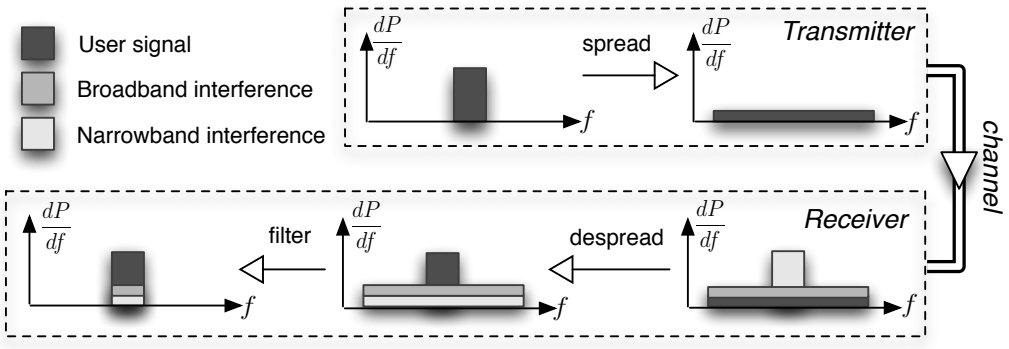

Figure 1.6: Spread spectrum: using spreading and despreading to resist narrowband interference.

Fading is another unavoidable phenomena in communications, generally refers to the degradation of the signal at the receiver. According to the coherence time of the channel which is large or small relative to the delay constraint of the channel, **slow fading** and **fast fading** can be therefore defined. The slow fading includes the following cases: the **large-scale fading** when the subscriber moves away significantly from the transmitter; or the **shadowing** when the subscriber moves behind a large object or in a tunnel. On the other side, the fast fading can be caused by different situations: either by the **multipath fading** which is known for the interference between two or more waves leaving the transmitter at the same time, but taking different paths to get to the receiver and thus arriving at different times; or by the **Doppler shift** because of the motion of the terminals (such as driving in a car), which is also called **Rayleigh fading**. [19]

It should be noticed that in communications, different frequencies propagate differently, so that fading can often be frequency selective, hence as shown in Figure 1.7, it's obvious that a system using a wider frequency band could resist a fading environment better than a narrowband system: *If a narrowband signal and a spectrum spread signal transport through the same frequency selective fading channel, it's possible that narrowband one is located in a very deep fading frequency point, which could consequently cancel most of its power. On the other hand, it's not as possible that all the spread spectrum locate in the deep fading points, so that the spectrum spread signal in the receiver can be used to reconstruct the original data with the enough remaining signal*

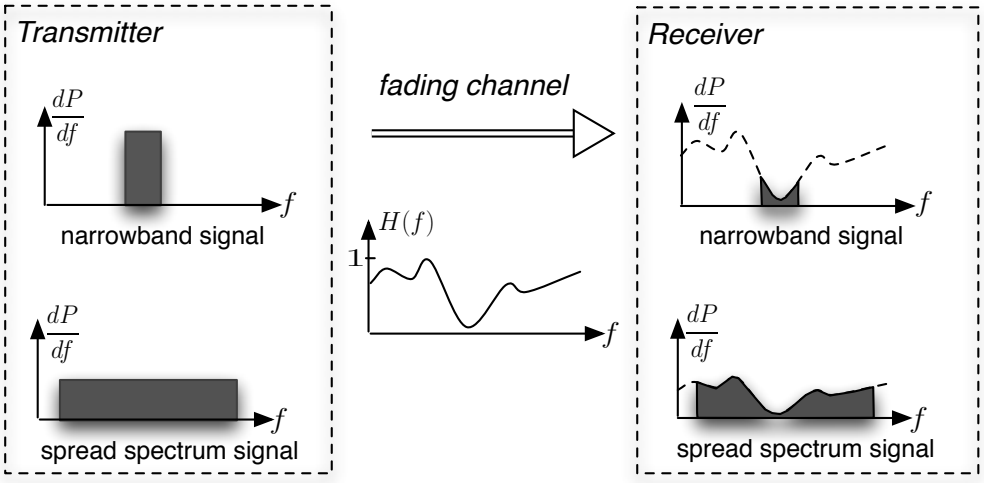

Figure 1.7: Spread spectrum signal resists better deep fading than narrowband signal. (In order to better observe the received spread spectrum signal after transmitting in deep fading channel, the magnitude of power per frequency, i.e., dP/df, is amplified, but the proportion of attenuation stays invariant.)

power.

Finally, how to spread spectrum?

There are several ways to spread a signal. The most practical and dominant methods of spread-spectrum communications in recent research and industry domains are *direct-sequence spread spectrum* (DSSS) [20][21], *frequency-hopping spread spectrum* (FHSS) [20] and *orthogonal frequency-division multiplexing* (OFDM) [22][21]. Since every wideband/spread spectrum modulation schemes is more or less based on and extended from the principles of narrowband modulations, we will first briefly talk about the conventional digital modulation schemes, known as **shift keying** [23], before introducing each spread spectrum method.

1.3.1 Shift Keying

In communications, modulation is the process of varying a waveform, which is more suitable for transmission, in order to use that signal to convey a message. Such a waveform is often called **carrier** or **basis function**. The three key parameters of a basis function are its amplitude, phase and frequency, all of which can be modified

in accordance with a low frequency information signal to obtain the modulated signal. Besides, digital modulation aims to transfer a digital bit stream over an analog bandpass channel or a certain *radio frequency* (RF) band. Generally, shifts from one state to another can be used to signify a one or a zero, where the states could be one of the three parameters of an RF carrier, and sometimes a combination of two.

Amplitude-shift keying (ASK) [23] simply varies the amplitude of the carrier between two states, one representing a one, the other representing a zero. Obviously, this method is linear and sensitive to atmospheric noise, distortions, propagation conditions, and speed is also a problem. Thus, it is not practical for advanced systems (although some systems do use a combination of ASK and another method).

Frequency-shift keying (FSK) [23] shifts the frequency of the carrier between the states to represent different data values, and it's actually used quite extensively in analog system signaling.

Phase-shift keying (PSK) [23][21] is the system best suited for today's cellular and *personal communication services* (PCS) systems. Essentially, the phase of the carrier is shifted, depending on the data to be sent. The simplest form of this is *binary PSK* (BPSK), where two phase states which are separated by 180° represent either a one or a zero. It's also the most robust modulation of all the PSKs since it takes serious distortion to make the demodulator reach an incorrect decision. For example, if a phase at 0° presents a zero, and at 180° presents a one, the binary data can be consequently conveyed as:

$$s(t) = A\cos\left(2\pi f_c t + d(t)\pi\right) \tag{1.9}$$

where A is the signal amplitude, $d(t)$ is the data symbol.

In the receiver, a demodulation is designed specifically for the set of symbols used by the modulator, where the amplitude, frequency or phase of the received signal is determined, and mapped back to the data symbol it represents, thus recovering the original data. According to the principle of demodulation, the receiver can be divided into two types [21]:

- **Coherent detection receiver**

  Coherent detection receivers are those in which the exact copies of all the basis functions are known. They are usually applied to demodulate ASK, PSK, etc.

- **Noncoherent detection receiver**

  In noncoherent detection receivers, the basis functions are unknown, but one or more robust characteristics of modulated signals can be determined, so that the demodulation is performed by evaluating one or more selected characteristics of the received signals. Noncoherent detection is often used in FSK.

It's often claimed that coherent detection outperforms noncoherent detection in the presence of additive channel noise. But noncoherent detection is the only possible solution when propagation conditions are so poor that the basis functions cannot be recovered from the received signal. Furthermore, noncoherent detections can often be implemented using easy circuitry.

In communications, the *bit error ratio* (BER) is a standard criterion to judge the performance of a system, which stands for the incorrectly detected symbol ratio in the receiver during a specified time interval. Note that BER is related to certain propagation conditions, i.e., transmission channels. The *additive white Gaussian noise* (AWGN) channel model is one in which the additive Gaussian noise is the only imperfection during the transmission. For a communication system, its BER in AWGN channel model is the most basic performance parameter, which is widely considered as a basic system performance parameter by researchers and engineers in this domain. Furthermore, E_b/N_0 is a term especially useful when comparing the BER performance of different digital modulation schemes without taking bandwidth into account. Here E_b is the energy of one bit transmitted information, $N_0/2$ is the double sided noise power spectral density.

Take the BER in AWGN of the robust BPSK with coherent detection for example, which is the most often considered reference for the comparison of digital modulation schemes. It can be calculated mathematically as [21]:

$$\mathrm{BER}_{\mathrm{BPSK}} = \frac{1}{2}\mathrm{erfc}(\sqrt{\frac{E_b}{N_0}}) \tag{1.10}$$

where $\mathrm{erfc}(\cdot)$ is the complementary error function defined as:

$$\mathrm{erfc}(x) = \frac{2}{\sqrt{\pi}}\int_x^\infty e^{-t^2}dt \tag{1.11}$$

It should be be noticed that, the coherent detected BPSK masters the limit BER performance in AWGN channel. Although the other modulation systems can't outperform

it, they could own other advantages, such as better **symbol error rate** of high-order PSK, simpler receivers of the noncoherent systems, multipath fading resistance of the spread spectrum systems, etc.

1.3.2 Direct-Sequence Spread Spectrum

A *direct-sequence* (DS) signal is a spread-spectrum signal generated by the direct mixing of the data with a spreading waveform before the final carrier modulation [20]. For example, a direct-sequence signal with BPSK data modulation can be represented by [20]

$$s(t) = Ad(t)p(t)\cos(2\pi f_c t + \theta) \tag{1.12}$$

where A is the signal amplitude, $d(t)$ is the data symbol, $p(t)$ is the spreading waveform stream, f_c is the carrier frequency, and θ is the phase at $t = 0$. The data symbol stream is a sequence of nonoverlapping rectangular pulses of duration T_s, each of them has an amplitude $d_n = +1$ if the associated data symbol is a one and $d_n = -1$ if it is a zero. Furthermore, the spreading waveform has the form [20]:

$$p(t) = \sum_{n=-\infty}^{\infty} p_n U(t - nT_c) \tag{1.13}$$

where each p_n equals $+1$ or -1 and represents one chip of the spreading sequence, and T_c is the chip duration. The DS **processing gain** $G = T_s/T_c$ is an integer equal to the number of chips per symbol. If W is the bandwidth of spreading waveform $p(t)$, and B is the bandwidth of data symbol $d(t)$, the spreading ensures that the DS signal $s(t)$ has a bandwidth $W \gg B$.

In order to recover the received signal, the same spreading sequence is reproduced in the receiver and mixed with the spread signal. If the incoming signal and the locally generated spreading code are synchronized, the original signal after correlation can be recovered. Figure 1.8 is a conceptual block diagram of DSSS system transceiver, where the modulate and demodulate modules could be any shift keying or other methods, often PSK as in the cited example.

The spreading sequence in DSSS is normally *pseudorandom noise* (PN) codes with good cross- and autocorrelation properties [24]. In a multiuser environment, the user signals can be distinguished by different orthogonal PN codes, and the receiver needs

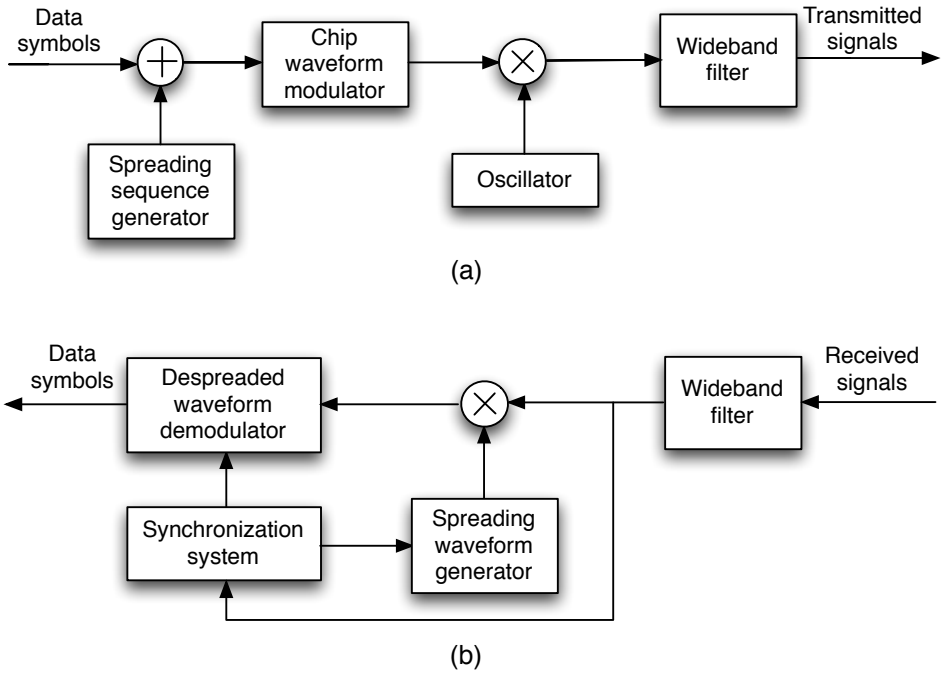

Figure 1.8: Conceptual block diagram of DSSS system [20]: (a) transmitter; (b) receiver.

only knowledge of the user's PN code. The longer the PN code is, the more noise-like signals appear. The drawback is that synchronization becomes more difficult unless synchronization information such as pilot signals is sent to aid acquisition. A **maximum length sequence** [25], also called m-**sequence**, is a type of widely used PN sequence.

DSSS is applied in many communications systems, such as *direct-sequence code-division multiple access* (DS-CDMA) system [22] and wireless local area network (WLAN) standards, e.g., 802.11b Wi-Fi.

1.3.3 Frequency-Hopping Spread Spectrum

Frequency hopping (FH) is similar to direct sequence spreading where a code is used to spread the signal over a much larger bandwidth than that required to transmit the signal [20]. A FH signal is generated by rapidly switching a carrier among many frequency channels, according to a specified algorithm, although the signal bandwidth keeps unchanged and has the same bandwidth as the transmitted signal at any instant.

The specific order in which frequencies are occupied is a function of a code sequence known by both transmitter and receiver, called FH pattern, as illustrated in Figure 1.9, where B is the frequency bandwidth of a single carrier, W is the total hopping bandwidth, and the hop interval is denoted by T_h. The FH pattern is generated usually by a PN sequence generator, such as m-sequences and Reed-Solomon codes [20].

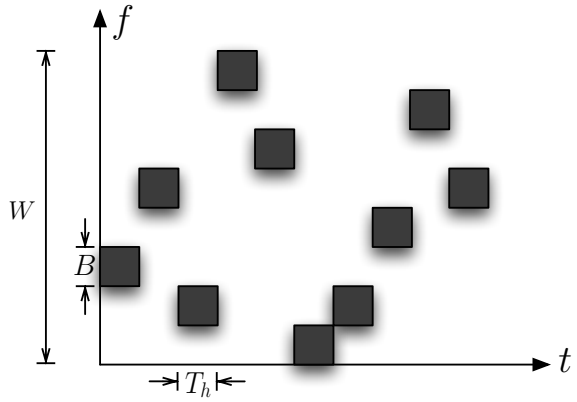

Figure 1.9: A frequency-hopping pattern.

In a FHSS system, the transmitter should operate in synchronization with the receiver, which remains tuned to the same center frequency as the transmitter. Though FHSS requires a much wider bandwidth than is needed to transmit the same information using only one carrier frequency, a short burst of data is transmitted on a narrowband, so that FH can enjoy the coexistence of several access points in the same area.

FHSS can provide a security transmission by choosing secret and complex hopping pattern, hence it is especially applied in military use, i.e., U.S. military employes separate encryption devices with FH.

1.3.4 Orthogonal Frequency-Division Multiplexing

OFDM is a multi-carrier spread spectrum method [22]. The principle of multi-carrier modulation is to convert a serial high-rate data stream (with the source symbol duration T_d) into N_c parallel low-rate sub-streams. Each sub-stream is modulated on one sub-carrier, so that the symbol rate on each sub-carrier is $1/N_c$ the initial serial data symbol rate [22]. An example of multi-carrier modulation with four sub-carriers $N_c = 4$ is illustrated in Figure 1.10 in three dimensional representation, i.e., time, frequency

and power density. Note that in the frequency domain, the spectra of the modulated symbol is spread to the total spectrum of N_c sub-carriers, therefore the power density is lowered. Here the A axis stands for the power density distribution trend, and does not make any sense in the context of pulse or spectrum shaping.

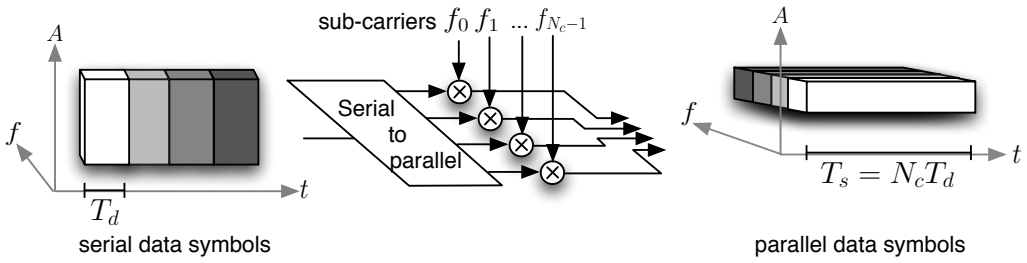

Figure 1.10: Conceptual block diagram of multi-carrier spread spectrum with four sub-carriers.

The principle of OFDM is to modulate the N_c sub-streams on N_c sub-carriers with a spacing of $F_s = 1/T_s$ in order to achieve orthogonality between the signals on the sub-carriers [22]. Here $T_s = N_c T_d$ is the OFDM symbol duration, and an OFDM symbol includes the N_c parallel modulated source symbols S_n, $n = 0, ..., N_c - 1$. The complex envelope of an OFDM symbol can be presented as [22]

$$x(t) = \frac{1}{N_c} \sum_{n=0}^{N_c-1} S_n e^{j2\pi f_n t}, \quad 0 \le t < T_s \tag{1.14}$$

where the sub-carrier frequencies are located at $f_n = n/T_s$, $n = 0, 1, ..., N_c - 1$. By sampling the complex envelope $x(t)$ of an OFDM symbol with rate $1/T_d$, we can get a sampled sequence as

$$x_m = \frac{1}{N_c} \sum_{n=0}^{N_c-1} S_n e^{j2\pi n \frac{m}{N_c}}, \quad m = 0, 1, ...N_c - 1 \tag{1.15}$$

Obviously, x_m, $m = 0, 1, ...N_c - 1$ is the *inverse discrete Fourier transform* (IDFT) of S_n, $n = 0, 1, ...N_c - 1$. Hence, a key advantage of using OFDM is that multi-carrier modulation can be implemented in the discrete domain by using an IDFT, or a computationally more efficient *inverse fast Fourier transform* (IFFT). Meanwhile, the corresponding demodulation can also be implemented by using *discrete Fourier transform* (DFT) or *fast Fourier transform* (FFT). This is why OFDM is known as

a low-complex technique to efficiently modulate multiple sub-carriers by using digital signal processing [22][26]. OFDM is widely used in various multi-carrier-based communications standards, such as *digital audio/video broadcasting* (DAB/DVB), WLAN and *wireless local loop* (WLL), etc. [22]

1.4 Chaos-based Wideband Communications

According to Section 1.3, wideband systems are considered to be more robust than narrowband systems in certain propagation conditions, such as multipath fading channel. Hence, they are widely required in modern communications, especially wireless communications in severe transmission environments. Different spread-spectrum schemes are developed and applied in different communication systems, which are introduced and compared briefly. Because the conventional modulation schemes are usually based on periodic carrier waveforms, such as the sinusoidal waveforms, which are normally narrowband, the spread spectrum methods try to either use the PN codes (which have flat band) to spread the frequency bandwidth of the carrier, or use simultaneously the total frequency bands of multi-carrier to form a globally larger bandwidth.

In Section 1.2, the basic behaviors of dynamical systems are presented. The revealed characteristics are very specific and different from those of periodic systems. A variety of chaotic waveforms can be generated by dynamical systems simply on choosing suitable parameter values. Talking about in the signal level, although chaotic signals are essentially deterministic, their pseudo-stochastic appearance leads to naturally wideband in the spectral distribution, which makes them very attractive for using as the carriers in spread spectrum communications. Furthermore, the sensitivity to initial conditions of the chaotic signals causes difficulty in eavesdropping. In other words, this sensitivity brings security to communications, while the deterministic essential ensures the possibility of detection under certain conditions. Above all, the developement of research of chaos in electronic circuits in late 1980s brought a research opportunity in chaos-based wideband communications.

In this section, the state of the art of the research on chaos-based wideband communications is given. According to the fact that chaotic signals are applied as spreading codes or directly as modulation carrier waveforms, **chaotic spreading sequence modulation** and **chaotic signal direct modulation** are separated and defined.

1.4.1 Chaotic Spreading Sequence Modulation

As mentioned in the previous section, modern spread spectrum communications, such as DSSS and FHSS, use PN sequences as spreading codes. In this section, chaotic spreading sequence modulation is defined in case that the chaotic sequences are used in place of PN sequences in spread spectrum systems, such as **chaotic DSSS** and **chaotic FHSS**.

1.4.1.1 Chaotic Direct-Sequence Spread Spectrum

The research on chaotic DSSS can be dated back to references [27] and [28], where the chaotic sequences were proposed for DSSS for the first time. The auto-/cross-correlation properties and the *power spectral density* (PSD) of these proposed sequences are similar to random white noise, as shown in Figure 1.11 with the corresponding correlations and the spectra of logistic map of equation (1.3) with parameter $a = 4$. The numbers and lengths of chaotic sequences are theoretically not restricted like m-sequences, however, due to the limited precision of practical systems, there is only a finite number that can be used. This number augments with the increase of the precision, with a cost of longer generation time. The simulations in reference [27] show that the BER performance of DSSS using random binary PN sequences and chaotic sequences generated by logistic map is comparable in the presence of AWGN for different numbers of users. Another advantage of chaotic sequences is that due to the noise-like appearance, they outperform PN sequences in *low probability of intercept* (LPI).

The application of chaotic DSSS for DS-CDMA system has been studied in references [29], [30] and [31] when AWGN channels are considered and multi-user interference is the dominant cause of the channel's non-ideality. Under such environment, theoretical performance bounds have been studied which show that significant improvement can be achieved by employing a properly designed family of chaotic systems generating real trajectories that are then quantized and periodically repeated to yield the users signatures.

1.4.1.2 Chaotic Frequency-Hopping Spread Spectrum

The research of chaotic sequence for FHSS began with reference [32], which showed that the FH sequences generated by chaotic systems are harder to intercept and give

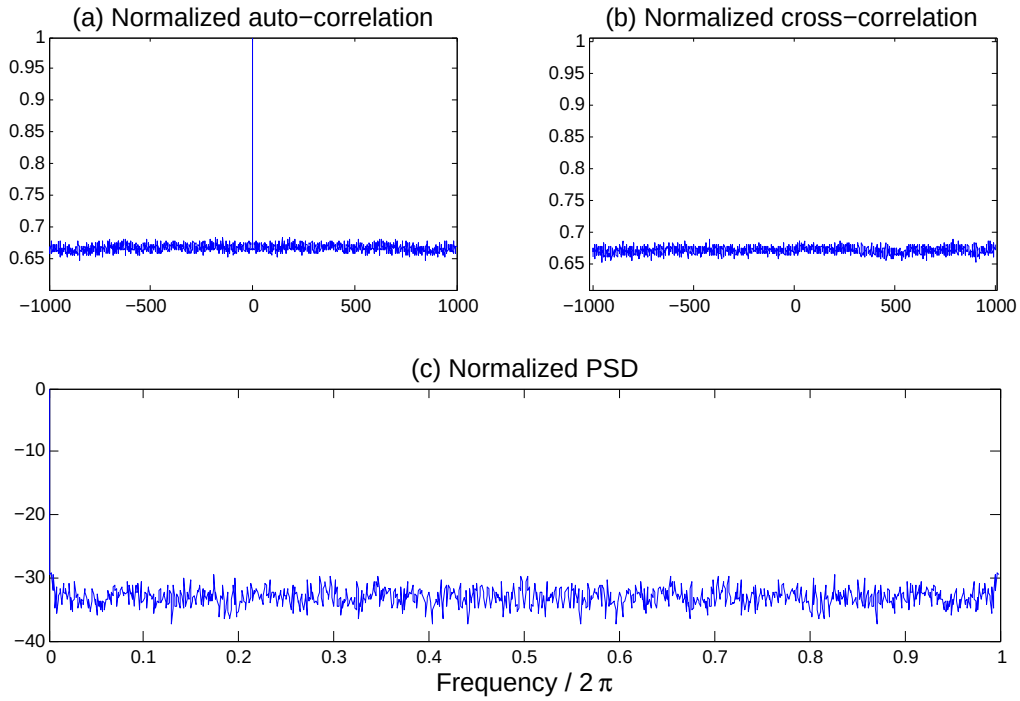

Figure 1.11: Properties of chaotic (logistic map with $a = 4$) sequences of length 5000 (the first 1000 iterations are abandoned): (a) Normalized auto-correlation property of a sequence with initial condition $x_0 = 0.1$, only the middle 2000 points are shown; (b) Normalized cross-correlation property between a sequence with initial condition $x_0 = 0.1$ and a sequence with initial condition $x_0 = 0.3$, only the middle 2000 points are shown; (c) PSD of the sequence with initial condition $x_0 = 0.1$ under 1028 points of FFT.

a uniform spread over the entire frequency bandwidth. Meanwhile, they own the good Hamming correlation properties and the ideal linear span which is attractive in multiple-access applications.

The application of chaotic FH sequence in the CDMA systems has been studied [33][34]. Reference [33] realized a chaostic FH sequence generator prototype in *field programmable gate arrays* (FPGA), and the BER performance evaluation of the chaos-based asynchronous FH-CDMA system suggests that the cost-effective and well-performing generator has the potential to be incorporated into existing FH systems.

1.4.2 Chaotic Signal Direct Modulation

As introduced above, chaotic spreading sequence modulations use chaotic sequences to spread the spectrum of conventional narrowband modulation systems, such as BPSK. In other words, spreading and modulation are realized in two different processes.

In this section, another way of using chaotic signals directly to realize wideband communications is discussed, named chaotic signal direct modulation in the context of this thesis. It uses similar schemes of shift keying as in Section 1.3.1 for narrowband modulation, while a chaotic carrier differs to a conventional periodic carrier at least in two domains: in the time domain, a chaotic basis function is nonperiodic [35], hence, the transmitted waveform is never periodic, even if the same data symbol is transmitted repeatedly; in the frequency domain, the spectrum of a chaotic carrier is nature-wideband, while a periodic carrier is narrowband without spread spectrum techniques.

Chaotic signal direct modulation is concerned with directly mapping data symbols to the chaotic waveforms generated by the dynamical systems. For example, *chaos shift keying* (CSK) [36] is proposed to map informations to weighted chaotic basis functions. According to the detection scheme, different types of CSK can be divided, such as antipodal CSK [6], *chaotic on-off keying* (COOK) [37], *chaotic parameter modulation* (CPM) [38], etc. *Differential chaos shift keying* (DCSK) [39] is a variety of CSK, in which the basis function is composed by both reference and information-bearing functions, so that the detection can be realized differentially.

1.4.2.1 Coherent Chaos Shift Keying

CSK is a digital modulation scheme where chaotic signals generated by different attractors or chaotic signals generated by the same attractor but emerging from different initial conditions are used as basis functions [36][6]. The number of attractors or initial conditions is equal to the number of basis functions N, which can form M elements of signal set using the combination of them, with $M \geq N$. The attractors may be produced by the same dynamical system with different values of bifurcation parameter, or by different dynamical systems.

The M elements of the signal set can be defined as [40]

$$s_m(t) = \sum_{n=1}^{N} s_{mn} g_n(t), \quad m = 1, 2, ..., M \tag{1.16}$$

where the basis functions $g_n(t)$ $(n = 1, 2, ..., N)$ are chaotic waveforms, and $s_m(t)$ $(m = 1, 2, ..., M)$ can be conceptually shown in Figure 1.12.(a).

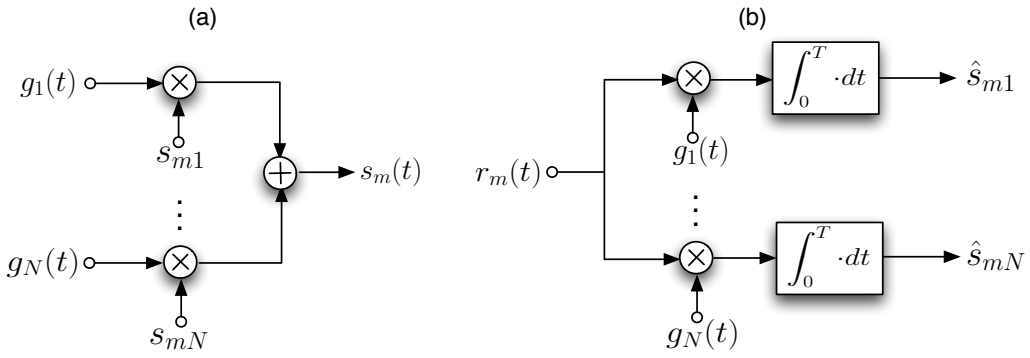

Figure 1.12: Conceptual diagram of CSK [40]: (a) generation of the elements of the modulated signal set; (b) observation signals using coherent detection.

Suppose that the chaotic basis functions $g_n(t)$ $(n = 1, 2, ..., N)$ are all zero mean and normalized, i.e., $E\left[\int_0^T g_n(t)dt\right] = 0$ and $E\left[\int_0^T g_n^2(t)dt\right] = 1$, where $E[\cdot]$ denotes the expectation operator, and T is the symbol duration. They are considered to be orthonormal in the mean CSK [6] as:

$$E\left[\int_0^T g_n(t) g_{n'}(t)dt\right] = \begin{cases} 1 & \text{if } n' = n \\ 0 & \text{otherwise} \end{cases} \tag{1.17}$$

Hence, the weights s_{mn} of the signal vector can be recovered by correlating the received signal with locally generated copies of the basis functions $g_n(t)$, as shown in Figure 1.12.(b), where $r_m(t)$ is the received signal, and $r_m(t) = s_m(t)$ if the transmission channel is distortion and noise free. The estimated element $\hat{s}_{mn}$ of the observation vector when $r_m(t) = s_m(t)$ can be given by

$$\begin{aligned} \hat{s}_{mn} &= \int_0^T s_m(t) g_n(t) dt \\ &= \int_0^T \left[\sum_{n'=1}^{N} s_{mn'} g_{n'}(t) \right] g_n(t) dt \\ &= s_{mn} \int_0^T g_n^2(t) dt \\ &\approx s_{mn} \end{aligned} \tag{1.18}$$

where the bit duration T is long enough.

It should be noted that, since each basis function $g_n(t)$ is not periodic, the waveform is not fixed for different symbol times, and the bit duration T is limited by the data rate. Therefore the estimated element $\hat{s}_{mn}$ of the observation vector are random numbers, so that the observation vector can only be considered as an estimation of the signal vector.

The simplest case of binary coherent **antipodal CSK** uses only one basis function, i.e., symbol '1' is represented by $s_1(t) = \sqrt{E_b} g_1(t)$ and symbol '0' is represented by $s_2(t) = -\sqrt{E_b} g_1(t)$. The bit energy E_b is assumed constant. Consider AWGN in the transmission channel so that $r_m(t) = s_m(t) + n(t)$ $(m = 1, 2)$, where $n(t)$ stands for the added noise, the theoretical noise performance was reported in reference [40] by

$$\mathrm{BER}_{\text{antipodal CSK}} = \frac{1}{2} \mathrm{erfc} \left(\sqrt{\frac{E_b}{N_0}} \right) \tag{1.19}$$

which is identical to the BER of BPSK in equation (1.10). An approach to calculating the BER of coherent CSK has been presented by reference [41].

Equation (1.19) shows the ideal AWGN performance on assuming that the basis function $g_1(t)$ can be properly regenerated from the received signal and perfectly synchronized. However, the high sensitivity of chaotic signals to initial conditions and poor propagation conditions may cause the recovering very difficult, if not impossible. Several strategies for recovering the basis functions have been proposed under the title 'chaotic synchronization' [5][12][42], but the problem still keeps unrealistic from the

practical or engineering point of view [43][35][6]. Hence, in real applications, a coherent detection may be impractical and a noncoherent or differentially coherent receiver should be considered.

1.4.2.2 Noncoherent Chaos Shift Keying

Remind that in a noncoherent detection, one or more robust characteristics of modulated signals can be determined, so that the demodulation is performed by evaluating one or more selected characteristics of the received signals. Under this principle, COOK observes the symbol energy as characteristic to be evaluated, while CPM treats the bifurcation parameter as characteristic to be estimated.

Chaotic On-Off Keying

COOK is a binary CSK ($M = 2$) using one basis function ($N = 1$) with noncoherent detection, which maps data '1' to $s_1(t) = \sqrt{2E_b}g_1(t)$ and data '0' to $s_2(t) = 0$, where E_b is the average energy per bit [37][6].

Since the symbol energy is the selected characteristic for noncoherent detection, the observation variable after the distortion and noise free transmission ($r_m(t) = s_m(t)$) can be consequently given as [40]:

$$\begin{aligned} \hat{s}_{m1} &= \sqrt{\int_0^T s_m^2(t)dt} \\ &= \sqrt{s_{m1}^2 \int_0^T g_1^2(t)dt} \\ &= s_{m1}\sqrt{\int_0^T g_1^2(t)dt} \\ &\approx s_{m1} \end{aligned} \tag{1.20}$$

where $m = 1, 2$ and $[s_{11}\ s_{21}] = [\sqrt{2E_b}\ 0]$.

The noncoherent receiver of COOK can be shown schematically in Figure 1.13. As a noncoherent system, the noise performance in AWGN depends on both bit duration T and RF channel bandwidth $2B$, where B stands for the **Nyquist frequency**. Furthermore, though AWGN is a zero-mean noise, it adds a non-zero noise energy to the observation variable $\hat{s}_{m1}$, $(m = 1, 2)$, hence, noncoherent COOK has a biased detection and the decision threshold should be adjusted depending on the SNR measured in the receiver.

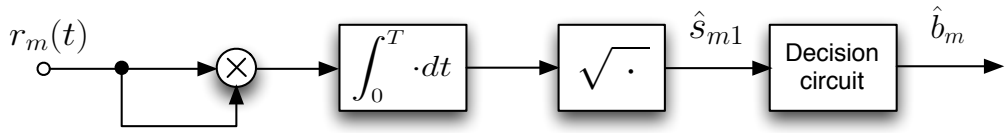

Figure 1.13: Noncoherent receiver for COOK system [6].

Chaotic Parameter Modulation

CPM [38] is another type of CSK, in which the basis functions $g_n(t)$ $(n = 1, 2, ..., N)$ are generated from the same dynamical system with distinct bifurcation parameters, and each value of information data corresponding to one of such parameters, i.e., $g_n(t) = g_{a_n}(t)$, where a_n is the parameter value mapped to s_{nn}. In this way, only $M = N$ elements are possible in the signal set.

Since the bifurcation parameter is the selected characteristic for noncoherent detection, the observation of the changes of the parameter should be considered in the receiver. Noted that the parameter characteristic is not a general characteristic for any dynamical systems, hence, different solutions could be optimal under certain selected dynamical systems or circuits. Authors of reference [38] have studied a binary CPM based on Chua's circuit [44], with the detection realized using the synchronization error to decide whether the received signal corresponds to one parameter, or to the other. Authors of reference [45] have proposed an *ergodic chaotic parameter modulation* (ECPM), using certain chaotic maps whose mean value functions are monotonic, such as Chebyshev's map given by $x(t) = \cos\left(\theta \cos^{-1}(x(t-1))\right)$, and based on this monotone property, it's possible to estimate a particular parameter value θ_0 by a mean value method. Authors of reference [46] have provided a method of using different chaotic signals which have different average frequencies, and the detection can be realized by measuring the average value of the zero-crossing rate of the received signals.

1.4.2.3 Differential Chaos Shift Keying

DCSK is a variety of binary CSK, in which the basis function is formed together by both reference and information-bearing parts, so that the detection can be realized differentially (noncoherently) [39][40][6].

Using the notations in Section 1.4.2.1, a binary DCSK can be shown as

$$s_m(t) = s_{m1}g_1(t) + s_{m2}g_2(t),\ m = 1, 2 \tag{1.21}$$

where the weight set of s_{mn} $(m = 1, 2,\ n = 1, 2)$ is

$$\begin{bmatrix} s_{11} & s_{12} \\ s_{21} & s_{22} \end{bmatrix} = \begin{bmatrix} \sqrt{E_b} & 0 \\ 0 & \sqrt{E_b} \end{bmatrix} \tag{1.22}$$

and the basis functions $g_n(t)$ $(n = 1, 2)$ have the special form as

$$\begin{aligned} g_1(t) &= \begin{cases} +\frac{1}{\sqrt{E_b}}c(t) & 0 \le t < \frac{T}{2} \\ +\frac{1}{\sqrt{E_b}}c(t - \frac{T}{2}) & \frac{T}{2} \le t < T \end{cases} \\ g_2(t) &= \begin{cases} +\frac{1}{\sqrt{E_b}}c(t) & 0 \le t < \frac{T}{2} \\ -\frac{1}{\sqrt{E_b}}c(t - \frac{T}{2}) & \frac{T}{2} \le t < T \end{cases} \end{aligned} \tag{1.23}$$

where $c(t)$ is the chaotic waveform. The first half symbol duration in each basis function is the reference chip, while the latter half is the information-bearing chip. The conceptual diagram of DCSK modulator is shown in Figure 1.14.(a).

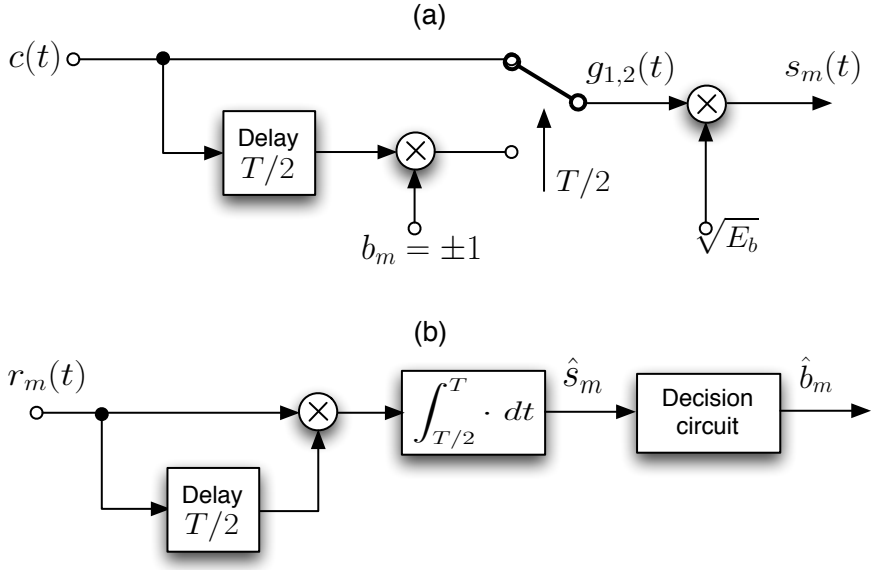

Figure 1.14: Conceptual diagram of DCSK system [39]: (a) modulator; (b) differential coherent demodulator.

The observation variable for DCSK can be the correlation between the reference chip and the information-bearing chip of the received symbol $r_m(t)$ [39], which can

therefore be presented under distortion and noise free conditions, i.e., $r_m(t) = s_m(t)$, as:

$$\begin{aligned} \hat{s}_m &= \int_{T/2}^{T} s_m(t) s_m(t - T/2) dt \\ &= E_b \int_{T/2}^{T} g_m(t) g_m(t - T/2) dt \end{aligned} \tag{1.24}$$

Since $E[\int_{T/2}^{T} g_m^2(t) dt] = 1/2$, it comes that $[\hat{s}_1 \ \hat{s}_2] \approx [\frac{E_b}{2} \ -\frac{E_b}{2}]$. The block diagram of the differential coherent receiver is shown in Figure 1.14.(b).

The exact analytical expression for the noise performance of differentially coherent DCSK was reported in reference [47], and the approximated expression of BER in AWGN was given by reference [48] as:

$$\mathrm{BER}_{\mathrm{DCSK}} = \frac{1}{2}\mathrm{erfc}\left(\sqrt{\frac{E_b}{4N_0}\left(1 + \frac{2}{5M_s}\frac{E_b}{N_0} + \frac{N_0}{2E_b}M_s\right)^{-1}}\right) \tag{1.25}$$

where $2M_s = 2BT$ is the number of samples per symbol using a sampling rate $2B$.

According to reference [35], in the radio propagation environments, DCSK offers the best noise performance among the chaotic signal direct modulations mentioned above. Hence, in the past twenty years after the publication of DCSK by Kolumbán, lots of performance analysis, enhancement and amelioration have been proposed based on DCSK.

For example, caused by the nonperiodicity of chaotic signals and the finite-length of each modulated symbol, DCSK (similar for the other chaotic signal direct modulations) has the non-constant bit energy, which leads to a estimation problem. In order to avoid this problem, DCSK can be combined with *Frequency Modulation* (FM), which forms the FM-DCSK modulation system [35][49][6][50], which can be treated as an amelioration of DCSK. Furthermore, the multipath, multi-user as well as multiple access schemes and performance of DCSK have been basically researched [51][52][53]. [51] and reference [52] have analyzed the multipath multi-user performance of DCSK respectively. As long as the application of DCSK is concerned, authors of reference [54] have talked about the low-rate UWB systems utilizing DCSK.

1.5 Conclusion

This chapter firstly presented a general introduction of chaos theory and dynamical systems. Definitions of specific notations of the behavior and stability of the discrete-time dynamical systems, as well as the simplest mathematical methods for analyzing

such systems have been given. They will be applied in Chapter 2 for studying our dynamical system. Secondly, another general introduction is concentrated on the target and advantages of the wideband communications, and the conventional spread spectrum communication systems, such as DSSS, FHSS and OFDM. Finally, the state of the art in the chaos-based modulation systems has been given, including the chaotic spreading sequence modulation and the chaotic signal direct modulation.

Based on the fundamental knowledge of chaos theory, further study of a selected dynamical system will be processed in Chapter 2. Specific properties of the studied system will be concluded, and application of these properties in the chaos-based communications will be given in the next chapters.

2

Chaotic Cyclic Attractors and Characteristics

2.1 Introduction

According to the Poincaré-Bendixson theorem [55][56][15], a continuous dynamical system on the plane cannot be chaotic; among the continuous-time dynamical systems, only those whose phase space is non-planar (having dimension at least three, or with a non-Euclidean geometry) can exhibit chaotic behavior. However, a discrete-time dynamical system can exhibit chaotic behavior in a one-dimensional or two-dimensional phase space. Furthermore, the continuous-time dynamical systems are often represented by the differential equations as (1.6)-(1.7), e.g., the Lorenz dynamical system in equation (1.8); in contrary, the discrete-time dynamical systems can be represented by simpler difference equation (map) as (1.1) or (1.2), e.g., logistic map in equation (1.3), which can be more easily simulated by the numerical computer. Therefore, the lower dimension discrete-time dynamical systems are usually considered by the researchers on chaos-based communications.

In the terminology of communications, chaotic signals are wideband, deterministic, nonperiodic, and random-like signals derived from nonlinear dynamical systems, which offer a number of attractive features as introduced in Chapter 1: the inherent wideband characteristic and the corresponding multipath fading resistance; the sensitive dependence on the initial conditions and parameter values so that a large number of spreading waveforms can be easily produced, hence, a cheap alternative solution for

spread-spectrum communications; very good spectral properties, especially that they can easily be generated by simple circuits.

A lot of dynamical systems can serve as the chaotic signal generators for chaos-based communications, and many of them have been studied in the research domain, such as piecewise-linear maps [10][57], tent maps [58][59], logistic maps [60][61] and chebyshev maps [62]. Another type of dynamical systems, which has a structure of n-dimensional digital filter, has been proposed by reference [63] to generate chaotic signals, and to be used in cryptography as in reference [64], etc.

The aim of this thesis is not to provide an overview or innovations of chaotic signals generators, but to study novel approaches of chaos-based communications, especially when noncoherent detection is concerned. During our study, a 2-dimensional digital filter structure system has been selected as a chaotic signal generator, which exhibits chaotic behavior in a 2-dimensional phase plane. The model of this dynamical system is given by

$$\mathbf{g}(x, y) = \Big(\sin(a\pi x + b\pi y), x \Big) \tag{2.1}$$

where $\mathbf{g} : \mathbb{R}^2 \to \mathbb{R}^2$ is a continuous function, and a, b are real valued parameters, which should be held fixed when the map is iterated. The conceptual diagram can be illustrated as in Figure 2.1, in which (x_k, y_k) is the iteration vector in state k.

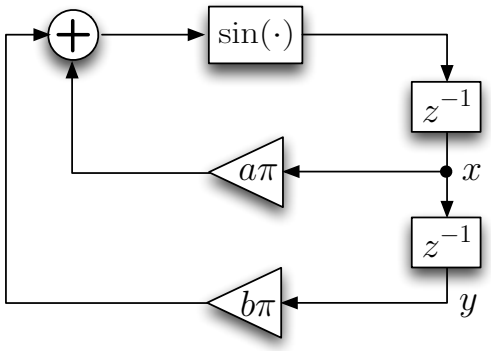

Figure 2.1: Conceptual diagram of system (2.1).

If we set the parameter values with $(a, b) = (0.05, -0.63)$, and choose initial conditions such that $(x_0, y_0) \in [-1, 1]^2$, the iterations will be attracted by a period-4 orbit:

$(-0.9198, -0.9765) \mapsto (0.9765, -0.9198) \mapsto (0.9198, 0.9765) \mapsto (-0.9765, 0.9198)$ ↻, as illustrated in Figure 2.2.(a). On the other hand, if we set $(a, b) = (0.05, -0.93)$ under

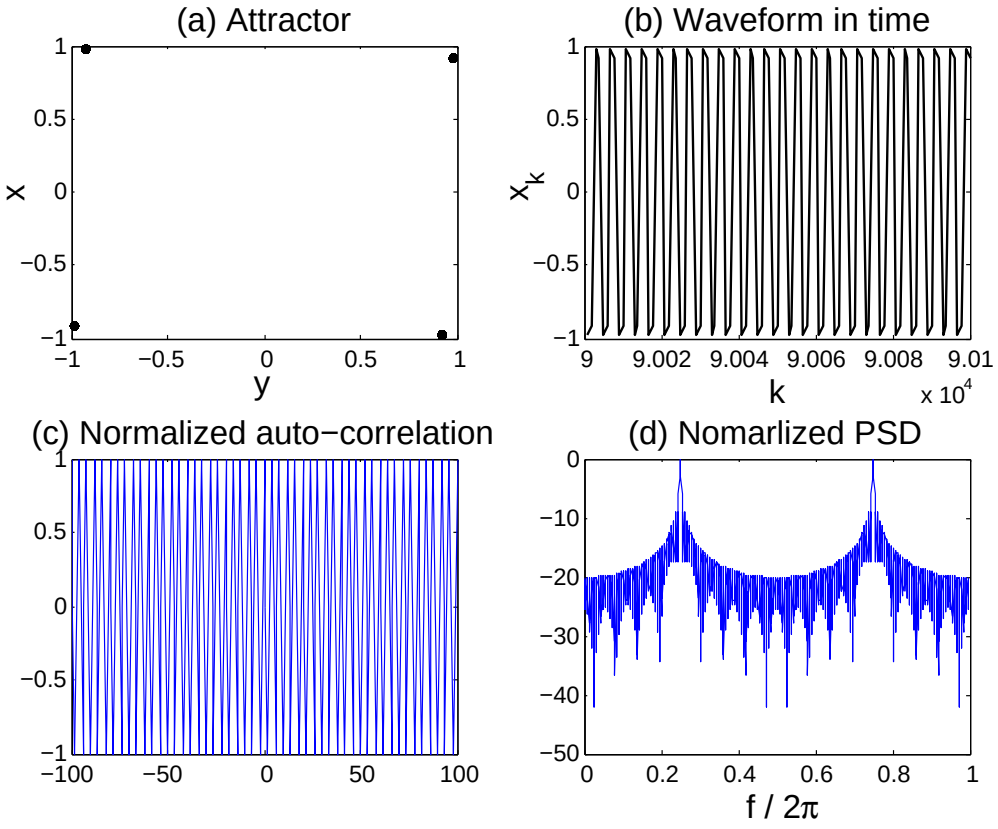

Figure 2.2: Analysis of x_k of system (2.1) with a=0.05, b=-0.63, $k \in [90\ 000, 90\ 100]$: (a) attractor; (b) waveform in time; (c) autocorrelation; (d) PSD (obtained by 1028 points of FFT).

the same initial conditions, the iterations will be attracted by a chaotic attractor, which is composed by four zones, as shown in Figure 2.3.(a). In both of the two trajectories, 10^5 points of iterations are computed, but only the last 10^4 points are depicted, in order to better observe the attractor.

Furthermore, the waveform in time, auto-correlation and PSD of 100 points ($k \in [90\ 000, 90\ 100]$) of both iterations are also shown in Figure 2.2 and Figure 2.3. From the comparison between them, an interesting phenomena can be observed namely that, though the attractors and waveforms in time are completely different between the two types of iterations, they have a very similar auto-correlation property and spectrum.

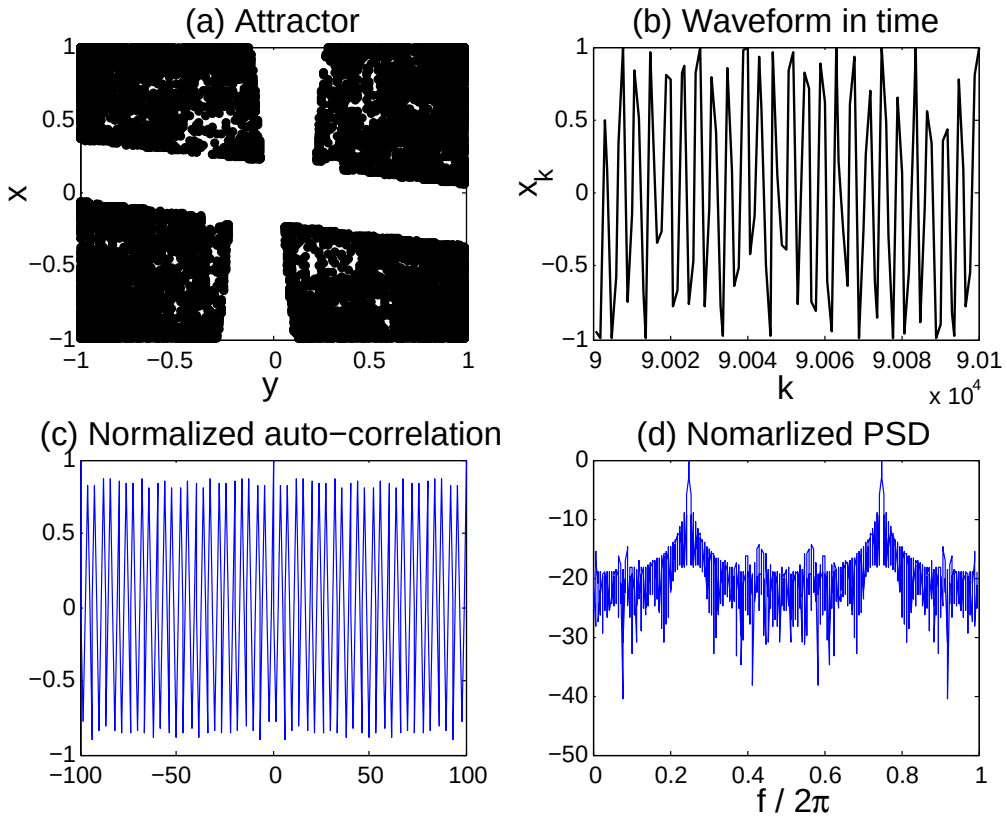

Figure 2.3: Analysis of x_k of system (2.1) with a=0.05, b=-0.93, $k \in [90\,000, 90\,100]$: (a) attractor; (b) waveform in time; (c) autocorrelation; (d) PSD (obtained by 1028 points of FFT).

How to get the type of chaotic attractors as in Figure 2.3.(a)? Is there some relationship between this type of attractors and the period-q orbits? What interesting properties do they own on applying in chaos-based communications? The further study of system (2.1) has been done in this chapter to answer these questions.

2.2 Bifurcations Analysis and Attractors

2.2.1 Basic Bifurcations Analysis

It has been briefly introduced in Section 1.2.1.2 that, in order to analyze the stability of a two-dimensional map, three basic bifurcations should be concerned, i.e., the tangent bifurcation, the period-doubling bifurcation, and the Neimark-Sacker bifurcation. For this sake, the eigenvalues of the system (2.1) should be obtained.

Rewrite the map of the dynamical system $\mathbf{f} : \mathbb{R}^2 \to \mathbb{R}^2$ in equation (2.1) as:

$$\mathbf{X} = \begin{bmatrix} x \\ y \end{bmatrix} \mapsto \mathbf{g}(\mathbf{X}; \mathbf{A}) = \begin{bmatrix} \sin(a\pi x + b\pi y) \\ x \end{bmatrix} \tag{2.2}$$

where $x, y \in \mathbb{R}$, $\mathbf{A} = \begin{bmatrix} a \\ b \end{bmatrix}$ is the parameter with $a, b \in \mathbb{R}$. Note $\mathbf{X}^* = \begin{bmatrix} x^* \\ y^* \end{bmatrix}$ as a fixed point, then we can get:

$$\mathbf{g}(\mathbf{X}^*) = \mathbf{X}^* \tag{2.3}$$

or

$$\begin{cases} x^* = \sin(a\pi x^* + b\pi x^*) \\ y^* = x^* \end{cases} \tag{2.4}$$

Let $D_{\mathbf{g}}$ be the derivative of $\mathbf{g}$, wet get

$$\begin{aligned} D_{\mathbf{g}}(\mathbf{X}^*; \mathbf{A}) &= \begin{bmatrix} \frac{\partial \sin(a\pi x + b\pi y)}{\partial x} & \frac{\partial \sin(a\pi x + b\pi y)}{\partial y} \\ 1 & 0 \end{bmatrix} \Bigg|_{(x^*, y^*)} \\ &= \begin{bmatrix} a\pi \cos(a\pi x^* + b\pi y^*) & b\pi \sin(a\pi x^* + b\pi y^*) \\ 1 & 0 \end{bmatrix} \end{aligned} \tag{2.5}$$

so that the eigenvalues λ of the fixed point $\mathbf{X}^*$ can be obtained by solving the following equation:

$$|D_{\mathbf{g}}(\mathbf{X}^*; \mathbf{A}) - \lambda \mathbf{I}| = 0 \tag{2.6}$$

where $\mathbf{I}$ is the two-dimensional identity matrix. Assume that the fixed point has at least a pair of complex conjugate eigenvalues described by:

$$\lambda, \overline{\lambda} = \rho e^{\pm j\theta} \tag{2.7}$$

where j stands for the imaginary unit, ρ is the radius of the eigenvalues, and θ is the argument. Inserting equation (2.7) into equation (2.6), we get:

$$\rho^2 e^{j2\theta} - a\pi \cos(a\pi x^* + b\pi y^*) \rho e^{j\theta} - b\pi \cos(a\pi x^* + b\pi y^*) = 0 \tag{2.8}$$

Define $\chi = \Re\chi + j\Im\chi$ to present the left side of equation (2.8), with $\Re\chi$ and $\Im\chi$ being the corresponding real and imaginary parts, i.e.,

$$\begin{cases} \Re\chi = \rho^2\cos(2\theta) - (a\pi\rho\cos(\theta) - b\pi)\cos(a\pi x^* + b\pi y^*) \\ \Im\chi = \rho^2\sin(2\theta) - a\pi\rho\sin(\theta)\cos(a\pi x^* + b\pi y^*) \end{cases} \tag{2.9}$$

Combining equation (2.3) and (2.8), we can get:

$$\begin{bmatrix} \mathbf{g}(\mathbf{X}^*;\mathbf{A}) - \mathbf{X}^* \\ \Re\chi \\ \Im\chi \end{bmatrix} = 0 \tag{2.10}$$

or

$$\begin{cases} \sin(a\pi x^* + b\pi x^*) - x^* = 0 \\ \rho^2\cos(2\theta) - (a\pi\rho\cos(\theta) - b\pi)\cos(a\pi x^* + b\pi x^*) = 0 \\ \rho^2\sin(2\theta) - a\pi\rho\sin(\theta)\cos(a\pi x^* + b\pi x^*) = 0 \end{cases} \tag{2.11}$$

According to Section 1.2.1, for a two-dimensional discrete-time dynamical system, the change of stability of a fixed point can be observed in three basic bifurcation cases, i.e., the tangent (or fold) bifurcation, the period-doubling (or flip) bifurcation, and the Neimark-Sacker bifurcation. The mathematical method for obtaining these bifurcations is given by calculating the eigenvalues λ, i.e., one eigenvalue equal to 1 ($\rho = 1, \theta = 0$) for the fold bifurcation, one eigenvalue equal to -1 ($\rho = 1, \theta = \pi$) for the flip bifurcation, while two complex conjugate eigenvalues with $\rho = 1$ ($\theta \neq 0, \pi$) for the Neimark-Sacker bifurcation.

By replacing the typical value of the eigenvalues into equation (2.11), the three basic bifurcations of fixed points of system (2.1) can be derived, which are illustrated in the parameter space (a, b) in Figure 2.4.(a)-(c) respectively. In this way, the parameter region corresponding to the existence of attractive fixed points is surrounded by these bifurcations, as shown in Figure 2.4.(d).

Furthermore, since a period-q point of the map $\mathbf{g}$ is also a fixed point of the map $\mathbf{g}^q$ [15], i.e., $\mathbf{g}^q(\mathbf{X}^*;\mathbf{A}) = \mathbf{X}^*$, the analysis of the bifurcations of the other periodic points, as well as the parameter region corresponding to the existence of period-q points in the parameter space (a, b) can also be manipulated like those in equations (2.5)-(2.10) by replacing $\mathbf{g}$ by $\mathbf{g}^q$, and the complexity of calculation increases a lot with the value of period q. In our research, a numerical method has been operated instead of the analysis, in which the parameter regions in the parameter space (a, b) for the existence of period-q points with $q < 15$ can be obtained simultaneously, as shown in Figure 2.5.

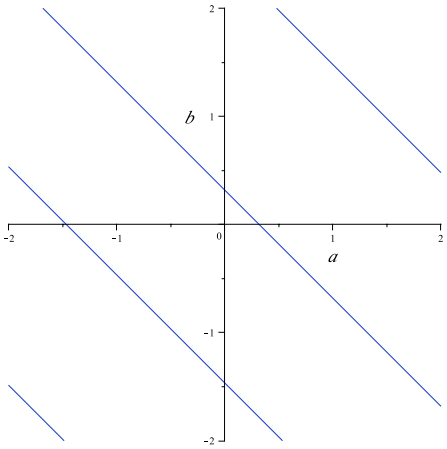

(a) Fold bifurcation

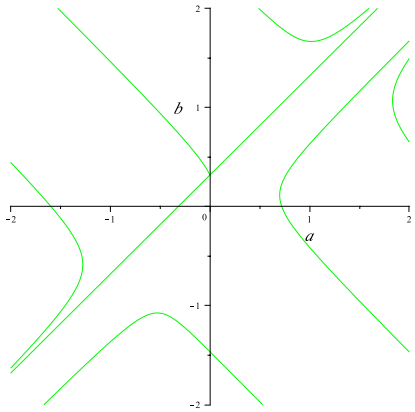

(b) Flip bifurcation

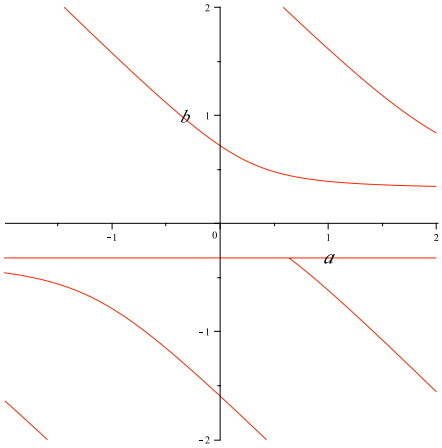

(c) Neimark-Sacker bifurcation

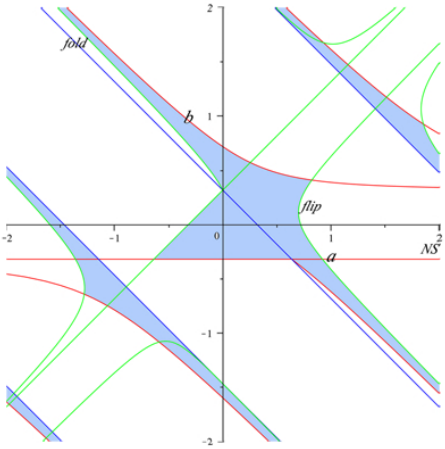

(d) Parameter region of fixed point

Figure 2.4: Three basic bifurcations of fixed points of system (2.1) in the parameter plane, and the corresponding parameter region of existence of a fixed point.

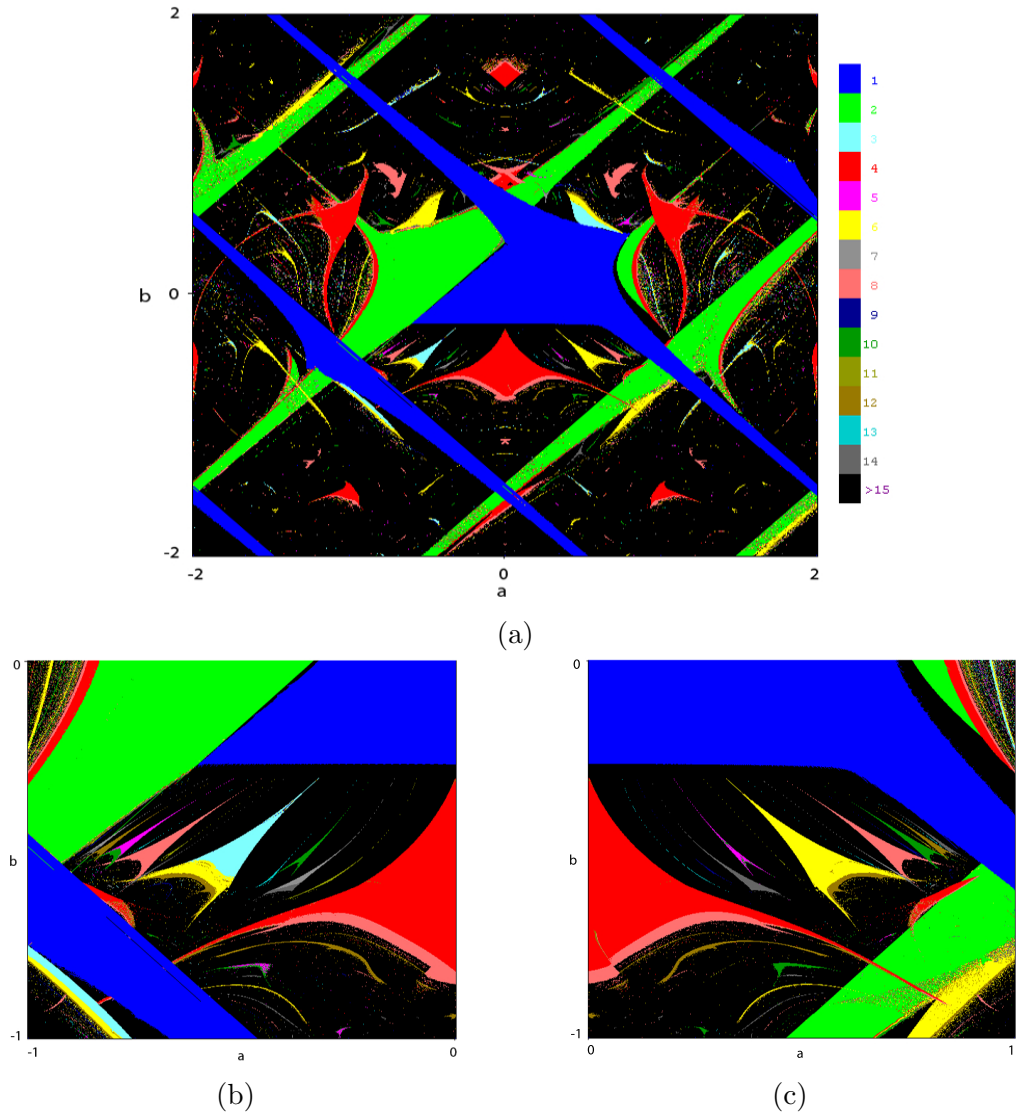

Figure 2.5: Simulated bifurcation diagram of system (2.1) in the phase plane (a, b) with: (a) $a \in [-2, 2], b \in [-2, 2]$; (b) $a \in [-1, 0], b \in [-1, 0]$; (c) $a \in [0, 1], b \in [-1, 0]$. The colored areas denote parameter values of existence of period-q ($q \leq 14$) points, where the periods q are differed by colors. Black denotes the parameter region of the existence of period-q orbits with $q > 14$, or other attractors, including chaotic attractors.

Observing the details of the diagram in Figure 2.5.(b)-(c), we can see the phenomenon of some special tongue-like colored zones (colors denoting different periods) surrounding a bifurcation, with their cusps pointing to the bifurcation. From the comparison between the analytical basic bifurcations in Figure 2.4 and the numerical result in Figure 2.5, it can be proved that the bifurcation with the cusps of tongue-like zones intersected is a Neimark-Sacker bifurcation. This phenomenon is called frequency locking and is characterized as **structure of Arnold tongues** [65] in the two-parameter bifurcation plane.

Authors of reference [66] proposed a numerical method to obtain the accurate location and the parameter value of the fixed point corresponding to a specified argument $\theta = 2\pi p/q$ (p, q are coprime intergers) of the complex conjugate eigenvalues $\lambda, \overline{\lambda}$. As the parameter changes, such solution draws as an isocline in the parameter space. The intersection point of the isocline of $\theta = 2\pi p/q$ and the Neimark-Sacker bifurcation coincide on the cusp of Arnold tongue of period-q. This method is chosen in our research to localize more precisely the parameter regions of the existence of periodic points.

A **super stable fixed point** exists when one eigenvalue is equal to 0. Therefore, in case of $\rho = 0$ (so that the eigenvalue $\lambda = 0$), through analyzing equation (2.11), we can get $b = 0$ and $a = 0,\ 0.5 + 2m$ ($m \in \mathbb{Z}$). In other words, the parameter values $(0, 0),\ (0.5 + 2m, 0)$ ($m \in \mathbb{Z}$) in the parameter space (a, b) correspond to the existence of super stable fixed points of our system.

Otherwise, in case of $\rho \neq 0$, for each specified argument $\theta \in [0, \pi]$, the radius of the complex conjugate eigenvalues can be represented by $\rho = -\frac{2b}{a}\cos(\theta)$. Hence, the location of one parameter of the fixed point $\mathbf{X}^*$ forms an isocline as the value of the other parameter varies. By replacing $\rho = -\frac{2b}{a}\cos(\theta)$ into equation (2.11), the expression of the isocline of argument θ can be obtained as:

$$\sqrt{1 - \frac{16b^2\cos^4(\theta)}{a^4\pi^2}} - \frac{\pi - \arccos\left(\frac{4b\cos^2(\theta)}{a^2\pi}\right)}{\pi(a+b)} - \frac{2m}{a+b} = 0 \tag{2.12}$$

where the coefficient $m \in \mathbb{Z}$ is caused by the periodicity of sinus.

Each isocline corresponding to the specified arguments θ in equation (2.12) can be drawn in the parameter plane (a, b) by plotting the solution a as the incremental parameter. Figure 2.6 shows the isoclines with the arguments $\theta = 2\pi/3$ (dashed lines) and $\theta = 2\pi/8$ (dash-dotted lines), which are illustrated on top of the parameter region

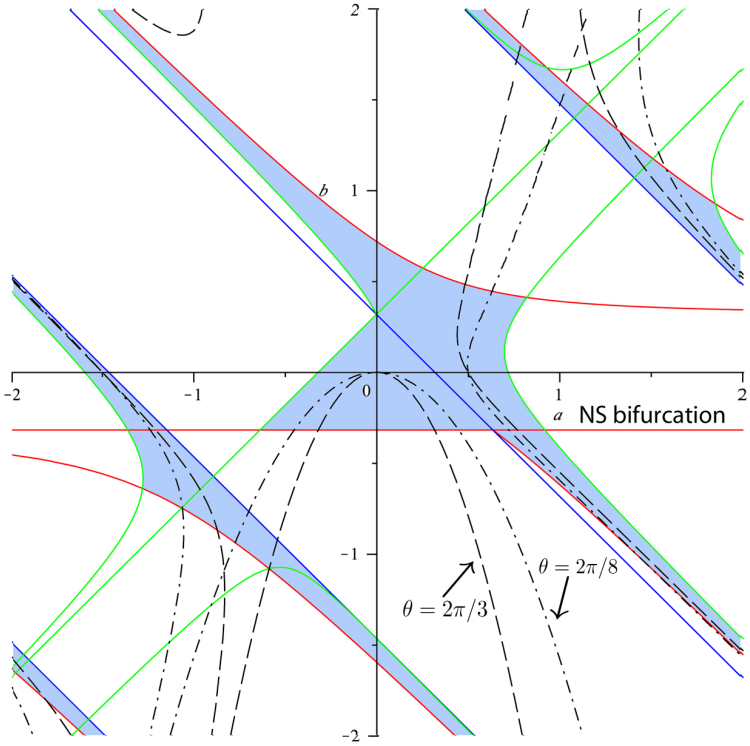

Figure 2.6: Isoclines corresponding to the arguments $\theta = 2\pi/3$ (dashed lines) and $\theta = 2\pi/8$ (dash-dotted lines).

of the existence of fixed points in Figure 2.4.(d). It can be noticed that all the isoclines pass by one of the mentioned points $(0, 0)$, $(0.5 + 2m, 0)$ $(m \in \mathbb{Z})$.

Furthermore, Figure 2.7 puts the analytical bifurcations and isoclines of the fixed points in the parameter space together with the simulated bifurcation diagram. As expected, it can be observed that the blue regions (parameter region corresponding to the existence of fixed points) in both results correspond one to the other; while the cross points of Neimark-Sacker bifurcation and the isoclines with $\theta = 2\pi/3$ and $\theta = 2\pi/8$ coincide with the cusps of the Arnold tongues of period-3 points and period-8 points, respectively.

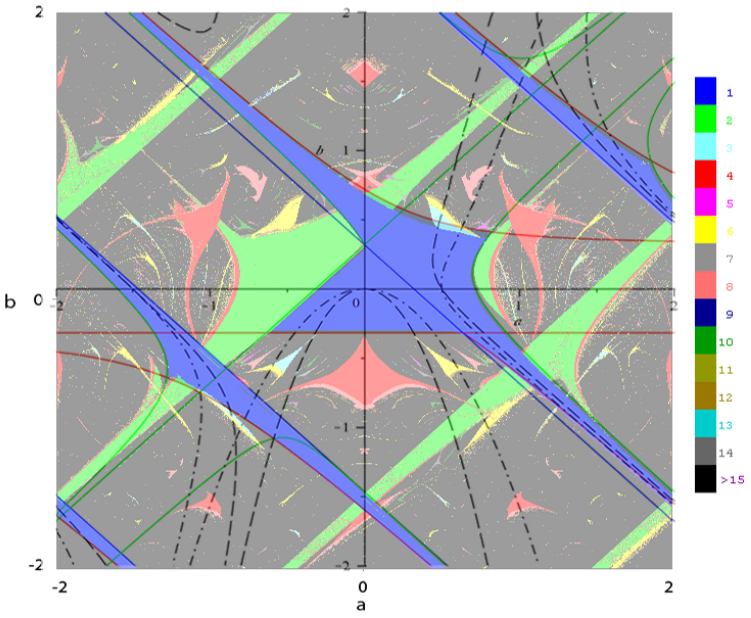

(a)

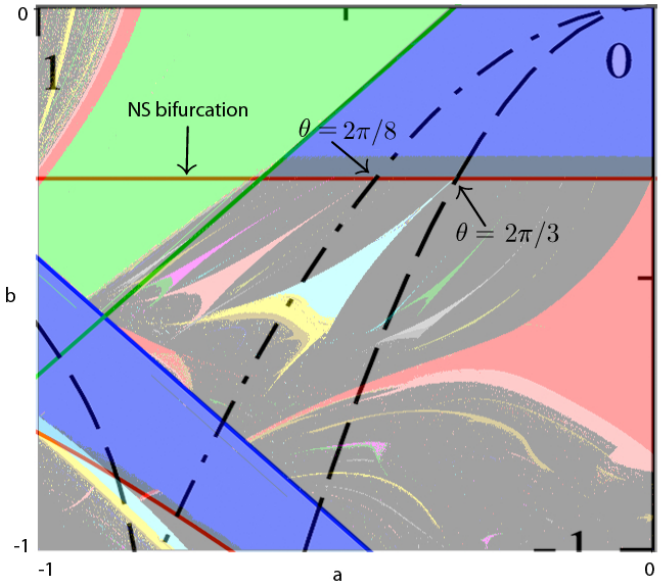

(b)

Figure 2.7: (a) Analytical bifurcations of the fixed points on top of the simulated bifurcation diagram(top); (b) Coincidence between the cusps of the parameter regions corresponding to the existence of period-q ($q = 3, 8$) orbits and the cross points of the Neimark-Sacker bifurcation with the isoclines of θ ($\theta = 2\pi/3, 2\pi/8$).

2.2.2 Diversity of Attractors

Based on the analysis and simulation of isoclines and bifurcation diagram in section 2.2.1, the rule of choosing suitable parameter values for different types of attractors for the dynamical system (2.1), i.e., fixed point, periodic orbit, closed invariant curve and chaotic attractor can be discussed. In this section, we will choose the isocline of $\theta = 2\pi/8$ to give an example, which can be presented as

$$\sqrt{1-\frac{4b^2}{a^4\pi^2}}-\frac{\pi-\arccos\left(\frac{2b}{a^2\pi}\right)}{\pi(a+b)}-\frac{2m}{a+b}=0, \quad m\in\mathbb{Z} \tag{2.13}$$

Let's only consider part of this isocline, i.e., $b=-a^2\pi/2$, which intersects the corresponding part of Neimark-Sacker bifurcation $b=-1/\pi$ in the point $(a_8,b_8)=(\pm\sqrt{2},-1/\pi)$. Remind that this point coincides with the cusp of the parameter region corresponding to the existence of period-8 orbits, which is indicated by light red in Figure 2.7, according to the structure of Arnold tongues.

Choose the parameter values to satisfy $b=-a^2\pi/2$ and $b\in(b_8,0)$, so that $\rho<1$, then iterations attracted by the stable fixed point $\mathbf{X}^*=(0,0)$ can be generated, as shown in Figure 2.8.(a) using $(a,b)=(0.4495,-0.3173)$. Notice that the trajectory is formed by 8 branches, each of them approaches toward the fixed point $\mathbf{X}^*$ quickly.

According to the definition, the Neimark-Sacker bifurcation is the birth of a closed invariant curve from a fixed point. Choose the parameters locating on the isocline with $b<b_8$ so that $\rho>1$, but not far from the cusp (a_8,b_8). As expected, iterations attracted by a closed invariant curve are generated, as shown in Figure 2.8.(b) using $(a,b)=(0.4509,-0.3193)$.

Again, choose the parameters around the cusp (a_8,b_8) to make $\rho>1$, meanwhile to make sure that the parameters locate in the parameter region corresponding to the existence of period-8 orbits (indicated by light red in Figure 2.5), the expected iterations attracted by a period-8 orbit are generated, as shown in Figure 2.8.(c) with $(a,b)=(0.7,-0.5)$.

Select the parameters locate slightly out of the region corresponds to the existence of period-8 orbits by the direction opposite to the cusp (a_8,b_8), iterations attracted by a chaotic attractor are generated, as shown in Figure 2.8.(d) with $(a,b)=(0.75,-0.55)$. This attractor is composed by several cyclic zones, and the iteration jumps from one zone to another with a regular order, but the position of iteration in each zone is chaotic.

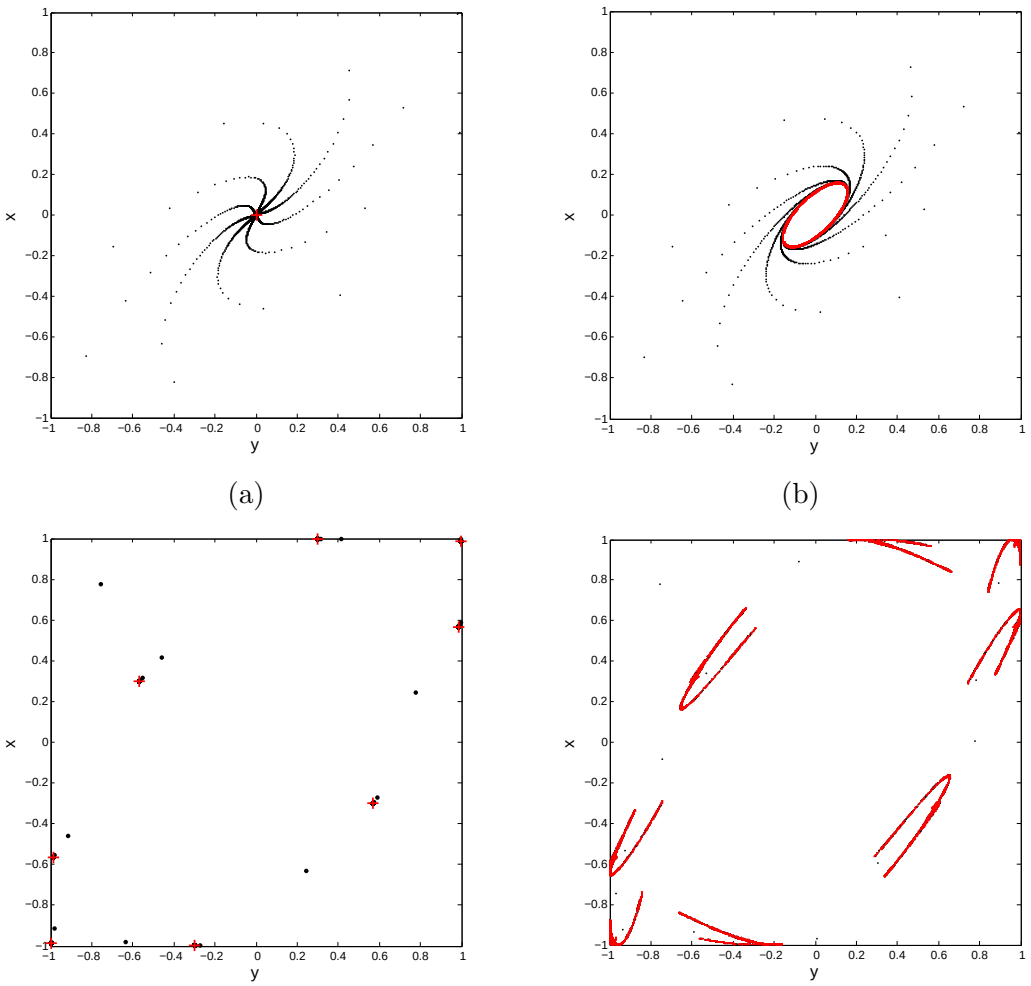

Figure 2.8: Iterations in the phase plane (y, x) with: (a) $(a, b) = (0.4495, -0.3173)$, attracted by a fixed point $\mathbf{X}^* = (0, 0)$ (denoted by a cross); (b) $(a, b) = (0.4509, -0.3193)$, attracted by a closed invariant curve; (c) $(a, b) = (0.7, -0.5)$, attracted by a period-8 orbit (denote by the crosses); (d) $(a, b) = (0.75, -0.55)$, attracted by a CCA-8. Each trajectory is obtained by 10^5 iterations with initial condition $x_0, y_0 \in [-1, 1]$ selected randomly, and all the attractors are denoted in red).

Name here this type of attractor as *chaotic cyclic attractor* (CCA), and Figure 2.8.(d) shows a CCA of period 8. In the later text, CCA-q will be used to denote the CCA of period q.

2.3 Properties of Chaotic Cyclic Attractor

As introduced in the previous section, CCA-q is a chaotic attractor, which is composed by q cyclic zones, and the iteration jumps from one zone to another with a regular order, but its position in each zone is chaotic.

In this section, the specific properties of the output $\mathbf{x}$ of CCA-q generator will be discussed, including the auto-correlation property, the spectral property and the statistical property. As iteration result of the discrete-time dynamical system, $\mathbf{x}$ can be denoted as a sequence $\mathbf{x} = (x_1,\ x_2,\ ...,\ x_L)$, where L stands for the finite length in the analysis. Furthermore, caused by the composition of q zones, the iterations in each zone can be denoted as a sub-sequence $\mathbf{x}_{q,l} = (x_l,\ x_{l+q},\ x_{l+2q},\ ...,\ x_{l+L_l q})$, with $l \in \{1, 2, ...q\}$ indicating the index of the q zones, and $L_l + 1 = \lfloor \frac{L-l}{q} \rfloor + 1$ standing for the length of each sub-sequence ($\lfloor \cdot \rfloor$ denotes the floor function which maps a real number to the next smallest integer). It is known that for a electronic signal in the communications, the *direct current* (DC) component does not transport information, which should always be subtracted to optimize the signal energy. The DC component equals to the mean of a signal side, alternatively speaking, we can simply make $\langle \mathbf{x} \rangle = 0$ to drop the unnecessary component, where $\langle \cdot \rangle$ denotes the mean operator.

For sake of verification of the properties, the CCA-31 of system (2.1) with the parameter $(a, b) = (0.3590, -0.6184)$ will be chosen as an example, and its iteration in phase plane (x_{n-1}, x_n) as well as in the time domain are illustrated in Figure 2.9, with the signal made zero mean.

2.3.1 Auto-Correlation Property

The auto-correlation of the iteration sequence of CCA-q $\mathbf{x} = (x_1,\ x_2,\ ...,\ x_L)$ can be performed as:

$$R_{\mathbf{xx}}[m] = \sum_{n=1}^{L} x_n x_{n-m} = \sum_{l=1}^{q} \sum_{k=0}^{L_l} x_{l+kq} x_{l+kq-m} \tag{2.14}$$

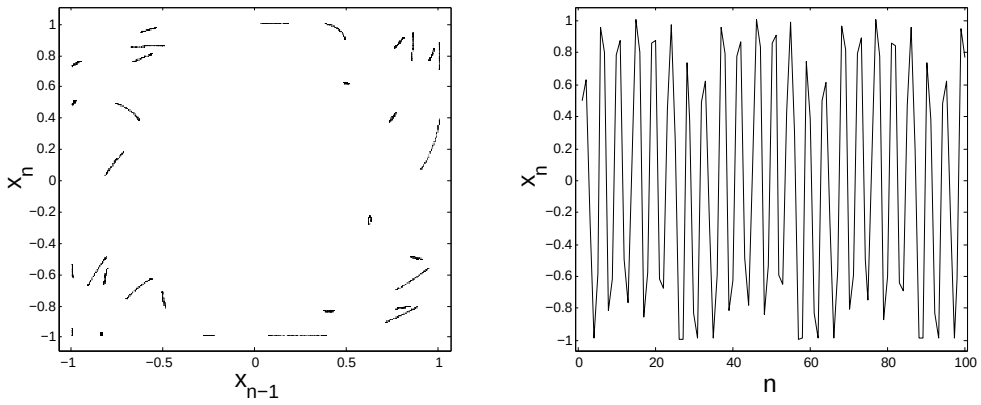

Figure 2.9: CCA-31 of system (2.1) with the parameter $(a, b) = (0.3590, -0.6184)$ using 10^5 iterations (first 100 points are abandoned) with initial condition ($-1 \leq x_0 \leq 1, -1 \leq y_0 \leq 1$) generated randomly: the iteration in phase plane (left) and the waveform in time (right).

where $L_l = \lfloor \frac{L-l}{q} \rfloor$. Let's define $l' = \text{mod}(l - m, q)$, with $\text{mod}(\cdot)$ being the modulo operation, so that the second sum in the above equation corresponds to the cross-correlation between the sub-sequence $\mathbf{x}_{q,l}$ and $\mathbf{x}_{q,l'}$, i.e.,

$$\sum_{k=0}^{L_l} x_{l+kq} x_{l+kq-m} = R_{\mathbf{x}_{q,l}\mathbf{x}_{q,l'}}[m'] \tag{2.15}$$

where $m' = \lfloor \frac{m}{q} \rfloor$. Especially, when m is the multiple of q, i.e., $m = \ell q$ ($\ell \in \mathbb{Z}, \ell \neq 0$), we can get $m' = 0$, and this sum equals to the auto-correlation of $\mathbf{x}_{q,l}$.

Since each zone of CCA appears as a dense chaotic attractor, it has the characteristics similar to a chaotic attractor. Denote the statistics of the l^{th} zone of CCA-q as $\langle \mathbf{x}_{q,l} \rangle = \mu_l$, and $\langle \mathbf{x}_{q,l}^2 \rangle = \mu_l^2 + \delta_l^2$. According to reference [6] and equation (1.17), we can say that:

$$\Big\langle \sum_{k=0}^{L_l} x_{l+kq} x_{l+kq-m} \Big\rangle = \begin{cases} (L_l+1)(\mu_l^2 + \delta_l^2), & \text{if } m = 0 \\ (L_l+1)\mu_l^2, & \text{if } m = \ell q \ (\ell \in \mathbb{Z}, \ell \neq 0) \\ (L_l+1)\mu_l \mu_{l'}, & \text{otherwise} \end{cases} \tag{2.16}$$

where $l' = \text{mod}(l - m, q) \neq l$. Inserting equation (2.16) into equation (2.14), we can get:

$$R_{\mathbf{xx}}[m] = \begin{cases} \sum_{l=1}^{q} (L_l+1)(\mu_l^2 + \delta_l^2), & \text{if } m = 0 \\ \sum_{l=1}^{q} (L_l+1)\mu_l^2, & \text{if } m = \ell q \ (\ell \in \mathbb{Z}, \ell \neq 0) \\ \sum_{l=1}^{q} (L_l+1)\mu_l \mu_{l'}, & \text{otherwise} \end{cases} \tag{2.17}$$

Since $\langle \mathbf{x} \rangle = 0$, we can say that $\sum_{l=1}^{q} \mu_l = 0$, and $\sum_{l=1}^{q}(L_l+1)\mu_l\mu_{l'} < \sum_{l=1}^{q}(L_l+1)\mu_l^2$. Therefore, the auto-correlation property of a CCA can be concluded as: when $m = 0$, the auto-correlation $R_{\mathbf{xx}}[m]$ of the iteration sequence of CCA-q has a maximum value, just as the auto-correlation of any sequence; while when $m \neq 0$, it has relatively larger value if m is multiple of q than if not. In other words, CCA-q owns a quasi-cyclic auto-correlation property, which is similar to a period-q sequence.

Example: The unbiased (divided by the length of calculated elements) auto-correlation of an iteration sequence of CCA-31 of system (2.1) with length $L = 10^4$ is simulated, and the center part ($m \in [-100, 100]$) is illustrated in Figure 2.10.

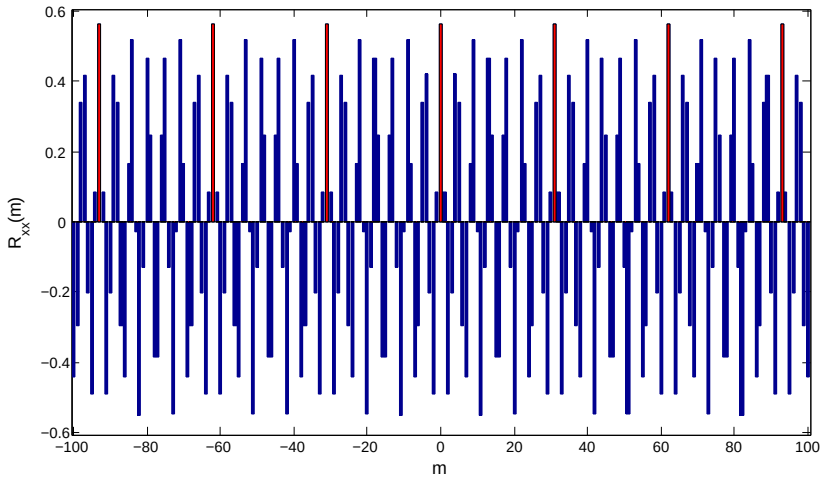

Figure 2.10: Unbiased auto-correlation of iteration sequence of CCA-31 of system (2.1) with length $L = 10^4$, and the center $m \in [-100, 100]$ is shown.

2.3.2 Spectral Property

Perform a p-point ($p \in \mathbb{N}$) DFT on the iteration sequence $\mathbf{x} = (x_1,\ x_2,\ ...,\ x_L)$ of CCA-q, so that

$$\begin{aligned} X[K] &= \sum_{n=1}^{L} x_n e^{-j\frac{K}{p}2\pi n} \\ &= \sum_{l=1}^{p} \vartheta(p,l) e^{-j2\pi\frac{K}{p}l} \end{aligned} \tag{2.18}$$

where $K \in \{1, 2, ..., p\}$, and $\vartheta(p, l) = \sum_{k=0}^{L_l} x_{l+kp}$ ($l \in \{1, 2, ..., p\}$, $L_l = \lfloor \frac{L-l}{p} \rfloor$) is used to represent the sum of the elements of the down-sampled sequence $\mathbf{x}_{p,l} = (x_l,\ x_{l+p},\ ...,\ x_{l+L_l p})$. Three cases corresponding to different values of p should be considered separately, as:

1. $p = \ell q$ ($\ell \in \mathbb{N}$)

   In case that p equals to the multiple of the period of CCA-q, the corresponding down-sampled sequence $\mathbf{x}_{p,l}$ ($l \in \{1, 2, ..., \ell q\}$) is a gathering of iterations belonging to the l' $^{\text{th}}$ zone of CCA-q, with

   $$l' = l - q\lfloor \frac{l}{q} \rfloor$$

   Hence, it can be obtained that $\langle \mathbf{x}_{p,l} \rangle = \langle \mathbf{x}_{q,l'} \rangle$, and $\vartheta(p, l) = (L_l + 1)\langle \mathbf{x}_{q,l'} \rangle$.

2. $p \perp q$ (p, q are coprime)

   In case that p is coprime to q, the corresponding down-sampled sequence $\mathbf{x}_{p,l}$ ($l \in \{1, 2, ..., p\}$) is a gathering of iterations from all the q zones of CCA-q. Hence, $\langle \mathbf{x}_{p,l} \rangle = \langle \mathbf{x} \rangle = 0$, and $\vartheta(p, l) = (L_l + 1)\langle \mathbf{x} \rangle = 0$.

3. p is other fraction of q

   In case that p is other fraction of q, which can be represented by $p = \frac{\ell_1}{\ell_2} q$ ($\ell_1, \ell_2 \in \mathbb{N}$, $1 < \ell_1 < p$, $1 < \ell_2 < q$, and $\ell_1 \perp \ell_2$), the corresponding down-sampled sequence $\mathbf{x}_{p,l}$ ($l \in \{1, 2, ..., p\}$) is a gathering of iterations from ℓ_2 zones of CCA-q. Hence, $\langle \mathbf{x}_{p,l} \rangle = \frac{1}{\ell_2} \sum_{m=1}^{\ell_2} \langle \mathbf{x}_{q,l'_m} \rangle$, with

   $$l'_m = l + (m-1)\frac{q}{\ell_2} - q\lfloor \frac{l + (m-1)\frac{q}{\ell_2}}{q} \rfloor$$

   In this case, $\vartheta(p, l) = (L_l + 1)\frac{1}{\ell_2} \sum_{m=1}^{\ell_2} \langle \mathbf{x}_{q,l'_m} \rangle$.

As a result, the p-point DFT of the iteration sequence of CCA-q corresponds to a low and pseudo-random distribution if $p \perp q$, where the pseudo-random distribution is caused by the chaoticity in each zone.

Especially, when q is a prime number, the above mentioned cases can be simplified as follows: the p-point DFT of the iteration sequence of CCA-q has much larger magnitudes when $p = \ell q$ compared to $p \neq \ell q$ ($\ell \in \mathbb{N}$). It could be explained in a more visual description that, the spectrum magnitude of the CCA-q waveform has a comb-like distribution, in which the majority of power is distributed on q equally spaced angular

frequencies $\omega = \frac{K}{q}2\pi$ ($K \in \{1, 2, ..., q\}$), while the remaining minority is distributed on the other frequencies $\omega \neq \frac{K}{q}2\pi$ ($\omega \in (0, 2\pi]$).

Remind that the power distribution among the main frequency points cannot be formulated generally, since it depends on each individual CCA, e.g., the location of each zone in the phase plane, the form and size of them, etc.

Example: Through a matlab simulation, the CCA-31 of system (2.1) as shown in Figure 2.9 has been generated, and p-point ($1 \leq p \leq 63$) DFT have been operated on $L = 10^4$ length of iterations sequence. The mean magnitude of p-point DFT is calculated, i.e., $\langle |X| \rangle = \frac{1}{p}\sum_{K=1}^{p} |X(K)|$, and is depicted versus different values of p in Figure 2.11 ($\langle |X| \rangle$ is normalized by the largest element). Similarly, $|X[K]|$ ($K \in \{1, 2, ..., p\}$) is also normalized and depicted in Figure 2.12 to show the distribution form of the passed spectrum by p-point DFT with different p ($p = 31, 29, 35$).

2.3.3 Statistical Property

Define the statistics of iteration sequence $\mathbf{x}$ as: $E(\mathbf{x}) = U$, $\mathrm{Var}(\mathbf{x}) = \Delta^2$, where $E(\cdot)$ is the expectation operator, and $\mathrm{Var}(\cdot)$ is the variance operator. Similarly, set the statistics of the sub-sequence of each zone $\mathbf{x}_{q,l}$ ($l \in \{1, 2, ..., q\}$) as: $E(\mathbf{x}_{q,l}) = \mu_l$, $\mathrm{Var}(\mathbf{x}_{q,l}) = \delta_l^2$. Obviously, we can get $U = \langle \mathbf{x} \rangle = 0$, $\mu_l = \langle \mathbf{x}_{q,l} \rangle$, as well as $U = \frac{1}{q}\sum_{l=1}^{q} \mu_l$. Meanwhile, since the variance of a sequence is a way to capture its scale or degree of being spread out, and δ_l^2 is the variance of the l^{th} zone of CCA-q, while Δ^2 is the variance of all the q zones together, hence, we can say that $\sum_{l=1}^{q} \delta_l^2 < \Delta^2$, and $\frac{1}{q}\sum_{l=1}^{q} \delta_l^2 \ll \Delta^2$ for large value of q.

Downsample $\mathbf{x}$ using factor p ($p \in \mathbb{N}$) to get $\mathbf{x}_{p,l} = [x_l \ x_{l+p} \ x_{l+2p} \ ...]$, where the offset $l \in \{1, 2, ...p\}$. According to the definition of CCA, $\mathbf{x}_{p,l}$ could be treated as a chaotic sequence, and its statistics can also be analyzed similarly under three cases corresponding to different value of p, as:

1. $p = \ell q$ ($\ell \in \mathbb{N}$)

   In this case, $\mathbf{x}_{p,l}$ ($l \in \{1, 2, ..., \ell q\}$) is a gathering of iterations belonging to the l' th zone of CCA-q, with $l' = l - q\lfloor \frac{l}{q} \rfloor$. Hence, $\langle \mathbf{x}_{p,l} \rangle = \langle \mathbf{x}_{q,l'} \rangle$, so that $E(\mathbf{x}_{p,l}) = \mu_{l'}$, and $\mathrm{Var}(\mathbf{x}_{p,l}) = \delta_{l'}^2$.

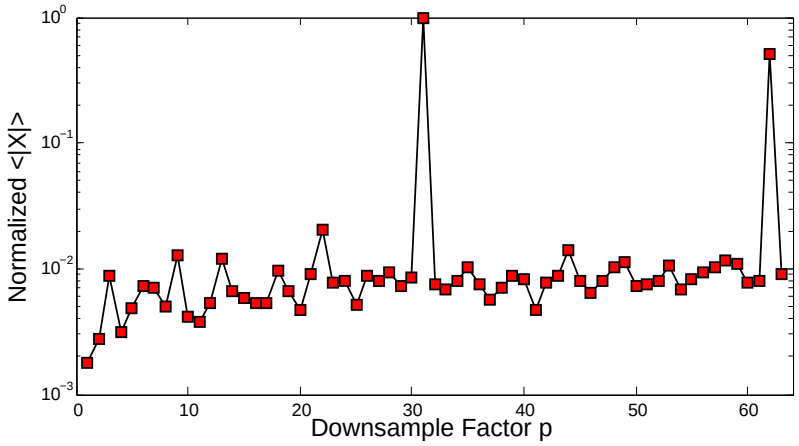

Figure 2.11: Normalized mean magnitude of p-point DFT on iteration sequence of CCA-31 of system (2.1) with length $L = 10^4$.

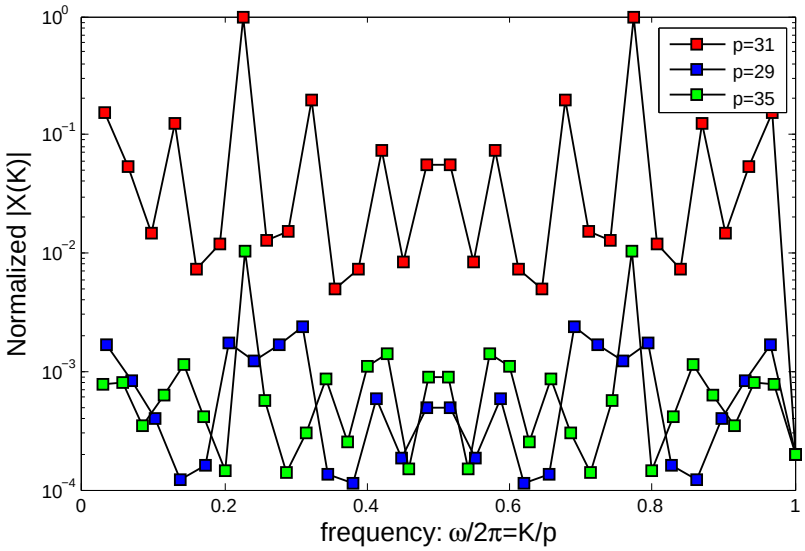

Figure 2.12: Normalized distribution form of $|X[K]|$ ($K \in \{1, 2, ..., p\}$ using p-DFT with $p = 31$ (red square), $p = 29$ (blue square) and $p = 35$ (green square) respectively.

2. $p \perp q$

   In this case, $\mathbf{x}_{p,l}$ ($l \in \{1, 2, ..., p\}$) is a gathering of iterations averagely from all the q zones of CCA-q. Therefore, $E(\mathbf{x}_{p,l}) = U$, and $\mathrm{Var}(\mathbf{x}_{p,l}) = \Delta^2$.

3. p is other fraction of q

   In this case, $p = \frac{\ell_1}{\ell_2} q$ ($\ell_1, \ell_2 \in \mathbb{N}$, $1 < \ell_1 < p$, $1 < \ell_2 < q$, and $\ell_1 \perp \ell_2$), so that $\mathbf{x}_{p,l}$ ($l \in \{1, 2, ..., p\}$) is a gathering of iterations from ℓ_2 zones of CCA-q. Hence, $E(\mathbf{x}_{p,l}) = \frac{1}{\ell_2} \sum_{m=1}^{\ell_2} \mu_{l'_m}$, and $\sum_{m=1}^{\ell_2} \delta^2_{l'_m} \leq \mathrm{Var}(\mathbf{x}_{p,l}) < \Delta^2$, where

$$l'_m = l + (m-1)\frac{q}{\ell_2} - q\lfloor \frac{l + (m-1)\frac{q}{\ell_2}}{q} \rfloor$$

   with $m \in \{1, ..., \ell_2\}$.

Denote $\langle \mathrm{Var}(\mathbf{x}_p) \rangle$ to be the *p-downsampled mean variance* (p-DMV) of $\mathbf{x}$, and we can get

$$\langle \mathrm{Var}(\mathbf{x}_p) \rangle = \frac{1}{p} \sum_{l=1}^{p} \mathrm{Var}(\mathbf{x}_{p,l}) = \begin{cases} \frac{1}{q} \sum_{l'=1}^{q} \delta^2_{l'}, & \text{if } p = \ell q \\ \Delta^2, & \text{if } p \perp q \\ \delta^2_{\frac{\ell_1}{\ell_2}}, & \text{if } p = \frac{\ell_1}{\ell_2} q \end{cases} \tag{2.19}$$

where $\ell, \ell_1, \ell_2 \in \mathbb{N}$, $1 < \ell_2 < q$, $\ell_1 \perp \ell_2$, and $\delta^2_{\frac{\ell_1}{\ell_2}}$ stands for the mean value of ℓ_2 variances in the above third case, which has $\frac{1}{q} \sum_{l'=1}^{q} \delta^2_{l'} < \delta^2_{\frac{\ell_1}{\ell_2}} < \Delta^2$.

Hence, the statistical property of the CCA-q signal can be concluded from Equation (2.19) as: the p-DMV of CCA-q has a maximum value when $p \perp q$, and has a minimum value when $p = \ell q$ ($\ell \in \mathbb{N}$).

Example: A matlab simulation of the CCA-31 of system (2.1) as shown in Figure 2.9 has been done, and $L = 10^5$ iterations have been generated. The statistical values have been calculated by this simulation, among which μ_l, δ^2_l ($l \in \{1, 2, ..., 31\}$) are shown in Figure 2.13, in which the mean values indicated by the red lines show that $\frac{1}{q} \sum_{l=1}^{31} \mu_l = 0$ and $\frac{1}{q} \sum_{l=1}^{31} \delta^2_l = 1.28 \times 10^{-3}$. p-DMV versus different downsample factors p is illustrated in Figure 2.14. Since $q = 31$ is a prime number, all the $25 \leq p \leq 63$ are either coprime or multiple to q, hence, all the p-DMV are equal to the maximum value except $p = 31, 62$ (the minimum ones).

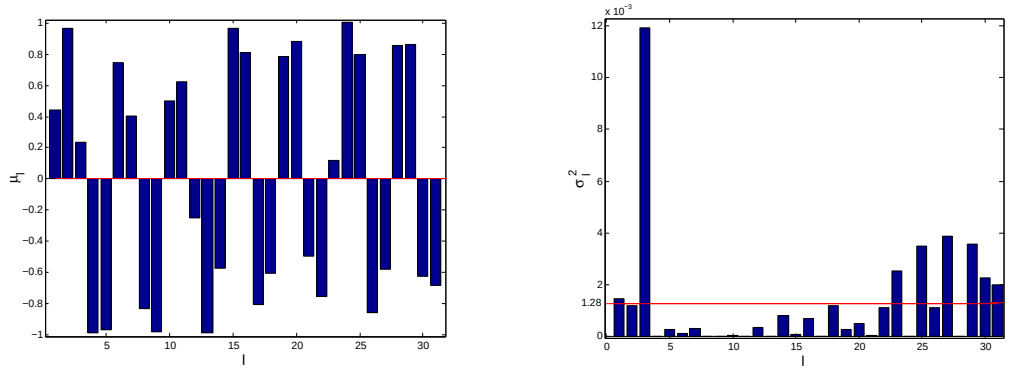

(a) (b)

Figure 2.13: Simulated statistical values of CCA-31 of system (2.1): (a) the expected value of each zone μ_l ($l \in \{1, 2, ..., 31\}$); (b) the variance value of each zone δ_l^2 ($l \in \{1, 2, ..., 31\}$). The mean values are indicated by the red lines.

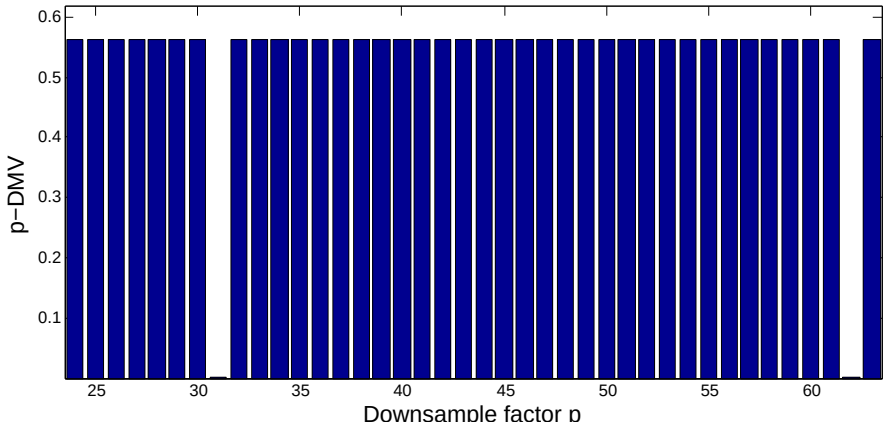

Figure 2.14: p-DMV of CCA-31 versus different downsample factor p. Minimum can be found when $p = 31, 62,$ etc., which corresponds to the mean variance value 1.28×10^{-3} in Figure 2.13.(b).

2.4 CCA Property Enhancement

As mentioned in Section 1.3, one of the important reasons why the spread spectrum systems are widely applied in wireless communications, is that they could resist the fading environment much better than the narrowband ones. The direct cause of the fading resistance is that in the frequency selective radio channel, it is less possible for all the spread spectrum to locate in the deep fading points, as shown in Figure 1.7.

As a chaotic signal, the waveform generated by a CCA generator can be considered as a wideband signal, and the bandwidth is determined by the iteration period T_s of the generator, i.e., $W = 1/T_s$. However, the spectral distribution in this band is not as flat as the other spread spectrum signals. The reasons can be considered as the followings:

1. Caused by the cyclicity of q zones of CCA-q, in an angular frequency period 2π, there exists q frequency peaks equally spaced at: $\omega = \frac{K}{q}2\pi$ $(K \in \{1, 2, ..., q\})$, which makes the spectral distribution on the other frequency points $\omega \neq \frac{K}{q}2\pi$ less important.

2. Among the q frequency peaks, the difference of the magnitudes could be so large that only several frequency points among them, if not only one, should be considered in the real applications, such that when a 3-dB bandwidth or 10-dB bandwidth is applied. It increases the possibility that all these considered important frequencies locate in the deep fading points.

Since the operation of q-point DFT of the iteration sequence of CCA shields the power distributed on all the less important frequency points, this shielded part of power should be as few as possible. Hence, we treat the first point in above as a favorable property in our later applications. In contrary, the second point is considered as an unfavorable point, which should be avoided if possible, e.g., manipulate the signals in order to make the power distribution on the q main equal spaced frequency points as flat as possible.

Generally speaking, the more white random a signal is, the more flat spectrum it owns. The cyclicity of a signal of CCA-q is due to the separation of the q zones, while its aperiodicity is caused by the chaotic iterations in each zone. Hence, in order to make the power distribution more flat on the main q equally spaced frequency points, while keep the comb-like spectrum, all the zones should be as close to each other as possible.

It should be noticed that the optimal manipulation for spectral enhancement differs with the particular CCA generator. Here, we talk about the manipulations which have been applied to system (2.1). Again, the CCA-31 in Figure 2.9 is taken to give a visual comparison of spectral properties, with and without these manipulations.

A. Folding function

Observing Figure 2.9.(a), we can see that most of the 31 zones of CCA-31 in the phase plane are more often away from the origin than close to it, which is obviously caused by the sinus operation in system (2.1). A simple folding function f_1 can be applied to the output x to the system to inverse this situation, hence to make the zones closer to the origin on keeping the zone size:

$$f_1(x) = \text{sgn}(x) - x \tag{2.20}$$

where $\text{sgn}(\cdot)$ is the sign operation.

The output iterations of $f_1(x)$ with the CCA-31 in Figure 2.9 as input is illustrated in Figure 2.15, both in phase plane and in time. Remind that the iteration of $f_1(x)$ is also made zero mean after generation. The p-point DFT analysis on the output sequence of $f_1(x)$ with $p = 31, 29, 35$ are also illustrated in Figure 2.16, from which we can see that the spectral distribution by 31-point DFT is more flat compared to the one in Figure 2.12.

B. Exponential function

Since $x \in [-1, 1]$, an exponential operation f_2 can also be used to approach the zones to the origin:

$$f_2(x) = x^3 \tag{2.21}$$

The output iteration of $f_2(x)$ with the CCA-31 in Figure 2.9 as input is illustrated in Figure 2.17, both in phase plane and in time, and it is also made zero mean after generation. The p-point DFT analysis on the output sequence of $f_2(x)$ with $p = 31, 29, 35$ are also illustrated in Figure 2.18, from which we can see that the spectral distribution of 31-point DFT is slightly more flat compared to the one in Figure 2.12.

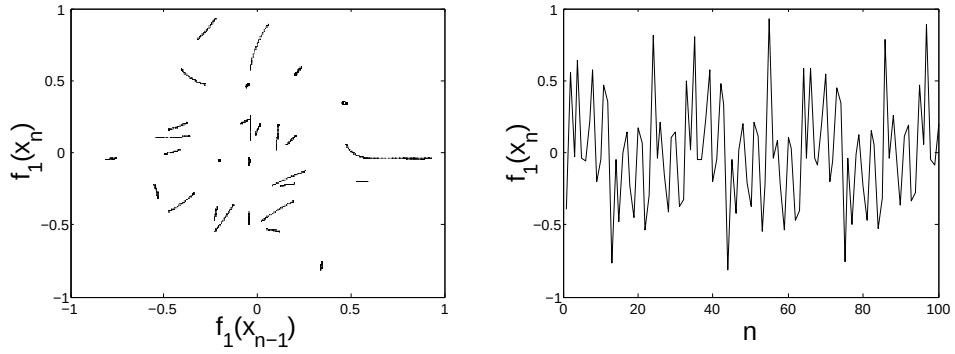

Figure 2.15: The iterations with length $L = 10^4$ of CCA-31 of system (2.1) on adding the folding function $f_1(x)$, shown in the phase plane (left) and the corresponding waveform in time (right).

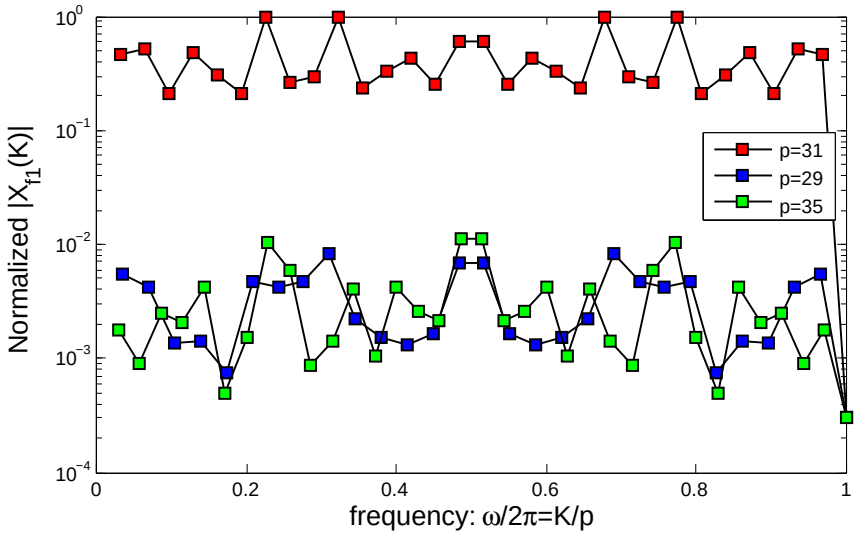

Figure 2.16: Normalized distribution form of $|X_{f_1}[K]|$ ($K \in \{1, 2, ..., p\}$) using p-DFT with $p = 31$ (red square), $p = 29$ (blue square) and $p = 35$ (green square).

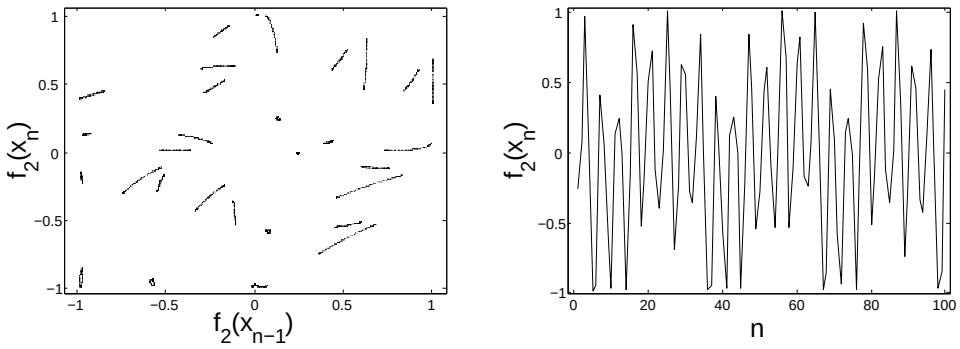

Figure 2.17: 10^4 iterations of enhanced CCA-31 of system (2.1) after applying the exponential function $f_2(x)$, shown in the phase plane (left) and the corresponding waveform in time (right).

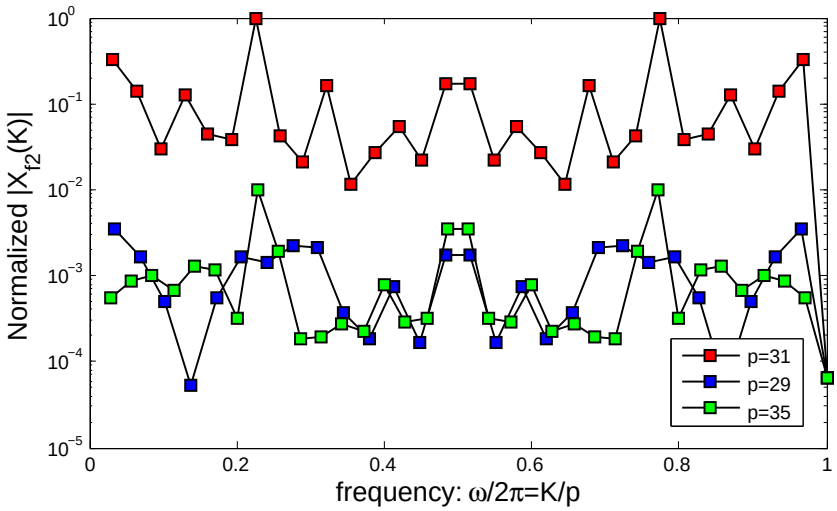

Figure 2.18: Normalized distribution form of $|X_{f_2}[K]|$ ($K \in \{1, 2, ..., p\}$) using p-DFT with $p = 31$ (red square), $p = 29$ (blue square) and $p = 35$ (green square).

C. Combination function

The above two function modules could individually make the spectral distribution of the 31-point DFT on the iterations of CCA-31 more flat, as in the figures illustrated above. However, the combination of them performs even better, by:

$$f_3(x) = f_2(f_1(x)) = (\text{sgn}(x) - x)^3 \tag{2.22}$$

The output iteration of $f_3(x)$ with the CCA-31 in Figure 2.9 as input is illustrated in Figure 2.19, both in phase plane and in time. Remind again that the output of $f_3(x)$ is made zero mean after generation. Similarly, the p-point DFT on the output iteration sequence of $f_3(x)$ with $p = 31, 29, 35$ are illustrated in Figure 2.20, from which we can see that the spectral distribution using 31-point DFT is even more flat compared to the one in Figure 2.16.

D. Selected function and the enhanced properties

Through the above analyses, it can be observed that the combination function allows to well improve the spectral distribution of the CCA generated by system (2.1). From Figure 2.20, the manipulated CCA-31 owns a very interesting spectral distribution: a high flat distribution on q equally spaced frequency points if p is chosen as multiple of q, while a low flat distribution for the other values of p. Furthermore, Figure 2.19 shows a much more irregular waveform in time compared to the one before the additional manipulations in Figure 2.9.

Since the combination function is considered to be the spectral enhancement of CCA, how does it influence the other two properties, i.e., the auto-correlation and statistical property? The similar simulations are done to observe these two properties of the manipulated CCA-31 in Figure 2.19, and the results are illustrated in Figure 2.21-2.22 respectively. The comparison can be done with the corresponding properties of the original CCA-31, as shown in Figure 2.10-2.14. It shows that a better auto-correlation property is obtained after the combination function, where the value of $R_{f_3(x)f_3(x)}[m]$ keeps large when m is multiple of q, but the value becomes very small with the other m. Meanwhile, the statistical property keeps more or less the same with or without the spectral enhancement manipulations.

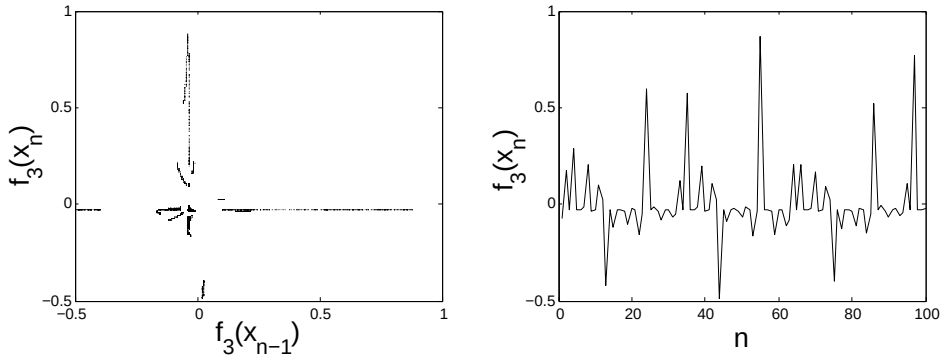

Figure 2.19: 10^4 iterations of enhanced CCA-31 of system (2.1) after applying the combination function $f_3(x)$, shown in the phase plane (left) and the corresponding waveform in time (right).

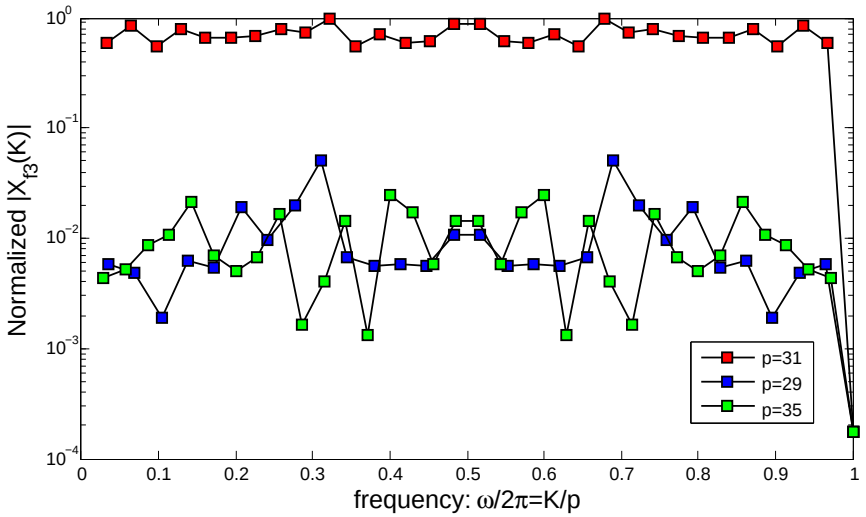

Figure 2.20: Normalized distribution form of $|X_{f_3}[K]|$ ($K \in \{1, 2, ..., p\}$) using p-point DFT with $p = 31$ (red square), $p = 29$ (blue square) and $p = 35$ (green square).

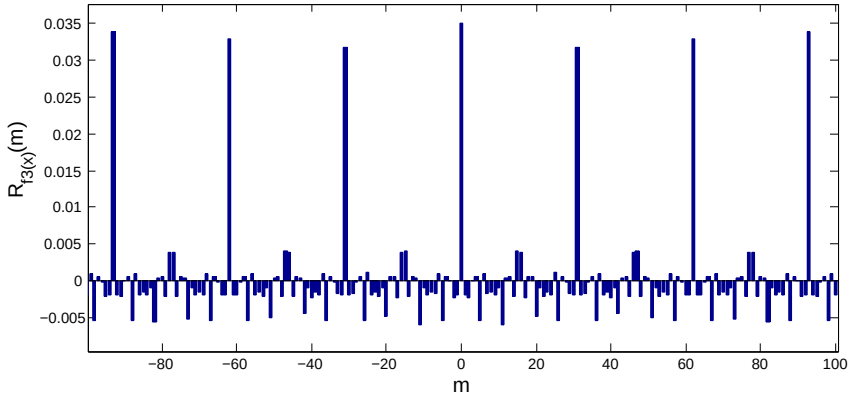

Figure 2.21: Normalized auto-correlation of 10^4 iterations of enhanced CCA-31 of system (2.1) after applying the combination function $f_3(x)$.

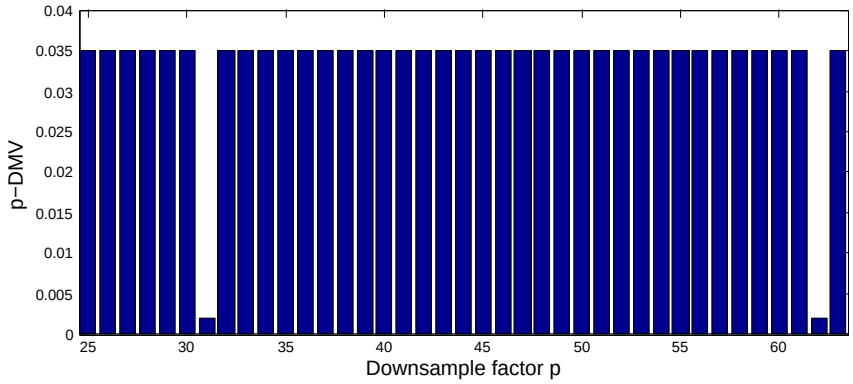

Figure 2.22: p-DMV of operated CCA-31 versus different downsample factor p. Minimum can be found when $p = 31, 62,$ etc..

2.5 Conclusion

In this chapter, the bifurcations of fixed points of the selected discrete-time dynamical system have been analyzed, and the bifurcations of periodic points have been simulated, with a period q less than 15. The structure of Arnold's tongues and the isoclines corresponding to the specified argument of the eigenvalues have been given, as well as their relationship. Various types of attractors of the selected system have been presented, together with the method of choosing the suitable parameters.

Among different type of attractors, the one processing simultaneously the chaoticity and cyclicity is called CCA in the context of this thesis. The period of a CCA is determined by the argument of the eigenvalues. In other words, different periods of CCAs can be easily obtained by changing the parameter values. The specific properties of the CCA-q signal have been discussed, including the auto-correlation property, the spectral property, and the statistical property. All the three properties depend upon the period q.

These analysis and discussion results give us the possibilities to detect the CCA signals non-coherently. Furthermore, to a certain extent, the comb-like spectrum of a CCA signal can be treated as a wideband signal. Therefore, the application of CCA in the chaos-based wideband modulations, or the CCA-based wideband modulations, will be proposed in the following chapter.

3

CCA-based Modulation Systems

3.1 Introduction

As introduced in Section 1.4.2, the chaotic signal direct modulation systems map the data symbols onto wideband chaotic waveforms directly, and processes the advantages of the conventional spread spectrum systems over the narrowband systems. In addition, the transceiver could be less complex than the conventional ones, thanks for the possibility of generating chaotic signals by some simple electronic circuits. As long as the demodulation is considered, a non-coherent detection is preferred, since the regeneration and synchronization of the basis function in the receiver could be very difficult or impossible, caused by the severe propagation condition of wireless channel, and the sensitive dependence of the chaotic signals on the initial conditions.

A type of attractor called CCA is presented in the previous chapter, with the period of zones determined by the parameter of the dynamical systems. Hence, a variety of CCA waveforms with different periods can be generated by the dynamical systems simply on choosing suitable parameter values. The chaoticity of a CCA assures the large spectrum of the iterated signal; while its cyclicity makes the signal owning several specific properties, as discussed in Section 2.3, which are all functions of the period. Therefore, the CCA-based wideband modulations can be simply realized by mapping the data symbols onto CCA waveforms, and detecting one of the specific properties in the receiver.

In this chapter, the context is organized as follow: Firstly, before the presentation of the schemes of CCA-based modulation systems, the equivalent CCA signals generated

by the iteration of the discrete-time dynamical systems will be discussed in Section 3.2, both in baseband and passband (RF band). Secondly, the modulation/demodulation schemes of a CCA-based chaos shift keying will be introduced in 3.3, as well as its performance evaluations in different channel models. Then, another CCA-based frequency shift keying will be proposed in 3.4, which can be considered to be an improvement of the first system. Similarly, the modulation/demodulation schemes will be explained and the performance evaluations in different channel models will be analyzed. Finally, the conclusion of this chapter will be given.

3.2 Equivalent CCA Signals in Baseband and Passband

In the chaos-based modulation systems, the chaotic signals serve as the basis functions. It's known that the chaotic iterations generated by the discrete-time dynamical systems have real continuous values in discrete time, such as $\mathbf{x} = (x_1, x_2, ...)$ of system (2.1). According to the **sampling theorem**, a signal in the baseband $[-W/2, W/2]$ can be generated from a discrete-time signal, with the band determined by the sampling rate of the discrete signal, i.e., $W = f_s = 1/T_s$, which can be presented by [21]:

$$x(t) = \sum_n x_n \text{sinc}(Wt - n) \tag{3.1}$$

where x_n is the iterated discrete-time chaotic sequence, $\text{sinc}(\cdot)$ denotes the sinc function as follows:

$$\text{sinc}(t) = \frac{\sin(\pi t)}{\pi t} \tag{3.2}$$

and its Fourier transform is a rectangular function, i.e.,

$$\int_{-\infty}^{+\infty} \text{sinc}(t) e^{-j2\pi ft} dt = \text{rect}(f) = \begin{cases} 0, & \text{if } |f| > \frac{1}{2} \\ \frac{1}{2}, & \text{if } |f| = \frac{1}{2} \\ 1, & \text{if } |f| < \frac{1}{2} \end{cases} \tag{3.3}$$

Obviously, $x(n/W) = x_n$ is the signal value in the sampling instant $t = n/W$. Since the aperiodic signals have no Fourier transform, they are represented in the frequency domain by their PSD, which means, by the Fourier transform of their auto-correlation functions. According to the theorem of **Fourier analysis**, the PSD of $\mathbf{x}$, denoted as $P_{x_d}(f)$, is the periodic extension of the PSD of $x(t)$, denoted as $P_x(f)$, with

$$P_{x_d}(f) = \sum_{k=-\infty}^{+\infty} P_x(f - kW) \tag{3.4}$$

Since a propagation channel for a typical radio communication is actually effected in the passband $[f_c - W/2, f_c + W/2]$ ($W < 2f_c$), with the values of f_c and W under certain spectrum allocation. A passband equivalent signal $x_p(t)$ can be converted from the baseband chaotic waveform $x(t)$ by [21]

$$x_p(t) = \Re[x(t)e^{j2\pi f_c t}] = x(t)\cos(2\pi f_c t) \tag{3.5}$$

The above mentioned baseband and passband equivalent signals have the same form of spectral distribution envelope, with

$$P_{x_p}(f) = \begin{cases} P_x(f - f_c)/2, & |f - f_c| < W/2 \\ 0, & \text{elsewhere} \end{cases} \tag{3.6}$$

where $P_{x_p}(f)$ stands for the PSD of $x_p(t)$.

In the rest part of this thesis, without of notification, **enhanced CCA of system** (2.1) will be used to short for CCA generated by system (2.1) applying the property enhancement function as introduced in Section 2.4. As an example, the baseband signal $x(t)$ of the enhanced CCA-31 of system (2.1) is illustrated in Figure 3.1.(a), in which the time axis is normalized by T_s. Its spectrum is correspondingly illustrated in Figure 3.1.(b), with the frequency axis normalized by $W/2$. Similarly, the baseband equivalent signal $x(t)$ of the enhanced CCA-29 of system (2.1) in time domain as well as in frequency domain are also illustrated in Figure 3.2. Remind that the above signals $x(t)$ are made zero mean and mean energy normalized, i.e., $E(x(t)) = 0$, and $E(x^2(t)) = 1$, with the former to drop the DC part which doesn't transport information (see Section 2.3), and the latter to keep the transmission energy statistically constant.

It is known that for the communication systems, the modulation and demodulation are usually operated in the baseband. In other words, the data symbols are firstly modulated in the baseband $[-W/2, W/2]$ by the basis function $x(t)$, and then transformed by the passband carrier to the RF band $[f_c - W/2, f_c + W/2]$ as in equation (3.5), before transmitted in the radio. In the receiver, the passband carrier of the received signal $y_p(t)$ is removed before the demodulation, by

$$\tilde{y}(t) = \text{LPF}\{2y_p(t)e^{-j2\pi f_c t}\} \tag{3.7}$$

here $\text{LPF}\{\cdot\}$ stands for the lowpass filter. As all the signals in the passband, $y_p(t)$ can be presented by its baseband complex envelope $y(t)$ in the form of equation (3.5) as

$$\begin{aligned} y_p(t) &= \Re[y(t)e^{j2\pi f_c t}] \\ &= y_I(t)\cos(2\pi f_c t) - y_Q(t)\sin(2\pi f_c t) \end{aligned} \tag{3.8}$$

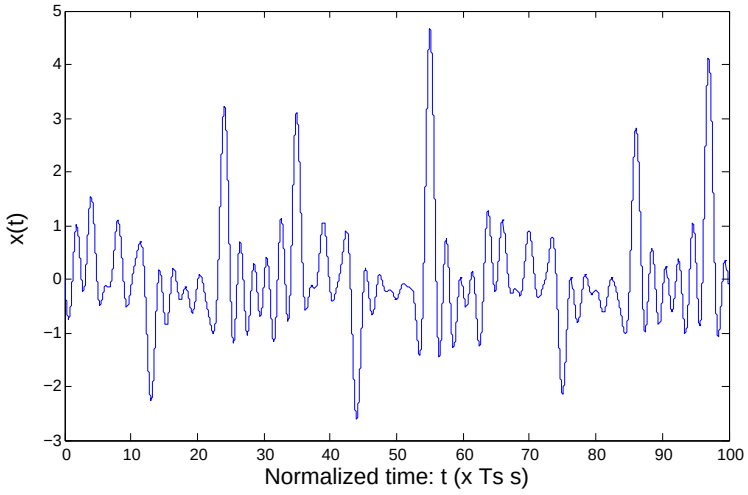

(a)

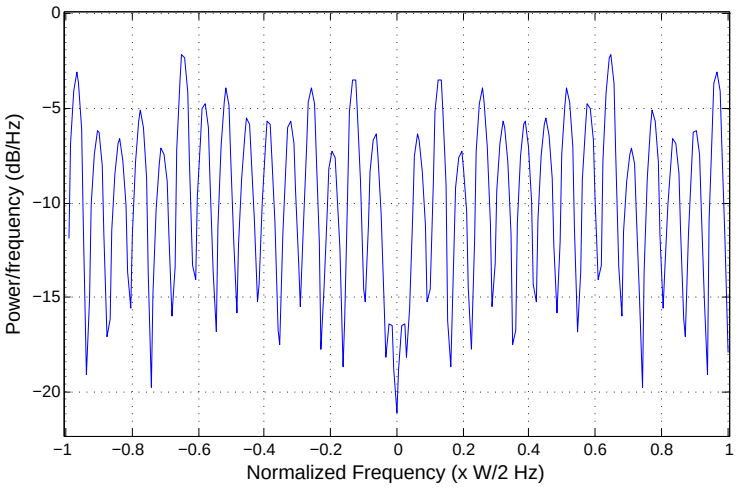

(b)

Figure 3.1: (a) Waveform and (b) spectrum of the baseband signal $x(t)$ of the enhanced CCA-31 of system (2.1).

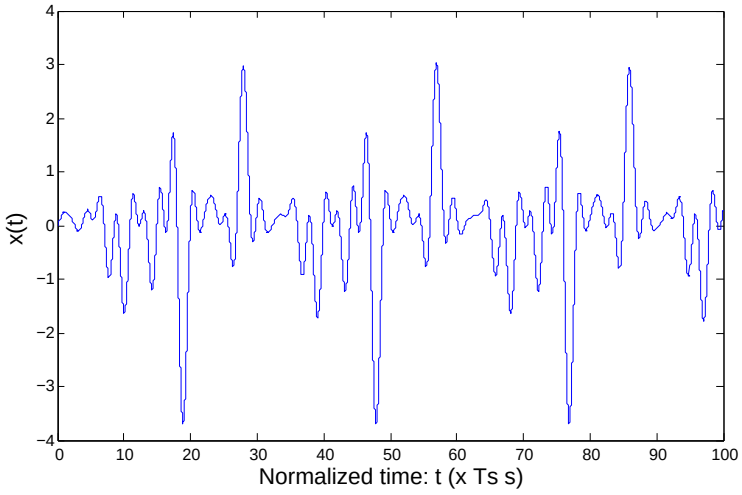

(a)

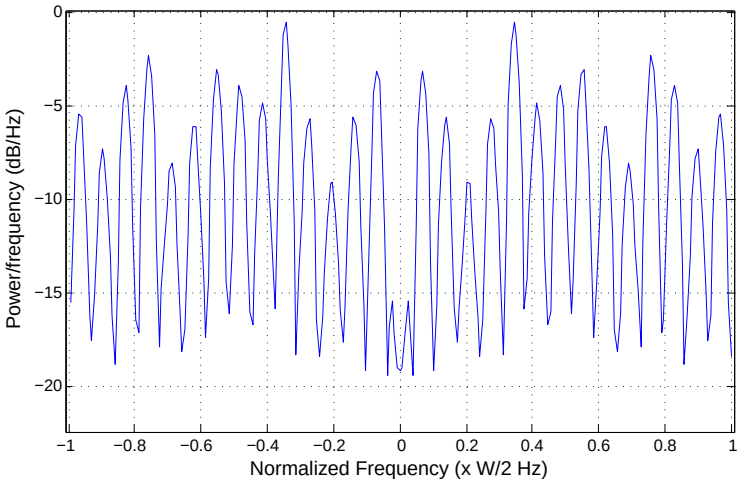

(b)

Figure 3.2: (a) Waveform and (b) spectrum of the baseband signal $x(t)$ of the enhanced CCA-29 of system (2.1).

where $y_I(t)$ and $y_Q(t)$ are the in-phase and quadrature components of the complex envelope. Inserting equation (3.8) into (3.7) to get

$$\begin{aligned}\tilde{y}(t) &= y_I(t) + jy_Q(t) \\ &= y(t)\end{aligned} \tag{3.9}$$

we can see that the passband carrier removing operation in equation (3.7) corresponds to the complex envelope recovering.

The object of this thesis is concentrated on the modulation/demodulation of the chaos-based systems, hence, in the later context, the discussion and analysis will be operated in the baseband equivalent channel models without notification.

3.3 CCASK: A Chaos Shift Keying Utilizing CCA

Chaotic cyclic attractors shift keying (CCASK) is a modulation system concerned with mapping data symbols to chaotic waveforms generated by CCA-q generators, of which the periods q are differed by the values of data. The demodulation is done by estimating one of the specific properties of these CCAs, which have been introduced in Section 2.3.

In this section, the modulation and demodulation schemes of CCASK using different detections are presented, as well as the noise performance in AWGN and multipath channel models.

3.3.1 Modulation Scheme of CCASK

An *M-ary* system is a system which transmits $\log_2 M$ bits of data in each symbol. As a simplest case, a binary system transmits only one bit of data per symbol.

Let's firstly talk about the general case. The *M-ary* CCASK uses chaotic signals generated by M different CCA generators as basis functions. The CCA generators differ by their periods q_v ($v \in \{0, 1, ..., M-1\}$). According to equation (3.1), the M basis functions can be presented as

$$x^{(v)}(t) = \sum_n x_n^{(v)} \text{sinc}(Wt - n) \tag{3.10}$$

where $x_n^{(v)}$ is the sample of the iterated sequence $\mathbf{x}^{(v)}$ generated by CCA-q_v. For the sake of frequency interference reduction, the values of q_v are chosen to be coprime to each other, i.e., $q_v \perp q_{v'}$, for $v' \neq v$ and $v, v' \in \{0, 1, ..., M-1\}$.

Define T_b as the bit time duration, and T as the symbol time duration, so that $T = T_b \log_2 M$. Suppose that each symbol is modulated by L samples of iteration of CCA, then the symbol time duration can be given by $T = LT_s$, with T_s being defined to be the sampling period. In this thesis, L is also defined as the **symbol modulation rate** since one symbol is modulated by L samples.

Under the above definitions, the modulated symbols of CCASK can be denoted by

$$s(t) = \sum_{m} \sum_{v=0}^{M-1} \sum_{n=1}^{L} \delta_{d_m,v} x_{mL+n}^{(v)} \text{sinc}(Wt - (mL + n)) \tag{3.11}$$

where $d_m \in \{0, 1, ..., M-1\}$ is the m^{th} data symbol, and $\delta_{i,j}$ stands for the **Kronecker's delta**:

$$\delta_{i,j} = \begin{cases} 1, & \text{if } i = j \\ 0, & \text{if } i \neq j \end{cases} \tag{3.12}$$

The Kronecker's delta in equation (3.11) can be simply realized by a key shifting among M different CCA generators, so comes the name of the system CCASK. The diagram of the baseband modulation in the *M-ary* CCASK transmitter can be illustrated as in Figure 3.3

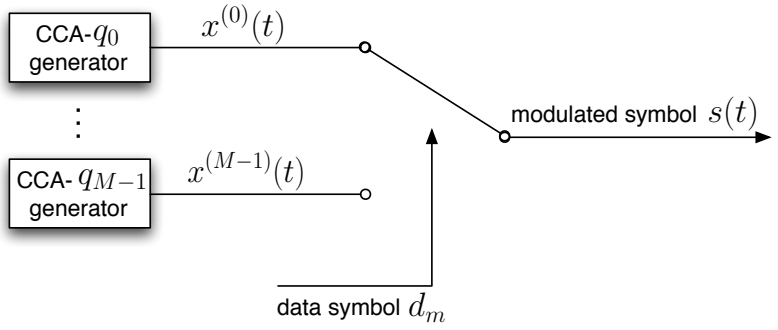

Figure 3.3: Modulation structure in *M-ary* CCASK transmitter.

The equivalent sampled sequence of the m^{th} modulated symbol $s(t)$ ($t \in [mT, (m+1)T]$) can be denoted by $\mathbf{s}_m = (s_m[1], s_m[2], ..., s_m[L])$, with

$$s_m[n] = s(mT + nT_s), \quad n \in \{1, 2, ..., L\} \tag{3.13}$$

Comparing equation (3.11) with equation (3.13), we can get that $s_m[n] = x^{(i)}_{mL+n}$ when $d_m = i$ ($i \in \{0, 1, ..., M-1\}$) was transmitted.

Especially, in case of the simplest binary CCASK ($M = 2$), only two different CCA generators are needed, i.e., a CCA-q_0 generator when a data symbol '0' is transmitted, and another CCA-q_1 generator when a data symbol '1' is transmitted. Hence the expression of the modulated symbols can be simplified as

$$s(t) = \sum_m \sum_{n=1}^{L} \Big(d_m x^{(1)}_{mL+n} + (1 - d_m) x^{(0)}_{mL+n} \Big) \mathrm{sinc}(Wt - (mL + n)) \tag{3.14}$$

where $d_m \in \{0, 1\}$. For binary CCASK, the sampled sequence of the m^{th} modulated symbol is $\mathbf{s}_m = (x^{(1)}_{mL+1},\ x^{(1)}_{mL+2},\ ...,\ x^{(1)}_{mL+L})$ when an '1' is transmitted, and $\mathbf{s}_m = (x^{(0)}_{mL+1},\ x^{(0)}_{mL+2},\ ...,\ x^{(0)}_{mL+L})$ when a '0' is transmitted.

The baseband modulated signal $s(t)$ will be transferred to the RF band $[f_c - W/2, f_c + W/2]$ to form the passband signal $s_p(t)$ before the transmission, using the operation in equation (3.5).

3.3.2 Demodulation Scheme of CCASK

As introduced in Section 2.3, the robust properties of CCA-q, such as the auto-correlation property, the spectral property and the statistical property, can be determined as functions of the period q. One of these properties can be observed to get the evaluating factor for the received symbols, hence, a noncoherent detection can be realized as the scheme of demodulation.

Denote the received passband signal by $r_p(t)$, and its equivalent complex envelope by $r(t)$. According to Section 3.2, a passband carrier removing operation in equation (3.7) will be processed on $r_p(t)$ before the baseband demodulation. Let's simply use $r(t)$ to stand for this baseband received signal without bringing the confusion, which is also the input of the demodulation block.

Due to the imperfect transmission channel, the received signal $r_p(t)$ could be the noised, filtered and/or multipath distorted result of the transmitted signal $s_p(t)$, so that the mismatch of amplitude and phase can be happened between them. Although the baseband equivalent transmitted signal $s(t)$ is real valued, the baseband received

signal $r(t)$ could have complex values, owing to the phase distortion in the propagation channel. Hence, both the in-phase and quadrature components of $r(t)$ should be demodulated simultaneously.

Let's consider the passband carrier removed signal of the m^{th} received symbol: $r(t)$ ($t \in [mT, (m+1)T]$). Since all the specific properties in Section 2.3 are analyzed in the discrete-time domain, we sample the baseband signal $r(t)$ at a sampling rate T_s to get a sampled sequence $\mathbf{r}_m = (r_m[1],\ r_m[2],\ ...,\ r_m[L])$, with

$$r_m[n] = r(mT + nT_s), \quad n \in \{1, 2, ..., L\} \tag{3.15}$$

In case of single user so that the interference from the other users does not exist, if the transmission channel is noise and distortion free, as well as the ideal transmitting and receiving antennas are applied, we can get $r_m[n] = s_m[n]$; or else, $r_m[n]$ differs from $s_m[n]$, and can be presented by its in-phase and quadrature components as $r_m[n] = r_{m,I}[n] + jr_{m,Q}[n]$.

In the following sub-sections, the detection methods using auto-correlation, spectral and statistical properties will be introduced respectively. In sake of simplicity, the detections will be discussed after the sampling operation, i.e., the detections of the sampled sequence $\mathbf{r}_m$ will be considered.

3.3.2.1 Auto-Correlation Detection

Firstly, remind that the basic schemes of CCASK using auto-correlation detection have been published, see reference [67].

The auto-correlation detection of the *M-ary* CCASK relies on the quasi-periodic auto-correlation property of each received symbol. Through applying the auto-correlation operation on both the in-phase and quadrature components of the sampled symbol sequence $\mathbf{r}_m$, we can get:

$$R_{r_m r_m,I}[\eta] = \sum_{n=1+\eta}^{L} r_{m,I}[n] r_{m,I}[n-\eta] \tag{3.16}$$

$$R_{r_m r_m,Q}[\eta] = \sum_{n=1+\eta}^{L} r_{m,Q}[n] r_{m,Q}[n-\eta] \tag{3.17}$$

where $\eta \in \{0, 1, ..., L-1\}$. Since $\mathbf{r}_m$ is a length limited sequence, i.e., $r_m[n] = 0$ for $n \notin \{1, 2, ..., L\}$, only $L - \eta$ points of multiplications are concerned for each η. Adding

the auto-correlation results of the in-phase and quadrature components to get

$$R_{r_m r_m}[\eta] = R_{r_m r_m,I}[\eta] + R_{r_m r_m,Q}[\eta] \tag{3.18}$$

According to the auto-correlation property of CCA in Section 2.3.1, in the ideal case that $\mathbf{r}_m = \mathbf{s}_m$, if an '$i$' ($i \in \{0, 1, ..., M-1\}$) was transmitted, $R_{r_m r_m}[\ell q_v]$ ($v \in \{0, 1, ..., M-1\}, \ell \in \mathbb{N}$) have relatively big values when $v = i$, and much smaller values when $v \neq i$. Hence, for each q_v, adding $R_{xx_k}[\ell q_v]$ with all the possible $\ell \in \mathbb{N}$ and normalizing the sum by the total concerned points of multiplications to form

$$C_m[v] = \frac{\sum_{\ell=1}^{L_v} R_{r_m r_m}[\ell q_v]}{\sum_{\ell=1}^{L_v}(L - \ell q_v)} \tag{3.19}$$

where $L_v = \lfloor \frac{L}{q_v} \rfloor$.

In a tolerably noisy and/or distortional channel, C_m can serve as the decision variable for the m^{th} received symbol, with the demodulated symbols $\hat{d}_m$ (in base-M) given by

$$\hat{d}_m = \underset{v}{\operatorname{argmax}}\, C_m[v] \tag{3.20}$$

where argmax stands for the operation of finding argument of the maximum.

Especially, in case of the simplest binary CCASK using auto-correlation detection, the decision variable for the m^{th} received symbol can be simplified by the difference between $C_m[1]$ and $C_m[0]$, as:

$$\begin{aligned} C_{b_m} &= C_m[1] - C_m[0] \\ &= \frac{\sum_{\ell=1}^{L_1} R_{r_m r_m}[\ell q_1]}{\sum_{\ell=1}^{L_1}(L - \ell q_1)} - \frac{\sum_{\ell=1}^{L_0} R_{r_m r_m}[\ell q_0]}{\sum_{K=1}^{L_0}(L - \ell q_0)} \end{aligned} \tag{3.21}$$

while the consequently demodulated symbol $\hat{d}_m$ can be represented by:

$$\hat{d}_m = \begin{cases} 1, & \text{if } C_{b_m} \geq 0 \\ 0, & \text{if } C_{b_m} < 0 \end{cases} \tag{3.22}$$

The structure of baseband demodulation in binary CCASK receiver using auto-correlation detection can be designed as shown in Figure 3.4.

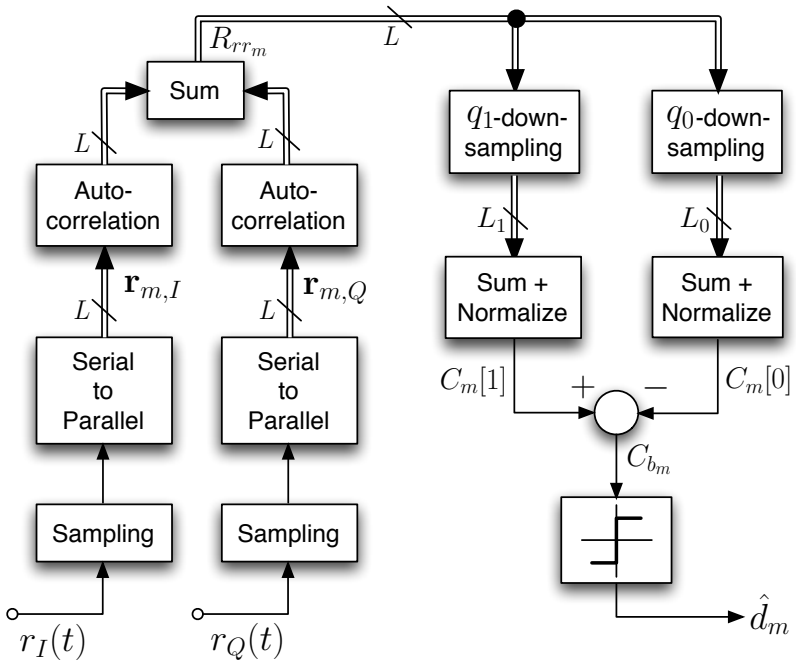

Figure 3.4: Demodulation structure in binary CCASK receiver using auto-correlation detection.

3.3.2.2 Spectral Detection

The basic schemes of CCASK using spectral detection and the AWGN performance evaluation have been published, see reference [68].

The spectral detection of the *M-ary* CCASK relies on the comb-like distribution of the main frequency peaks of each received symbol. Since the Fourier transform can be performed on a complex signal, without separating the in-phase and quadrature component, we can directly apply q_v-point DFT ($v \in \{0, 1, ..., M-1\}$) on the sampled symbol sequence $\mathbf{r}_m$ to get the magnitudes of the observing frequencies as:

$$A_m^v[K] = \Big| \sum_{n=1}^{L} r_m[n] e^{-j2\pi \frac{K}{q_v} n} \Big| \tag{3.23}$$

where $v \in \{0, 1, ..., M-1\}$, and $K \in \{1, 2, ..., q_v\}$.

According to the spectral property of CCA in Section 2.3.2, in the ideal case that $\mathbf{r}_m = \mathbf{s}_m$, if a '$d_m = i$' ($i \in \{0, 1, ..., M-1\}$) was transmitted, $A_m^v[K]$ ($K \in \{1, 2, ..., q_v\}$) have relatively large values when $v = i$, and much smaller values when $v \neq i$. Hence,

for each $v \in \{0, 1, ..., M-1\}$, the mean squared value of $A_m^v[K]$ can be obtained, as

$$D_m[v] = \frac{1}{q_v} \sum_{K=1}^{q_v} \left(A_m^v[K] \right)^2 \tag{3.24}$$

In a tolerably noisy and/or distortional channel, D_m can be observed as the decision variable for the m^{th} received symbol. Hence, the demodulated symbol $\hat{d}_m$ (in base-M) can be given by

$$\hat{d}_m = \underset{v}{\operatorname{argmax}}\, D_m(v) \tag{3.25}$$

Especially, when binary CCASK using spectral detection is concerned, the decision variable for the m^{th} received symbol can be simplified by the difference between $D_m[1]$ and $D_m[0]$, as:

$$\begin{aligned} D_{b_m} &= D_m[1] - D_m[0] \\ &= \frac{1}{q_1} \sum_{K=1}^{q_1} \left(A_m^1[K] \right)^2 - \frac{1}{q_0} \sum_{K=1}^{q_0} \left(A_m^0[K] \right)^2 \end{aligned} \tag{3.26}$$

and the consequently demodulated symbol $\hat{d}_m$ can be represented by:

$$\hat{d}_m = \begin{cases} 1, & \text{if } D_{b_m} \geq 0 \\ 0, & \text{if } D_{b_m} < 0 \end{cases} \tag{3.27}$$

The structure of baseband demodulation of binary CCASK receiver using spectral detection can be designed as shown in Figure 3.5.

3.3.2.3 Statistical Detection

The basic schemes of CCASK using statistical detection and the AWGN performance evaluation will be published soon, see reference [69].

The statistical detection of the *M-ary* CCASK relies on the specific statistics of each received symbol, i.e., the p-DMV as proposed in equation (2.19). Downsampling both the in-phase and quadrature components of the sampled received symbol $\mathbf{r}_m$ with factor q_v ($v \in \{0, 1, ..., M-1\}$) and offset $l-1$ ($l \in \{1, 2, ..., q_v\}$) to get the sub-sequences $\mathbf{r}_{m_{q_v,l},I} = (r_{m,I}[l],\ r_{m,I}[l+q_v],\ ...,\ r_{m,I}[l+L_v^l q_v])$ and $\mathbf{r}_{m_{q_v,l},Q} = (r_{m,Q}[l],\ r_{m,Q}[l+q_v],\ ...,\ r_{m,Q}[l+L_v^l q_v])$, where $L_v^l = \left\lfloor \frac{L-l}{q_v} \right\rfloor$. Define the variance value of the sub-sequences $\mathbf{r}_{m_{q_v,l}}$ and $\mathbf{r}_{m_{q_v,Q}}$ as $\mathrm{Var}(\mathbf{r}_{m_{q_v,l},I})$ and $\mathrm{Var}(\mathbf{r}_{m_{q_v,l},Q})$, hence the q_v-DMV of

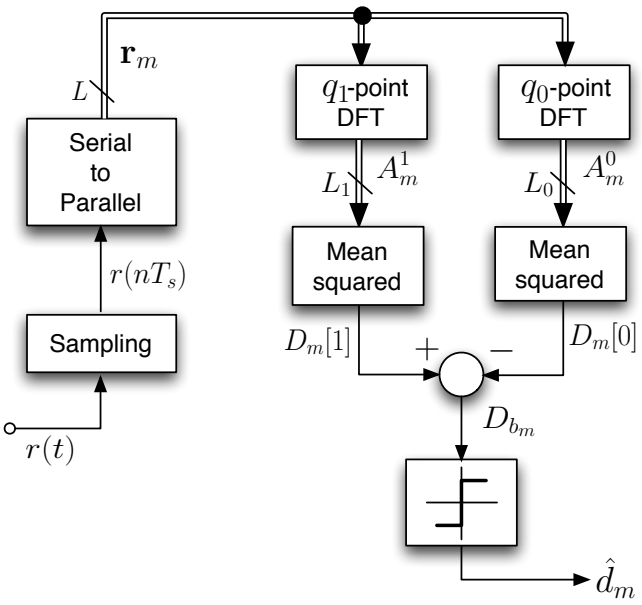

Figure 3.5: Demodulation structure in binary CCASK receiver using spectral detection.

$\mathbf{r}_{m,I}$ and $\mathbf{r}_{m,Q}$ can be presented as:

$$V_{m,I}[v] = \left\langle \mathrm{Var}(\mathbf{r}_{m_{q_v},I}) \right\rangle = \frac{1}{q_v} \sum_{l=1}^{q_v} \mathrm{Var}(\mathbf{r}_{m_{q_v,l},I}) \tag{3.28}$$

$$V_{m,Q}[v] = \left\langle \mathrm{Var}(\mathbf{r}_{m_{q_v},Q}) \right\rangle = \frac{1}{q_v} \sum_{l=1}^{q_v} \mathrm{Var}(\mathbf{r}_{m_{q_v,l},Q}) \tag{3.29}$$

Adding the q_v-DMV of $\mathbf{r}_{m,I}$ and $\mathbf{r}_{m,Q}$ to get:

$$V_m[v] = V_{m,I}[v] + V_{m,Q}[v] \tag{3.30}$$

According to the statistical property in Section 2.3.3, in the ideal case that $\mathbf{r}_m = \mathbf{s}_m$, if a '$d_m = i$' ($i \in \{0, 1, ..., M-1\}$) was transmitted, q_v-DMV ($v \in \{0, 1, ..., M-1\}$) of $\mathbf{r}_m$ has relatively small value when $v = i$, and much bigger value when $v \neq i$.

Hence, in a tolerably noisy and/or distortional channel, V_m can be used as the decision variable for the m^{th} received symbol, and the demodulated symbol $\hat{d}_m$ (in base-M) can be given by:

$$\hat{d}_m = \underset{v}{\mathrm{argmin}}\, V_m(v) \tag{3.31}$$

where argmin stands for the operation of finding argument of the minimum.

Especially, in the simplest case of binary CCASK using statistical detection, the decision variable for the m^{th} received symbol can be simplified as the difference between $V_m[0]$ and $V_m[1]$, as

$$\begin{aligned} V_{b_m} &= V_m[0] - V_m[1] \\ &= \frac{1}{q_0}\sum_{l=1}^{q_0}\Big(\mathrm{Var}(\mathbf{r}_{m_{q_0,l},I}) + \mathrm{Var}(\mathbf{r}_{m_{q_0,l},Q})\Big) \\ &\quad -\frac{1}{q_1}\sum_{l=1}^{q_1}\Big(\mathrm{Var}(\mathbf{r}_{m_{q_1,l},I}) + \mathrm{Var}(\mathbf{r}_{m_{q_1,l},Q})\Big) \end{aligned} \tag{3.32}$$

Consequently, the demodulated symbol $\hat{d}_m$ of binary CCASK using statistical detection can be represented by:

$$\hat{d}_m = \begin{cases} 1, & \text{if } V_{b_m} \geq 0 \\ 0, & \text{if } V_{b_m} < 0 \end{cases} \tag{3.33}$$

The structure of baseband demodulation in binary CCASK receiver using statistical detection can be designed as shown in Figure 3.6, in which the block modulo of q-DMV stands for the operation of downsampled variance with factor q, as defined in Section 2.3.3.

3.3.3 AWGN Performance of CCASK

Noise performance of a system can be usually presented by the BER. Since that BER is related to propagation conditions, different transmission channel models could be considered. In this section, the AWGN performance of single user binary CCASK in the simplest AWGN channel will be given by theoretical analysis as well as computer simulations.

Conventionally, the BER of AWGN is a function of E_b/N_0 as mentioned in Section 1.3.1, in which E_b is the energy of one bit transmitted information, while $N_0/2$ is the double-sided PSD of the added Gaussian noise. In other words, E_b/N_0 is the parameter of the passband transmission channel over $[f_c - W/2, f_c + W/2]$. However, the modulation/demodulation schemes of CCASK are discussed in the equivalent baseband, hence, it's necessary to derive the bit energy and the PSD of the Gaussian noise in the baseband equivalent model from E_b and N_0 respectively.

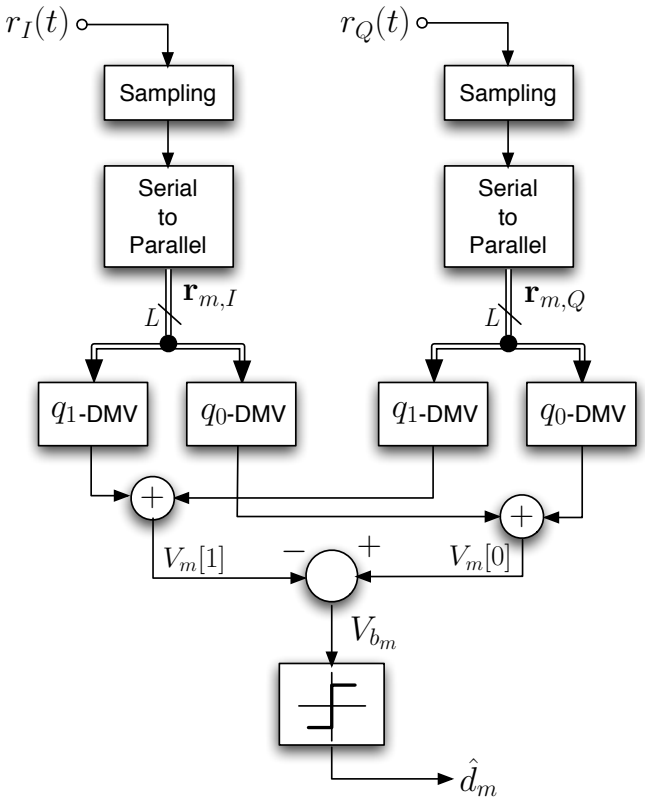

Figure 3.6: Demodulation structure in binary CCASK receiver using statistical detection.

3.3.3.1 Baseband Equivalent AWGN Channel Model

AWGN channel is a simplest channel model in which only a linear addition of white noise is considered as the impairment, which can be represented by

$$r_p(t) = s_p(t) + b_p(t) \tag{3.34}$$

where $b_p(t)$ is the Gaussian noise in the RF band with a double-sided PSD $N_0/2$, i.e.,

$$N_p(f) = \begin{cases} N_0/2, & |f \pm f_c| < W/2 \\ 0, & \text{elsewhere} \end{cases} \tag{3.35}$$

and its variance can be obtained as $\sigma_p^2 = N_0 W$.

Define $b(t) = b_I(t) + jb_Q(t)$ to be the complex envelope of $b_p(t)$ in the equivalent baseband, with $b_I(t)$ and $b_Q(t)$ being the in-phase and quadrature components of $b(t)$, we have:

$$\begin{aligned} b_p(t) &= \Re(b(t)e^{j2\pi f_c t}) \\ &= b_I(t)\cos(2\pi f_c t) - b_Q(t)\sin(2\pi f_c t) \end{aligned} \tag{3.36}$$

Hence, the baseband equivalent AWGN channel model can be denoted by

$$r(t) = s(t) + b(t) \tag{3.37}$$

According to reference [21], a complex Gaussian noise has the *independent and identically-distributed* (i.i.d.) components. Let's define the PSD of baseband equivalent noise $b(t)$ to be $N(f)$, which has non-zero value only when $|f| < W/2$, so that the PSD of both quadrature components equal to $N(f)/2$. By performing the Fourier transform on equation (3.36), we can get:

$$N_p(f) = \frac{N(f + f_c) + N(f - f_c)}{4} \tag{3.38}$$

or

$$N(f) = \begin{cases} 2N_0, & |f| < W/2 \\ 0, & \text{elsewhere} \end{cases} \tag{3.39}$$

and the variance of $b(t)$ can be obtained as $\sigma_c^2 = 2N_0 W$.

On the other side, $b(t)$ can also be presented by the sampled sequence b_n as

$$b(t) = \sum_n b_n \text{sinc}(Wt - n) \tag{3.40}$$

where $b_n = b(nT_s)$ is the sampled sequence of $b(t)$ in the sampling instant $t = nT_s$ using the sampling rate $1/T_s$, which can also be presented by its quadrature components as $b_n = b_{n,I} + jb_{n,Q}$. Therefore, the discrete-time baseband equivalent AWGN channel model can be obtained as

$$r_n = s_n + b_n \tag{3.41}$$

Since the samples of a white Gaussian noise are independent, b_n has the same variance as $b(t)$, i.e., $\sigma_d^2 = \sigma_c^2 = 2N_0W$, and the variance of the quadrature components of b_n, i.e., $b_{n,I}$ and $b_{n,Q}$, can be derived as

$$\sigma^2 = \sigma_d^2/2 = N_0W \tag{3.42}$$

Now, the relationship among the PSD of AWGN in the passband and the PSD of its equivalent complex envelope in the baseband, as well as the variance of the sampled complex envelope has been derived.

3.3.3.2 Symbol Energy in Passband and Equivalent Baseband

If the BER performance of a system on function of E_b/N_0 is required, while the analysis or simulation of modulation/demodulation is done in the equivalent baseband channel, we need not only the power (variance) relationship of the equivalent additive Gaussian noise in different band, but also the quantitive connection of the symbol energy of the passband transmitted signal, its equivalent complex envelope, as well as the sampled complex sequence.

When a binary system is considered, the symbol energy is equal to the bit energy. Let's talk about the CCA signals concerned in binary CCASK. According to equation (3.5) and equation (3.14), the transmitted signal for data symbol 'i' ($i \in \{0, 1\}$) in the RF band can be presented by

$$x_p^{(i)}(t) = x^{(i)}(t)\cos(2\pi f_c t) \tag{3.43}$$

The average power of this transmitted passband signal can be derived as

$$\begin{aligned}
P_{x_p} &= \lim_{\tau\to\infty}\frac{1}{\tau}\int_{-\frac{\tau}{2}}^{\frac{\tau}{2}}\Big(x^{(i)}(t)\cos(2\pi f_c t)\Big)^2 dt \\
&= \frac{1}{2}\lim_{\tau\to\infty}\frac{1}{\tau}\int_{-\frac{\tau}{2}}^{\frac{\tau}{2}} {x^{(i)}}^2(t)dt + \frac{1}{2}\lim_{\tau\to\infty}\frac{1}{\tau}\int_{-\frac{\tau}{2}}^{\frac{\tau}{2}} {x^{(i)}}^2(t)\cos(4\pi f_c t)dt \\
&= \frac{1}{2}\lim_{\tau\to\infty}\frac{1}{\tau}\int_{-\frac{\tau}{2}}^{\frac{\tau}{2}}\Big(\sum_n x_n^{(i)}\mathrm{sinc}(Wt-n)\Big)^2 dt \\
&= \frac{1}{2}\lim_{\tau\to\infty}\frac{1}{W\tau}\int_{-\frac{W\tau}{2}}^{\frac{W\tau}{2}}\Big(\sum_n x_n^{(i)}\mathrm{sinc}(t'-n)\Big)^2 dt' \\
&= \frac{1}{2}\lim_{\tau\to\infty}\frac{1}{W\tau}\sum_{n=\lceil -\frac{W\tau}{2}\rceil}^{\lceil\frac{W\tau}{2}\rceil} {x_n^{(i)}}^2 \\
&= \frac{1}{2}\langle {\mathbf{x}^{(i)}}^2\rangle
\end{aligned} \tag{3.44}$$

In order to avoid the transmission of DC part of a signal, and keep the bit energy symmetric for different data symbol $'i'$, the iterated sequence $\mathbf{x}^{(i)}$ $(i \in \{0,1\})$ of CCA-q_i is assumed to be zero mean and normalized, i.e., $\langle \mathbf{x}^{(i)}\rangle = U^{(i)} = 0$, and $\langle {\mathbf{x}^{(i)}}^2\rangle = {\Delta^{(i)}}^2 = \Delta^2$. Hence, the bit energy E_b in the RF band can be derived as

$$E_b = P_{x_p}T = \frac{T}{2}\Delta^2 == \frac{L\Delta^2}{2W} \tag{3.45}$$

Since the average power of the equivalent baseband signal $s(t)$ (complex envelope) can be presented by

$$\begin{aligned}
P_x &= \lim_{\tau\to\infty}\frac{1}{\tau}\int_{-\frac{\tau}{2}}^{\frac{\tau}{2}} x^{(i)}(t)^2 dt \\
&= 2P_{x_p}
\end{aligned} \tag{3.46}$$

the bit energy of $s(t)$ is twice the one of $s_p(t)$, i.e., $E_{b_c} = 2E_b = T\Delta^2$. As long as the discrete-time equivalent baseband signal s_n (sampled complex sequence) is concerned, the bit energy can be given as

$$\begin{aligned}
E_{b_d} &= L\lim_{N\to\infty}\frac{1}{N}\sum_{n=1}^{N} {x_n^{(i)}}^2 \\
&= L\Delta^2 \\
&= 2WE_b
\end{aligned} \tag{3.47}$$

where $T_s = T/L$ is the sampling period, and L is the number of samples per symbol (bit) as defined above.

Besides, let's denote the statistics of the l^{th} ($l \in \{1, 2, ..., q_i\}$) zone of CCA-q_i by

$$\mu_l^{(i)} = \lim_{N\to\infty} \frac{1}{N+1} \sum_{k=0}^{N} x_{l+kq_i}^{(i)} \tag{3.48}$$

$$\delta_l^{(i)^2} = \lim_{N_l\to\infty} \frac{1}{N} \sum_{k=0}^{N} \left(x_{l+kq_i}^{(i)} - \mu_l^{(i)} \right)^2 \tag{3.49}$$

as well as several important mean values of these statistics by

$$\begin{aligned}
\langle \mu^2 \rangle^{(i)} &= \frac{1}{q_i} \sum_{l=1}^{q_i} \mu_l^{(i)^2} \\
\langle \delta^2 \rangle^{(i)} &= \frac{1}{q_i} \sum_{l=1}^{q_i} \delta_l^{(i)^2} \\
\langle \mu^4 \rangle^{(i)} &= \frac{1}{q_i} \sum_{l=1}^{q_i} \mu_l^{(i)^4} \\
\langle \delta^4 \rangle^{(i)} &= \frac{1}{q_i} \sum_{l=1}^{q_i} \delta_l^{(i)^4} \\
\langle \mu^2 \delta^2 \rangle^{(i)} &= \frac{1}{q_i} \sum_{l=1}^{q_i} \mu_l^{(i)^2} \delta_l^{(i)^2}
\end{aligned} \tag{3.50}$$

It can be obtained that $\langle \mu^2 \rangle^{(i)} + \langle \delta^2 \rangle^{(i)} = \Delta^2$, and the bit energy of the sampled baseband signal of the CCA-q_i modulated symbol can also be presented by its specific statistics as

$$E_{b_d} = L\Big(\langle \mu^2 \rangle^{(i)} + \langle \delta^2 \rangle^{(i)} \Big) \tag{3.51}$$

Until now, with the results in equation (3.42) and equation (3.47), we can finally represent the parameter of the passband AWGN channel, i.e., E_b/N_0, by the statistics of sampled signal and noise in the baseband equivalent complex channel as follows:

$$E_b/N_0 = \frac{L\Delta^2}{2\sigma^2} \tag{3.52}$$

In this way, the BER performance of CCASK can also be obtained in the equivalent baseband channel model.

3.3.3.3 CCASK AWGN Performance Evaluation

Let's talk about the performance evaluation in the AWGN channel. Since the baseband modulation symbols of CCASK have real values, the real statistics of the equivalent discrete-time baseband AWGN channel model in equation (3.41) are sufficient for the detection, i.e.,

$$r_{n,I} = s_n + b_{n,I} \tag{3.53}$$

Note that the expressions of the decision variables in equation (3.21), (3.26) and (3.32) have a similar structure: the average of a large number of identically distributed uncorrelated quasi-random variables, and each of these variables has a finite mean and variance value. By using the central limit theorem under the condition of large modulation ($L \gg q_1, q_0$), it can be assumed that these detection variables, i.e., C_{b_m} for auto-correlation detection, D_{b_m} for spectral detection and V_{b_m} for statistical detection respectively, are normally distributed random variables [23]. Define ε_m to generally present these detection variables. Two cases need to be considered in order to evaluate the noise performance of a system: when a '0' was transmitted ($d_m = 0$), and when an '1' was transmitted ($d_m = 1$), which can be denoted as

$$\begin{cases} \varepsilon_m^{(0)} = \varepsilon_m|_{d_m=0} \\ \varepsilon_m^{(1)} = \varepsilon_m|_{d_m=1} \end{cases} \tag{3.54}$$

According to reference [23], the BER of a binary system owning such observation variable as ε_m can be given as

$$\text{BER} = P_0 \text{Prob}(\varepsilon_m^{(0)} > 0) + P_1 \text{Prob}(\varepsilon_m^{(1)} < 0) \tag{3.55}$$

where P_0 and P_1 are the probabilities of a '0' and an '1' being transmitted, $\text{Prob}(\varepsilon_m^{(0)} > 0)$ is the probability of a transmitted '0' wrongly detected as '1', and $\text{Prob}(\varepsilon_m^{(1)} < 0)$ is the probability of a transmitted '1' wrongly detected as '0'. Generally, we can suppose $P_0 = P_1 = \frac{1}{2}$, while $\text{Prob}(\varepsilon_m^{(0)} > 0)$ and $\text{Prob}(\varepsilon_m^{(1)} < 0)$ can be obtained by

$$\text{Prob}(\varepsilon_m^{(0)} > 0) = \frac{1}{2}\text{erfc}\left(\frac{-E(\varepsilon_m^{(0)})}{\sqrt{2\text{Var}(\varepsilon_m^{(0)})}}\right) \tag{3.56}$$

$$\text{Prob}(\varepsilon_m^{(1)} < 0) = \frac{1}{2}\text{erfc}\left(\frac{E(\varepsilon_m^{(1)})}{\sqrt{2\text{Var}(\varepsilon_m^{(1)})}}\right) \tag{3.57}$$

Replacing ε_m by C_{b_m}, D_{b_m} or V_{b_m}, the BER of binary CCASK using auto-correlation, spectral and statistical detections can be respectively obtained. In this way, the expressions of the expectation and variance of each detection variable are indispensable.

During the performance evaluation of chaos-based systems, several hypothesis are usually considered for quantifying the chaotic signals in communication systems, such that the chaotic signals are usually supposed to be uncorrelated (although it's valid only if infinitely long chaotic sequences are considered), as proposed in reference [6] and also presented in equation (1.17). As long as the iterated sequence of CCA-q is concerned, it has been supposed that $E(\mathbf{x}) = U = 0$. Here, we furthermore assume that the iteration sequence $\mathbf{x}$, which is collected averagely from all the q zones of CCA-q, is orthogonal; meanwhile, $\mathbf{x}_{q,l}$ ($l \in \{1, 2, ..., q\}$) is a chaotic sub-sequence with $E(\mathbf{x}_{q,l}) = \mu_l$, so that the sub-sequence of the iteration belonging to each zone will be assumed to be uncorrelated.

It should be noticed that CCA-q stands for all the CCAs of period q, which can be generated by different dynamical systems with certain fixed parameters. Therefore, the particular values of the specific statistics of CCA-q, e.g., μ_l and δ_l^2, can vary among different CCA-q generators. Hence, these statistics cannot be formulated, but only be obtained by computer simulations for each particular dynamical system. For example, the statistics of one of the realizations of CCA-31 and CCA-29 have been listed in Table 3.1. These statistics are obtained by 10^6 points of computer simulation for the enhanced CCA-31 and CCA-29 of system (2.1) as illustrated in Figure 3.1 and Figure 3.1. Remind that the simulated chaotic signals of both CCAs are made zero mean and normalized, i.e., $U = 0$, and $\Delta^2 = 1$. Furthermore, the important mean values in equation (3.50) of these simulated statistics are calculated from Table 3.1, and listed in Table 3.2.

Since the probabilities in equations (3.56)-(3.57) are functions of unformulated statistics, the performance can be obtained by the combination of the analytical and numerical methods (or **analytic-numerical method**), using the statistics of certain realization of CCAs, such as listed in Table 3.1; or else, approximations should be done to get an approximated expression, which will be mentioned in the analysis. In addition, the Monte-Carlo simulations of binary CCASK with each detections will also be operated to give a pure numerical performance. The same CCA generator realizations for getting the statistics in Table 3.1 will be selected in the simulations, i.e., the en-

CCA-31			CCA-29		
l	μ_l	δ_l^2	l	μ_l	δ_l^2
1	-0.3410	4.6283×10^{-3}	1	0.2661	2.1597×10^{-3}
2	0.7888	3.9186×10^{-2}	2	0.1572	7.1455×10^{-6}
3	-0.1724	3.6561×10^{-6}	3	-0.0706	4.6227×10^{-3}
4	2.4662	1.1582	4	0.1305	5.5897×10^{-6}
5	-0.1738	5.3843×10^{-14}	5	0.2042	1.0666×10^{-3}
6	-0.1740	3.8926×10^{-8}	6	0.3474	2.1850×10^{-3}
7	-0.0815	1.5581×10^{-4}	7	0.0670	8.8767×10^{-4}
8	1.0117	1.1200×10^{-2}	8	-0.8544	6.1898×10^{-3}
9	-0.1960	1.9568×10^{-6}	9	0.1537	8.7496×10^{-6}
10	-0.1738	1.6418×10^{-10}	10	-1.8195	2.6121×10^{-1}
11	0.5255	1.2930×10^{-3}	11	0.1512	1.3185×10^{-14}
12	0.1273	1.5372×10^{-4}	12	0.1513	3.2926×10^{-9}
13	-2.3597	2.7558×10^{-2}	13	0.2614	7.6038×10^{-5}
14	-0.1738	1.1893×10^{-13}	14	-1.0224	4.5165×10^{-3}
15	-0.5683	6.4848×10^{-3}	15	0.1217	7.5244×10^{-8}
16	-0.1733	9.5369×10^{-8}	16	0.1512	9.5158×10^{-12}
17	-0.1295	2.8309×10^{-4}	17	1.0558	3.4875×10^{-4}
18	-0.2067	1.0897×10^{-5}	18	-0.0570	3.1193×10^{-6}
19	-0.4849	7.0315×10^{-3}	19	-3.5883	6.6933×10^{-3}
20	-0.1146	1.9304×10^{-4}	20	0.1513	1.0014×10^{-10}
21	-0.1623	3.5183×10^{-5}	21	0.1209	9.9599×10^{-6}
22	-0.8359	7.8778×10^{-4}	22	0.1232	8.0869×10^{-6}
23	-0.2456	8.9109×10^{-4}	23	0.5512	1.4044×10^{-4}
24	3.6438	4.2529×10^{-1}	24	0.1853	4.6910×10^{-6}
25	-0.1738	3.0378×10^{-17}	25	0.1450	1.0692×10^{-6}
26	-0.1113	2.0207×10^{-3}	26	-0.3979	1.8087×10^{-3}
27	-0.1890	1.0666×10^{-4}	27	0.2583	6.0430×10^{-6}
28	-0.5696	2.9685×10^{-2}	28	2.9053	6.8106×10^{-2}
29	-0.1561	1.2623×10^{-6}	29	0.1512	4.2602×10^{-15}
30	-0.1489	5.7563×10^{-4}			
31	-0.4475	1.0725×10^{-2}			

Table 3.1: Statistics of CCA-31 and CCA-29 generated by the enhanced CCAs of system (2.1), obtained by 10^6 points of computer simulations.

	CCA-31	CCA-29
Δ^2	1	1
$\langle\mu^2\rangle$	0.9443	0.9877
$\langle\delta^2\rangle$	0.0557	0.0124
$\langle\mu^4\rangle$	7.9554	8.6579
$\langle\delta^4\rangle$	0.0492	0.0025
$\langle\mu^2\delta^2\rangle$	0.4161	0.0529

Table 3.2: Mean values of the statistics of CCA-31 and CCA-29 in Table 3.1.

hanced CCA-31 of system (2.1) will be the basis function for modulating data '1', while the similar CCA-29 will be chosen for modulating data '0'.

In the rest part of this section, the AWGN performance evaluation obtained by the analytic-numerical method, the approximated analytical method, as well as the pure numerical method will be given for each detection, and the results using different evaluation methods will be compared. In addition, the comparison of AWGN performance of CCASK using different detections, as well as the comparison of AWGN performance between CCASK and DCSK will also be discussed.

A. AWGN Performance Evaluation of CCASK Using Auto-Correlation Detection

It has been pointed out in the beginning of this section that the noise performance of binary CCASK using auto-correlation detection is a function of the expectation and variance of the detection variable C_{b_m}. The analytical evaluation in case of single user is given in Appendix A.1, and the result of the general expression of BER performance is given as

$$\begin{aligned}
&\mathrm{BER}_{\mathrm{CCASK}} \\
&= \frac{1}{4}\sum_{i=0}^{1}\mathrm{erfc}\Bigg[\Bigg(\frac{8(L+q_i)}{3L(L-q_i)}\frac{\langle\mu^2\delta^2\rangle^{(i)}}{\langle\mu^2\rangle^{(i)^2}}+\frac{4q_i}{L(L-q_i)}\frac{\langle\delta^4\rangle^{(i)}}{\langle\mu^2\rangle^{(i)^2}}+\frac{4q_{1-i}}{L(L-q_{1-i})}\frac{\Delta^4}{\langle\mu^2\rangle^{(i)^2}} \\
&\qquad +\Big(\frac{8(2L-q_i)}{3L(L-q_i)}\frac{\langle\mu^2\rangle^{(i)}}{\langle\mu^2\rangle^{(i)^2}}+\frac{8q_i}{L(L-q_i)}\frac{\langle\delta^2\rangle^{(i)}}{\langle\mu^2\rangle^{(i)^2}}+\frac{8q_{1-i}}{L(L-q_{1-i})}\frac{\Delta^2}{\langle\mu^2\rangle^{(i)^2}}\Big)\sigma^2 \\
&\qquad +\frac{4}{L}\Big(\frac{q_i}{L-q_i}+\frac{q_{1-i}}{L-q_{1-i}}\Big)\frac{\sigma^4}{\langle\mu^2\rangle^{(i)^2}}\Bigg)^{-\frac{1}{2}}\Bigg]
\end{aligned} \tag{3.58}$$

which depends not only on the noise spectral density σ^2 (determined by E_b/N_0 if bit energy is constant), but also on the symbol modulation rate L, the periods q_0, q_1 of the taken CCAs, as well as the statistics of these CCAs.

Hence, the analytic-numerical noise performance will be a function of L and E_b/N_0 if certain CCAs are chosen, i.e., q_1, q_0 as well as the statistics are fixed. For example, when the CCA-29 and CCA-31 in Table 3.2 are considered, the analytic-numerical BER of CCASK using auto-correlation detection versus L corresponding to certain E_b/N_0 is illustrated in Figure 3.7. The result shows that the AWGN noise performance of CCASK using auto-correlation detection augments with the increase of number of samples per symbol L.

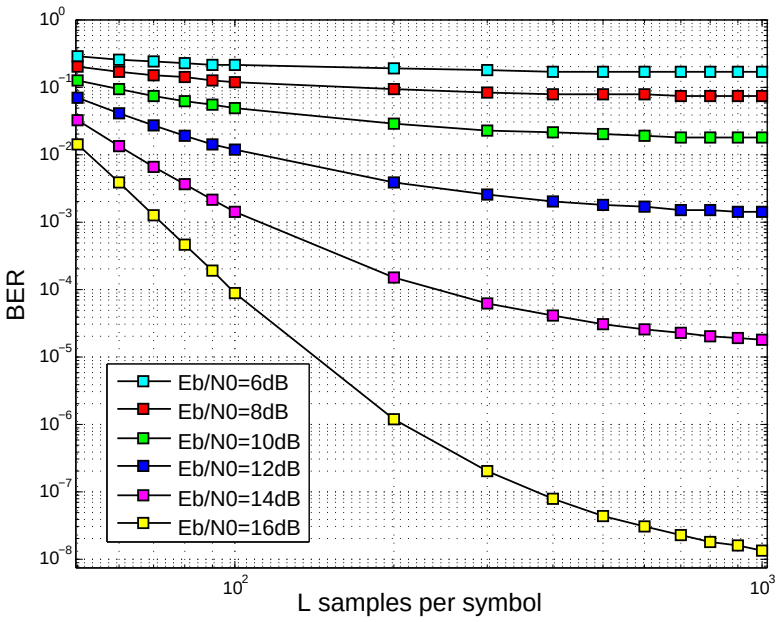

Figure 3.7: Analytic-numerical noise performance of binary CCASK using auto-correlation detection versus the number of samples per symbol L, when the enhanced CCA-29 and CCA-31 of system (2.1) are considered.

The Monte-Carlo simulations are done in order to verify the analytical AWGN performance of binary CCASK using auto-correlation detection. During the simulations, the enhanced CCA-29 and CCA-31 of system 2.1 are generated, in which the signals are centered and energy normalized before the transmission. Under each modulation rate L, 10^6 points of symbols are transmitted through 10^4 AWGN channels in parallel.

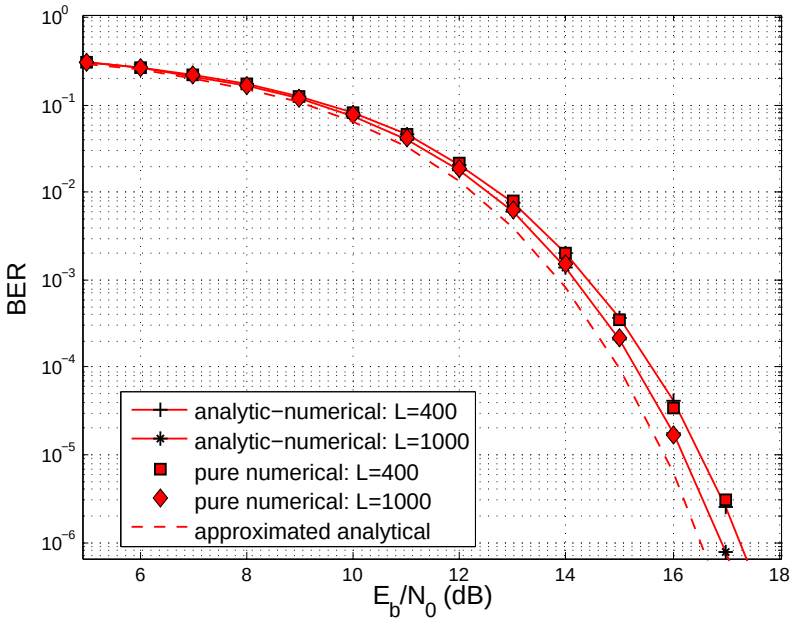

Figure 3.8: Analytic-numerical result in Figure 3.7 with $L = 400$ and $L = 1000$, compared with the approximated analytical and pure numerical results under the same conditions.

Figure 3.8 illustrates the pure numerical results with $L = 400, 1000$, together with the corresponding analytic-numerical results. The comparison shows a good coincidence between them, which affirms the procedure of analysis in A.1.

Furthermore, according to the performance analysis of auto-correlation detection, it's also possible to approximate the analytical result if the statistics of CCAs are not acknowledged. A.1 gives the approximation under the conditions of large number of samples per symbol, i.e., $L \gg q_0, q_1$, and relative small zones of CCAs:

$$\mathrm{BER}_{\mathrm{CCASK}} \approx \frac{1}{4}\sum_{i=0}^{1}\mathrm{erfc}\left[\left(\frac{8}{3}\frac{N_0}{E_b}+(q_i+q_{1-i})\frac{N_0^2}{E_b^2}\right)^{-\frac{1}{2}}\right] \tag{3.59}$$

which is a function of E_b/N_0, as well as the periods q_0, q_1 of the CCAs. The comparison between this approximated analytical result and the above mentioned analytic-numerical result has sense only if L is large enough. Figure 3.8 also illustrates the approximated analytical result (dashed line) with $q_0 = 29$, $q_1 = 31$. Notice that the difference between the approximated analytical result and the analytic-numerical result diminishes with the increase of L, because the approximation was made in case of large

L. Furthermore, the difference will also diminish if the value of $\langle\delta^2\rangle/\langle\mu^2\rangle$ decreases, according to the conditions under which the approximation was done in A.1.

B. AWGN Performance Evaluation of CCASK Using Spectral Detection

The noise performance of binary CCASK using spectral detection is a function of the expectation and variance of the detection variable D_{b_m}. The procedure of this analysis in case of single user is given in A.2, and the result of the general expression of BER performance is given by

$$\begin{aligned}
&\mathrm{BER}_{\mathrm{CCASK}} \\
&= \frac{1}{4}\sum_{i=0}^{1}\mathrm{erfc}\Bigg[\Bigg(\frac{8(L+q_i)}{3L(L-q_i)}\frac{\langle\mu^2\delta^2\rangle^{(i)}}{\langle\mu^2\rangle^{(i)^2}} + \frac{4q_i}{L(L-q_i)}\frac{\langle\delta^4\rangle^{(i)}}{\langle\mu^2\rangle^{(i)^2}} + \frac{4(L-q_{1-i})q_i^2}{L(L-q_i)^2q_{1-i}}\frac{\Delta^4}{\langle\mu^2\rangle^{(i)^2}} \\
&\qquad + \Big(\frac{8(2L-q_i))}{3L(L-q_i)}\frac{\langle\mu^2\rangle^{(i)}}{\langle\mu^2\rangle^{(i)^2}} + \frac{8q_i}{L(L-q_i)}\frac{\langle\delta^2\rangle^{(i)}}{\langle\mu^2\rangle^{(i)^2}} + \frac{8(L-q_{1-i})q_i^2}{L(L-q_i)^2q_{1-i}}\frac{\Delta^2}{\langle\mu^2\rangle^{(i)^2}}\Big)\sigma^2 \\
&\qquad + \frac{4}{L}\frac{L(q_i+q_{1-i})q_i - 2q_i^2q_{1-i}}{(L-q_i)^2q_{1-i}}\frac{\sigma^4}{\langle\mu^2\rangle^{(i)^2}}\Bigg)^{-\frac{1}{2}}\Bigg]
\end{aligned} \tag{3.60}$$

which depends on the noise spectral density σ^2, the symbol modulation rate L, the periods q_0, q_1 of the taken CCAs, as well as the statistics of these CCAs.

Similarly as the auto-correlation detection, the analytic-numerical noise performance of binary CCASK using spectral detection is also a function of L and E_b/N_0 if certain CCAs are chosen, i.e., q_1, q_0 as well as the statistics are fixed. When the CCA-29 and CCA-31 in Table 3.2 are considered, this analytic-numerical result with $L = 400$ and $L = 1000$ are illustrated in Figure 3.9, which shows that the noise performance using spectral detection also augments with the increase of number of samples per symbol L.

The similar Monte-Carlo simulations as in auto-correlation detection are done in order to verify the analytical AWGN performance of binary CCASK using spectral detection. The pure numerical results with $L = 400, 1000$ are illustrated in Figure 3.9. The comparison shows a good agreement between the analytic-numerical and pure numerical results, which means the correctness of the procedure of analysis in A.2.

Furthermore, according to the performance analysis of spectral detection, it's also possible to approximate the analytical result if the statistics of CCAs are not acknowl-

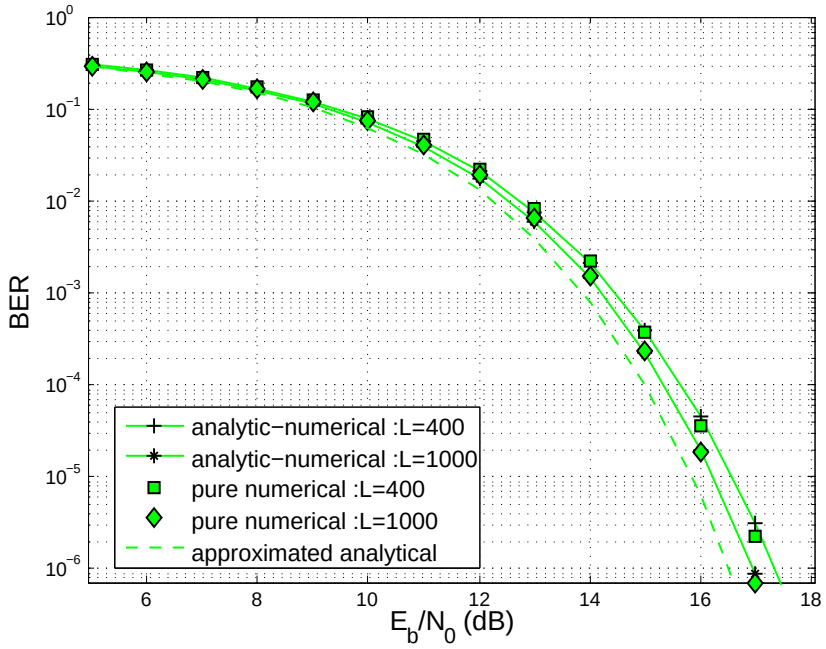

Figure 3.9: Analytic-numerical noise performance of binary CCASK using spectral detection with $L = 400$ and $L = 1000$ when the enhanced CCA-29 and CCA-31 of system (2.1) are considered, as well as the approximated analytical and pure numerical results under the same conditions.

edged. A.2 gives the approximation under the conditions of large number of samples per symbol, i.e., $L \gg q_0, q_1$, and relative small zones of CCAs:

$$\mathrm{BER}_{\mathrm{CCASK}} \approx \frac{1}{4}\sum_{i=0}^{1}\mathrm{erfc}\left[\left(\frac{8}{3}\frac{N_0}{E_b}+\left(q_i+\frac{q_i^2}{q_{1-i}}\right)\frac{N_0^2}{E_b^2}\right)^{-\frac{1}{2}}\right] \tag{3.61}$$

which is also a function of E_b/N_0 and q_0, q_1. The comparison between this approximated analytical result and the above mentioned analytic-numerical result has sense only if L is large enough. Figure 3.9 also illustrates the approximated analytical result with $q_0 = 29$, $q_1 = 31$. Similarly, the difference between the approximated analytical result and the analytic-numerical result using spectral detection diminishes with the increase of L, and it will also diminish if the value of $\langle\delta^2\rangle/\langle\mu^2\rangle$ decreases, according to the conditions under which the approximation was done in A.2.

C. AWGN Performance Evaluation of CCASK Using Statistical Detection

The noise performance of binary CCASK using statistical detection is a function of the expectation and variance of the detection variable V_{b_m}. The procedure of this analysis in case of single user is given in A.3, and the result of the general expression of BER performance is given as

$$\begin{aligned}
&\mathrm{BER}_{\mathrm{CCASK}} \\
&= \frac{1}{4}\sum_{i=0}^{1}\mathrm{erfc}\Bigg[\Bigg(\frac{8(L+q_i)}{3L(L-q_i)}\frac{\langle\mu^2\delta^2\rangle^{(i)}}{\langle\mu^2\rangle^{(i)^2}}+\frac{4q_i}{L(L-q_i)}\frac{\langle\delta^4\rangle^{(i)}}{\langle\mu^2\rangle^{(i)^2}}+\frac{4q_{1-i}}{L(L-q_{1-i})}\frac{\Delta^4}{\langle\mu^2\rangle^{(i)^2}} \\
&\qquad +\Big(\frac{4(2L-q_i)}{3(L-q_i)}\frac{\langle\mu^2\rangle^{(i)}}{\langle\mu^2\rangle^{(i)^2}}+\frac{4q_i}{(L-q_i)}\frac{\langle\delta^2\rangle^{(i)}}{\langle\mu^2\rangle^{(i)^2}}+\frac{4q_{1-i}}{(L-q_{1-i})}\frac{\Delta^2}{\langle\mu^2\rangle^{(i)^2}}\Big)\frac{2\sigma^2}{L} \\
&\qquad +\Big(\frac{q_i}{L(L-q_i)}+\frac{q_{1-i}}{L(L-q_{1-i})}\Big)\frac{4\sigma^4}{\langle\mu^2\rangle^{(i)^2}}\Bigg)^{-\frac{1}{2}}\Bigg]
\end{aligned} \tag{3.62}$$

which depends on the noise spectral density σ^2, the symbol modulation rate L, the periods q_0, q_1 of the taken CCAs, as well as the statistics of these CCAs.

Similarly as the other two detections, the analytic-numerical noise performance of binary CCASK using statistical detection is also a function of L and E_b/N_0 if certain CCAs are chosen, i.e., q_1, q_0 as well as the statistics are fixed. When the CCA-29 and CCA-31 in Table 3.2 are considered, this analytic-numerical result with $L = 400$ and $L = 1000$ are illustrated in Figure 3.10, which shows that the noise performance of statistical detection also augments with the increase of number of samples per symbol L.

The similar Monte-Carlo simulations as in the other two detections are done in order to verify the analytical AWGN performance of binary CCASK using statistical detection. The pure numerical results with $L = 400, 1000$ are illustrated in Figure 3.10 for comparison. It shows a good coincidence between the analytic-numerical and pure numerical results, which means the correctness of the procedure of analysis in A.3.

Furthermore, according to the performance analysis of statistical detection, it's also possible to approximate the analytical result if the statistics of CCAs are not acknowledged. A.3 gives a method to approximate the performance under the conditions of relative large number of samples per symbol, i.e., $L \gg q$, and relative small zones of

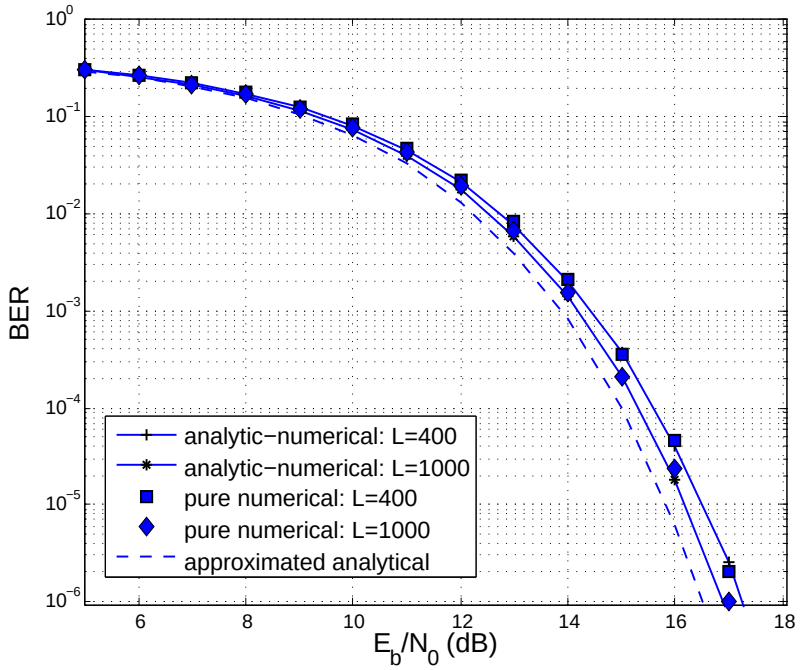

Figure 3.10: Analytic-numerical noise performance of binary CCASK using statistical detection with $L = 400$ and $L = 1000$ when the enhanced CCA-29 and CCA-31 of system (2.1) are considered, as well as the approximated analytical and pure numerical results under the same conditions.

CCAs, with a simple expression as:

$$\mathrm{BER}_{\mathrm{CCASK}} \approx \frac{1}{4}\sum_{i=0}^{1}\mathrm{erfc}\left[\left(\frac{8}{3}\frac{N_0}{E_b}+(q_i+q_{1-i})\frac{N_0^2}{E_b^2}\right)^{-\frac{1}{2}}\right] \tag{3.63}$$

which is also a function of E_b/N_0 and q_0, q_1. The comparison between this approximated analytical result and the above mentioned analytic-numerical result has sense only if L is large enough. Figure 3.10 also illustrates the approximated analytical result with $q_0 = 29$, $q_1 = 31$. Similarly, the difference between the approximated analytical result and the analytic-numerical result using statistical detection diminishes with the increase of L, and it will also diminish if the value of $\langle\delta^2\rangle/\langle\mu^2\rangle$ decreases, according to the conditions under which the approximation was done in A.3.

D. Comparison of Different Detection Schemes

Firstly, let's compare the auto-correlation and spectral detections of CCASK. According to **Wiener-Khinchin theorem**, the autocorrelation $R_{rr}(\tau)$ of a function $r(t)$, i.e., $R_{rr}(\tau) = \int_{-\infty}^{+\infty} r^*(t)r(t+\tau)dt$, can be simply given by the inverse Fourier transform of the absolute square of $\hat{r}(k)$, here $\hat{r}(k)$ is the Fourier transform of $r(t)$, i.e., $\hat{r}(k) = \mathcal{F}[r(t)]$, and $R_{rr}(\tau) = \mathcal{F}^{-1}[|\hat{r}(k)|^2]$. The decision variable $C_m[v]$ in equation (3.21) is a collection of auto-correlation of $\mathbf{r}_m$, i.e., $R_{r_m r_m}(\ell q_v)$, i.e.. Meanwhile the decision variable $D_m[v]$ in equation (3.26) is a collection of the absolute square of DFT of received symbol sequence $\mathbf{r}_m$, i.e., $|\hat{r}(\frac{K}{q_v})|^2$. Obviously, it can be found that $R_{r_m r_m}[\ell q_v]$ is the IDFT of $|\hat{r}(\frac{K}{q_v})|^2$, with

$$\begin{aligned} R_{r_m r_m}[\ell q_v] &= \epsilon(\ell) \sum_{K=1}^{q_v} |\hat{r}(\frac{K}{q_v})|^2 e^{j2\pi \frac{K}{q_v} \ell q_v} \\ &= \epsilon(\ell) \sum_{K=1}^{q_v} |\hat{r}(\frac{K}{q_v})|^2 \end{aligned} \tag{3.64}$$

where $\epsilon(\ell)$ stands for the coefficient caused by the finite length L of each symbol $\mathbf{r}_m$. Inserting this relationship into the expression of the decision variable $C_m[v]$ of auto-correlation detection in (A.1) in section A.1, we can get

$$\begin{aligned} C_m[v] &\approx \frac{2q_v}{L(L-q_v)} \sum_{l=1}^{q_v} R_{r_m r_m}[\ell q_v] \\ &= \frac{2q_v}{L(L-q_v)} \sum_{\ell=1}^{L_v} \epsilon(\ell) \sum_{K=1}^{q_v} |\hat{r}(\frac{K}{q_v})|^2 \\ &= \frac{2q_v^2}{L(L-q_v)} \sum_{\ell=1}^{L_v} \epsilon(\ell) D_m[v] \end{aligned} \tag{3.65}$$

Hence, the auto-correlation detection and spectral detection should have a similar performance with slight difference in coefficient, which can be noticed by the comparison of the AWGN performance expressions in equations (3.58) and (3.62), as well as the simulation results in Figure 3.8 and Figure 3.9. Especially, the approximated analytical results of both detections are identical, see equation (3.59) and (3.61), which is caused by the approximations which have been done during the analysis. Actually, in order to get the approximated analytical performance, it has been supposed that $L \gg q_0, q_1$, hence several slight proportions of coefficients have been dropped to get the simpler

expression, such as $L \pm q_i \approx L$ (see the details in Appendix A.1 and A.2). Hence, the slight coefficient difference on performance between the auto-correlation detection and the spectral detection have been dropped by the way.

As long as the auto-correlation and statistical detections is concerned, the relationship can't been explained directly. According to the performance analysis in section A.3, the expression of the decision variable $V_m[v]$ of statistical detection can be represented as in (A.30). However, it can be rewritten in another form as

$$\begin{aligned}
V_m[v] &\approx \frac{1}{L}\sum_{n=1}^{L} r_n^2 - \frac{2q_v(L+q_v)}{L^2(L-q_v)} \sum_{l=1}^{q_v}\sum_{k=0}^{L_v^l}\sum_{k'=0}^{k-1} r_{l+\ell q_v} r_{l+k'q_v} \\
&\underline{\underline{\ell = k-k'}}\ \frac{1}{L}\sum_{n=1}^{L} r_n^2 - \frac{2q_v(L+q_v)}{L^2(L-q_v)} \sum_{l=1}^{q_v}\sum_{k=0}^{L_v^l}\sum_{\ell=1}^{k} r_{l+\ell q_v} r_{l+(k-\ell)q_v} \\
&= \frac{1}{L}\sum_{n=1}^{L} r_n^2 - \frac{2q_v(L+q_v)}{L^2(L-q_v)} \sum_{l=1}^{q_v}\sum_{\ell=1}^{L_v^l}\sum_{k=\ell}^{L_v^l} r_{l+\ell q_v} r_{l+(k-\ell)q_v} \\
&= \frac{1}{L}\sum_{n=1}^{L} r_n^2 - \frac{2q_v(L+q_v)}{L^2(L-q_v)} \sum_{l=1}^{q_v} R_{r_m r_m}[\ell q_v] \\
&= \frac{1}{L}\sum_{n=1}^{L} r_n^2 - (1+\frac{q_v}{L}) C_m[v]
\end{aligned} \tag{3.66}$$

Therefore, the decision variable of binary CCASK using statistical detection can be represented by

$$\begin{aligned}
V_{b_m} &= V_m[0] - V_m[1] \\
&= (1+\frac{q_1}{L}) C_m[1] - (1+\frac{q_0}{L}) C_m[0]
\end{aligned} \tag{3.67}$$

Hence, the auto-correlation detection and statistical detection also have a similar performance with slight difference in coefficient, which could be proven by the comparison of the AWGN performance expressions in equations (3.58) and (3.62), as well as the simulation results in Figure 3.8 and Figure 3.10.

Therefore, a conclusion can be given on the three detections of CCASK: though the scheme as well as the circuit implementation in the receiver are different for each detection, it has been proven by the analysis and simulations that they obtain similar AWGN noise performance. Since that the expression of each decision variable has a linear relationship with the others, naturally they will obtain a performance in almost any channel model similar to each other.

E. Comparison of AWGN Performance between CCASK and DCSK

As a chaotic signal direct modulation system, CCASK needs to own some strongpoints compared with the other direct modulation systems, in order to outperform in certain conditions. As a noncoherent system, neither CCASK nor DCSK requires the regeneration of the transmitted chaotic signals in the receiver, therefore the synchronization between the transmitted signals and the received ones can be avoided. Furthermore, they have the comparable complexity in the transceiver implementation. Above all, DCSK is one of the most studied chaotic signal direct modulation system in the research domain. Hence, we would like to make the comparison between CCASK and DCSK.

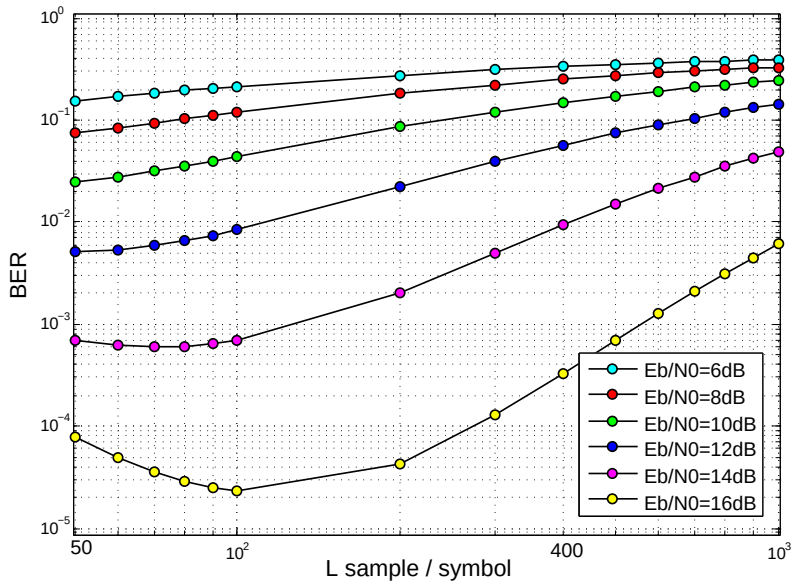

Figure 3.11: AWGN performance of DCSK versus the number of samples per symbol L.

The approximated analytical expression of AWGN performance of DCSK has been given in equation (1.25), where $2M_s$ is the number of samples per symbol, hence $L = 2M_s$. The BER of DCSK versus the number of samples per symbol L can therefore be illustrated as in Figure 3.11. From comparing Figure 3.11 with Figure 3.7, it can be observed that for DCSK, the AWGN performance firstly enhanced with the increase of L under the condition of small L, then it worsens with the increase of L when

L is enough large. Meanwhile, the value of L for the optimal AWGN performance changes with E_b/N_0, and it is relatively small, e.g., $L < 100$. In contrary, the AWGN performance of CCASK firstly enhances with the increase of the value of L, then it keeps constant after a certain value of L.

For better comparison, the AWGN performance of DCSK and CCASK versus L when E_b/N_0 = 4dB, 10dB and 14dB are illustrated together in Figure 3.12. We can see that in the AWGN channel with E_b/N_0 <14dB, CCASK outperforms DCSK when $L > 100$, and the improvement augments with the increase of L.

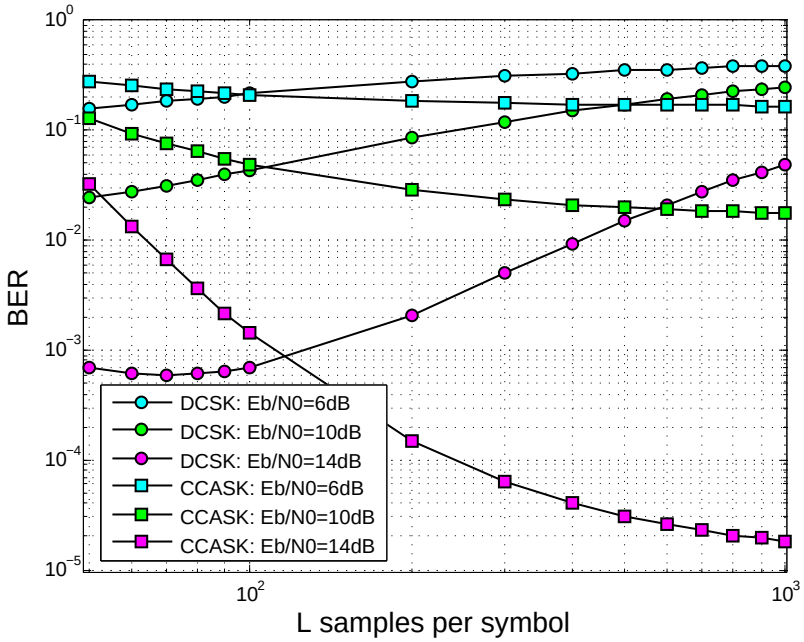

Figure 3.12: Comparison of AWGN performance of DCSK and CCASK versus the number of samples per symbol L.

The AWGN performance of DCSK when $L = 400$ and 1000, as well as the analytic-numerical performance of CCASK using different detections under the same conditions are illustrated respectively in Figure 3.13. It shows that CCASK has an improvement of about 3dB compared with DCSK in case of $L = 400$, while about 4dB in case of $L = 1000$.

It has been defined that the symbol duration is related with the number of samples per symbol as $T = LT_s$. Under the condition of fixed sampling rate T_s (which equals

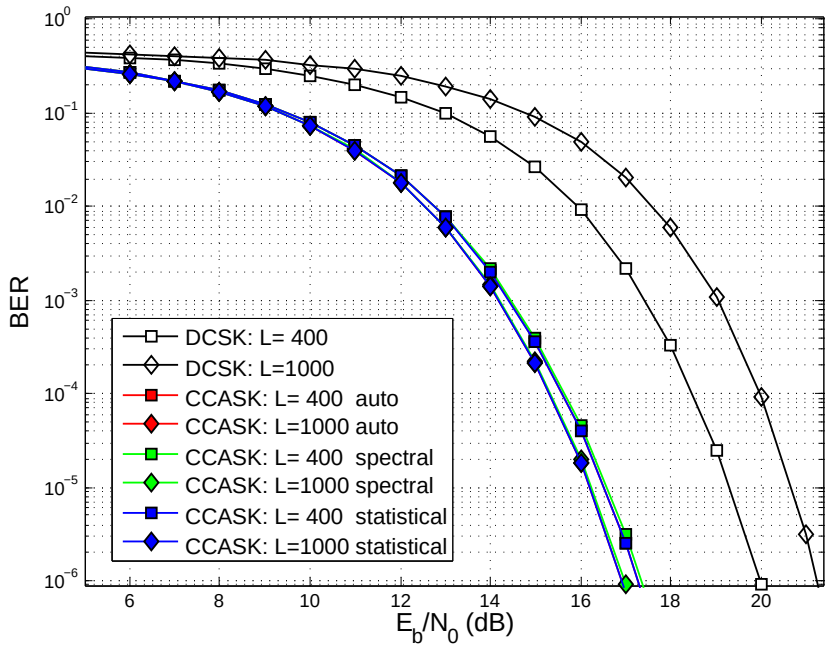

Figure 3.13: Comparison of AWGN performance of DCSK and CCASK with different detections, in case that $L = 400$ and 1000 respectively.

to the oscillation rate of the discrete-time chaotic generator), the larger value of L means the longer symbol duration T. Therefore, if transmitting rate is considered, DCSK outperforms CCASK. However, CCASK shows better noise performance in the low-rate wideband applications.

3.3.4 Multipath Performance of CCASK

It has been discussed in the precedent section that the AWGN channel model considers the additive noise as the only imperfection. However, in certain applications, such as indoor wireless applications and mobile communications, the received signal is composed by the components traveling via multiple paths with different propagation delays, which may add destructively (or constructively) in the receiver. In such an environment, it's rather the multipath fading than the additive noise which decides the performance of a system.

Generally, the continuous-time multipath fading channel can be written as [21]

$$r_p(t) = \sum_i \alpha_i(f,t) s_p(t - \tau_i(f,t)) + b_p(t) \tag{3.68}$$

where $\alpha_i(f,t)$ is the overall attenuation on frequency f (frequency dependent) at time t from the transmitter to the receiver on path i, while $\tau_i(f,t)$ stands for the respectively propagation delay.

In a special case that the transmission is over the RF band W relatively narrow to the carrier frequency f_c, and in addition, the transmitter, receiver and environment are all stationary, the attenuation $\alpha_i(f,t)$ and propagation delays $\tau_i(f,t)$ can be assumed to be independent of the frequency f and time t. Hence, they can be denoted simply by α_i and τ_i, and the linear time-invariant multipath fading channel can be derived as [21]

$$r_p(t) = \sum_i \alpha_i s_p(t - \tau_i) + b_p(t) \tag{3.69}$$

and the total multipath power gain of this channel is as follows:

$$G = \sum_i \alpha_i^2 \tag{3.70}$$

The baseband equivalent multipath channel model can be derived as

$$r(t) = \sum_i \alpha_i e^{-j2\pi f_c \tau_i} s(t - \tau_i) + b(t) \tag{3.71}$$

as well as the discrete-time baseband equivalent model in terms of channel filter taps as [21]

$$r[n] = \sum_\ell h_\ell[n] s[n - \ell] + b[n] \tag{3.72}$$

where $r[n] = r(n/W)$, $s[n] = s(n/W)$, $b[n] = b(n/W)$ and

$$h_\ell[n] = \sum_i \alpha_i e^{-j2\pi f_c \tau_i} \mathrm{sinc}[\ell - \tau_i W] \tag{3.73}$$

Since the values of attenuation α_i and propagation delay τ_i can't be measured exactly for each particular environment, channel models have been developed to present the typical or average behavior of a channel [70]. Based on the fact that the CCA-based

systems in this thesis use the chaotic signals generated by simple circuits which are naturally wideband, they can be proposed to be a modulation scheme for the short distance (or indoor) wireless communications. Hence, in the multipath analysis and simulation parts, the two-ray multipath channel model will be considered, which is simple and often considered for the indoor wireless environments.

3.3.4.1 Model of Two-Ray Multipath Channel

The two-ray channel model includes only a direct path with attenuation α_1, and a reflected path with attenuation α_2 and propagation delay τ_d [71]. Hence, the **mean excess delay** can be derived as $\tau_\mu = \tau_d/2$. According to equation (3.69), the two-ray multipath channel model can be presented as

$$r_p(t) = \alpha_1 s_p(t) + \alpha_2 s_p(t - \tau_d) \tag{3.74}$$

Remind that the additive noise is not mentioned in this model, but once multipath performance evaluation is required, an additive Gaussian noise will be added as in the AWGN channel model. The path delay profile of this model is illustrated in Figure 3.14. This channel model can also be characterized by its frequency response as

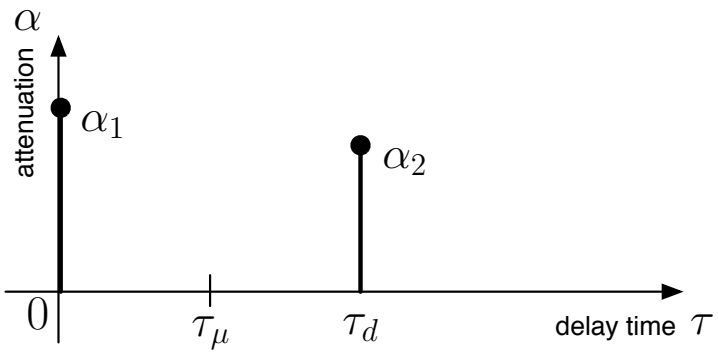

Figure 3.14: Path delay profile of a two-ray channel model.

$$\begin{aligned} H_p(f) &= \mathcal{F}\Big(\alpha_1\delta(t) + \alpha_2\delta(t - \tau_d)\Big) \\ &= \alpha_1 + \alpha_2 e^{-j2\pi\tau_d f} \end{aligned} \tag{3.75}$$

Suppose that the attenuation in the channel is only caused by the multipath transmission, in other words, the power loss in the channel will not be considered, so that

the total channel power gain is $G = 1$, we get $\alpha_1^2 + \alpha_2^2 = 1$. Hence, in case of equal attenuation, i.e., $\alpha_1^2 = \alpha_2^2 = 1/2$, the magnitude of the frequency response of the two-ray multipath channel model in equation (3.75) can be derived as $|H_p(f)|^2 = 1+\cos(2\pi\tau_d f)$, which is illustrated in Figure 3.15.

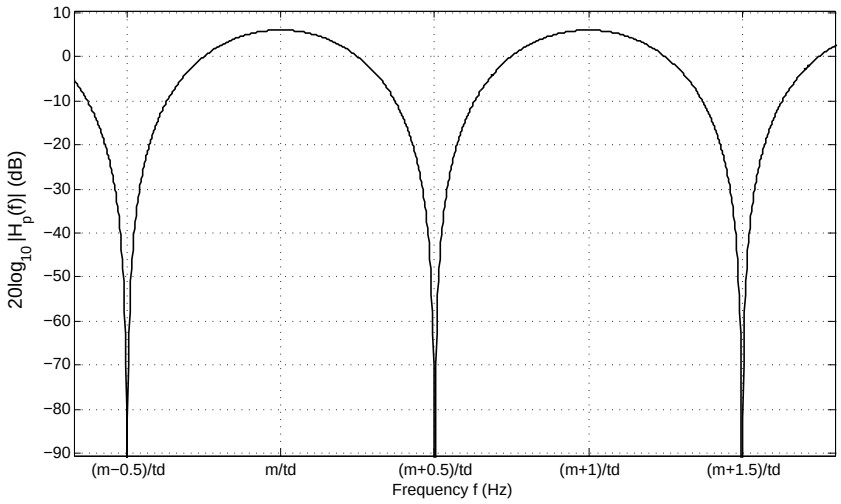

Figure 3.15: Magnitude of frequency response of the two-ray multipath channel model with equal attenuation $\alpha_1^2 = \alpha_2^2 = 1/2$.

The frequency response of the equal attenuation two-ray multipath channel shows intuitively the multipath-related nulls caused by the cancellation (destructively add) between two paths, locating in the equally spaced frequency points

$$f_{\text{null},p} = \frac{2m-1}{2\tau_d}, \quad m \in \mathbb{N} \tag{3.76}$$

where the attenuation becomes infinitely large [72], and the distance between two mulipath-related nulls is

$$\Delta f_{\text{null},p} = \frac{1}{\tau_d} \tag{3.77}$$

In contrary, the multipath related maximal gains caused by the constructively add between two paths can also be observed in the channel frequency response, locating in $f_{\text{maxgain}} = m/\tau_d$ $(m \in \mathbb{N})$.

For the narrow-band communication systems, the worst case in the two-ray multipath channel is that when the channel has equal attenuation, and the parts of the

signal energy distributed in the two paths cancel each other completely on the carrier frequency, i.e., $f_c = (m - 1/2)/\tau_d$ ($m \in \mathbb{N}$).

As long as the analysis in the baseband is concerned, the equivalent baseband model of the two-ray multipath channel can be derived from equation (3.71) and (3.74) as

$$r(t) = \alpha_1 s(t) + \alpha_2 e^{-j2\pi f_c \tau_d} s(t - \tau_d) \tag{3.78}$$

Similarly, the channel frequency response in the equivalent baseband can also be derived, i.e.,

$$H(f) = \alpha_1 + \alpha_2 e^{-j2\pi\tau_d(f+f_c)} \tag{3.79}$$

In case of equal attenuation, the equivalent multipath-related nulls in the baseband

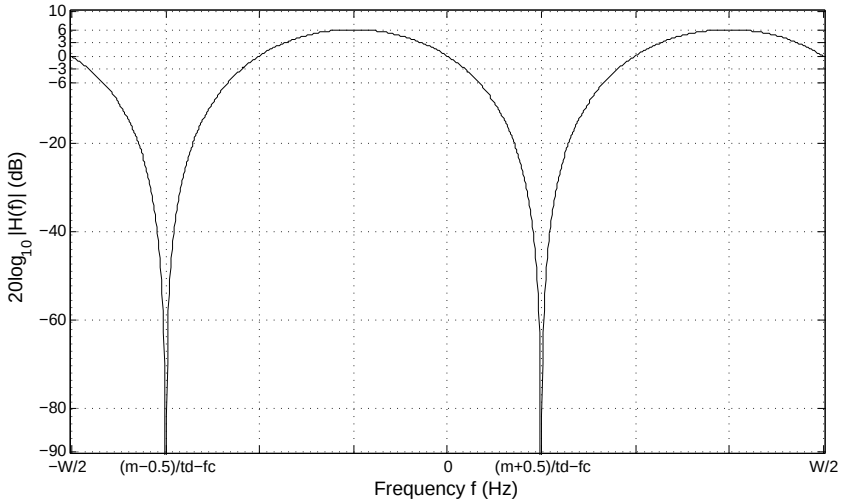

Figure 3.16: Magnitude of frequency response of the two-ray multipath channel model in the equivalent baseband, with equal attenuation $\alpha_1^2 = \alpha_2^2 = 1/2$.

locates in the following equally spaced frequency points

$$f_{\text{null}} = \frac{2m-1}{2\tau_d} - f_c, \quad m \in \mathbb{R} \tag{3.80}$$

which can be illustrated as in Figure 3.16. The distance between two multipath-related nulls is

$$\Delta f_{\text{null}} = \frac{1}{\tau_d} \tag{3.81}$$

and the number of multipath-related nulls in the baseband $[-W/2, W/2]$ could be $\lceil W\tau_d \rceil$ or $\lfloor W\tau_d \rfloor$.

Similarly, the discrete-time baseband equivalent model of the two-ray channel can be derived from equation (3.72) as

$$\begin{aligned} r[n] &= \sum_{\ell} \Big(\alpha_1 \text{sinc}[\ell] + \alpha_2 e^{-j2\pi f_c \tau_d} \text{sinc}[\ell - \tau_d W] \Big) s[n-\ell] \\ &= \alpha_1 s[n] + \alpha_2 e^{-j2\pi f_c \tau_d} \sum_{\ell} \text{sinc}[\ell - \tau_d W] s[n-\ell] \end{aligned} \tag{3.82}$$

3.3.4.2 Qualitative Multipath Performance of CCASK in the Two-Ray Channel

The spread spectrum systems usually possess a large RF band around the center frequency, so that at least part of the spectrum doesn't locate in the multipath-related nulls of the channel frequency response in Figure 3.15. Hence, the spread spectrum systems are often considered to outperform the narrowband systems under the multipath channel models.

Since that CCASK utilizes a spectral or spectrum-determined (e.g., auto-correlation and variance) detection in baseband, its performance in the two-ray channel model can be qualitatively evaluated by the spectrum attenuation of the received signal in baseband. Let's take an applicable scenario to quantify the attenuation. Suppose that CCASK is implemented in one of the three channels in the 2.4 GHz *industrial, scientific and medical* (ISM) band [73][72], with $f_c \in [2.400, 2.412]$ GHz, $W = 17$ MHz. As reported in reference [73], the typical values of propagation delay for the applications in this band are $\tau_d = 91$ ns for large warehouses and $\tau_d = 75$ ns for office buildings, hence, $\Delta f_{\text{null}} = 10.989$ MHz for large warehouses and $\Delta f_{\text{null}} = 13.333$ MHz for office buildings. In both environments, there could be only one or two multipath-related nulls in the band.

Let's consider the environment of office buildings. The frequency response of the equal attenuation two-ray multipath channel in the equivalent baseband with $\tau_d = 75$ ns can be illustrated in Figure 3.17, which the RF center frequency equals to 2.4 GHz, 2.406 GHz and 2.412 GHz respectively. The channel frequency response shows that the power attenuation for a transmitted signal with a flat spread spectrum varies for

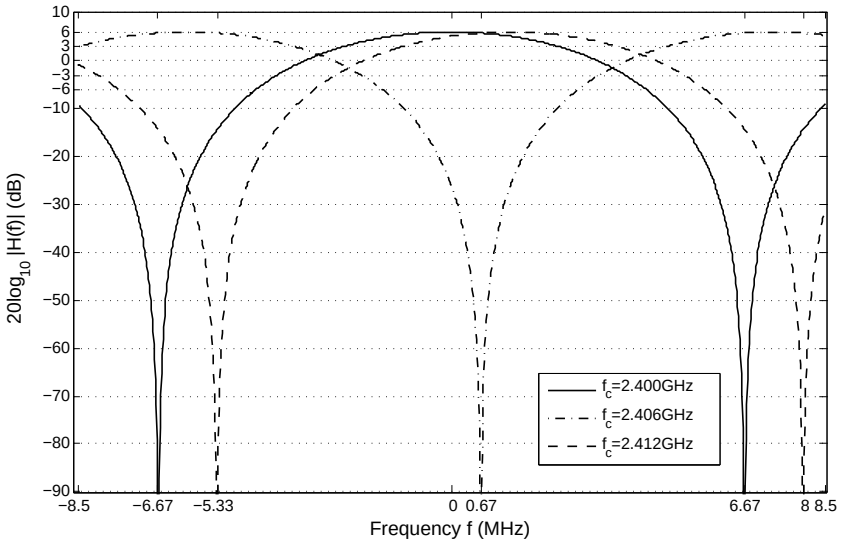

Figure 3.17: Magnitude of frequency response of the equal attenuation two-ray multipath channel model in the equivalent baseband of the 2.4 GHz ISM band, with propagation delay $\tau_d = 75$ ns, and RF center frequency $f_c = 2.4$ GHz, 2.406 GHz, 2.412 GHz.

different value of f_c: if the 10dB bandwidth is considered, the most attenuation happens when f_c=2.4 GHz.

However, for the same RF band, if the propagation delay is reduced to $\tau_d = 50$ ns, there could be only zero or one multipath-related null. The corresponding frequency response of the equal attenuation two-ray multipath channel in the equivalent baseband is illustrated in Figure 3.18, which the RF center frequency equals to 2.4 GHz, 2.406 GHz and 2.410 GHz respectively. In this case, when f_c=2.4 GHz, there exists the least spectrum attenuation, while the most attenuation happens when f_c=2.410 GHz.

Generally speaking, the worst case for a signal with a flat spread spectrum in baseband $[-W/2, W/2]$ transmitted in the two-ray multipath channel with the propagation delay τ_d is that, the attenuation of both rays have equal value, and the value of centered frequency f_c makes $\lceil W\tau_d \rceil$ number of multipath-related nulls locating in the baseband, and the nulls are symmetric. Hence, $\lceil W\tau_d \rceil$ is even, such as the situation in Figure 3.17, the worst case happens if $\cos(2\pi f_c \tau_d) = 1$, i.e., $f_c = m/\tau_d$ ($m \in \mathbb{N}$); or else, if $\lceil W\tau_d \rceil$ is odd, the worst case is that when $\cos(2\pi f_c \tau_d) = -1$, i.e., $f_c = (m - 0.5)/\tau_d$ ($m \in \mathbb{N}$). Furthermore, it can be observed from Figure 3.17-3.18 that, the smaller τ_d a

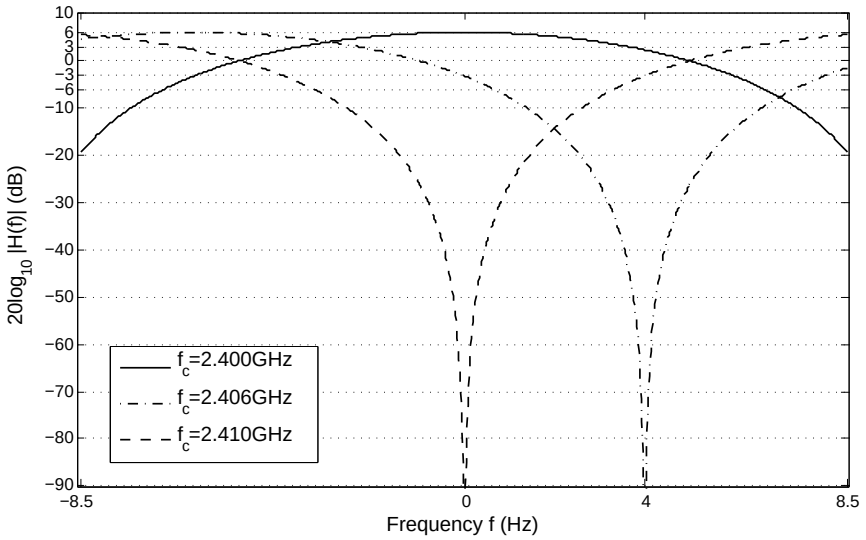

Figure 3.18: Magnitude of frequency response of the equal attenuation two-ray multipath channel model in the equivalent baseband of the 2.4 GHz ISM band, with propagation delay $\tau_d = 50$ ns, and RF center frequency $f_c = 2.4$ GHz, 2.406 GHz, 2.412 GHz.

channel has, the more energy a transmitted flat spread spectrum signal could lose.

Although a CCA signal is not strictly a flat spread spectrum, its spectrum is indeed spread, with the energy distributed in lots of frequency points equally located in the baseband. We expect that the total spectrum attenuation of a CCA signal is not worse than a signal with strictly flat spread spectrum, at least in some particular application environments.

Take the CCAs generated by system (2.1) for example. The comparison of the spectra between the equivalent baseband signal generated by the enhanced CCA-31 and the received signal after transmitting in the channel with f_c=2.4 GHz in Figure 3.17 is given in Figure 3.19.(a). The spectra comparison of the transmitted and received signal of the similar CCA-29 is also given in Figure 3.19.(b). It can be obtained from both comparisons that, although the magnitudes of several main frequency points are deeply attenuated because of the deconstructive add of the signal components of two rays, the magnitudes of several other main frequency points increase thanks for the constructive add. We expect that the total loss in energy is tiny, and the performance loss is still acceptable for certain applications.

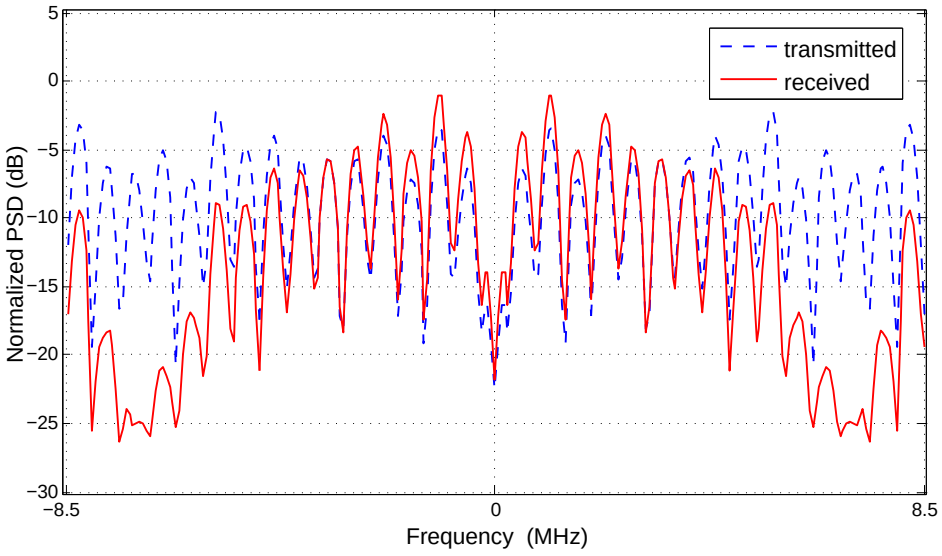

(a)

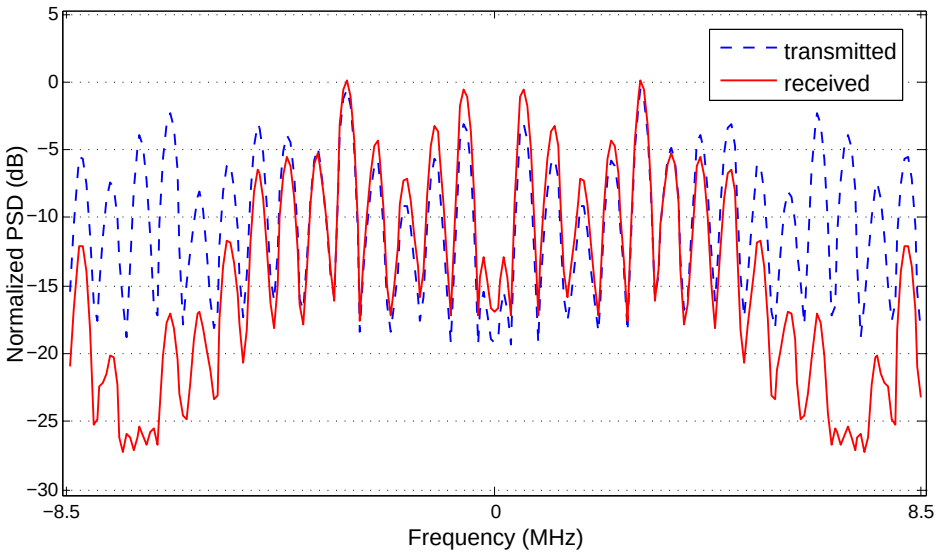

(b)

Figure 3.19: Spectra of the transmitted and received baseband signal of enhanced CCA-q of system (2.1) through the equal-attenuation two-ray channel model in Figure 3.17 with f_c=2.4 GHz, and (a) q=31, (b) q=29.

3.3.4.3 Quantitative Multipath Performance of CCASK in the Two-Ray Channel

In order to quantify the multipath performance, the channel model under certain environment parameters are required, such as RF band W, center frequency f_c, as well as the propagation delay τ_d. We have realized the matlab simulation using the discrete-time baseband equivalent two-ray multipath channel model in equation (3.82), with different power gain on two rays, i.e., equal power gain $\alpha_1^2 = \alpha_2^2 = 1/2$ and 10dB difference power gain $\alpha_1^2 = 10/11, \alpha_2^2 = 1/11$. The environment parameters are chosen to fit the 2.4 GHz ISM band, with RF bandwidth $W = 17$ MHz (sampling rate $T_s = 1/W$), and $\tau_d = 75$ ns for office buildings application. The center frequency f_c varies from 2.4 GHz to 2.412 GHz in step of 3 MHz.

The binary CCASK is designed using the enhanced CCA-31 and CCA-29 of system (2.1), and the modulated symbols are transmitted through the above designed multipath channels, in which the additive Gaussian noise is added with the same amount as in the AWGN channel without multipath. The number of samples per symbol is chosen to be L=400, as we have discussed in Section 3.3.3.3 that CCASK performs better than DCSK when L is large. In this case, the symbol duration is $T = L/W = 23.5\mu$s, hence, the data transmission rate is 42.6 kbps.

For each realization, a Monte-Carlo simulation is operated using the spectral detection, with 10^6 symbols transmitted through 10^4 i.i.d. channels. For comparison, the simulations of DCSK in the same channels are also done, using the chaotic signals generated by the logistic map $g(x) = 4x(1-x)$ as introduced in Section 1.2.1, with the same configuration on the symbol design (symbol duration, sampling rate, etc.).

The simulation result of the noise performance of CCASK and DCSK in the two-ray multipath channel, with both equal power gain and unequal power gain with 10dB difference, are illustrated in Figure 3.20, together with their AWGN performance without multipath. From the comparison, we can see that the worst case for both CCASK and DCSK is when f_c=2.4 GHz, which corresponds with the qualitative analysis in the above sub-section. The worst performance loss is about 2dB for CCASK and 2.5dB for DCSK in the two-ray multipath channel with equal power gain, and still 0.5dB less for both systems in case of unequal gain with 10dB difference. This result shows that CCASK can have a good multipath performance just as the other spread spectrum systems in certain indoor application environments.

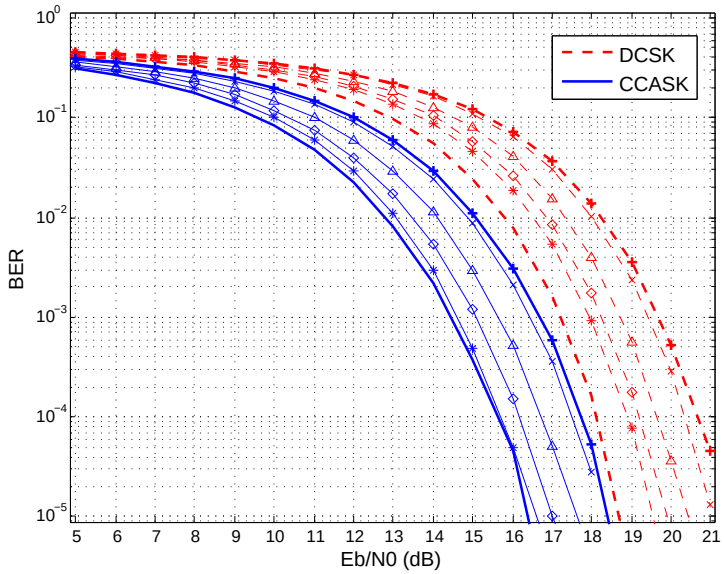

(a)

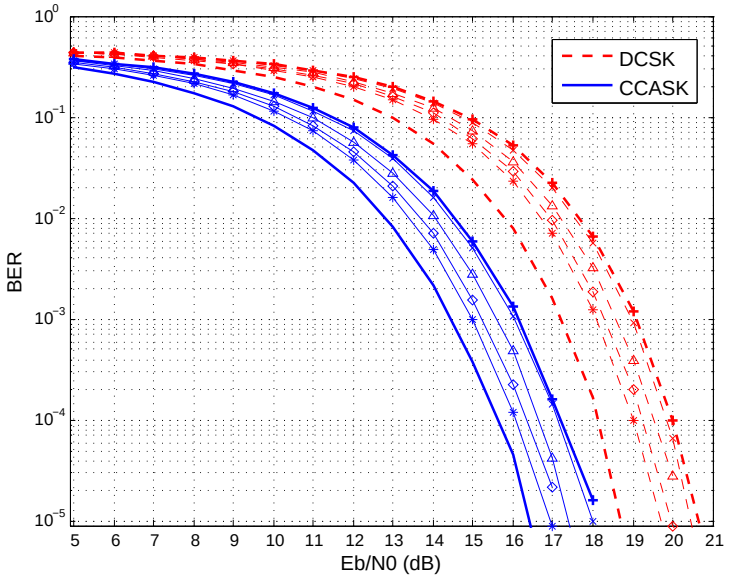

(b)

Figure 3.20: Noise performance of CCASK and DCSK in the two-ray channel model with: (a) equal power gain; (b) unequal power gain with 10dB difference. The channel parameter is: τ_d=75ns, W=17MHz, and the value of f_c differed by forms: 2.4 GHz (+), 2.403 GHz ($\triangle$), 2.406 GHz ($*$), 2.409 GHz ($\Diamond$) 2.4012 GHz ($\times$). For comparison, the AWGN performance without multipath is also given (lines without form).

3.4 CCAFSK: A Frequency Shift Keying Utilizing CCA

In binary CCASK, the spectrum of CCA-q_v ($v \in \{0, 1\}$) with coprime periods is quasi-orthogonal to each other thanks for the comb-like spectral distribution differed by q_v. However, the considered detections are not strictly antipodal for different symbols. Take the spectral detection of binary CCASK for example. Most of the bit energy is collected either from the observed q_0 frequency points using q_0-point DFT, or from the observed q_1 frequency points using q_1-point DFT, depending on which data symbol was transmitted. **Most of the bit energy** means how much? The proportion can't be quantified precisely. In fact, it is determined by the specific trajectory of CCA-q_v in the phase plane, hence not possible to be guaranteed identical between different q_v. The similar situation also exists for the other two detection methods. Hence, the not exactly antipodal observing variables, such as C_{m_b}, D_{m_b} and V_{m_b}, which are detected by a '0' threshold, lead to the not optimal performance.

Undoubtedly, if only one CCA generator is used for each user, the above considered shortcoming will disappear. Since all the detections of CCASK discussed in Section 3.3 utilize the specific properties of CCA-q_v differed by q_v, these detections can't function anymore if the same CCA is taken for different data symbols. Hence, some new parameters which could differ the data symbols should be introduced to the modulation. Here comes an example to generate frequency quasi-orthogonal signals by only one CCA generator.

Suppose that a CCA-q is considered with q being odd. As discussed in Section 2.3.2, the signal sequence $\mathbf{x} = (x_1, x_2, ..., x_L)$ of CCA-q owns a comb-like spectral distribution with q equally spaced main angular frequencies locating in $\{\frac{W}{q}2\pi, \frac{2W}{q}2\pi, ..., 2\pi\}$, and the power distributed on them can be simply obtained by a q-point DFT. In other words, if the sequence of CCA-q is transformed by a $2q$-point DFT, we can get

$$X[K] = \sum_{n=1}^{L} x_n e^{-j2\pi\frac{K}{2q}n}, \qquad K \in [1, 2q] \tag{3.83}$$

Let's define $|X[K]|$ as the even index spectrum magnitude if $K = 2K_1$ ($K_1 \in [1, q]$), as well as the odd index spectrum magnitude if $K = 2K_1 - 1$ for the $2q$-point DFT. Hence, the even index spectrum magnitudes of CCA-q are relatively large compared to the odd index spectrum magnitudes.

On the other side, a signal sequence $\breve{\mathbf{x}} = (\breve{x}_1,\ \breve{x}_2, ...,\ \breve{x}_L)$ can be created from the CCA-q signal sequence $\mathbf{x}$ by changing the sign of each second x_n as

$$\begin{aligned}\breve{x}_n &= (-1)^n x_n \\ &= \begin{cases} x_n, & n \text{ is even} \\ -x_n, & n \text{ is odd} \end{cases}\end{aligned} \tag{3.84}$$

Define this operation as **second-sign-changing**, hence, $\breve{\mathbf{x}}$ is a signal sequence of second-sign-changed CCA-q. Transforming $\breve{\mathbf{x}}$ also by a $2q$-point DFT to get

$$\breve{X}[K] = \sum_{n=1}^{L} \breve{x}_n e^{-j2\pi \frac{K}{2q} n}, \qquad K \in \{1, 2, ..., 2q\} \tag{3.85}$$

Therefore, the relationship between the $2q$-point DFT of the original sequence $\mathbf{x}$ and the second-sign-changed sequence $\breve{\mathbf{x}}$ can be derived as

$$\begin{aligned}\breve{X}[K] &= \sum_{n=1}^{L} (-1)^n x_n e^{-j2\pi \frac{K}{2q} n} \\ &= \sum_{n=1}^{L} e^{jn\pi} x_n e^{-j2\pi \frac{K}{2q} n} \\ &= \sum_{n=1}^{L} x_n e^{-j2\pi \frac{K-q}{2q} n} \\ &= X[K - q \bmod q] \\ &= \begin{cases} X[K+q], & \text{if } K \in [1, q] \\ X[K-q], & \text{if } K \in [q+1, 2q] \end{cases}\end{aligned} \tag{3.86}$$

where $K \in [1, 2q]$. It's known that in case of q being odd, $K \pm q$ is odd when K is even with $K = 2K_1$ ($K_1 \in [1, q]$), while $K \pm q$ is even when K is odd with $K = 2K_1 - 1$. Hence, the even index spectrum magnitudes of $\breve{\mathbf{x}}$ correspond to the odd index spectrum magnitudes of $\mathbf{x}$; and conversely, the odd index spectrum magnitudes of $\breve{\mathbf{x}}$ correspond to the even index spectrum magnitudes of $\mathbf{x}$.

Therefore, the signal sequence of the original CCA-q and the signal sequence of the second-sign-changed CCA-q are quasi-orthogonal in the frequency domain, with the quasi-orthogonality defined as: one has the dominant even index spectrum magnitudes, while the other has the dominant odd index spectrum magnitudes, and both dominant parts own an antipodal proportion.

Take the enhanced CCA-31 in Figure 2.19 for example, the magnitudes of 62-point DFT of both original and second-sign-changed signal sequences are illustrated in

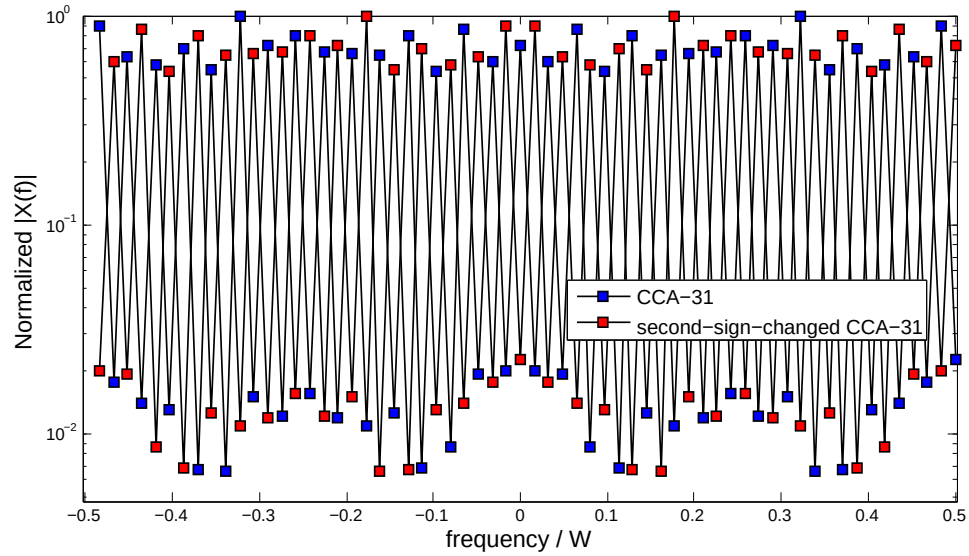

(a)

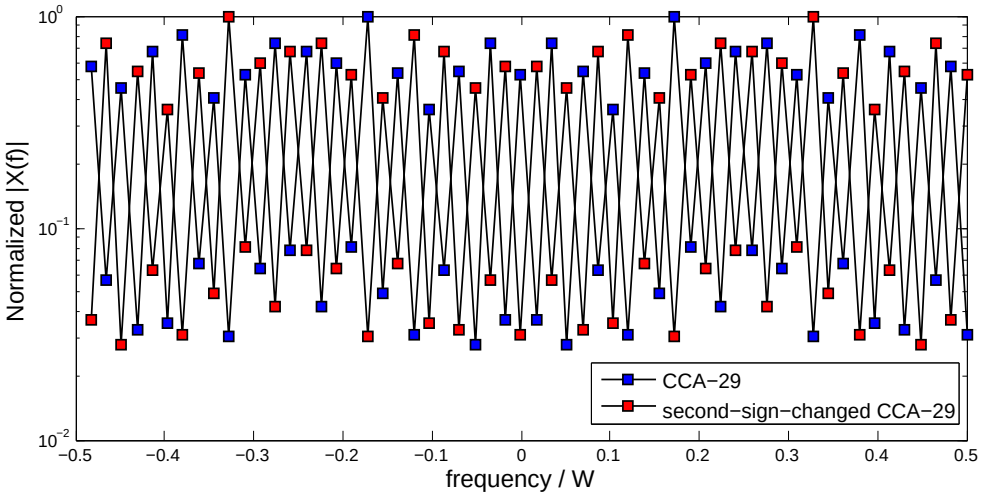

(b)

Figure 3.21: Normalized magnitude of $2q$-point DFT of both the original (blue square) and second-sign-changed (red square) signals of the enhanced CCA-q of system (2.1) with (a) q=31, (b) q=29. PSD are carried out for the sequences with length $L = 10^4$.

Figure 3.21.(a), where the quasi-orthogonality can be observed clearly. Similar spectral distributions can be found after the 58-point DFT for the sequence of the enhanced CCA-29 of system (2.1), as shown in Figure 3.21.(b).

This quasi-orthgonal spectral distributions between the original signal and second-sign-changed signal of CCA-q will be applied in another CCA-based modulation system: *chaotic cyclic attractors frequency-shift keying* (CCAFSK). CCAFSK is concerned with mapping data symbols of one user to the chaotic waveforms generated by the CCA-q generator, while the data symbols are differed by operating or not operating the second-sign-changing on the iterations, hence, differed by the quasi-orthogonal spectra. The demodulation of CCAFSK could be realized by applying $2q$-point DFT on the received symbols.

As long as multiplexing is considered, CCAs of different periods can be allocated for different users, with the periods coprime to each other.

3.4.1 Modulation Scheme of CCAFSK

In the simplest case of binary CCAFSK, two basis signals generated by one CCA-q generator with two different sign-changing operations are needed: the original signal and the second-sign-changed signal. Remind that the original signal generated by the CCA-q generator is $x(t) = \sum_n x_n \text{sinc}(Wt - n)$, hence the second-sign-changed signal $\breve{x}(t)$ can be presented by

$$\begin{aligned} \breve{x}(t) &= \sum_n (-1)^n x_n \text{sinc}(Wt - n) \\ &= x(t)\tilde{u}(t) \end{aligned} \tag{3.87}$$

in which $\breve{x}(n/W) = (-1)^n x_n$ is the value of the sample at the sampling instant n/W, and $\tilde{u}(t)$ is the square wave:

$$\tilde{u}(t) = \sum_n (-1)^n \sqcap (t - nT_s) \tag{3.88}$$

with $\sqcap(t)$ denoting the rectangular function.

Suppose that the basis function for modulating data symbol '0' is $x(t)$, while the basis function for modulating data symbol '1' is $\breve{x}(t)$. Then, the modulated symbols in the baseband can be derived as

$$s(t) = \sum_m \sum_{n=1}^{L} \Big(d_m x_{mL+n} + (1 - d_m)\breve{x}_{mL+n} \Big) \text{sinc}(Wt - (mL + n)) \tag{3.89}$$

where $d_m \in \{0, 1\}$ denotes the m^{th} data symbol.

The equivalent sampled sequence of the m^{th} modulated symbol $s(t)$ ($t \in [mT, (m+1)T]$) can be denoted as $\mathbf{s}_m = (s_m[1], s_m[2], ..., s_m[L])$, with

$$s_m[n] = s(mT + nT_s), \quad n \in \{1, 2, ..., L\} \tag{3.90}$$

hence, $s_m[n] = x_{mL+n}$ if a data symbol $d_m = 1$ is transmitted, and $s_m[n] = \breve{x}_{mL+n}$ if a data symbol $d_m = 0$ is transmitted.

The diagram of baseband modulation in binary CCAFSK transmitter is illustrated in Figure 3.22.

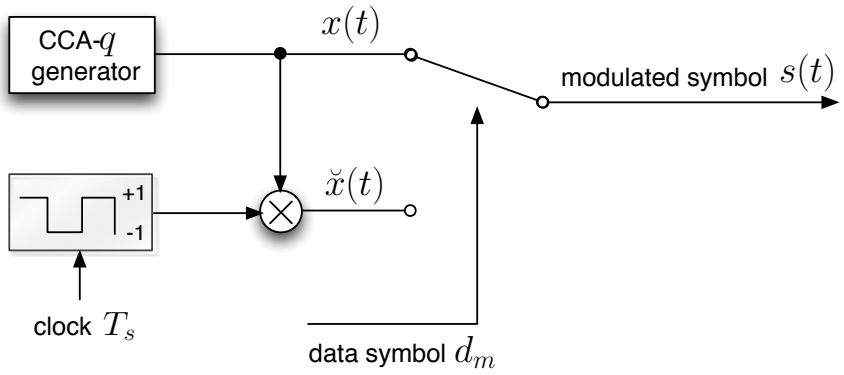

Figure 3.22: Modulation structure in binary CCAFSK transmitter.

3.4.2 Demodulation Scheme of CCAFSK

According to the introduced quasi-orthogonality in spectrum of the original signal and second-sign-changed signal of CCA-q, a noncoherent detection can be realized for CCAFSK using $2q$-point DFT. As in the demodulation scheme of CCASK, we consider the passband carrier removed signal of the m^{th} received symbol $r(t)$ ($t \in [mT, (m+1)T]$) in the demodulation, the sampled sequence of which is $\mathbf{r}_m = (r_m[1],\ r_m[2],\ ...,\ r_m[L])$, with $r_m[n] = r(mT + nT_s)$ ($n \in \{1, 2, ..., L\}$). Therefore, the detection will be realized in the discrete-time domain.

In case of single user application so that the interference from the other users doesn't exist, if the transmission channel is noise and distortion free, as well as the ideal transmitting and receiving antennas are applied, we can get $r_m[n] = s_m[n]$; or

else, $r_m[n]$ differs from $s_m[n]$, and can be presented by its in-phase and quadrature components as $r_m[n] = r_{m,I}[n] + jr_{m,Q}[n]$.

Similarly to the spectral detection of CCASK, the detection of binary CCAFSK relies on the comb-like frequency distribution of each received symbol. Through applying $2q$-point DFT on the sampled sequence $\mathbf{r}_m$, the magnitudes of the observing frequencies can be easily obtained by:

$$A_m[K] = \Big| \sum_{n=1}^{L} r_m(n) e^{-j2\pi \frac{K}{2q} n} \Big| \tag{3.91}$$

where $K \in \{1, 2, ..., 2q\}$.

According to the discussion in the beginning of this section, in the ideal case that $\mathbf{r}_m = \mathbf{s}_m$, if a '0' was transmitted, the even index spectrum magnitudes $A_m[2K_1]$ ($K_1 = 1, 2, ..., q$) have relative large values compared to the odd index spectrum magnitudes $A_m[2K_1 - 1]$; in contrary, if an '1' was transmitted, the odd ones have relative large values compared to the even ones. Hence, in a tolerably noisy and/or distortional channel, the decision variable for the m^{th} received symbol could simply be the difference between the mean squared value of $A_m[2K_1-1]$ and the mean squared value of $A_m[2K_1]$, denoted as

$$B_{b_m} = \frac{1}{q} \sum_{K_1=1}^{q} \Big(A_m^2[2K_1 - 1] - A_m^2[2K_1] \Big) \tag{3.92}$$

Consequently, the demodulated data symbol $\hat{d}_m$ can be represented as follows:

$$\hat{d}_m = \begin{cases} 1, & \text{if } B_{b_m} \geq 0 \\ 0, & \text{if } B_{b_m} < 0 \end{cases} \tag{3.93}$$

The structure of the baseband demodulation in binary CCAFSK receiver can be designed as shown in Figure 3.23.

3.4.3 AWGN Performance of CCAFSK

In this section, the AWGN performance of binary CCAFSK in case of single-user and multi-user applications will be given. The single-user noise performance will be analyzed as well as simulated, while the multi-user noise performance will be given only by simulation. The comparison of AWGN performance between CCAFSK and CCASK, as well as between CCAFSK and DCSK will also be discussed.

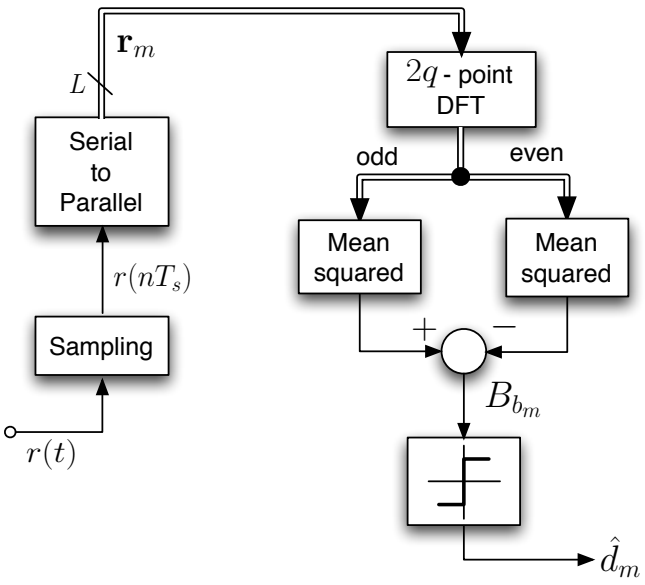

Figure 3.23: Demodulation structure in binary CCAFSK receiver.

A. AWGN Performance Evaluation in Single User Application

The AWGN noise performance of binary CCAFSK is a function of the expectation and variance of the detection variable B_{b_m}. The detail of the performance analysis in case of single user is given in Appendix B, with the result of the general expression of BER performance obtained as

$$\begin{aligned}\mathrm{BER}_{\mathrm{CCAFSK}} = \frac{1}{4}\sum_{i=0}^{1}\mathrm{erfc}\Bigg[\Bigg(&\frac{2(4L^2+16Lq+15q^2)}{3(L-q)(L+q)^2}\frac{\langle\mu^2\delta^2\rangle}{\langle\mu^2\rangle^2}+\frac{8q}{(L^2-q^2)}\frac{\langle\delta^4\rangle}{\langle\mu^2\rangle^2}\\&+\Big(\frac{4(4L^2+4Lq+3q^2)}{3(L-q)(L+q)^2}\frac{\langle\mu^2\rangle}{\langle\mu^2\rangle^2}+\frac{16q}{(L^2-q^2)}\frac{\langle\delta^2\rangle}{\langle\mu^2\rangle^2}\Big)\sigma^2\\&+\frac{8q}{(L^2-q^2)}\frac{\sigma^4}{\langle\mu^2\rangle^2}\Bigg)^{-\frac{1}{2}}\Bigg]\end{aligned} \tag{3.94}$$

which depends on the noise spectral density σ^2, the symbol modulation rate L, the period q of the taken CCA, as well as the specific statistics of the CCA as defined in Section 3.3.3.

Hence, the analytic-numerical AWGN performance of CCAFSK is a function of L and E_b/N_0 for a given CCA, i.e., the period q as well as the statistics are fixed.

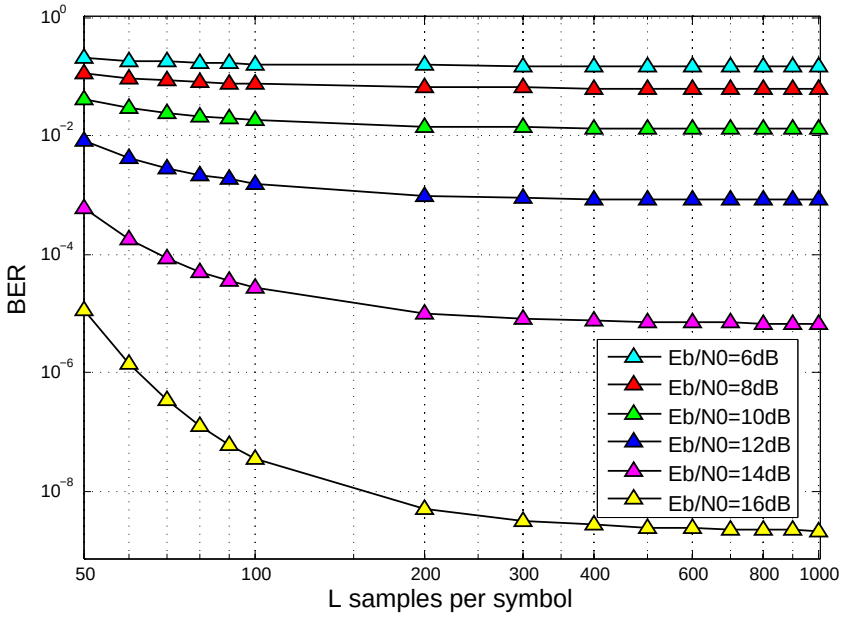

Figure 3.24: Analytic-numerical AWGN performance of binary CCAFSK versus the number of samples per symbol L, when the statistics of the enhanced CCA-29 of system (2.1) are considered.

For example, when the statistics of CCA-29 in Table 3.2 are considered, the analytic-numerical BER of CCAFSK versus L corresponding to certain E_b/N_0 is illustrated in Figure 3.24. The result shows that, the AWGN performance of CCAFSK firstly aemliorates with the increase of the number of samples per symbol L when $L < 200$ is small; and the performance keeps more or less constant when $L > 200$. This analytic-numerical AWGN performance of CCAFSK with $L = 100$ and $L = 400$ is illustrated in Figure 3.25.

The Monte-Carlo simulation of single user binary CCAFSK using the enhanced CCA-29 of system (2.1) are also done, and the pure numerical results with $L = 100$ and $L = 400$ are illustrated in Figure 3.25, each of which is obtained by 10^6 symbols transmitted through 10^4 i.i.d. AWGN channels. The results show a good correspondence between the analytic-numerical and pure numerical results.

Furthermore, based on the analytical expression in equation (3.94), the AWGN performance of CCAFSK can also be approximated to a certain degree if the statistics of

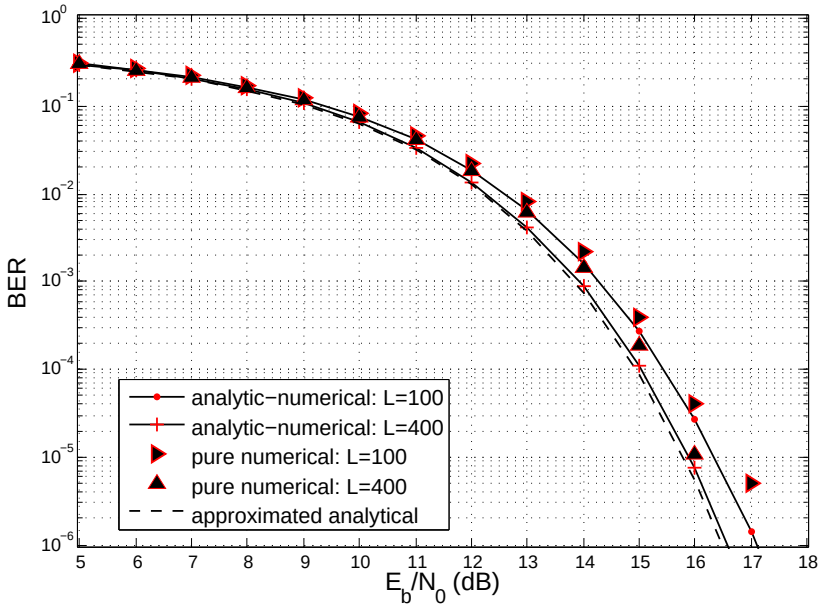

Figure 3.25: Analytic-numerical AWGN performance of binary CCAFSK using the enhanced CCA-29 of system (2.1), with $L = 100$ and $L = 400$, compared to the approximated analytical and pure numerical results under the same conditions.

CCA are not acknowledged. Appendix B gives a method to approximate the performance under the conditions of relative large number of samples per symbol, i.e., $L \gg q$, and relative small zones of CCAs, with a simple expression as:

$$\mathrm{BER}_{\mathrm{CCAFSK}} \approx \frac{1}{2}\mathrm{erfc}\left[\left(\frac{8}{3}\frac{N_0}{E_b} + 2q\frac{N_0^2}{E_b^2}\right)^{-\frac{1}{2}}\right] \tag{3.95}$$

Though this approximated analytical performance doesn't depend on L, the comparison between it and the above mentioned analytic-numerical result has sense only if L is large enough. The approximated analytical result with $q = 29$ is also illustrated in Figure 3.25 for comparison. Since the analytic-numerical results in Figure 3.24 shows that the noise performance of CCAFSK keeps constant when $L > 200$, the approximated analytical result in Figure 3.25 is a good approximation of the optimal performance of CCAFSK.

B. AWGN Performance Evaluation in Dual-User Application

It's mentioned in the beginning of Section 3.4 that the multiplexing of CCAFSK can be realized simply by allocating coprime periods of CCAs to different users. Since

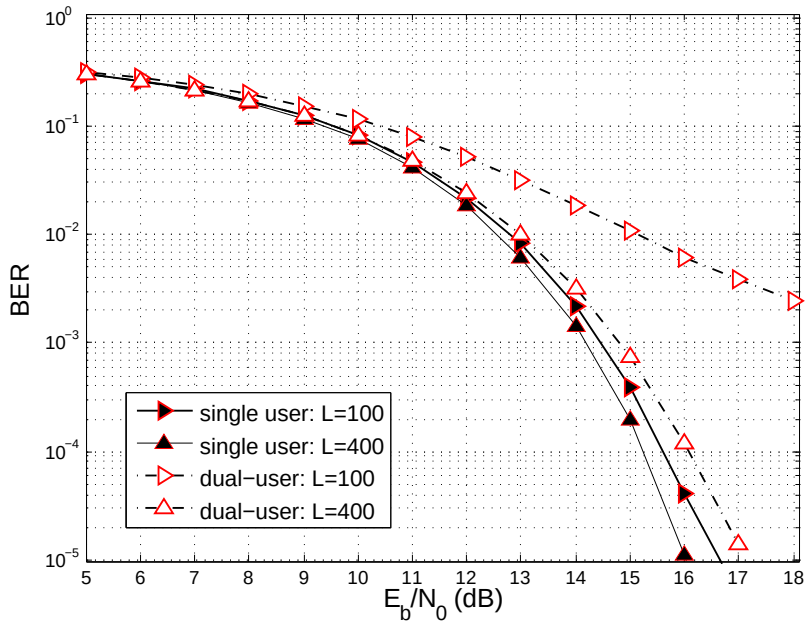

Figure 3.26: Comparison of AWGN performance of CCAFSK using CCA-29 between single user and dual-user cases, with $L = 100$ and $L = 400$ respectively. The CCA-31 generator is used for the modulation of the interference user.

the spectra of signals of CCAs of coprime periods are quasi-orthogonal as discussed in Section 2.3, generally speaking, the multi-user interference won't make the performance much worse, just as the other multiplexing systems.

In order to quantify the multiple-access performance of CCAFSK, a Monte-Carlo simulation of dual-user CCAFSK is operated, using the enhanced CCA-29 of system (2.1) for user-1, and the similar CCA-31 for user-2. 10^6 independent symbols of each user are transmitted simultaneously through 10^4 i.i.d. AWGN channels, and the result is illustrated in Figure 3.26 with $L = 100$ and $L = 400$, together with the single user performance under the same conditions. From the comparison, we can see that CCAFSK can prevent the interference from the other users when number of samples per

symbol L is large, with only little loss in BER performance; however, with the decrease of the value of L, the multi-user interference can make the detection very difficult.

C. AWGN Performance Comparison between CCAFSK and CCASK

In order to better compare the AWGN performance of CCASK and CCAFSK, part

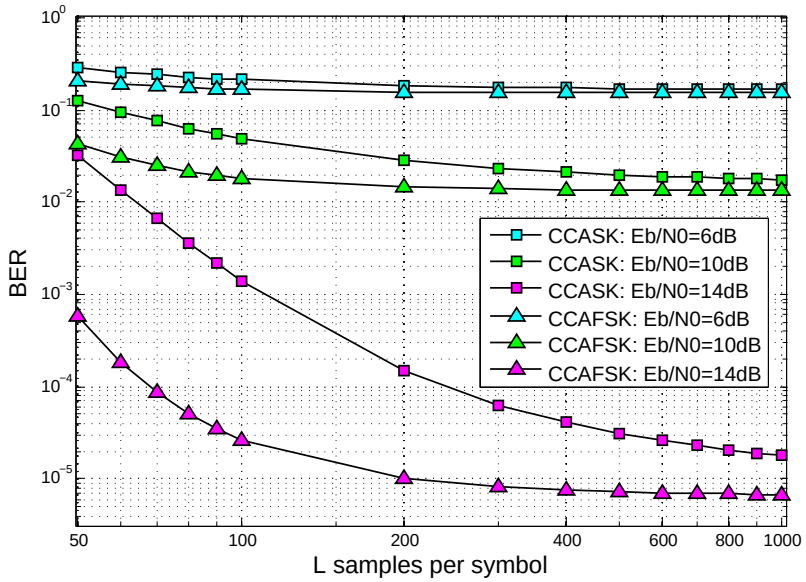

Figure 3.27: Comparison of performance versus L between CCASK using CCA-31 and CCA-29 and spectral detection, and CCAFSK using CCA-29.

of the performance in Figure 3.7 and Figure 3.24 are illustrated together in Figure 3.27. From the comparison, we can see clearly the performance gain of CCAFSK over CCASK, which diminishes with the increase of the value of L. For example, the performance of CCASK with $L = 700$ can be obtained by CCAFSK with $L = 100$. It means that, CCAFSK is more efficiency than CCASK when certain BER is required, since the former needs smaller number of samples per symbol compared with the latter.

D. AWGN Performance Comparison between CCAFSK and DCSK

Similarly, in order to better compare the AWGN performance of DCSK and CCAFSK, part of the performance in Figure 3.11 and Figure 3.24 are illustrated together in Figure

3.28. We can see that in the AWGN channel with E_b/N_0 <14dB, CCAFSK outperforms

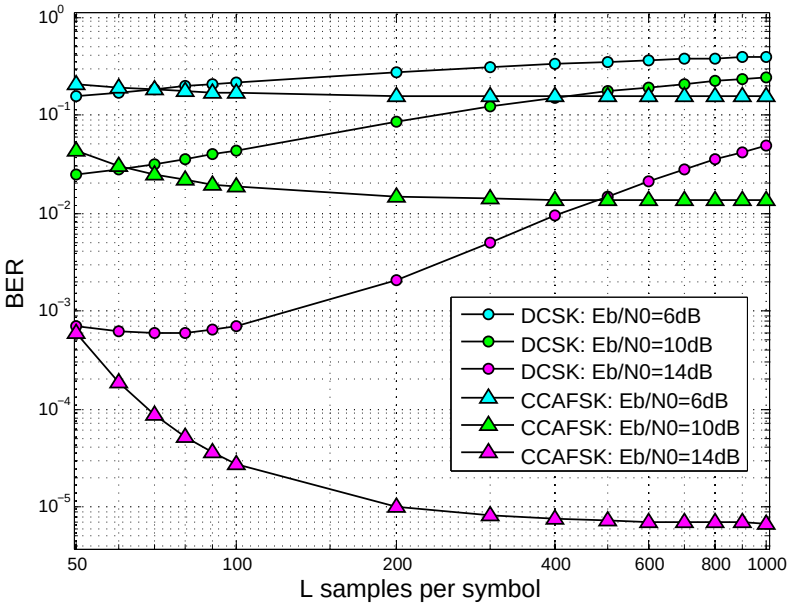

Figure 3.28: Comparison of AWGN performance of DCSK and CCASK versus the number of samples per symbol L.

DCSK when $L > 50$, and the gain of CCAFSK over DCSK increases with the increase of L.

The theoretical AWGN performance of DCSK and the analytic-numerical performance of CCAFSK with $L = 100$ and $L = 400$ are illustrated respectively in Figure 3.29. It shows that when BER is 10^{-4}, CCAFSK has an improvement of about 2dB compared with DCSK in case of $L = 100$, and an improvement of about 3.5dB in case of $L = 400$. Hence, CCAFSK has better AWGN performance in the low-rate wideband applications.

3.4.4 Multipath Performance of CCAFSK

The quantitative multipath performance in Section 3.3.4.2 is analyzed generally and roughly for the CCA-based systems. Indeed, it's an advantage that shared by all the spread spectrum systems. Since both CCASK and CCAFSK are CCA-based systems using spectral detection, both of them should possess a similar multipath performance,

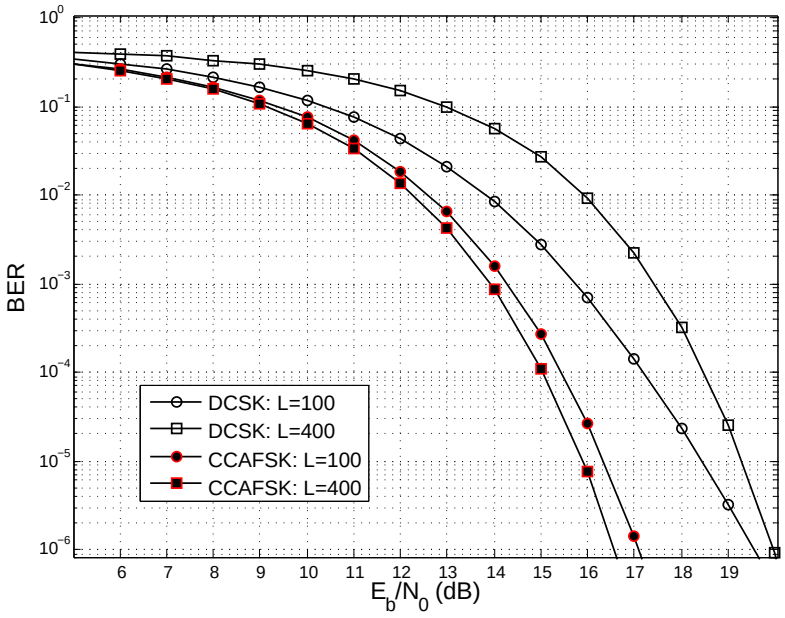

Figure 3.29: Comparison of AWGN performance of DCSK and CCAFSK with $L = 100$ and $L = 400$ respectively.

or a comparable performance loss compared with their AWGN performance without multipath.

In order to quantify the multipath performance of CCAFSK, binary CCAFSK is designed using the enhanced CCA-29 of system (2.1), and the modulated symbols are transmitted through the same two-ray multipath channels designed for CCASK in Section 3.3.4.3. According to Section 3.4.3, for obtaining certain BER, CCAFSK can realize with a much smaller number of symbols than DCSK. Hence, we chose L=100 for the CCAFSK multipath performance evaluation. In this case, the symbol duration is $T = L/W = 5.88\mu$s, which results a more efficient data transmission rate, i.e., 170 kbps.

The Monte-Carlo simulations are operated with 10^6 symbols transmitted through 10^4 i.i.d. two-ray channels, in case of both equal power gain and unequal power gain with 10dB difference. The results are illustrated in Figure 3.30, together with the AWGN performance of CCAFSK without multipath. From the comparison of CCAFSK noise performance in the channels with and without multipath, we can see that the

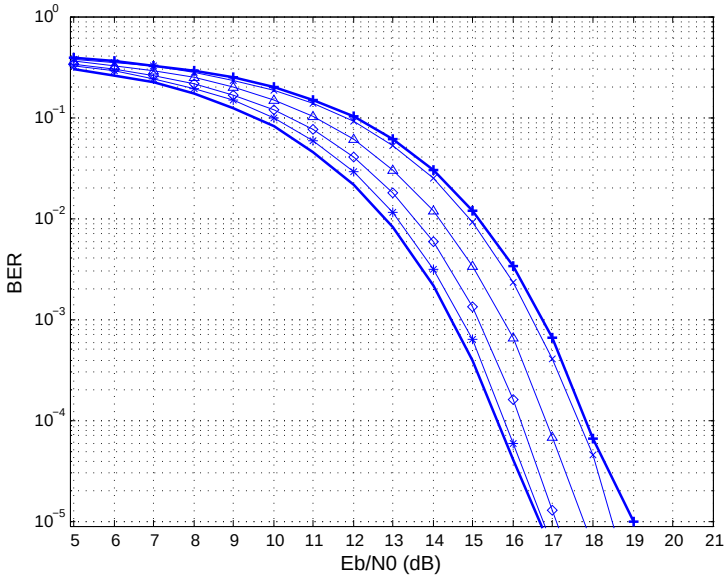

(a)

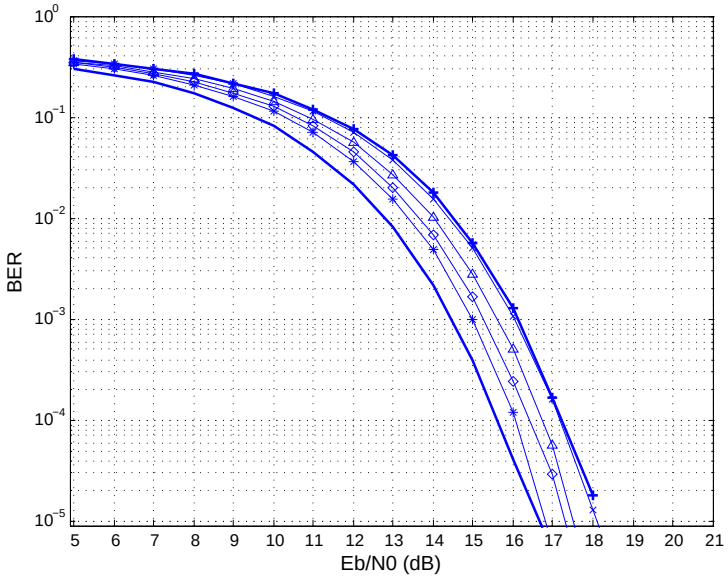

(b)

Figure 3.30: Noise performance of CCAFSK in the two-ray channel model with: (a) equal power gain; (b) unequal power gain with 10dB difference. The channel parameter is: τ_d=75ns, W=17MHz, and the value of f_c differed by forms: 2.4 GHz (+), 2.403 GHz ($\triangle$), 2.406 GHz ($*$), 2.409 GHz ($\Diamond$) 2.4012 GHz ($\times$). For comparison, the AWGN performance without multipath is also given (line without form).

worst performance loss is about 2dB in the two-ray multipath channel with equal power gain, and 1.5dB in case of unequal gain with 10dB difference. This result shows that CCAFSK has a similar multipath performance as CCASK. However, based on the fact that CCAFSK has a generally better noise performance, especially for small L, we can say that it outperforms CCASK.

3.5 Conclusion

In this chapter, the modulation/demodulation schemes of two CCA-based systems have been introduced, called CCASK and CCAFSK.

CCASK utilizes different period values of CCAs for modulating different data symbols, and the demodulation can be realized by the detection of the auto-correlation property, the spectral property, or the statistical property of the received symbols. Since CCA signals can be generated by simple electronic circuits, with the period controlled simply by the value of bifurcation parameters, the transceiver of CCASK is considered to have low-complexity, hence, low-cost. Besides, CCASK shows a good AWGN performance in case of large number of samples per symbol, i.e., lower bit transmission rate if the RF frequency band is fixed. Meanwhile, its multipath performance in the two-ray channel model is comparable to that of DCSK, in other words, much better than the narrow-band systems. Hence, we propose CCASK to be used for the short-range indoor applications with low-complexity, low-cost transceivers.

However, the detections of CCASK are not strictly antipodal for different data symbols, since coprime periods are required to make the quasi-orthogonality on spectrum. CCAFSK is actually an improvement of CCASK. It uses only one CCA for each user, with the data symbols differed by a second-sign-changing operation on the CCA iteration, which introduces the quasi-orthogonality on spectrum with a same number of observed frequency points. The modulation/demodulation schemes of CCAFSK is similar to that of CCASK, and to obtain the certain noise performance, the former requires a shorter symbol duration than the latter. Besides, both of them have a similar multipath performance. Furthermore, a simple evaluation of multi-user performance has been done for CCAFSK, which shows the possibility and the robust performance on multi-access. Hence, CCAFSK can serve in the short-range, low-rate muti-user applications.

Conclusion and Perspective

Recently, the quickly expanding field of wideband communications has encountered lots of developments, innovations as well as challenges, which will doubtlessly continue in the predictable future. From the point of view of signal processing, the chaotic signals are statistically uncorrelated in the time domain, and have naturally large-band in the frequency domain, both of them are in contrary to the periodic signals. Hence, the application of chaos in the wideband communication systems sounds attractive and practical, which has formed a research field called chaos-based wideband communications in the past twenty years.

The state of the art in the first chapter has been given in two research branches of chaos-based wideband communications: the application of chaos in the chaotic spectrum spreading, or the direct chaotic signal modulation. The latter can be realized by low-complexity transceivers, based on the possibility of generating wideband signals directly by simple electronic circuits of the dynamical systems. The synchronization of chaotic signals is another research subject, which has been proved to be difficult to achieve in the wireless transmissions. Hence, for the direct chaotic signal modulation systems, a noncoherent (or differential) detection is preferred. DCSK has been widely studied and considered to be the most practical chaos-based modulation scheme when the radio propagation environment is concerned.

Our study has been carried out in two steps. In the first step, the sinusoidal two-dimensional discrete-time dynamical system has been selected, and its periodic behaviors have been studied based on the fundamental knowledge of chaos theory. Variety of attractors have been derived, including CCA. CCA is a type of attractors processing simultaneously the chaoticity and cyclicity, and different periods of CCAs can be obtained easily by changing the parameter values of the dynamical system. The specific characteristics of CCAs have been analyzed, including the auto-correlation

property, the spectral property, and the statistical property. All the three properties are functions of the period q. In the frequency domain, CCA-q has a comb-like spectrum, with q main frequency points equally spaced in the band. The presentation on this part of work can be found in Chapter 2.

The second step of the work has been concentrated on the application of CCA properties in the wideband communications. Two CCA-based modulation schemes have been proposed. The first one is a CCA-based chaos shift keying, called CCASK. The modulation scheme of CCASK is mapping data symbols to CCA signals with different periods, and the detection can be realized by observing one of the introduced properties. The second one is a CCA-based frequency shift keying, called CCAFSK. It comes from the fact that the second-sign-changed signal of CCA has a spectrum quasi-orthogonal to the one of the original signal. It's considered to be an improvement of CCASK. The performance evaluation of each CCA-based system in the AWGN channel has been theoretically analyzed and simulated. The AWGN performance has been compared between CCASK/CCAFSK and DCSK, which shows that the former systems have better noise performance than the latter, in case of long symbol duration with fixed radio frequency band. The performance evaluation in the basic multipath channel model shows that CCASK/CCAFSK have the comparable multipath performance to DCSK in the 2.4 GHz ISM environment. Furthermore, a simple evaluation of multi-user performance has been simulated for CCAFSK, which shows the possibility of multiple access for the CCA-based systems. In a conclusion, the CCA-based modulation systems can serve in the short-range, low-rate muti-user applications which require low-complexity transceivers, such as local personal applications. Chapter 3 has given in detail the this second part of work.

As a PhD study of a period of three years, our work is far from being complete. A lot of further studies can be done for the CCA-based modulation systems, here we give several examples:

1. The multipath performance of CCASK/CCAFSK in this thesis have been discussed in the two-ray multipath channel, which is the simplest linear time-invariant model. However, in a large RF band, the attenuation and propagation delay of each path could be frequency selective and time dependent, hence, the performance evaluation of CCA-based systems in more complex multipath channel models will make sense, with a raised complexity in analysis and simulations.

2. Based on the quasi-orthogonal spectrum of different period of CCA, the multiple access of CCA-based systems could be an advantage compared to the other chaos-based systems, such as DCSK. The performance of multiple access in this thesis is simply evaluated for CCAFSK by the simulations of dual-user applications. Hence, the noise performance in case of multiple access could be theoretically analyzed, and the applications of more users could be considered.

3. Inspired by the reference [74], the sign-changing operation on the signal of CCA for modulating different data symbol of CCAFSK equals to a multiplication of a pair of Walsh-code-similar codes with length L (number of samples per symbol), i.e., '1 1 1 1...' and '1 -1 1 -1 ...' . Then, if L is selected to be $L = m2^M$ $(m, M \in \mathbb{N})$, M signals with quasi-orthogonal spectrum between each other can be generated by cyclically multiplying the signal of CCA by the first M Walsh codes with length 2^M. The scheme of M-ary CCAFSK could be considered by mapping the data symbols to one of these generated signals. Hence, the further analysis on this scheme, as well as the performance evaluation, may lead to interesting results.

4. During the study of dynamical systems, we have always taken sinusoidal two-dimensional discrete-time system in equation (2.1). The other dynamical systems could be interesting, if the similar CCAs can be generated by simpler generator, or the CCAs with better properties can be generated.

There is a proverb: *throw a sprat to catch a whale*, which means a modest spur to induce others to come forward with valuable contributions. We hope that our study can serve as a sprat for some further researches.

Appendix A

Analytical Evaluation of AWGN Noise Performance of CCASK

In this appendix, the analytical evaluation of noise performance of CCASK using different detections in the discrete-time baseband equivalent AWGN channel will be given. All the analysis are based on the passband carrier removed signal of the m^{th} received symbol $r(t) = s(t) + b(t)$ $(t \in [mT, (m+1)T])$. The equivalent sampled sequence of the observed signal is $\mathbf{r}_m = (r_m[1],\ r_m[2],\ ...,\ r_m[L])$, with $r_m[n] = s_m[n] + b_m[n]$ $(n \in \{1, 2, ..., L\})$. For the sake of simplification in notations, the index m will be dropped, hence r_n, s_n, x_n and b_n will be used to stand for $r_m[n]$, $s_m[n]$, $x_m[n]$ and $b_m[n]$, without loss of generality.

It should be reminded that CCASK use the real valued basis functions generated by the dynamical systems. According to Section 3.3.3.3, the real statistics of the equivalent discrete-time baseband AWGN channel model is sufficient for the detection of the real valued baseband modulated symbols, i.e., $r_{n,I} = s_n + b_{n,I}$ $(n \in \{1, 2, ..., L\})$, where $b_{n,I}$ stands for the in-phase component of the sampled complex envelope of the additive Gaussian noise. Again, for the reason of simplification in notations, r_n and b_n will be used to present $r_{n,I}$ and $b_{n,I}$ in Sections A.1, A.2 and A.3. In other words, b_n in these sections won't stand for the sampled complex envelope of additive noise, but for its real component, with the variance equal to σ^2 as defined in equation (3.42); and similarly, r_n is real valued, so that the part of the observation variables collected from the quadrature component of $r(t)$ in Section 3.3.2 will be neglected without notification.

A. ANALYTICAL EVALUATION OF AWGN NOISE PERFORMANCE OF CCASK

A.1 Performance of Auto-Correlation Detection

According to equations (3.55)-(3.57), the general expression of noise performance of the binary CCASK using auto-correlation detection can be obtained as a function of the expectation and variance of the detection variable C_{b_m} in equation (3.21). Hence, the analysis of these two statistics are indispensable.

The normalized sum of the auto-correlation elements $R_{r_m r_m}[\ell q_v]$ ($\ell \in \mathbb{N}$) of $\mathbf{r}_m$, as defined in equation (3.19), can be written under the form of equation (2.18) as

$$\begin{aligned} C_m[v] &= \frac{\sum_{\ell=1}^{L_v} R_{r_m r_m}[\ell q_v]}{\sum_{\ell=1}^{L_v}(L-\ell q_v)} \\ &= Q_v \sum_{\ell=1}^{L_v} \sum_{n=1+\ell q_v}^{L} r_n r_{n-\ell q_v} \\ &= Q_v \sum_{l=1}^{q_v} \sum_{\ell=1}^{L_v} \zeta(q_v, l) \end{aligned} \tag{A.1}$$

where $v \in \{0,1\}$, $L_v = \lfloor \frac{L}{q_v} \rfloor$, $Q_v = \frac{2}{2LL_v - L_v(L_v+1)q_v}$, and $\zeta(q_v, l) = \sum_{k=\ell}^{L_v^l} r_{l+\ell q_v} r_{l+(k-\ell)q_v}$ with $L_v^l = \left\lfloor \frac{L-l}{q_v} \right\rfloor$. The elements $\sum_{\ell=1}^{L_v} \zeta(q_v, l)$ in (A.1) can be extended as

$$\begin{aligned} \sum_{\ell=1}^{L_v} \zeta(q_v, l) &= \sum_{\ell=1}^{L_v} \sum_{k=\ell}^{L_v^l} (s_{l+\ell q_v} + b_{l+\ell q_v})(s_{l+(k-\ell)q_v} + b_{l+(k-\ell)q_v}) \\ &= \sum_{\ell=1}^{L_v} \sum_{k=\ell}^{L_v^l} s_{l+\ell q_v} s_{l+(k-\ell)q_v} + \sum_{\ell=1}^{L_v} \sum_{k=\ell}^{L_v^l} b_{l+\ell q_v} b_{l+(k-\ell)q_v} \\ &\quad + \sum_{\ell=1}^{L_v} \sum_{k=\ell}^{L_v^l} (s_{l+\ell q_v} b_{l+(k-\ell)q_v} + s_{l+(k-\ell)q_v} b_{l+\ell q_v}) \end{aligned} \tag{A.2}$$

Inserting (A.1) and (A.2) into equation (3.21), we can get the extended expression of

decision variable C_{b_m} as

$$\begin{aligned} C_{b_m} &= Q_1 \sum_{l=1}^{q_1} \sum_{\ell=1}^{L_1} \sum_{k=\ell}^{L_1^l} s_{l+kq_1} s_{l+(k-\ell)q_1} - Q_0 \sum_{l=1}^{q_0} \sum_{\ell=1}^{L_0} \sum_{k=\ell}^{L_0^l} s_{l+kq_0} s_{l+(k-\ell)q_0} \\ &+ Q_1 \sum_{l=1}^{q_1} \sum_{\ell=1}^{L_1} \sum_{k=\ell}^{L_1^l} b_{l+kq_1} b_{l+(k-\ell)q_1} - Q_0 \sum_{l=1}^{q_0} \sum_{\ell=1}^{L_0} \sum_{k=\ell}^{L_0^l} b_{l+kq_0} b_{l+(k-\ell)q_0} \\ &+ Q_1 \sum_{l=1}^{q_1} \sum_{\ell=1}^{L_1} \sum_{k=\ell}^{L_1^l} (s_{l+kq_1} b_{l+(k-\ell)q_1} + s_{l+(k-\ell)q_1} b_{l+kq_1}) \\ &- Q_0 \sum_{l=1}^{q_0} \sum_{\ell=1}^{L_0} \sum_{k=\ell}^{L_0^l} (s_{l+kq_0} b_{l+(k-\ell)q_0} + s_{l+(k-\ell)q_0} b_{l+kq_0}) \end{aligned} \tag{A.3}$$

In order to simplify the notations, under the condition that $L \gg q_1, q_0$, we can define $\overline{L_v} = \frac{1}{q_v} \sum_{l=1}^{q_v} L_v^l$ to approximate L_v^l ($l \in \{1, 2, ..., q_v\}$), which agrees with $L = (\overline{L_v} + 1)q_v$. In case that $d_m = i$ ($i \in \{0, 1\}$) was transmitted, the expectation of $C_{b_m}^{(i)}$ can be calculated as:

$$\begin{aligned} &E(C_{b_m}^{(i)}) \\ &= Q_1 \sum_{l=1}^{q_1} \sum_{\ell=1}^{L_1} \sum_{k=\ell}^{L_v^l} E(s_{l+kq_1} s_{l+(k-\ell)q_1}) - Q_0 \sum_{l=1}^{q_0} \sum_{\ell=1}^{L_0} \sum_{k=\ell}^{L_0^l} E(s_{l+kq_0} s_{l+(k-\ell)q_0}) \\ &+ Q_1 \sum_{l=1}^{q_1} \sum_{\ell=1}^{L_1} \sum_{k=\ell}^{L_1^l} E(b_{l+kq_1} b_{l+(k-\ell)q_1}) - Q_0 \sum_{l=1}^{q_0} \sum_{\ell=1}^{L_0} \sum_{k=\ell}^{L_0^l} E(b_{l+kq_0} b_{l+(k-\ell)q_0}) \\ &+ Q_1 \sum_{l=1}^{q_1} \sum_{\ell=1}^{L_1} \sum_{k=\ell}^{L_1^l} E(s_{l+kq_1} b_{l+(k-\ell)q_1} + s_{l+(k-\ell)q_1} b_{l+kq_1}) \\ &- Q_0 \sum_{l=1}^{q_0} \sum_{\ell=1}^{L_0} \sum_{k=\ell}^{L_0^l} E(s_{l+kq_0} b_{l+(k-\ell)q_0} + s_{l+(k-\ell)q_0} b_{l+kq_0}) \\ &= (-1)^{i+1} Q_i \left(\sum_{l=1}^{q_i} \sum_{\ell=1}^{L_i} \sum_{k=\ell}^{L_i^l} \left\langle \mathbf{x}_{q_i,l}^{(i)} \right\rangle^2 - Q_{1-i} \sum_{l=1}^{q_{1-i}} \sum_{\ell=1}^{L_{1-i}} \sum_{k=\ell}^{L_{1-i}^l} \left\langle \mathbf{x}_{q_{1-i},l}^{(i)} \right\rangle^2 \right) \\ &= (-1)^{i+1} \langle \mu^2 \rangle^{(i)} \end{aligned} \tag{A.4}$$

A. ANALYTICAL EVALUATION OF AWGN NOISE PERFORMANCE OF CCASK

As long as the variance of $C_{b_m}^{(i)}$ is considered, the following expression can be given:

$$\begin{aligned}
&\mathrm{Var}(C_{b_m}^{(i)}) \\
&= Q_1^2\mathrm{Var}\Big(\sum_{l=1}^{q_1}\sum_{\ell=1}^{L_1}\sum_{k=\ell}^{L_1^l} s_{l+kq_1}s_{l+(k-\ell)q_1}\Big) + Q_0^2\mathrm{Var}\Big(\sum_{l=1}^{q_0}\sum_{\ell=1}^{L_0}\sum_{k=\ell}^{L_0^l} s_{l+kq_0}s_{l+(k-\ell)q_0}\Big) \\
&\quad + Q_1^2\mathrm{Var}\Big(\sum_{l=1}^{q_1}\sum_{\ell=1}^{L_1}\sum_{k=\ell}^{L_1^l} b_{l+kq_1}b_{l+(k-\ell)q_1}\Big) + Q_0^2\mathrm{Var}\Big(\sum_{l=1}^{q_0}\sum_{\ell=1}^{L_0}\sum_{k=\ell}^{L_0^l} b_{l+kq_0}b_{l+(k-\ell)q_0}\Big) \\
&\quad + Q_1^2\mathrm{Var}\Big(\sum_{l=1}^{q_1}\sum_{\ell=1}^{L_1}\sum_{k=\ell}^{L_1^l}(s_{l+kq_1}b_{l+(k-\ell)q_1} + s_{l+(k-\ell)q_1}b_{l+kq_1})\Big) \\
&\quad + Q_0^2\mathrm{Var}\Big(\sum_{l=1}^{q_0}\sum_{\ell=1}^{L_0}\sum_{k=\ell}^{L_0^l}(s_{l+kq_0}b_{l+(k-\ell)q_0} + s_{l+(k-\ell)q_0}b_{l+kq_0})\Big)
\end{aligned} \tag{A.5}$$

The variances of the auto-correlations of $\mathbf{s}_m$ in $(A.5)$ can be extended as

$$\begin{aligned}
&\mathrm{Var}\Big(\sum_{l=1}^{q_v}\sum_{\ell=1}^{L_v}\sum_{k=\ell}^{L_v^l} s_{l+\ell q_v}s_{l+(k-\ell)q_v}\Big) \\
&= \sum_{l=1}^{q_v}\sum_{k=1}^{L_v^l}\mathrm{Var}\Big(s_{l+\ell q_v}\sum_{K=1}^{k} s_{l+(k-\ell)q_v}\Big) \\
&= \sum_{l=1}^{q_v}\sum_{k=1}^{L_v^l}\left[E\Big(s_{l+\ell q_v}^2(\sum_{K=1}^{k} s_{l+(k-\ell)q_v})^2\Big) - E^2\Big(s_{l+\ell q_v}\sum_{K=1}^{k} s_{l+(k-\ell)q_v}\Big)\right] \\
&= \sum_{l=1}^{q_v}\sum_{k=1}^{L_v^l}\left[E\Big(s_{l+\ell q_v}^2\Big)E\Big((\sum_{K=1}^{k} s_{l+(k-\ell)q_v})^2\Big) - E^2\Big(s_{l+\ell q_v}\Big)E^2\Big(\sum_{K=1}^{k} s_{l+(k-\ell)q_v}\Big)\right] \\
&= \begin{cases} \frac{\overline{L_i}(\overline{L_i}+1)(\overline{L_i}+2)}{3}\sum_{l=1}^{q_i}(\mu_l^{(i)^2} + \frac{3}{2\overline{L_i}+4}\delta_l^{(i)^2})\delta_l^{(i)^2}, & v = i \\ \frac{L\overline{L_{1-i}}}{2}\Delta^4 & v \neq i \end{cases} \\
&= \begin{cases} \frac{L}{3}(\frac{L^2}{q_i^2}-1)\langle\mu^2\delta^2\rangle^{(i)} + \frac{L}{2}(\frac{L}{q_i}-1)\langle\delta^4\rangle^{(i)}, & v = i \\ \frac{L}{2}(\frac{L}{q_{1-i}}-1)\Delta^4 & v \neq i \end{cases}
\end{aligned} \tag{A.6}$$

where the extensions of the elements can be obtained from:

$$E\Big(s_{l+\ell q_v}^2\Big) = \begin{cases} \langle\mathbf{x}_{q_i,l}^{(i)^2}\rangle, & v = i \\ \langle\mathbf{x}_{q_{1-i},l}^{(i)^2}\rangle, & v \neq i \end{cases} = \begin{cases} \mu_l^{(i)^2} + \delta_l^{(i)^2}, & v = i \\ \Delta^2, & v \neq i \end{cases} \tag{A.7}$$

$$E^2\Big(s_{l+\ell q_v}\Big) = \begin{cases} \langle\mathbf{x}_{q_i,l}^{(i)}\rangle^2, & v = i \\ \langle\mathbf{x}_{q_{1-i},l}^{(i)}\rangle^2, & v \neq i \end{cases} = \begin{cases} \mu_l^{(i)^2}, & v = i \\ 0, & v \neq i \end{cases} \tag{A.8}$$

$$
\begin{aligned}
E\Big((\sum_{K=1}^{k} s_{l+(k-\ell)q_v})^2\Big) &= E\Big(\sum_{K=1}^{k} s^2_{l+(k-\ell)q_v} + \sum_{K=1}^{k}\sum_{\substack{K'=1\\K'\neq K}}^{k} s_{l+(k-\ell)q_v} s_{l+(k-K')q_v}\Big) \\
&= \begin{cases} k\langle \mathbf{x}^{(i)^2}_{q_i,l}\rangle + k(k-1)\langle \mathbf{x}^{(i)}_{q_i,l}\rangle^2, & v = i \\ k\langle \mathbf{x}^{(i)^2}_{q_{1-i},l}\rangle + k(k-1)\langle \mathbf{x}^{(i)}_{q_{1-i},l}\rangle^2, & v \neq i \end{cases} \\
&= \begin{cases} k(\mu_l^{(i)^2} + \delta_l^{(i)^2}) + k(k-1)\mu_l^{(i)^2}, & v = i \\ k\Delta^2, & v \neq i \end{cases}
\end{aligned} \tag{A.9}
$$

$$
\begin{aligned}
E^2\Big(\sum_{K=1}^{k} s_{l+(k-\ell)q_v}\Big) &= \begin{cases} k^2\langle \mathbf{x}^{(i)}_{q_i,l}\rangle^2, & v = i \\ k^2\langle \mathbf{x}^{(i)}_{q_{1-i},l}\rangle^2, & v \neq i \end{cases} \\
&= \begin{cases} k^2\mu_l^{(i)^2}, & v = i \\ 0, & v \neq i \end{cases}
\end{aligned} \tag{A.10}
$$

In the similar way, the variance of the auto-correlation of $\mathbf{b}_m$, as well as the variance of the cross-correlation between $\mathbf{s}_m$ and $\mathbf{b}_m$ in equation $(A.5)$, can also be extended as

$$
\mathrm{Var}\Big(\sum_{l=1}^{q_v}\sum_{\ell=1}^{L_v}\sum_{k=\ell}^{L_v^l} b_{l+\ell q_v} b_{l+(k-\ell)q_v}\Big) = \frac{L}{2}(\frac{\overline{L}}{q_v} - 1)\sigma^4 \tag{A.11}
$$

$$
\begin{aligned}
&\mathrm{Var}\Big(\sum_{l=1}^{q_v}\sum_{\ell=1}^{L_v}\sum_{k=\ell}^{L_v^l}(s_{l+\ell q_v} b_{l+(k-\ell)q_v} + s_{l+(k-\ell)q_v} b_{l+\ell q_v})\Big) \\
&= \begin{cases} \Big(\frac{L}{3}(\frac{L}{q_i} - 1)(2\frac{L}{q_i} - 1)\langle\mu^2\rangle^{(i)} + L(\frac{L}{q_i} - 1)\langle\delta^2\rangle^{(i)}\Big)\sigma^2, & v = i \\ L(\frac{L}{q_{1-i}} - 1)\Delta^2\sigma^2, & v \neq i \end{cases}
\end{aligned} \tag{A.12}
$$

Furthermore, $Q_v = \frac{2}{2LL_v - L_v(L_v+1)q_v} \approx \frac{2q_v}{L(L-q_v)}$. Hence, inserting $(A.6)$, $(A.11)$ and $(A.12)$ into $(A.5)$, the expression of the variance of $C^{(i)}_{b_m}$ can be obtained as

$$
\begin{aligned}
\mathrm{Var}(C^{(i)}_{b_m}) &= \frac{4(L+q_i)}{3L(L-q_i)}\langle\mu^2\delta^2\rangle^{(i)} + \frac{2q_i}{L(L-q_i)}\langle\delta^4\rangle^{(i)} + \frac{2q_{1-i}}{L(L-q_{1-i})}\Delta^4 \\
&\quad + \Big(\frac{4(2L-q_i)}{3L(L-q_i)}\langle\mu^2\rangle^{(i)} + \frac{4q_i}{L(L-q_i)}\langle\delta^2\rangle^{(i)} + \frac{4q_{1-i}}{L(L-q_{1-i})}\Delta^2\Big)\sigma^2 \\
&\quad + \frac{2}{L}\Big(\frac{q_i}{L-q_i} + \frac{q_{1-i}}{L-q_{1-i}}\Big)\sigma^4
\end{aligned} \tag{A.13}
$$

Consequently, replacing $E(\varepsilon^{(i)})$ and $\mathrm{Var}(\varepsilon^{(i)})$ in equations (3.55)-(3.57) by $E(C^{(i)}_{b_m})$ and $\mathrm{Var}(C^{(i)}_{b_m})$ in $(A.4)$ and $(A.13)$ respectively, the BER performance of the binary

A. ANALYTICAL EVALUATION OF AWGN NOISE PERFORMANCE OF CCASK

CCASK using auto-correlation detection can be presented as

$$\begin{aligned}
&\mathrm{BER}_{\mathrm{CCASK}} \\
&= \frac{1}{4}\sum_{i=0}^{1}\mathrm{erfc}\Bigg[\Bigg(\frac{8(L+q_i)}{3L(L-q_i)}\frac{\langle\mu^2\delta^2\rangle^{(i)}}{\langle\mu^2\rangle^{(i)^2}} + \frac{4q_i}{L(L-q_i)}\frac{\langle\delta^4\rangle^{(i)}}{\langle\mu^2\rangle^{(i)^2}} + \frac{4q_{1-i}}{L(L-q_{1-i})}\frac{\Delta^4}{\langle\mu^2\rangle^{(i)^2}} \\
&\qquad + \Big(\frac{8(2L-q_i)}{3L(L-q_i)}\frac{\langle\mu^2\rangle^{(i)}}{\langle\mu^2\rangle^{(i)^2}} + \frac{8q_i}{L(L-q_i)}\frac{\langle\delta^2\rangle^{(i)}}{\langle\mu^2\rangle^{(i)^2}} + \frac{8q_{1-i}}{L(L-q_{1-i})}\frac{\Delta^2}{\langle\mu^2\rangle^{(i)^2}}\Big)\sigma^2 \\
&\qquad + \frac{4}{L}\Big(\frac{q_i}{L-q_i} + \frac{q_{1-i}}{L-q_{1-i}}\Big)\frac{\sigma^4}{\langle\mu^2\rangle^{(i)^2}}\Bigg)^{-\frac{1}{2}}\Bigg]
\end{aligned} \tag{A.14}$$

In case of large number of samples per symbol and relative small zones of CCAs are considered, i.e., $L \gg q_0, q_1$, and $\langle\delta^2\rangle^{(i)} \ll \langle\mu^2\rangle^{(i)}$, it's reasonable to do the approximations as $E_{b_d} = L\Delta^2 = L(\langle\mu^2\rangle^{(i)} + \langle\delta^2\rangle^{(i)}) \approx L\langle\mu^2\rangle^{(i)}$. Furthermore, according to equation (3.47) and equation (3.42), $E_b = E_{b_d}/(2W)$ and $N_0 = W\sigma^2$. Under these conditions, the BER performance the binary CCASK using auto-correlation detection in $(A.14)$ can be approximated in function of E_b/N_0 as

$$\mathrm{BER}_{\mathrm{CCASK}} \approx \frac{1}{4}\sum_{i=0}^{1}\mathrm{erfc}\left[\left(\frac{8}{3}\frac{N_0}{E_b} + (q_i + q_{1-i})\frac{N_0^2}{E_b^2}\right)^{-\frac{1}{2}}\right] \tag{A.15}$$

A.2 Performance of Spectral Detection

According to equations (3.55)-(3.57), the general expression of noise performance of the binary CCASK using spectral detection can be obtained as a function of the expectation and variance of the detection variable D_{b_m} in equation (3.26). Hence, the analysis of these two statistical values are indispensable.

The mean squared value of the observed spectra magnitudes of $\mathbf{r}_m$, as defined in equation (3.24), can also be written under the form of equation (2.18) as

$$\begin{aligned} D_m[v] &= \frac{1}{q_v}\sum_{K=1}^{q_v}\Big(A_m^v[K]\Big)^2 \\ &= \frac{1}{q_v}\sum_{K=1}^{q_v}\Big|\sum_{n=1}^{L} r_n e^{-j2\pi\frac{K}{q_v}n}\Big|^2 \\ &= \frac{1}{q_v}\sum_{K=1}^{q_v}\Big|\sum_{l=1}^{q_v}\xi(q_v,l)e^{-j2\pi\frac{K}{q_v}l}\Big|^2 \\ &= \sum_{l=1}^{q_v}\xi^2(q_v,l) \end{aligned} \tag{A.16}$$

where $\xi(q_v,l) = \sum_{k=0}^{L_v^l}(s_{l+\ell q_v} + b_{l+\ell q_v})$ with $L_v^l = \left\lfloor\frac{L-l}{q_v}\right\rfloor$. Furthermore, the element $\xi^2(q_v,l)$ in (A.16) can be extended as

$$\begin{aligned} \xi^2(q_v,l) &= \sum_{k=0}^{L_v^l}\sum_{k'=0}^{L_v^l}(s_{l+\ell q_v}+b_{l+\ell q_v})(s_{l+k'q_v}+b_{l+k'q_v}) \\ &= \sum_{k=0}^{L_v^l}(s_{l+\ell q_v}+b_{l+\ell q_v})^2 + \sum_{k=0}^{L_v^l}\sum_{\substack{k'=0\\k'\neq k}}^{L_v^l}(s_{l+\ell q_v}+b_{l+\ell q_v})(s_{l+k'q_v}+b_{l+k'q_v}) \\ &= \sum_{k=0}^{L_v^l}(s_{l+\ell q_v}+b_{l+\ell q_v})^2 \\ &\quad +2\sum_{k=0}^{L_v^l}\sum_{k'=0}^{k-1}\left(s_{l+\ell q_v}s_{l+k'q_v} + b_{l+\ell q_v}b_{l+k'q_v} + s_{l+\ell q_v}b_{l+k'q_v} + b_{l+\ell q_v}s_{l+k'q_v}\right) \end{aligned} \tag{A.17}$$

Inserting (A.16) and (A.17) into equation (3.26), we can get the extended expression

of decision variable D_{b_m} as

$$\begin{aligned} D_{b_m} = & 2\sum_{l=1}^{q_1}\sum_{k=0}^{L_1^l}\sum_{k'=0}^{k-1}\left(s_{l+kq_1}s_{l+k'q_1}+b_{l+kq_1}b_{l+k'q_1}+s_{l+kq_1}b_{l+k'q_1}+b_{l+kq_1}s_{l+k'q_1}\right) \\ & -2\sum_{l=1}^{q_0}\sum_{k=0}^{L_0^l}\sum_{k'=0}^{k-1}\left(s_{l+kq_0}s_{l+k'q_0}+b_{l+kq_0}b_{l+k'q_0}+s_{l+kq_0}b_{l+k'q_0}+b_{l+kq_0}s_{l+k'q_0}\right) \end{aligned} \tag{A.18}$$

In order to simplify the notations, under the condition that $L \gg q_1, q_0$, $\overline{L_v} = \frac{1}{q_v}\sum_{l=1}^{q_v} L_v^l$ can be defined to approximate L_v^l ($l \in \{1,2,...,q_v\}$), which agrees with $L = (\overline{L_v}+1)q_v$. In case that $d_m = i$ ($i \in \{0,1\}$) was transmitted, the expectation of $D_{b_m}^{(i)}$ can be calculated as:

$$\begin{aligned} E(D_{b_m}^{(i)}) &= 2\sum_{l=1}^{q_1}\sum_{k=0}^{L_1^l}\sum_{k'=0}^{k-1}E\left(s_{l+kq_1}s_{l+k'q_1}+b_{l+kq_1}b_{l+k'q_1}+s_{l+kq_1}b_{l+k'q_1}+b_{l+kq_1}s_{l+k'q_1}\right) \\ &\quad -2\sum_{l=1}^{q_0}\sum_{k=0}^{L_0^l}\sum_{k'=0}^{k-1}E\left(s_{l+kq_0}s_{l+k'q_0}+b_{l+kq_0}b_{l+k'q_0}+s_{l+kq_0}b_{l+k'q_0}+b_{l+kq_0}s_{l+k'q_0}\right) \\ &= 2\sum_{l=1}^{q_1}\sum_{k=0}^{L_1}\sum_{k'=0}^{k-1}E\left(s_{l+kq_1}s_{l+k'q_1}\right)-2\sum_{l=1}^{q_0}\sum_{k=0}^{L_0}\sum_{k'=0}^{k-1}E\left(s_{l+kq_0}s_{l+k'q_0}\right) \\ &= (-1)^{i+1}\left(\frac{L\overline{L_i}}{q_i}\sum_{l=1}^{q_i}\left\langle \mathbf{x}_{q_i,l}^{(i)}\right\rangle^2-\frac{L\overline{L_{1-i}}}{q_{1-i}}\sum_{l=1}^{q_{1-i}}\left\langle \mathbf{x}_{q_{1-i},l}^{(i)}\right\rangle^2\right) \\ &= (-1)^{i+1}L(\frac{L}{q_i}-1)\langle\mu^2\rangle^{(i)} \end{aligned} \tag{A.19}$$

As long as the variance of $D_{b_m}^{(i)}$ is considered, the following expression can be given:

$$\begin{aligned} \mathrm{Var}(D_{b_m}^{(i)}) &= 4\mathrm{Var}\Big(\sum_{l=1}^{q_1}\sum_{k=0}^{L_1^l}\sum_{k'=0}^{k-1}s_{l+kq_1}s_{l+k'q_1}\Big)+4\mathrm{Var}\Big(\sum_{l=1}^{q_0}\sum_{k=0}^{L_0^l}\sum_{k'=0}^{k-1}s_{l+kq_0}s_{l+k'q_0}\Big) \\ &\quad +4\mathrm{Var}\Big(\sum_{l=1}^{q_1}\sum_{k=0}^{L_1^l}\sum_{k'=0}^{k-1}b_{l+kq_1}b_{l+k'q_1}\Big)+4\mathrm{Var}\Big(\sum_{l=1}^{q_0}\sum_{k=0}^{L_0^l}\sum_{k'=0}^{k-1}b_{l+kq_0}b_{l+k'q_0}\Big) \\ &\quad +4\mathrm{Var}\Big(\sum_{l=1}^{q_1}\sum_{k=0}^{L_1^l}\sum_{k'=0}^{k-1}(s_{l+kq_1}b_{l+k'q_1}+b_{l+kq_1}s_{l+k'q_1})\Big) \\ &\quad +4\mathrm{Var}\Big(\sum_{l=1}^{q_0}\sum_{k=0}^{L_0^l}\sum_{k'=0}^{k-1}(s_{l+kq_0}b_{l+k'q_0}+b_{l+kq_0}s_{l+k'q_0})\Big) \end{aligned} \tag{A.20}$$

The variances of the auto-correlation of $\mathbf{s}_m$ in $(A.20)$ can be extended as

$$\begin{aligned}
&\mathrm{Var}\Big(\sum_{l=1}^{q_v}\sum_{k=0}^{L_v^l}\sum_{k'=0}^{k-1} s_{l+\ell q_v}s_{l+k'q_v}\Big)\\
&=\sum_{l=1}^{q_v}\sum_{k=0}^{L_v^l}\mathrm{Var}\Big(s_{l+\ell q_v}\sum_{k'=0}^{k-1}s_{l+k'q_v}\Big)\\
&=\sum_{l=1}^{q_v}\sum_{k=0}^{L_v^l}\Big[E\Big(s_{l+\ell q_v}^2(\sum_{k'=0}^{k-1}s_{l+k'q_v})^2\Big)-E^2\Big(s_{l+\ell q_v}\sum_{k'=0}^{k-1}s_{l+k'q_v}\Big)\Big]\\
&=\sum_{l=1}^{q_v}\sum_{k=0}^{L_v^l}\Big[E(s_{l+\ell q_v}^2)E\Big((\sum_{k'=0}^{k-1}s_{l+k'q_v})^2\Big)-E^2(s_{l+\ell q_v})E^2\Big(\sum_{k'=0}^{k-1}s_{l+k'q_v}\Big)\Big]\\
&=\begin{cases}\frac{\overline{L_i}(\overline{L_i}+1)(\overline{L_i}+2)}{3}\sum_{l=1}^{q_i}(\mu_l^{(i)^2}+\frac{3}{2\overline{L_i}+4}\delta_l^{(i)^2})\delta_l^{(i)^2}, & v=i\\ \frac{L\overline{L_{1-i}}}{2}\Delta^4, & v\neq i\end{cases}\\
&=\begin{cases}\frac{L}{3}(\frac{L^2}{q_i^2}-1)\langle\mu^2\delta^2\rangle^{(i)}+\frac{L}{2}(\frac{L}{q_i}-1)\langle\delta^4\rangle^{(i)}, & v=i\\ \frac{L}{2}(\frac{L}{q_{1-i}}-1)\Delta^4, & v\neq i\end{cases}
\end{aligned}\tag{A.21}$$

where the extensions of the elements $E(s_{l+\ell q_v}^2)$ and $E^2(s_{l+\ell q_v})$ in (A.21) have been given in $(A.7)$-$(A.8)$, and the extensions of the other two elements in A.21 can be given as

$$\begin{aligned}
E\Big((\sum_{k'=0}^{k-1}s_{l+k'q_v})^2\Big)&=E\Big(\sum_{k'=0}^{k-1}s_{l+k'q_v}^2+\sum_{k'=0}^{k-1}\sum_{\substack{k''=0\\k''\neq k'}}^{k-1}s_{l+k'q_v}s_{l+k''q_v}\Big)\\
&=\begin{cases}k\big\langle\mathbf{x}_{q_i,l}^{(i)^2}\big\rangle+k(k-1)\big\langle\mathbf{x}_{q_i,l}^{(i)}\big\rangle^2, & v=i\\ k\big\langle\mathbf{x}_{q_{1-i},l}^{(i)^2}\big\rangle+k(k-1)\big\langle\mathbf{x}_{q_{1-i},l}^{(i)}\big\rangle^2, & v\neq i\end{cases}\\
&=\begin{cases}k^2\mu_l^{(i)^2}+k\delta_l^{(i)^2}, & v=i\\ k\Delta^2, & v\neq i\end{cases}
\end{aligned}\tag{A.22}$$

$$\begin{aligned}
E^2\Big(\sum_{k'=0}^{k-1}s_{l+k'q_v}\Big)&=\begin{cases}k^2\big\langle\mathbf{x}_{q_i,l}^{(i)}\big\rangle^2, & v=i\\ k^2\big\langle\mathbf{x}_{q_{1-i},l}^{(i)}\big\rangle^2, & v\neq i\end{cases}\\
&=\begin{cases}k^2\mu_l^{(i)^2}, & v=i\\ 0, & v\neq i\end{cases}
\end{aligned}\tag{A.23}$$

In the similar way, the variance of the auto-correlation of $\mathbf{b}_m$, as well as the cross-correlation between $\mathbf{s}_m$ and $\mathbf{b}_m$ in $(A.20)$, can also be extended and represented by

$$\mathrm{Var}\Big(\sum_{l=1}^{q_v}\sum_{k=0}^{L_v^l}\sum_{k'=0}^{k-1}b_{l+\ell q_v}b_{l+k'q_v}\Big)=\frac{L}{2}(\frac{L}{q_v}-1)\sigma^4\tag{A.24}$$

A. ANALYTICAL EVALUATION OF AWGN NOISE PERFORMANCE OF CCASK

$$\begin{aligned}
&\mathrm{Var}\Big(\sum_{l=1}^{q_v}\sum_{k=0}^{L_v^l}\sum_{k'=0}^{k-1}(s_{l+\ell q_v}b_{l+k'q_v}+b_{l+\ell q_v}s_{l+k'q_v})\Big)\\
&=\begin{cases}\frac{L}{3}(\frac{L}{q_i}-1)(\frac{2L}{q_i}-1)\langle\mu^2\rangle^{(i)}\sigma^2+L(\frac{L}{q_i}-1)\langle\delta^2\rangle^{(i)}\sigma^2, & v=i\\ L(\frac{L}{q_{1-i}}-1)\Delta^2\sigma^2, & v\neq i\end{cases}
\end{aligned}\tag{A.25}$$

Inserting $(A.21)$, $(A.24)$ and $(A.25)$ into $(A.20)$, the expression of the variance of $D_{b_m}^{(i)}$ can therefore be obtained as

$$\begin{aligned}
\mathrm{Var}(D_{b_m}^{(i)})=&\frac{4L}{3}(\frac{L^2}{q_i^2}-1)\langle\mu^2\delta^2\rangle^{(i)}+2L(\frac{L}{q_i}-1)\langle\delta^4\rangle^{(i)}+2L(\frac{L}{q_{1-i}}-1)\Delta^4\\
&+\Big(\frac{8L}{3}(\frac{L}{q_i}-1)(\frac{L}{q_i}-\frac{1}{2})\langle\mu^2\rangle^{(i)}+4L(\frac{L}{q_i}-1)\langle\delta^2\rangle^{(i)}+4L(\frac{L}{q_{1-i}}-1)\Delta^2\Big)\sigma^2\\
&+2L\Big(\frac{L}{q_i}+\frac{L}{q_{1-i}}-2\Big)\sigma^4
\end{aligned}\tag{A.26}$$

Consequently, replacing $E(\varepsilon^{(i)})$ and $\mathrm{Var}(\varepsilon^{(i)})$ in equations (3.55)-(3.57) by $E(D_{b_m}^{(i)})$ and $\mathrm{Var}(D_{b_m}^{(i)})$ in $(A.19)$ and $(A.26)$ respectively, the BER performance of the binary CCASK using spectral detection can be presented as

$$\begin{aligned}
&\mathrm{BER}_{\mathrm{CCASK}}\\
&=\frac{1}{4}\sum_{i=0}^{1}\mathrm{erfc}\Bigg[\Bigg(\frac{8(L+q_i)}{3L(L-q_i)}\frac{\langle\mu^2\delta^2\rangle^{(i)}}{\langle\mu^2\rangle^{(i)^2}}+\frac{4q_i}{L(L-q_i)}\frac{\langle\delta^4\rangle^{(i)}}{\langle\mu^2\rangle^{(i)^2}}+\frac{4(L-q_{1-i})q_i^2}{L(L-q_i)^2q_{1-i}}\frac{\Delta^4}{\langle\mu^2\rangle^{(i)^2}}\\
&\quad+\Big(\frac{8(2L-q_i))}{3L(L-q_i)}\frac{\langle\mu^2\rangle^{(i)}}{\langle\mu^2\rangle^{(i)^2}}+\frac{8q_i}{L(L-q_i)}\frac{\langle\delta^2\rangle^{(i)}}{\langle\mu^2\rangle^{(i)^2}}+\frac{8(L-q_{1-i})q_i^2}{L(L-q_i)^2q_{1-i}}\frac{\Delta^2}{\langle\mu^2\rangle^{(i)^2}}\Big)\sigma^2\\
&\quad+\frac{4}{L}\frac{L(q_i+q_{1-i})q_i-2q_i^2q_{1-i}}{(L-q_i)^2q_{1-i}}\frac{\sigma^4}{\langle\mu^2\rangle^{(i)^2}}\Bigg)^{-\frac{1}{2}}\Bigg]
\end{aligned}\tag{A.27}$$

In case of large number of samples per symbol and relative small zones of CCAs are considered, i.e., $L\gg q_0,q_1$, and $\langle\delta^2\rangle^{(i)}\ll\langle\mu^2\rangle^{(i)}$, it's reasonable to do the approximations as $E_{b_d}=L\Delta^2=L(\langle\mu^2\rangle^{(i)}+\langle\delta^2\rangle^{(i)})\approx L\langle\mu^2\rangle^{(i)}$. Since $E_b=E_{b_d}/(2W)$ and $N_0=W\sigma^2$ according to equation (3.47) and equation (3.42), the expression of BER performance the binary CCASK using spectral detection in $(A.27)$ can also be approximated and represented in function of E_b/N_0 as

$$\mathrm{BER}_{\mathrm{CCASK}}\approx\frac{1}{4}\sum_{i=0}^{1}\mathrm{erfc}\Bigg[\Bigg(\frac{8}{3}\frac{N_0}{E_b}+\Big(q_i+\frac{q_i^2}{q_{1-i}}\Big)\frac{N_0^2}{E_b^2}\Bigg)^{-\frac{1}{2}}\Bigg]\tag{A.28}$$

A.3 Performance of Statistical Detection

According to equations (3.55)-(3.57), the general expression of noise performance of the binary CCASK using statistical detection can be obtained as a function of the expectation and variance of the detection variable V_{b_m} in equation (3.32). Hence, the analysis of these two statistical values are required.

Since V_{b_m} is the difference between q_1-DMV and q_0-DMV of the the received symbol $\mathbf{r}_m$, the q_v-DMV ($v \in \{0,1\}$) of $\mathbf{r}_m$ should be analyzed firstly. Downsample $\mathbf{r}_m$ with factor q_v and offset l ($l \in \{1,2,...,q_v\}$) to get the sub-vector $\mathbf{r}_{q_v,l} = (r_l,\ r_{l+q_v},\ ...,\ r_{l+L_v^l q_v})$, with $r_{l+kq_v} = s_{l+kq_v} + b_{l+kq_v}$ ($k \in \{0,1,...,L_v^l\}, L_v^l = \left\lfloor \frac{L-l}{q_v} \right\rfloor$). Denote $\langle \mathbf{r}_{q_v,l} \rangle = \frac{1}{L_v^l+1} \sum_{k=0}^{L_v^l} r_{l+\ell q_v}$, so that the variance of the sub-vector $\mathbf{r}_{q_v,l}$ can be represented as

$$
\begin{aligned}
\mathrm{Var}(\mathbf{r}_{q_v,l}) &= \frac{1}{L_v^l} \sum_{k=0}^{L_v^l} (r_{l+\ell q_v} - \langle \mathbf{r}_{q_v,l} \rangle)^2 \\
&= \frac{1}{L_v^l} \sum_{k=0}^{L_v^l} \left(r_{l+\ell q_v}^2 - 2 \langle \mathbf{r}_{q_v,l} \rangle r_{l+\ell q_v} + \langle \mathbf{r}_{q_v,l} \rangle^2 \right) \\
&= \frac{1}{L_v^l} \sum_{k=0}^{L_v^l} r_{l+\ell q_v}^2 - 2 \langle \mathbf{r}_{q_v,l} \rangle \frac{1}{L_v^l} \sum_{k=0}^{L_v^l} r_{l+\ell q_v} + \langle \mathbf{r}_{q_v,l} \rangle^2 \\
&= \frac{1}{L_v^l} \sum_{k=0}^{L_v^l} r_{l+\ell q_v}^2 - \frac{L_v^l + 2}{L_v^l} \langle \mathbf{r}_{q_v,l} \rangle^2 \\
&= \frac{1}{L_v^l} \sum_{k=0}^{L_v^l} r_{l+\ell q_v}^2 - \frac{L_v^l + 2}{L_v^l (L_v^l + 1)^2} \Big(\sum_{k=0}^{L_v^l} r_{l+\ell q_v}^2 + \sum_{k=0}^{L_v^l} \sum_{\substack{k'=0 \\ k' \neq k}}^{L_v^l} r_{l+\ell q_v} r_{l+k' q_v} \Big) \\
&= \frac{L_v^{l^2} + L_v^l - 1}{L_v^l (L_v^l + 1)^2} \sum_{k=0}^{L_v^l} r_{l+\ell q_v}^2 - \frac{2(L_v^l + 2)}{L_v^l (L_v^l + 1)^2} \sum_{k=0}^{L_v^l} \sum_{k'=0}^{k-1} r_{l+\ell q_v} r_{l+k' q_v}
\end{aligned} \tag{A.29}
$$

Hence, the expression of q_v-DMV of $\mathbf{r}_m$ can be obtained as

$$
\begin{aligned}
V_m[v] &= \frac{1}{q_v} \sum_{l=1}^{q_v} \mathrm{Var}(\mathbf{r}_{q_v,l}) \\
&= \frac{1}{q_v} \sum_{l=1}^{q_v} \frac{1}{L_v^l} \sum_{k=0}^{L_v^l} r_{l+\ell q_v}^2 - \frac{1}{q_v} \sum_{l=1}^{q_v} \frac{L_v^l + 2}{L_v^l} \langle \mathbf{r}_{q_v,l} \rangle^2 \\
&= \frac{1}{q_v} \sum_{l=1}^{q_v} \frac{L_v^{l^2} + L_v^l - 1}{L_v^l (L_v^l + 1)^2} \sum_{k=0}^{L_v^l} r_{l+\ell q_v}^2 - \frac{2}{q_v} \sum_{l=1}^{q_v} \frac{L_v^l + 2}{L_v^l (L_v^l + 1)^2} \sum_{k=0}^{L_v^l} \sum_{k'=0}^{k-1} r_{l+\ell q_v} r_{l+k' q_v}
\end{aligned}
$$

A. ANALYTICAL EVALUATION OF AWGN NOISE PERFORMANCE OF CCASK

Again, in order to simplify the notations, under the condition that $L \gg q_1, q_0$, $\overline{L_v} = \frac{1}{q_v}\sum_{l=1}^{q_v} L_v^l$ can be defined to approximate L_v^l ($l \in \{1, 2, ..., q_v\}$), which agrees with $L = (\overline{L_v} + 1)q_v$. Therefore, $V_m(v)$ can be represented by

$$\begin{aligned} V_m[v] &= \frac{\overline{L_v}^2 + \overline{L_v} - 1}{L(\overline{L_v}^2 + \overline{L_v})} \sum_{l=1}^{q_v}\sum_{k=0}^{L_v^l} r_{l+\ell q_v}^2 - \frac{2q_v}{L^2}\frac{\overline{L_v}+2}{\overline{L_v}} \sum_{l=1}^{q_v}\sum_{k=0}^{L_v^l}\sum_{k'=0}^{k-1} r_{l+\ell q_v} r_{l+k'q_v} \\ &\approx \frac{1}{L}\sum_{n=1}^{L} r_n^2 - \frac{2q_v(L+q_v)}{L^2(L-q_v)} \sum_{l=1}^{q_v}\sum_{k=0}^{L_v^l}\sum_{k'=0}^{k-1} r_{l+\ell q_v} r_{l+k'q_v} \end{aligned} \tag{A.30}$$

Therefore, the detection variable V_{b_m} can be represented by

$$\begin{aligned} V_{b_m} &= V_m[0] - V_m[1] \\ &= \frac{2q_1(L+q_1)}{L^2(L-q_1)} \sum_{l=1}^{q_1}\sum_{k=0}^{L_1^l}\sum_{k'=0}^{k-1} r_{l+kq_1} r_{l+k'q_1} \\ &\quad - \frac{2q_0(L+q_0)}{L^2(L-q_0)} \sum_{l=1}^{q_0}\sum_{k=0}^{L_0^l}\sum_{k'=0}^{k-1} r_{l+kq_0} r_{l+k'q_0} \\ &= \frac{2q_1(L+q_1)}{L^2(L-q_1)} \sum_{l=1}^{q_1}\sum_{k=0}^{L_1^l}\sum_{k'=0}^{k-1} (s_{l+kq_1} + b_{l+kq_1})(s_{l+k'q_1} + b_{l+k'q_1}) \\ &\quad - \frac{2q_0(L+q_0)}{L^2(L-q_0)} \sum_{l=1}^{q_0}\sum_{k=0}^{L_0^l}\sum_{k'=0}^{k-1} (s_{l+kq_0} + b_{l+kq_0})(s_{l+k'q_0} + b_{l+k'q_0}) \\ &= \frac{2q_1(L+q_1)}{L^2(L-q_1)} \sum_{l=1}^{q_1}\sum_{k=0}^{L_1^l}\sum_{k'=0}^{k-1} (s_{l+kq_1} s_{l+k'q_1} + b_{l+kq_1} b_{l+k'q_1}) \\ &\quad + \frac{2q_1(L+q_1)}{L^2(L-q_1)} \sum_{l=1}^{q_1}\sum_{k=0}^{L_1^l}\sum_{k'=0}^{k-1} (s_{l+kq_1} b_{l+k'q_1} + b_{l+kq_1} s_{l+k'q_1}) \\ &\quad - \frac{2q_0(L+q_0)}{L^2(L-q_0)} \sum_{l=1}^{q_0}\sum_{k=0}^{L_0^l}\sum_{k'=0}^{k-1} (s_{l+kq_0} s_{l+k'q_0} + b_{l+kq_0} b_{l+k'q_0}) \\ &\quad - \frac{2q_0(L+q_0)}{L^2(L-q_0)} \sum_{l=1}^{q_0}\sum_{k=0}^{L_0^l}\sum_{k'=0}^{k-1} (s_{l+kq_0} b_{l+k'q_0} + b_{l+kq_0} s_{l+k'q_0}) \end{aligned} \tag{A.31}$$

Therefore, the expectation of V_{b_m} can be obtained as

$$\begin{aligned}
E(V_{b_m}) = & \frac{2q_1(L+q_1)}{L^2(L-q_1)} \sum_{l=1}^{q_1} \sum_{k=0}^{L_1^l} \sum_{k'=0}^{k-1} E(s_{l+kq_1} s_{l+k'q_1}) \\
& - \frac{2q_0(L+q_0)}{L^2(L-q_0)} \sum_{l=1}^{q_0} \sum_{k=0}^{L_0^l} \sum_{k'=0}^{k-1} E(s_{l+kq_0} s_{l+k'q_0}) \\
= & (-1)^{i+1} \Big(\frac{L+q_i}{Lq_i} \sum_{l=1}^{q_i} \big\langle \mathbf{x}_{q_i,l}^{(i)} \big\rangle^2 - \frac{L+q_{1-i}}{Lq_{1-i}} \sum_{l=1}^{q_{1-i}} \big\langle \mathbf{x}_{q_{1-i},l}^{(i)} \big\rangle^2 \Big) \\
= & (-1)^{i+1} (1 + \frac{q_i}{L}) \langle \mu^2 \rangle^{(i)})
\end{aligned} \tag{A.32}$$

As long as the variance of V_{b_m} is considered, firstly, it could be expanded as

$$\begin{aligned}
\mathrm{Var}(V_{b_m}) = & \frac{4q_1^2(L+q_1)^2}{L^4(L-q_1)^2} \mathrm{Var}\Big(\sum_{l=1}^{q_1} \sum_{k=0}^{L_1^l} \sum_{k'=0}^{k-1} (s_{l+kq_1} s_{l+k'q_1} + b_{l+kq_1} b_{l+k'q_1}) \Big) \\
& + \frac{4q_1^2(L+q_1)^2}{L^4(L-q_1)^2} \mathrm{Var}\Big(\sum_{l=1}^{q_1} \sum_{k=0}^{L_1^l} \sum_{k'=0}^{k-1} (s_{l+kq_1} b_{l+k'q_1} + b_{l+kq_1} s_{l+k'q_1}) \Big) \\
& + \frac{4q_0^2(L+q_0)^2}{L^4(L-q_0)^2} \mathrm{Var}\Big(\sum_{l=1}^{q_0} \sum_{k=0}^{L_0^l} \sum_{k'=0}^{k-1} (s_{l+kq_0} s_{l+k'q_0} + b_{l+kq_0} b_{l+k'q_0}) \Big) \\
& + \frac{4q_0^2(L+q_0)^2}{L^4(L-q_0)^2} \mathrm{Var}\Big(\sum_{l=1}^{q_0} \sum_{k=0}^{L_0^l} \sum_{k'=0}^{k-1} (s_{l+kq_0} b_{l+k'q_0} + b_{l+kq_0} s_{l+k'q_0}) \Big)
\end{aligned} \tag{A.33}$$

Since the extensions of the other elements of $\mathrm{Var}(V_{b_m})$ have been done in (A.21)-(A.25), inserting them into (A.33), the expression of $\mathrm{Var}(V_{b_m})$ can be obtained as

$$\begin{aligned}
\mathrm{Var}(V_{b_m}) = & \frac{4(L+q_i)^3}{3L^3(L-q_i)} \langle \mu^2 \delta^2 \rangle^{(i)} + \frac{2q_i(L+q_i)^2}{L^3(L-q_i)} \langle \delta^4 \rangle^{(i)} + \frac{2q_{1-i}(L+q_{1-i})^2}{L^3(L-q_{1-i})} \Delta^4 \\
& + \Big(\frac{(L+q_i)^2(2L-q_i)}{3L^3(L-q_i)} \langle \mu^2 \rangle^{(i)} + \frac{q_i(L+q_i)^2}{L^3(L-q_i)} \langle \delta^2 \rangle^{(i)} + \frac{q_{1-i}(L+q_{1-i})^2}{L^3(L-q_{1-i})} \Delta^2 \Big) 4\sigma^2 \\
& + \Big(\frac{q_i(L+q_i)^2}{L^3(L-q_i)} + \frac{q_{1-i}(L+q_{1-i})^2}{L^3(L-q_{1-i})} \Big) 2\sigma^4
\end{aligned} \tag{A.34}$$

Consequently, replacing $E(\varepsilon^{(i)})$ and $\mathrm{Var}(\varepsilon^{(i)})$ in equations (3.55)-(3.57) by $E(V_{b_m}^{(i)})$ and $\mathrm{Var}(V_{b_m}^{(i)})$ in $(A.32)$ and $(A.34)$ respectively, the BER performance of the binary

A. ANALYTICAL EVALUATION OF AWGN NOISE PERFORMANCE OF CCASK

CCASK using statistical detection can be presented as

$$\begin{aligned}
&\mathrm{BER}_{\mathrm{CCASK}} \\
&= \frac{1}{4}\sum_{i=0}^{1}\mathrm{erfc}\Bigg[\Bigg(\frac{8(L+q_i)}{3L(L-q_i)}\frac{\langle\mu^2\delta^2\rangle^{(i)}}{\langle\mu^2\rangle^{(i)^2}} + \frac{4q_i}{L(L-q_i)}\frac{\langle\delta^4\rangle^{(i)}}{\langle\mu^2\rangle^{(i)^2}} + \frac{4q_{1-i}}{L(L-q_{1-i})}\frac{\Delta^4}{\langle\mu^2\rangle^{(i)^2}} \\
&\qquad + \Big(\frac{4(2L-q_i)}{3(L-q_i)}\frac{\langle\mu^2\rangle^{(i)}}{\langle\mu^2\rangle^{(i)^2}} + \frac{4q_i}{(L-q_i)}\frac{\langle\delta^2\rangle^{(i)}}{\langle\mu^2\rangle^{(i)^2}} + \frac{4q_{1-i}}{(L-q_{1-i})}\frac{\Delta^2}{\langle\mu^2\rangle^{(i)^2}}\Big)\frac{2\sigma^2}{L} \\
&\qquad + \Big(\frac{q_i}{L(L-q_i)} + \frac{q_{1-i}}{L(L-q_{1-i})}\Big)\frac{4\sigma^4}{\langle\mu^2\rangle^{(i)^2}}\Bigg)^{-\frac{1}{2}}\Bigg]
\end{aligned} \tag{A.35}$$

In case of large number of samples per symbol and relative small zones of CCAs are considered, i.e., $L \gg q_0, q_1$, and $\langle\delta^2\rangle^{(i)} \ll \langle\mu^2\rangle^{(i)}$, it's reasonable to do the approximations as $E_{b_d} = L\Delta^2 = L(\langle\mu^2\rangle^{(i)} + \langle\delta^2\rangle^{(i)}) \approx L\langle\mu^2\rangle^{(i)}$. Furthermore, according to equation (3.47) and equation (3.42), $E_b = E_{b_d}/(2W)$ and $N_0 = W\sigma^2$ can be inserted in (A.35), and the expression of BER performance the binary CCASK using statistical detection can also be approximated in function of E_b/N_0 as

$$\mathrm{BER}_{\mathrm{CCASK}} \approx \frac{1}{4}\sum_{i=0}^{1}\mathrm{erfc}\left[\left(\frac{8}{3}\frac{N_0}{E_b} + (q_i + q_{1-i})\frac{N_0^2}{E_b^2}\right)^{-\frac{1}{2}}\right] \tag{A.36}$$

Appendix B

Analytical Evaluation of AWGN Noise Performance of CCAFSK

Similarly as in Appendix A, the analytical evaluation of the noise performance of CCAFSK in AWGN channel will be talked about in the discrete-time baseband equivalent AWGN channel model. The analysis will be done on the passband carrier removed signal of the m^{th} received symbol $r(t) = s(t) + b(t)$ $(t \in [mT, (m+1)T])$, and the sampled sequence of which is $\mathbf{r}_m = (r_m[1],\ r_m[2],\ ...,\ r_m[L])$, with $r_m[n] = s_m[n] + b_m[n]$ $(n \in \{1, 2, ..., L\})$. The index m will be dropped for the sake of simplification, and r_n, s_n, x_n and b_n will be used to stand for $r_m[n]$, $s_m[n]$, $x_m[n]$ and $b_m[n]$, without loss of generality.

Remind that for binary CCAFSK, the baseband modulated symbols also have real values: $s_n = x_n$ when a '0' was transmitted, while $s_n = (-1)^n x_n$ when an '1' was transmitted. In other words, $s_n = (-1)^{ni} x_n$ when an $'i'$ was transmitted. Hence, the real statistics of the equivalent discrete-time baseband AWGN channel model is sufficient for the detection of the real valued baseband modulated symbols, with $r_{n,I} = s_n + b_{n,I}$ $(n \in \{1, 2, ..., L\})$ Again, r_n and b_n will be used to present the real valued terms $r_{n,I}$ and $b_{n,I}$ for the simplification, with the variance of b_n equal to σ^2 as defined in equation (3.42).

According to equations (3.55)-(3.57), the general expression of noise performance of the binary CCAFSK can be obtained as a function of the expectation and variance of the detection variable B_{b_m} in equation (3.92). Hence, the expression of the two statistics should be analyzed firstly.

B. ANALYTICAL EVALUATION OF AWGN NOISE PERFORMANCE OF CCAFSK

Let's start with the analysis of the squared magnitudes of $2p$-point DFT of $\mathbf{r}_m$ in equation (3.91), which can be extended as

$$\begin{aligned} A_m^2[K] &= \Big| \sum_{n=1}^{L} r_n e^{-j2\pi \frac{K}{2q} n} \Big|^2 \\ &= \Big(\sum_{n=1}^{L} r_n \cos(2\pi \frac{K}{2q} n) \Big)^2 + \Big(\sum_{n=1}^{L} r_n \sin(2\pi \frac{K}{2q} n) \Big)^2 \end{aligned} \tag{B.1}$$

where $K \in \{1, 2, ..., 2q\}$. The mean of $(B.1)$ in case that the value of K is even, i.e., $K = 2K_1$ with $K_1 \in \{1, 2, ..., q\}$, can be extended in the form of equation (2.18) as

$$\begin{aligned} &\frac{1}{q} \sum_{K_1=1}^{q} A_m^2[2K_1] \\ &= \frac{1}{q} \sum_{K_1=1}^{q} \Big[\Big(\sum_{n=1}^{L} r_n \cos(2\pi \frac{2K_1}{2q} n) \Big)^2 + \Big(\sum_{n=1}^{L} r_n \sin(2\pi \frac{2K_1}{2q} n) \Big)^2 \Big] \\ &= \frac{1}{q} \sum_{K_1=1}^{q} \Big(\sum_{l=1}^{q} \sum_{k=0}^{L_l} r_{l+kq} \cos(2\pi \frac{2K_1}{2q} (l + kq)) \Big)^2 \\ &\quad + \frac{1}{q} \sum_{K_1=1}^{q} \Big(\sum_{l=1}^{q} \sum_{k=0}^{L_l} r_{l+kq} \sin(2\pi \frac{2K_1}{2q} (l + kq)) \Big)^2 \\ &= \frac{1}{q} \sum_{K_1=1}^{q} \Big[\Big(\sum_{l=1}^{q} \sum_{k=0}^{L_l} r_{l+kq} \cos(\frac{2K_1}{q} l\pi) \Big)^2 + \Big(\sum_{l=1}^{q} \sum_{k=0}^{L_l} r_{l+kq} \sin(\frac{2K_1}{q} l\pi) \Big)^2 \Big] \\ &= \frac{1}{q} \sum_{K_1=1}^{q} \Big[\Big(\sum_{l=1}^{q} \xi(q,l) \cos(\frac{2K_1}{q} l\pi) \Big)^2 + \Big(\sum_{l=1}^{q} \xi(q,l) \sin(\frac{2K_1}{q} l\pi) \Big)^2 \Big] \\ &= \frac{1}{q} \sum_{K_1=1}^{q} \sum_{l=1}^{q} \xi^2(q,l) + \frac{1}{q} \sum_{K_1=1}^{q} \sum_{l=1}^{q} \sum_{\substack{l'=1 \\ l' \neq l}}^{q} \xi(q,l)\xi(q,l') \cos\Big(\frac{K_1}{q} (l - l') 2\pi \Big) \\ &= \frac{1}{q} \sum_{K_1=1}^{q} \sum_{l=1}^{q} \xi^2(q,l) + \frac{1}{q} \sum_{l=1}^{q} \sum_{\substack{l'=1 \\ l' \neq l}}^{q} \xi(q,l)\xi(q,l') \Big[\sum_{K_1=1}^{q} \cos\Big(\frac{K_1}{q} (l - l') 2\pi \Big) \Big] \\ &= \sum_{l=1}^{q} \xi^2(q,l) \end{aligned} \tag{B.2}$$

where $L_l = \Big\lfloor \frac{L-l}{q} \Big\rfloor$, and $\xi(q,l) = \sum_{k=0}^{L_l} r_{l+kq}$. Similarly, the mean of $(B.1)$ in case that the value of K is odd, i.e., $K = 2K_1 - 1$ with $K_1 \in \{1, 2, ..., q\}$ can be also extended

and written in the same form as

$$
\begin{aligned}
&\frac{1}{q}\sum_{K_1=1}^{q} A_m^2[2K_1-1] \\
&= \frac{1}{q}\sum_{K_1=1}^{q}\Big(\sum_{l=1}^{q}\sum_{k=0}^{L_l}(-1)^k r_{l+kq}\cos(\frac{2K_1-1}{q}l\pi)\Big)^2 \\
&\quad +\frac{1}{q}\sum_{K_1=1}^{q}\Big(\sum_{l=1}^{q}\sum_{k=0}^{L_l}(-1)^k r_{l+kq}\sin(\frac{2K_1-1}{q}l\pi)\Big)^2 \\
&= \frac{1}{q}\sum_{K_1=1}^{q}\Big[\Big(\sum_{l=1}^{q}\breve{\xi}(q,l)\cos(\frac{2K_1-1}{q}l\pi)\Big)^2+\Big(\sum_{l=1}^{q}\breve{\xi}(q,l)\sin(\frac{2K_1-1}{q}l\pi)\Big)^2\Big] \\
&= \frac{1}{q}\sum_{K_1=1}^{q}\sum_{l=1}^{q}\breve{\xi}^2(q,l)+\frac{1}{q}\sum_{K_1=1}^{q}\sum_{l=1}^{q}\sum_{\substack{l'=1\\l'\neq l}}^{q}\breve{\xi}(q,l)\breve{\xi}(q,l')\cos\Big(\frac{2K_1-1}{q}(l-l')\pi\Big) \\
&= \sum_{K_1=1}^{q}\sum_{l=1}^{q}\breve{\xi}^2(q,l) \\
&\quad +\frac{1}{q}\sum_{l=1}^{q}\sum_{\substack{l'=1\\l'\neq l}}^{q}\breve{\xi}(q,l)\breve{\xi}(q,l')\cos\Big(\frac{1}{q}(l-l')\pi\Big)\Big[\sum_{K_1=1}^{q}\cos\Big(\frac{K_1}{q}(l-l')2\pi\Big)\Big] \\
&\quad +\frac{1}{q}\sum_{l=1}^{q}\sum_{\substack{l'=1\\l'\neq l}}^{q}\breve{\xi}(q,l)\breve{\xi}(q,l')\sin\Big(\frac{1}{q}(l-l')\pi\Big)\Big[\sum_{K_1=1}^{q}\sin\Big(\frac{K_1}{q}(l-l')2\pi\Big)\Big] \\
&= \sum_{l=1}^{q}\breve{\xi}^2(q,l)
\end{aligned}
\tag{B.3}
$$

where $\breve{\xi}(q,l)=\sum_{k=0}^{L_l}(-1)^k r_{l+kq}$. Remind that the expansions in (B.2) and (B.3) have used the following results:

$$\sum_{K_1=1}^{q}\cos\Big(\frac{K_1}{q}(l-l')2\pi\Big)=0 \tag{B.4}$$

$$\sum_{K_1=1}^{q}\sin\Big(\frac{K_1}{q}(l-l')2\pi\Big)=0 \tag{B.5}$$

Therefore, the decision variable B_{b_m} of CCAFSK in equation (3.92) can be extended

and represented by

$$\begin{aligned}
B_{b_m} &= \sum_{l=1}^{q}\left[\breve{\xi}^2(q,l) - \xi^2(q,l)\right] \\
&= \sum_{l=1}^{q}\sum_{k=0}^{L_l}\sum_{k'=0}^{L_l}\Big((-1)^{k+k'}-1\Big)r_{l+kq}r_{l+k'q} \\
&= 2\sum_{l=1}^{q}\sum_{k=0}^{L_l}\sum_{k'=0}^{k-1}\Big((-1)^{k+k'}-1\Big)r_{l+kq}r_{l+k'q} \\
&= -4\sum_{l=1}^{q}\sum_{k=1}^{L_l}\sum_{\Delta k=0}^{\lfloor\frac{k-1}{2}\rfloor} r_{l+kq}r_{l+(k-2\Delta k-1)q}
\end{aligned} \tag{B.6}$$

Since it was supposed that q is odd, it can be obtained that $s_{l+kq} = (-1)^{(l+kq)i}x_{l+kq} = (-1)^{(l+k)i}x_{l+kq}$. Hence, the decision variable B_{b_m} in (B.6) can be expanded as

$$\begin{aligned}
B_{b_m} &= -4\sum_{l=1}^{q}\sum_{k=1}^{L_l}\sum_{\Delta k=0}^{\lfloor\frac{k-1}{2}\rfloor}\Big(s_{l+kq}+b_{l+kq}\Big)\Big(s_{l+(k-2\Delta k-1)q}+b_{l+(k-2\Delta k-1)q}\Big) \\
&= -4\sum_{l=1}^{q}\sum_{k=1}^{L_l}\sum_{\Delta k=0}^{\lfloor\frac{k-1}{2}\rfloor}\Big((-1)^{(l+k)i}x_{l+kq}+b_{l+kq}\Big) \\
&\qquad\qquad \times\Big((-1)^{(l+k-2\Delta k-1)i}x_{l+(k-2\Delta k-1)q}+b_{l+(k-2\Delta k-1)q}\Big) \\
&= -4\sum_{l=1}^{q}\sum_{k=1}^{L_l}\sum_{\Delta k=0}^{\lfloor\frac{k-1}{2}\rfloor}(-1)^{i}x_{l+kq}x_{l+(k-2\Delta k-1)q} \\
&\quad -4\sum_{l=1}^{q}\sum_{k=1}^{L_l}\sum_{\Delta k=0}^{\lfloor\frac{k-1}{2}\rfloor}(-1)^{(l+k)i}x_{l+kq}b_{l+(k-2\Delta k-1)q} \\
&\quad -4\sum_{l=1}^{q}\sum_{k=1}^{L_l}\sum_{\Delta k=0}^{\lfloor\frac{k-1}{2}\rfloor}(-1)^{(l+k-1)i}s_{l+(k-2\Delta k-1)q}b_{l+kq} \\
&\quad -4\sum_{l=1}^{q}\sum_{k=1}^{L_l}\sum_{\Delta k=0}^{\lfloor\frac{k-1}{2}\rfloor}b_{l+kq}b_{l+(k-2\Delta k-1)q}
\end{aligned} \tag{B.7}$$

In order to simplify the notations, let's define $\overline{L} = \frac{1}{q}\sum_{l=1}^{q}L_l$ to approximate all the L_l ($l \in \{1,2,...,q\}$), which agrees with $L = (\overline{L}+1)q$. Hence, the expectation of B_{b_m}

when an $'i'$ was transmitted can be presented by these statistical values as

$$\begin{aligned}
E(B_{b_m}^{(i)}) &= -4\sum_{l=1}^{q}\sum_{k=1}^{L_l}\sum_{\Delta k=0}^{\lfloor\frac{k-1}{2}\rfloor} E\Big[(-1)^i x_{l+kq}x_{l+(k-2\Delta k-1)q}\Big] \\
&= (-1)^{i+1}4\sum_{l=1}^{q}\sum_{k=1}^{L_l}\sum_{\Delta k=0}^{\lfloor\frac{k-1}{2}\rfloor}\big\langle \mathbf{x}_{q,l}\big\rangle^2 \\
&= (-1)^{i+1}\overline{L}(\overline{L}+2)\sum_{l=1}^{q}\mu_l^2 \\
&= (-1)^{i+1}(L-q)(\frac{L}{q}+1)\langle\mu^2\rangle
\end{aligned} \tag{B.8}$$

Similarly, the variance of B_{b_m} when an $'i'$ was transmitted can be extended as

$$\begin{aligned}
\mathrm{Var}(B_{b_m}^{(i)}) &= 16\mathrm{Var}\Big[\sum_{l=1}^{q}\sum_{k=1}^{L_l}\sum_{\Delta k=0}^{\lfloor\frac{k-1}{2}\rfloor}\Big(s_{l+kq}+b_{l+kq}\Big)\Big(s_{l+(k-2\Delta k-1)q}+b_{l+(k-2\Delta k-1)q}\Big)\Big] \\
&= 16\mathrm{Var}\Big[\sum_{l=1}^{q}\sum_{k=1}^{L_l}\sum_{\Delta k=0}^{\lfloor\frac{k-1}{2}\rfloor} x_{l+kq}x_{l+(k-2\Delta k-1)q}\Big] \\
&\quad +16\mathrm{Var}\Big[\sum_{l=1}^{q}\sum_{k=1}^{L_l}\sum_{\Delta k=0}^{\lfloor\frac{k-1}{2}\rfloor}(-1)^{(l+k)i}x_{l+kq}b_{l+(k-2\Delta k-1)q}\Big] \\
&\quad +16\mathrm{Var}\Big[\sum_{l=1}^{q}\sum_{k=1}^{L_l}\sum_{\Delta k=0}^{\lfloor\frac{k-1}{2}\rfloor}(-1)^{(l+k)i}x_{l+(k-2\Delta k-1)q}b_{l+kq}\Big] \\
&\quad +16\mathrm{Var}\Big[\sum_{l=1}^{q}\sum_{k=1}^{L_l}\sum_{\Delta k=0}^{\lfloor\frac{k-1}{2}\rfloor} b_{l+kq}b_{l+(k-2\Delta k-1)q}\Big]
\end{aligned} \tag{B.9}$$

The further extensions of the elements of $\mathrm{Var}(B_{b_m})$ in (B.9) can be operated as

$$\begin{aligned}
&\mathrm{Var}\Big[\sum_{l=1}^{q}\sum_{k=1}^{L_l}\sum_{\Delta k=0}^{\lfloor\frac{k-1}{2}\rfloor} x_{l+kq}x_{l+(k-2\Delta k-1)q}\Big] \\
&= \sum_{l=1}^{q}\sum_{k=1}^{L_l}\mathrm{Var}\Big[x_{l+kq}\sum_{\Delta k=0}^{\lfloor\frac{k-1}{2}\rfloor} x_{l+(k-2\Delta k-1)q}\Big] \\
&= \frac{\overline{L}}{12}\sum_{l=1}^{q}\Big((\overline{L}^2+6\overline{L}+\frac{35}{4})\mu_l^2+3(\overline{L}+2)\delta_l^2\Big)\delta_l^2 \\
&= \frac{L-q}{12}\Big(\frac{L^2}{q^2}+4\frac{L}{q}+\frac{15}{4}\Big)\langle\mu^2\delta^2\rangle+\frac{L-q}{4}\Big(\frac{L}{q}+1\Big)\langle\delta^4\rangle
\end{aligned} \tag{B.10}$$

$$
\begin{aligned}
&\mathrm{Var}\Big[\sum_{l=1}^{q}\sum_{k=1}^{L_l}\sum_{\Delta k=0}^{\lfloor\frac{k-1}{2}\rfloor}(-1)^{(l+k)i}x_{l+kq}b_{l+(k-2\Delta k-1)q}\Big]\\
&=\mathrm{Var}\Big[\sum_{l=1}^{q}\sum_{k=1}^{L_l}\sum_{\Delta k=0}^{\lfloor\frac{k-1}{2}\rfloor}(-1)^{(l+k)i}x_{l+(k-2\Delta k-1)q}b_{l+kq}\Big]\\
&=\frac{\overline{L}}{12}\sum_{l=1}^{q}\Big((\overline{L}^2+3\overline{L}+\frac{11}{4})\mu_l^2+3(\overline{L}+2)\delta_l^2\Big)\sigma^2\\
&=\frac{L-q}{12}\Big(\frac{L^2}{q^2}+\frac{L}{q}+\frac{3}{4}\Big)\langle\mu^2\rangle\sigma^2+\frac{L-q}{4}\Big(\frac{L}{q}+1\Big)\langle\delta^2\rangle\sigma^2
\end{aligned}
\tag{B.11}
$$

$$
\begin{aligned}
&\mathrm{Var}\Big[\sum_{l=1}^{q}\sum_{k=1}^{L_l}\sum_{\Delta k=0}^{\lfloor\frac{k-1}{2}\rfloor}b_{l+kq}b_{l+(k-2\Delta k-1)q}\Big]\\
&=\frac{\overline{L}(\overline{L}+2)}{4}q\sigma^4\\
&=\frac{L-q}{4}\Big(\frac{L}{q}+1\Big)\sigma^4
\end{aligned}
\tag{B.12}
$$

Therefore, inserting $(B.10)$-$(B.12)$ into (B.9), the expression of variance of B_{b_m} using the statistics of signal and noise can be obtained as

$$
\begin{aligned}
\mathrm{Var}(B_{b_m}^{(i)})=&\frac{4}{3}(L-q)\Big(\frac{L^2}{q^2}+4\frac{L}{q}+\frac{15}{4}\Big)\langle\mu^2\delta^2\rangle+4(L-q)\Big(\frac{L}{q}+1\Big)\langle\delta^4\rangle\\
&+\frac{8}{3}(L-q)\Big(\frac{L^2}{q^2}+\frac{L}{q}+\frac{3}{4}\Big)\langle\mu^2\rangle+8(L-q)(\frac{L}{q}+1)\langle\delta^2\rangle\Big)\sigma^2\\
&+4(L-q)(\frac{L}{q}+1)\sigma^4
\end{aligned}
\tag{B.13}
$$

Consequently, replacing $E(\varepsilon^{(i)})$ and $\mathrm{Var}(\varepsilon^{(i)})$ in equations (3.55)-(3.57) by $E(B_{b_m}^{(i)})$ and $\mathrm{Var}(B_{b_m}^{(i)})$ in $(B.8)$ and $(B.13)$ respectively, the BER performance of the binary CCAFSK can be presented as

$$
\begin{aligned}
\mathrm{BER}_{\mathrm{CCAFSK}}=\frac{1}{4}\sum_{i=0}^{1}\mathrm{erfc}\Bigg[\Bigg(&\frac{2(4L^2+16Lq+15q^2)}{3(L-q)(L+q)^2}\frac{\langle\mu^2\delta^2\rangle}{\langle\mu^2\rangle^2}+\frac{8q}{(L^2-q^2)}\frac{\langle\delta^4\rangle}{\langle\mu^2\rangle^2}\\
&+\Big(\frac{4(4L^2+4Lq+3q^2)}{3(L-q)(L+q)^2}\frac{\langle\mu^2\rangle}{\langle\mu^2\rangle^2}+\frac{16q}{(L^2-q^2)}\frac{\langle\delta^2\rangle}{\langle\mu^2\rangle^2}\Big)\sigma^2\\
&+\frac{8q}{(L^2-q^2)}\frac{\sigma^4}{\langle\mu^2\rangle^2}\Bigg)^{-\frac{1}{2}}\Bigg]
\end{aligned}
\tag{B.14}
$$

In case of large number of samples per symbol and relative small zones of CCA are considered, i.e., $L \gg q$, and $\langle \delta^2 \rangle \ll \langle \mu^2 \rangle$, it's reasonable to do the approximations as $E_{b_d} = L\Delta^2 = L(\langle \mu^2 \rangle + \langle \delta^2 \rangle) \approx L\langle \mu^2 \rangle$. Similarly, the channel statistics derived in equation (3.47) and equation (3.42), i.e., $E_b = E_{b_d}/(2W)$ and $N_0 = W\sigma^2$, can be inserted in (B.14), and the expression of BER performance the binary CCAFSK can be approximated in function of E_b/N_0 as

$$\mathrm{BER}_{\mathrm{CCAFSK}} \approx \frac{1}{2}\mathrm{erfc}\left[\left(\frac{8}{3}\frac{N_0}{E_b} + 2q\frac{N_0^2}{E_b^2}\right)^{-\frac{1}{2}}\right] \tag{B.15}$$

B. ANALYTICAL EVALUATION OF AWGN NOISE PERFORMANCE OF CCAFSK

References

[1] V. Garg. *Wireless Commnications and Networking*. The Morgan Kaufmann Series in Networking. Morgan Kaufmann, 1 edition, June 2007. 1, 161

[2] B. P. Crow, I. Widjaja, L. G. Kim, and P. T. Sakai. **IEEE 802.11 Wireless Local Area Networks**. *Communications Magazine, IEEE*, **35**(9):116–126, September 1997. 1, 161

[3] K. J. Negus, A. P. Stephens, and J. Lansford. **HomeRF: wireless networking for the connected home**. *Personal Communications, IEEE*, **7**(1):20–27, 2000. 1, 161

[4] T. Matsumoto. **A chaotic attractor from Chua's circuit**. *IEEE Transactions on Circuits and Systems*, **31**(12):1055–1058, December 1984. 1, 5, 161

[5] L. M. Pecora and T. L. Carroll. **Synchronization in chaotic system**. *Phys. Rev. Lett.*, **64**(8):821–824, February 1990. 1, 5, 29, 161

[6] M. P. Kennedy, R. Rovatti, and G. Setti. *Chaotic Electronics In Telecommunications*. CRC, 1 edition, June 2000. 2, 27, 28, 30, 31, 33, 49, 85

[7] G. Kolumban and T. Krebesz. **UWB radio: A real chance for application of chaotic communications**. *International Symposium on Nonlinear Theory and its Applications*, pages 475–478, September 2006. 2

[8] G. Kolumban and T. Krebesz. **LR-WPAN and UWB data communication systems: A new possible application for chaotic carriers**. *IEEE Workshop on Nonlinear Maps and Applications (NOMA)*, 2007. 2

[9] A. F. Molisch, K. Balakrishnan, D. Cassioli, C. C. Chong, S. Emami, A. Fort, J. Karedal, J. Kunisch, H. Schantz, U. Schuster, and K. Siwiak. **IEEE 802.15.4a channel model - final report**. Technical report, Document IEEE 802.15.04-0662-02-004a, 2005. 2

[10] S. Bullett. **Invariant circles for the piecewise linear standard map**. *Communications in Mathematical Physics*, **107**(2):241–262, February 1986. 5, 36

[11] L. O. Chua and T. Lin. **Chaos in Digital Filters**. *IEEE Transaction on Circuits and Systems*, **36**(6):648–658, June 1988. 5

[12] U. Parlitz, L. O. Chua, L. Kocarev, K. S. Halle, and A. Shang. **Transmission of digital signals by chaotic synchronization**. *International Journal of Bifurcation and Chao*, **2**(4):973–977, December 1992. 5, 29

[13] M. J. Ogorzalek. **Taming chaos. I. Synchronization**. *IEEE Transactions on Circuits and Systems I: Fundamental Theory and Applications*, **40**(10):693–699, October 1993. 5

[14] K. T. Alligood, T. D. Sauer, and J. A. Yorke. *Chaos: an Introduction to Dynamical Systems*. Springer, 1996. 6, 7, 8, 13

[15] S. Wiggins. *Introduction to Applied Nonlinear Dynamical Systems and Chaos*. Springer, 2 edition, 2003. 6, 7, 8, 9, 11, 12, 13, 35, 40

[16] C. Mira. *Chaotic Dynamics*. World Scientific, 1987. 6, 7, 8

[17] G. Turin. **An introduction to matched filters**. *Information Theory, IRE Transactions on*, **6**(3):311–329, June 1960. 15

[18] J. Schiller. *Mobile Communications*. Addison Wesley, 2 edition, September 2003. 15

[19] A. Miceli. *Wireless Technician's Handbook*. Artech House moible communications series. Artech House Publishers, 2 edition, July 2003. 16

[20] D. Torrieri. *Principles of Spread-Spectrum Communication Systems*. Springer, 1 edition, Novembre 2004. 17, 20, 21, 22

[21] D. Tse and P. Viswanath. *Fundamentals of Wireless Communication*. Cambridge University Press, June 2005. 17, 18, 19, 66, 67, 80, 99, 168

[22] K. Fazel and S. Kaiser. *Multi-Carrier and Spread Spectrum Systems*. Wiley, 1 edition, November 2003. 17, 21, 22, 23, 24

[23] J. G. Proakis. *Communications Systems Engineering*. Englewook Cliffs, NJ: Prentice-Hall, 1994. 17, 18, 84

[24] R.L. Pickholtz, L.B. Milstein, and D.L. Schilling. **Spread spectrum for mobile communications**. *Vehicular Technology, IEEE Transactions on*, **40**(2):313–322, May 1991. 20

[25] M. Cohn and A. Lempel. **On fast M-sequence transforms (Corresp.)**. *IEEE Transactions on Information Theory*, **23**(1):135–137, January 1977. 21

[26] S. Weinstein and P. Ebert. **Data transmission by frequency-division multiplexing using the discrete Data Transmission by Frequency-Division Multiplexing Using the Discrete Fourier transform**. *Communication Technology, IEEE Transactions on*, **19**(5):628–634, October 1971. 24

[27] G. Heidari-Bateni and C. D. McGillem. **Chaotic sequences for spread spectrum: an alternative to PN-sequences**. *Wireless Communications, 1992. Conference Proceedings., 1992 IEEE International Conference on Selected Topics in*, pages 437–440, June 1992. 25

[28] G. Heidari-Bateni and C. D. McGillem. **A chaotic direct-sequence spread-spectrum communication system**. *Communications, IEEE Transactions on*, **42**(234):1524–1527, April 1994. 25

[29] G. Mazzini, G. Setti, and R. Rovatti. **Chaotic complex spreading sequences for asynchronous DS-CDMA. I. System modeling and result**. *Circuits and Systems I: Fundamental Theory and Applications, IEEE Transactions on*, **44**(10):937–947, October 1997. 25

[30] R. Rovatti, G. Setti, and G. Mazzini. **Chaotic complex spreading sequences for asynchronous DS-CDMA. Part II. Some theoretical performance bounds**. *Circuits and Systems I: Fundamental Theory and Applications, IEEE Transactions on*, **45**(4):496–506, April 1998. 25

[31] G. Mazzini, R. Rovatti, and G. Setti. **Chaos-based asynchronous DS-CDMA systems and enhanced Rake receivers: measuring the improvements**. *Circuits and Systems I: Fundamental Theory and Applications, IEEE Transactions on*, **48**(12):1445–1453, December 2001. 25

[32] C. Ling and S. Sun. **Chaotic Frequency Hopping Sequences**. *Communications, IEEE Transactions on*, **46**(11):1433–1437, November 1998. 25

[33] C. Ling and X. Wu. **Design and realization of an FPGA-based generator for chaotic frequency hopping sequences**. *IEEE Transactions on Circuits and Systems I: Fundamental Theory and Applications*, **48**(5):521–532, May 2001. 27

[34] Y. Akin and S. Erturk. **Chaotic frequency hopping for code division multiple access**. *Proceedings of the IEEE 12th Signal Processing and Communications Applications Conference*, pages 716–719, April 2004. 27

[35] G. Kolumban, M. P. Kennedy, and L. O. Chua. **The role of synchronization in digital communications using chaos. II. Chaotic modulation and chaotic synchronization**. *IEEE Transactions on Circuits and Systems—Part I: Fundamental Theory and Applications*, **45**(11):1129–1140, 1998. 27, 30, 33

[36] H. Dedieu, M. P. Kennedy, and M. Hasler. **Chaos shift keying: modulation and demodulation of a chaotic carrier using self-synchronizing Chua's circuits**. *Circuits and Systems II: Analog and Digital Signal Processing, IEEE Transactions on*, **40**(10):634–642, October 1993. 27, 28

[37] G. Kolumban, M. P. Kennedy, and G. Kis. **Performance improvement of chaotic communications systems**. *Proc. European Conf. on Circuit Theory and Design*, pages 284–289, September 1997. 27, 30

[38] T. Yang and L. O. Chua. **Secure communication via chaotic parameter modulation**. *Circuits and Systems I: Fundamental Theory and Applications, IEEE Transactions on*, **43**(9):817–819, September 1996. 27, 31

[39] G. Kolumban, B. Vizvari, W. Schwarz, and A. Abel. **Differential chaos shift keying: a robust coding for chaotic communication**. *Proc. Int. Specialist Workshop on Nonlinear Dynamics of Electronic Systems*, page 81, June 1996. 27, 31, 32

[40] G. Kolumban, M. P. Kennedy, Z. Jako, and G. Kis. **Chaotic communications with correlator receivers: theory and performance limits**. *Proceedings of the IEEE*, **90**(5):711–732, 2002. 28, 29, 30, 31

[41] W. M. Tam, F. C. M. Lau, C. K. Tse, and M. M. Yip. **An approach to calculating the bit-error rate of a coherent chaos-shift-keying digital communication system under a noisy multiuser environment**. *IEEE Transactions on Circuits and Systems I: Fundamental Theory and Applications*, **49**(2):210–223, 2002. 29

[42] H. Leung and Z. Zhu. **Performance evaluation of EKF-based chaotic synchronization**. *Circuits and Systems I: Fundamental Theory and Applications, IEEE Transactions on*, **48**(9):1118–1125, September 2001. 29

[43] G. Kolumban, M. P. Kennedy, and L. O. Chua. **The role of synchronization in digital communications using chaos. I . Fundamentals of digital communications**. *IEEE Transactions on Circuits and Systems—Part I: Fundamental Theory and Applications*, **44**(10):927–936, 1997. 30

[44] J. M. Cruz and L. O. Chua. **An IC chip of Chua's circuit**. *Circuits and Systems II: Analog and Digital Signal Processing, IEEE Transactions on*, **40**(10):614–625, October 1993. 31

[45] H. Leung, S. Shanmugam, N. Xie, and S. Wan. **An ergodic approach for chaotic signal estimation at low SNR with application to ultra-wideband communication**. *Signal Processing, IEEE Transactions on*, **54**(3):1091–1103, March 2006. 31

[46] T. Yang. **Recovery of digital signals from chaotic switching**. *International journal of circuit theory and applications*, **23**(6):611–615, 1995. 31

[47] G. Kolumban and M. P. Kennedy. **DCSK: Chaotic modulation for multipath environments**. *Presymp. Tutorial ISCAS'2000*, May 2000. 33

[48] M. Sushchik, Lev S. Tsimring, and A. R. Volkovskii. **Performance analysis of correlation-based communication schemes utilizing chaos**. *Circuits and Systems I: Fundamental Theory and Applications, IEEE Transactions*, **47**:1684–1691, December 2000. 33, 175

[49] G. Kolumban, Z. Jako, and M. P. Kennedy. **Enhanced versions of DCSK and FM-DCSK data transmission systems**. In *Proc. IEEE International Symposium on Circuits and Systems ISCAS '99*, **4**, pages 475–478 vol.4, 1999. 33

[50] G. Kolumban, G. Kis, F. C. M. Lau, and C. K. Tse. **Optimum noncoherent FM-DCSK detector: application of chaotic GML decision rule**. In *Proc. International Symposium on Circuits and Systems ISCAS '04*, **4**, pages IV–597–600 Vol.4, 2004. 33

[51] Y. Xia, C.K. Tse, and F.C.M. Lau. **Performance of differential chaos-shift-keying digital communication systems over a multipath fading channel with delay spread**. *IEEE Transactions on Circuits and Systems II: Express Briefs*, **51**(12):680–684, December 2004. 33

[52] Z. Zhou, T. Zhou, and J. Wang. **Performance of Multi-User DCSK Communication System Over Multipath Fading Channel**. *IEEE International Symposium on Circuits and Systems*, pages 2478–2481, May 2007. 33

[53] H. Li, X. Dai, and P. Xu. **A CDMA based multiple-access scheme for DCSK**. *Proceedings of the IEEE 6th Circuits and Systems Symposium on Emerging Technologies: Frontiers of Mobile and Wireless Communication*, **1**:313–316, May 2004. 33

[54] C. C. Chong and S. K. Yong. **UWB Direct Chaotic Communication Technology for Low-Rate WPAN Applications**. *IEEE Transactions on Vehicular Technology*, **57**(3):1527–1536, 2008. 33

[55] H. Poincare. **Sur les courbes definies par une equations differentielle**. *OEuvre*, **1**, 1892. 35

[56] S. Cantat. **Theoreme de Poincare-Bendixson**. *Le journal de maths des eleves*, **1**(3), 1995. 35

[57] P. Charge, D. Fournier-Prunaret, and V. Guglielm. **Features analysis of a parametric PWL chaotic map and its utilization for secure transmissions**. *Chaos, Solitons and Fractals*, **38**(5):1411–1422, December 2008. 36

[58] M. Hasler and Y. L. Maistrenko. **An introduction to the synchronization of chaotic systems: coupled skew tent maps**. *Circuits and Systems I: Fundamental Theory and Applications, IEEE Transactions on*, **44**(10):856–866, October 1997. 36

[59] T. Addabbo, M. Alioto, A. Fort, S. Rocchi, and V. Vignoli. **The Digital Tent Map: Performance Analysis and Optimized Design as a Low-Complexity Source of Pseudorandom Bits**. *Instrumentation and Measurement, IEEE Transactions on*, **55**(5):1451–1458, October 2006. 36

[60] M. J. S. Smith. **An analog integrated neural network capable of learning the Feigenbaum logistic map**. *Circuits and Systems, IEEE Transactions on*, **37**(6):841–844, June 1990. 36

[61] J. Tou, P. Yip, and H. Leung. **Spread-spectrum signals and the chaotic logistic map**. *Circuits, Systems, and Signal Processing*, **18**(1):59–73, January 1999. 36

[62] M. B. Luca, S. Azou, G. Burel, and A. Serbanescu. **On exact Kalman filtering of polynomial systems**. *Circuits and Systems I: Regular Papers, IEEE Transactions on*, **53**(6):1329–1340, June 2006. 36

[63] K. Kelber, M. Gotz, and W. Schwarz. **Generation of chaotic signals with n-dimensional uniform probability distribution by digital filter structures**. *Digital Signal Processing Workshop Proceedings, 1996., IEEE*, pages 486–489, September 1996. 36

[64] F. Dachselt and W. Schwarz. **Chaos and cryptography**. *Circuits and Systems I: Fundamental Theory and Applications, IEEE Transactions on*, **48**(12):1498–1509, December 2001. 36

[65] M. J. Ogorzalek and Z. Galias. **Arnold tongues and devil's staircase in a digital filter employing saturation arithmeti**. *Circuits and Systems, 1991., IEEE International Sympoisum on*, **1**:384–387, June 1991. 43, 165

[66] T. Ueta, S. Tsuji, T. Yoshinaga, and H. Kawakamt. **Calculation of the Isocline for the Fixed Point with a Specified Argument of Complex Multipliers**. *IEEE Digital Object Identifier*, **2**:755–758, 2001. 43

[67] Y. Xu, P. Charge, and D. Fournier-Prunaret. **Chaotic Cyclic Attractors Shift Keying**. *International Conference on Neural Networks and Signal Processing*, pages 62–66, june 2008. 73, 170

[68] Y. XU, P. Charge, and D. Fournier-Prunaret. **Chaotic Cyclic Attractors Shift Keying for Low-Rate UWB Chaotic Cyclic Attractors Shift Keying for Low-Rate UWB Communications**. *Internation Symposium on Nonlinear Theory and its Applications*, pages 648–651, September 2008. 75, 170

[69] Y. XU, P. Charge, and D. Fournier-Prunaret. **Chaos-based Communication Utilizing Attractor Statistic Detection**. *The 2nd Chaotic Modeling and Simulation International Conference*, June 2009. 76, 172

[70] K. Pahlavan and A. H. Levesque. *Wireless Information Networks*. Wiley, 2 edition, October 2005. 99

[71] K. Halfor and M. Webster. **Multipath Measurement in Wireless LANs**. Application note AN9895.1, Intersil, October 2001. 100

[72] M. P. Kennedy, G. Kolumban, G. Kis, and Z. Jako. **Performance evaluation of FM-DCSK modulation in multipath environments**. *IEEE Transactions on Circuits and Systems—Part I: Fundamental Theory and Applications*, **47**(12):1702–1711, 2000. 101, 103

[73] C. Andren. **A Comparison of Frequency Hopping and Direct Sequence Spread Spectrum Modulation for IEEE 802.11 Applications at 2.4 GHz**. Technical report, Harris Semiconductor, 1997. 103

[74] G. Kolumban. **A New Frequency-Domain FM-DCSK Detector**. *European Conference on Circuit Theory and Design*, (3):253–256, 2003. 127

Publications

- Y. XU, P. CHARGÉ, D. FOURNIER-PRUNARET, A.K.TAHA "A Digital Encoding Method Using Chaos", IEEE International Workshop on Nonlinear Maps and their Applications (NOMA 07) Toulouse, France, IEEE (December 2007)
- Y. XU, D. FOURNIER-PRUNARET, P. CHARGÉ "Utilisation du Chaos dans les Systèmes de Communications", EDSYS 2008 congrès des doctorants, INSA Toulouse, Toulouse, France (May 2008)
- Y. XU, P. CHARGÉ, D. FOURNIER-PRUNARET "Chaotic Cyclic Attractors Shift Keying", IEEE International conference on neural networks & signal processing (ICNNSP 08) Zhenjiang, China (June 2008) (Best Student Paper Award)
- Y. XU, P. CHARGÉ, D. FOURNIER-PRUNARET "Chaotic Cyclic Attractors Shift Keying for Low-Rate UWB Communications", International Symposium on Nonlinear Theory and its Applications (NOLTA2008) Budapest, Republic of Hungary (September 2008)
- Y. XU, P. CHARGÉ, D. FOURNIER-PRUNARET "Chaos-based Communication Utilizing Attractor Statistic Detection", The forthcoming 2nd International Conference (CHAOS2009) on Chaotic Modeling, Simulation and Applications, Chania, Greece (June 2009)

Résumé

Au cours de la dernière décennie, des changements importants sont apparus concernant les transmissions sans fil ; de nouvelles technologies ont été introduites qui permettent de transmettre des données de natures très diverses [1]. Dans ce contexte, non seulement la nature de l'information transmise a changé, mais aussi une grande variété d'échelle des réseaux de communications est apparue. En d'autres termes, en fonction des données à transmettre (parole, données multimédias,...) les réseaux sans fil peuvent être très étendus (*wireless wide-area networks*, WWAN), comme par exemple les réseaux de téléphonie mobile [1]; ces réseaux sans fil peuvent être déployés localement (*wireless local area networks*, WLAN) [2], comme IEEE 802.11a/b/g/n ; ces réseaux peuvent aussi avoir une portée très réduite et l'on parle alors de réseaux personnels sans fil (*wireless personal area networks*, WPAN) [3], etc. Devant une si grande diversité des données et des réseaux de communication sans fil, de nombreux systèmes de transmission ont été proposés afin de répondre à des contraintes de débit, de sécurité, mais aussi à des contraintes de complexité, de consommation et de coût des dispositifs d'émission/réception. De manière très générale, une communication consiste à véhiculer une information par l'émission d'un signal à travers un canal de transmission. Ce signal porteur d'information est bien souvent périodique mais peut tout aussi bien être chaotique ou aléatoire.

En particulier, l'idée d'utiliser des signaux chaotiques pour les télécommunications est apparue dans les années 1980. Suite à un rapport scientifique de l'*US Army Research Office*, cette idée révolutionnaire à l'époque s'est rapidement développée. La génération et la synchronisation de signaux chaotiques par des circuits électroniques simples ont été intensivement étudiées [4] [5]. Depuis, l'application du chaos au domaine des télécommunications continue de susciter beaucoup d'intérêt de la part des universitaires et des industriels. Ainsi, de nombreux procédés de modulation par chaos

ont été proposés jusqu'à ce jour. En effet, les signaux chaotiques possèdent a priori des propriétés particulièrement attractives pour les télécommuncations. Parmi ces propriétés on citera les suivantes : un signal chaotique est potentiellement large bande, non périodique, déterministe mais semble aléatoire. En raison de ces propriétés, beaucoup de travaux ont porté sur l'adaptation des techniques de modulation classiques aux signaux chaotiques, l'étalement de spectre par signaux chaotiques, ou encore le cryptage ou la sécurisation des transmissions par chaos. En outre, des signaux chaotiques peuvent être générés à l'aide de circuits électroniques simples. Cette capacité a rendu dernièrement l'attractivité du chaos encore plus forte en raison de l'intérêt que l'on porte aujourd'hui aux petits systèmes communicants de faible complexité, faible consommation, et faible coût.
La première motivation de cette thèse est d'étudier un système dynamique permettant de générer des signaux chaotiques, afin de déterminer quelques propriétés intéressantes pour les transmissions. Il s'agit ensuite de proposer de nouveaux procédés de modulation et de détection non cohérente qui utilisent les propriétés des signaux générés. Le domaine d'application des systèmes proposés est donc celui des transmissions large-bande en général, sans focaliser sur un type de données ou un réseau en particulier. Par conséquent, dans ce travail nous ne considérons pas le contrôle de puissance ou le respect de gabarit spectral d'émission. L'organisation de ce résumé de thèse est la suivante :

- Au chapitre 1, nous présentons l'état de l'art des systèmes de communication par chaos. Dans un premier temps, nous définissons les systèmes dynamiques chaotiques, puis nous présentons le principe des communications basées sur l'utilisation de signaux chaotiques.

- Dans le chapitre 2, nous proposons une structure de générateur de chaos, puis une étude théorique de ce système nous permet d'identifier des attracteurs aux propriétés spécifiques. En particulier nous focalisons notre attention sur certains signaux chaotiques ayant une composante période ; on parle alors d'Attracteur Chaotique Cyclique (CCA).

- Enfin, au chapitre 3 les signaux chaotiques CCA identifiés au chapitre précédent sont utilisés au sein de procédés de transmission sur une large bande de fréquence. La détection, au niveau du récepteur, se fait par exploitation des propriétés

spécifiques de ces CCA. En particulier, deux systèmes de modulation basés sur le CCA avec détection non-cohérente sont proposés. Les performances des ces deux systèmes sont évaluées pour des canaux de bruit additif et des canaux multi-trajet.

Chapitre 1: Communications par signaux chaotiques

Le premier chapitre de cette thèse est consacré globalement à l'utilisation de signaux chaotiques pour transmettre de l'information. La première partie du chapitre est alors naturellement dédiée aux systèmes dynamiques pouvant générer des signaux chaotiques, ainsi qu'aux méthodes d'analyse de ces systèmes. Plusieurs définitions fondamentales concernant les systèmes dynamiques sont données afin de décrire ces derniers de manière très générale. Puis de manière plus particulière, l'accent est mis sur les transformations ponctuelles non linéaires puisque le générateur de chaos qui sera utilisé dans les chapitres 2 et 3 entre dans cette catégorie.
La seconde partie du chapitre permet de faire un état de l'art des techniques de modulation large-bande. Selon le canal de propagation, nous illustrons l'intérêt que présente une transmission sur une large bande par rapport à une transmission dite bande étroite classique.
Enfin, ce chapitre se termine en évoquant les techniques de modulation/démodulation de la littérature qui utilisent des signaux chaotiques. Concernant les communications par chaos sur une large bande de fréquence, deux procédés peuvent être identifiés : l'étalement de spectre par signaux chaotiques et la modulation directe de signaux porteurs chaotiques à large bande. Parmi les techniques mentionnées dans cette fin de chapitre, la modulation dite "*Differential Chaos Shift Keying* (DCSK)" est aujourd'hui considérée comme la modulation par chaos la plus appropriée pour un canal de propagation radio-fréquence réaliste.

Chapitre 2: Attracteurs cycliques chaotiques

Dans ce chapitre, un système dynamique discret bidimensionnel a été choisi comme générateur de signaux chaotiques. Ce système dynamique peut être présenté par l'équation suivante :

$$\mathbf{g}(x,y) = \Big(\sin(a\pi x + b\pi y), x\Big) \tag{B.16}$$

où $\mathbf{g} : \mathbb{R}^2 \to \mathbb{R}^2$ est une fonction continue, et (a, b) sont des paramètres à valeurs réelles. Le schéma de ce système est donné dans la figure B.1, où (x_k, y_k) est le vecteur d'état

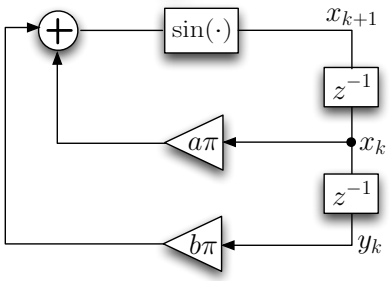

Figure B.1: Schéma du système $(B.16)$.

à l'itération k.

Les comportements périodiques du système $(B.16)$ ont été étudiés, en faisant l'analyse des bifurcations pour les points fixes définis au chapitre 1. Le diagramme de bifurcation dans le plan des paramètres $(a, b) \in [-1, 0]$ est illustré dans la figure B.2, où la zone bleue représente la région de paramètres correspondant à l'existence de points fixes. Au centre de la figure B.2, on peut remarquer plusieurs régions colorées en forme de

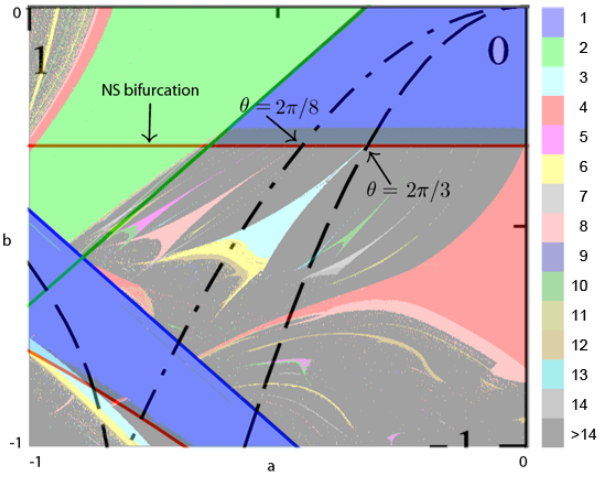

Figure B.2: Régions de paramètre du système $(B.16)$ correspondant à l'existence de cycles, dont les périodes sont indiquées par le code des couleurs. Les lignes à tirets et tiret-pointillées représentent les iscolines avec $\theta = 2\pi/3$ et $\theta = 2\pi/8$.

langues (ou de triangles). Ces zones correspondent à une structure de bifurcation, et

s'appellent des langues d'Arnold [65]. Chaque langue d'Arnold correspond à un ensemble de paramètres produisant un attracteur cyclique, dont la période est donnée par la couleur de la langue. Cette structure de bifurcation est très particulière dans la mesure où en choisissant des paramètres à proximité de ces langues, on observe des attacteurs chaotiques (non périodiques) qui présentent néanmoins une composante cyclique de même période que celle de la langue d'Arnold voisine. Ces attracteurs chaotiques sont alors qualifiés d'Attracteurs Chaotiques Cycliques (CCA). Un CCA est un attracteur pour lequel les états successifs passent périodiquement par plusieurs zones, mais la valeur précise de l'état dans chaque zone est parfaitement chaotique. En ce sens, un attracteur CCA est un véritable attracteur chaotique.
Dans notre étude, nous noterons CCA-q un CCA de période q, avec q égal au nombre de zones cycliques (déterminé par les paramètres du système). La figure B.3 montre un CCA-31 du système (B.16), qui est obtenu en choisissant les paramètres $(a, b) = (0,3590, -0,6184)$. La séquence produite est de moyenne nulle $\langle \mathbf{x} \rangle = 0$, avec $\langle \cdot \rangle$ l'opérateur de moyennage et $\mathbf{x} = (x_1,\ x_2,\ ...)$ la séquence des itérations (valeurs successives de l'état du système).

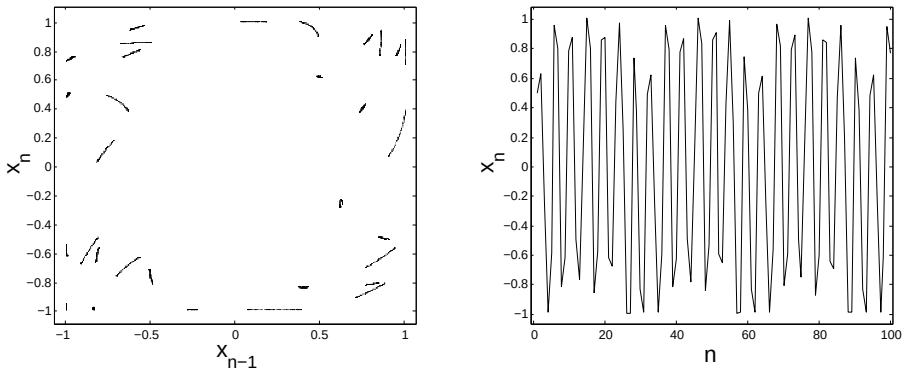

Figure B.3: CCA-31 du système (B.16): représentation des états du système, dans le plan de phase (à gauche) et selon l'indice d'itération (axe du temps) (à droite).

En analysant la séquence chaotique $\mathbf{x} = (x_1,\ x_2,\ ...)$ d'un CCA-q, les propriétés spécifiques suivantes du CCA peuvent être observées :

- Propriété d'autocorrélation : l'autocorrélation de la séquence chaotique du CCA-q, $R_{\mathbf{xx}}[m] = \sum_n x_n x_{n-m}$, a une valeur relativement importante si m est mul-

tiple de q. En d'autres termes, CCA-q possède une propriété quasi-cyclique d'autocorrélation, qui est semblable à une séquence périodique de période q.

- Propriété spectrale : l'amplitude du spectre de la forme d'onde du CCA-q a une distribution en forme de peigne, dans laquelle la majorité de la puissance est distribuée sur q fréquences angulaires équiréparties $\omega = \frac{K}{q}2\pi$ ($K \in \{1, 2, ..., q\}$), alors que la minorité restante est distribuée sur les autres fréquences $\omega \neq \frac{K}{q}2\pi$ ($\omega \in (0, 2\pi]$).

- Propriété statistique : la variance moyenne des sequences sous-échantillonnées d'un facteur p (p-*downsampled mean variance*, p-DMV) de la séquence chaotique du CCA-q a une valeur minimale lorsque $p = \ell q$ ($\ell \in \mathbb{N}$).

En outre, nous avons proposé un opérateur d'amélioration des propriétés des séquences CCA produitee par le système (B.16). Cet opérateur est le suivant :

$$f_3(x) = (\mathrm{sgn}(x) - x)^3$$

La séquence du CCA-31 amélioré est représentée dans la figure B.4, et ses propriétés d'autocorrélation, spectrales et statistiques sont visualisées dans la figure B.5.

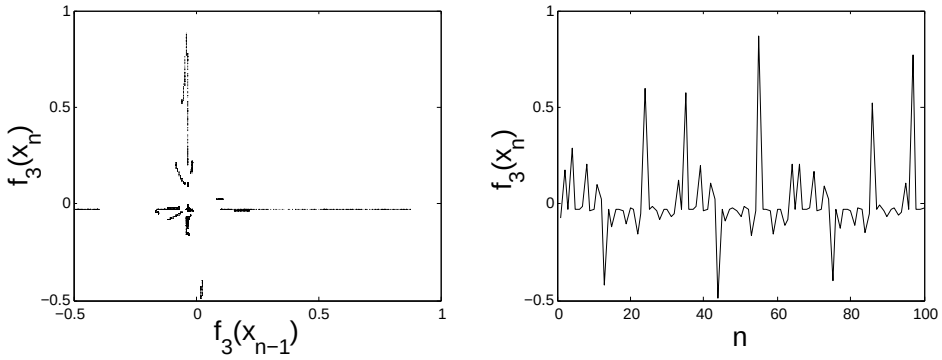

Figure B.4: Séquence CCA-31 améliorée après application de l'opérateur $f_3(x)$ dans le plan de phase (gauche), et selon l'indice d'itération (droite).

Au regard de la figure B.5, le spectre en forme de peigne d'un signal de CCA peut être traité comme un signal large-bande. En outre, il est facile de produire des séquences CCA de différentes périodes en changeant les valeurs des paramètres. Il apparait surtout que les trois propriétés des CCA-q sont facilement observables, et

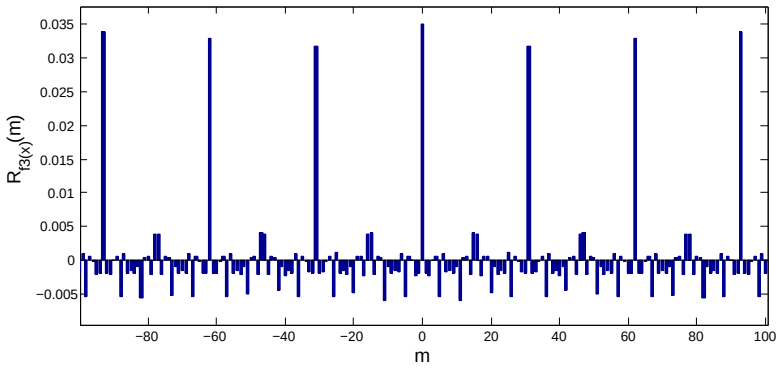

(a)

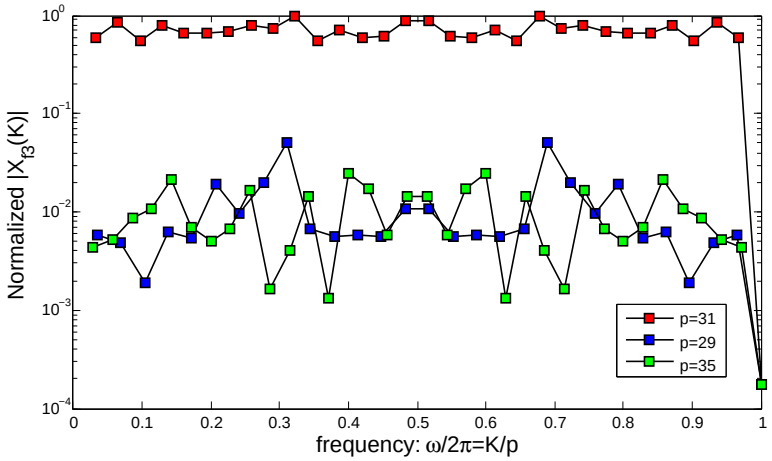

(b)

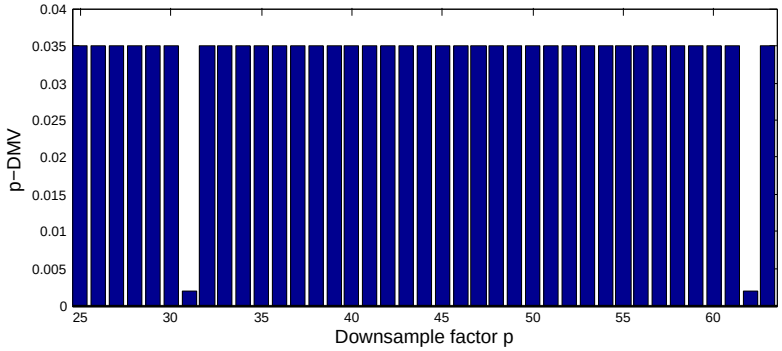

(c)

Figure B.5: Propriétés du CCA-31 amélioré : (a) autocorrélation ; (b) amplitudes normalisées de la p-point DFT avec $p = 31, 29, 35$; (c) p-DMV en fonction du facteur p de sous-échantillonnage.

nous offrent donc la possibilité de proposer des principes de détection originaux de ces séquences CCA-q sans recourir à aucune synchronisation (détection non cohérente). Par conséquent, dans le chapitre 3, nous allons exploiter cette possibilité d'identification simple de la période d'un CCA en proposant deux principes de modulation large bande par signaux CCA, ainsi que les techniques de détection associées.

Chapitre 3: Systèmes de modulation basés sur les CCA

Dans le dernier chapitre de cette thèse, nous proposons deux méthodes de modulation basées sur l'utilisation des propriétés de signaux chaotiques CCA, accompagnées de leurs méthodes de détection non-cohérente. Dans ce chapitre, nous faisons de plus l'analyse des performances de ces systèmes de transmission pour un canal de bruit additif ainsi que pour un canal multi-trajet. La première méthode de modulation est appelée *Chaotic Cyclic Attractors Shift Keying* (CCASK) et consiste à utiliser plusieurs séquences CCA de différentes périodes que l'on envoie selon la donnée à transmettre. La seconde méthode n'utilise qu'un seul CCA et consiste à décaler le spectre de fréquence de ce dernier selon l'information à transmettre, cette méthode est appelée *Chaotic Cyclic Attractors Frequency Shift Keying* (CCAFSK).

Concernant les systèmes de communication actuels, la modulation et la démodulation sont bien souvent réalisées en bande de base. Les séquences chaotiques produites par le système dynamique proposé ($B.16$) sont à valeurs réelles et à temps discret. Selon le **théorème de l'échantillonnage**, un signal occupant la bande de fréquence $[-W/2, W/2]$ peut être produit à l'aide d'un signal à temps discret, la largeur de bande étant déterminée par la période d'échantillonnage du signal discret, $W = f_s = 1/T_s$. On peut alors écrire [21] :

$$x(t) = \sum_n x_n \text{sinc}(Wt - n)$$

où x_n est la séquence chaotique.

▼ Technique de modulation/démodulation CCASK

La technique de modulation CCASK consiste à faire un codage en associant les différents symboles à transmettre des attracteurs CCA de différents ordres. Pour transmettre Q

symboles différents, il est nécessaire de pouvoir générer Q CCA de périodes distinctes. La démodulation est faite en détectant l'ordre des CCA reçus. Cette détection est possible puisque les CCA possèdent les propriétés spécifiques mentionnées au chapitre 2.

► Principe de la modulation

Le CCASK binaire emploie les signaux chaotiques produits par deux générateurs de CCA différents. Ces CCA sont en quelque sorte des fonctions de base : un générateur de CCA-q_0 pour moduler le symbole de données "0" , et un générateur différent de CCA-q_1 pour moduler le symbole de données "1". Les valeurs de q_0 et de q_1 sont sélectionnées pour être des nombres premiers entre eux. Cette contrainte est essentielle afin d'assurer la discrimination des ordres des deux CCA. L'expression des symboles modulés est la suivante :

$$s(t) = \sum_{m} \sum_{n=1}^{L} \Big(d_m x_{mL+n}^{(1)} + (1 - d_m) x_{mL+n}^{(0)} \Big) \mathrm{sinc}(Wt - (mL + n))$$

où $d_m \in \{0, 1\}$ est le $m^{\text{ième}}$ symbole de données, T est la durée du symbole, et L représente la longueur de la séquence chaotique CCA par symbole. Le diagramme de la modulation CCASK en bande de base est illustré dans la figure B.6.

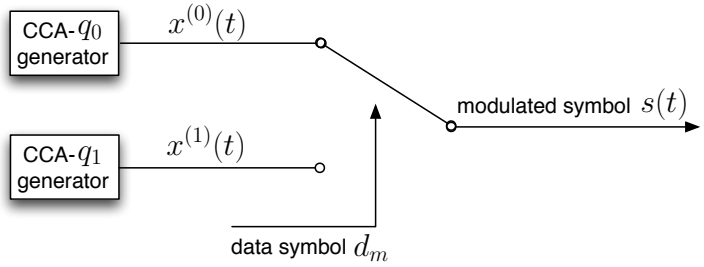

Figure B.6: Structure du modulateur CCASK binaire.

► Principe de la démodulation

On notera $r(t)$ le signal reçu au récepteur. De manière très générale, à cause du canal de propagation, $r(t)$ peut être à valeurs complexes. La propriété d'autocorrélation, la propriété spectrale ou encore la propriété statistique, présentées au chapitre 2,

peuvent être exploitées pour permettre l'opération de démodulation sur $r(t)$. Par conséquent, trois techniques de détections non-cohérentes différentes peuvent être appliquées pour démoduler l'information. Afin de procéder à une analyse temporelle, nous devons échantillonner le $m^{\text{ième}}$ symbole reçu $r(t)$ $(t \in [mT, (m+1)T])$ à un taux d'échantillonage T_s pour obtenir la séquence suivante $\mathbf{r}_m = (r_m[1],\ r_m[2],\ ...,\ r_m[L])$, avec $r_m[n] = r_{m,I}[n] + jr_{m,Q}[n] = r(mT + nT_s)$ $(n \in \{1, 2, ..., L\})$.

– ***Détection par autocorrélation des CCA***[67]
La détection par autocorrélation du signal modulé CCASK binaire, comme son nom l'indique, exploite la propriété d'autocorrélation quasi-périodique de chaque symbole reçu. En additionnant l'autocorrélation des composantes en phase et en quadrature du signal $\mathbf{r}_m$, nous pouvons obtenir :

$$R_{r_m r_m}[\eta] = \sum_{n=1+\eta}^{L} \Big(r_{m,I}[n] r_{m,I}[n-\eta] + r_{m,Q}[n] r_{m,Q}[n-\eta] \Big)$$

où $\eta \in \{0, 1, ..., L-1\}$.

Pour chaque q_v $(v \in \{0, 1\})$, en ajoutant les résultats de toutes les autocorrélations possibles telles que $R_{xx_k}[\ell q_v]$ avec $\ell \in \mathbb{N}$, puis en normalisant cette somme par le nombre de points concernés, on obtient la quantité suivante :

$$C_m[v] = \frac{\sum_{\ell=1}^{L_v} R_{r_m r_m}[\ell q_v]}{\sum_{\ell=1}^{L_v} (L - \ell q_v)}$$

où $L_v = \lfloor \frac{L}{q_v} \rfloor$. Selon la propriété d'autocorrélation des CCA, la variable de décision pour le $m^{\text{ième}}$ symbole reçu peut être donnée par la différence entre $C_m[1]$ et $C_m[0]$:

$$C_{b_m} = C_m[1] - C_m[0]$$

Une estimation du symbole transmis $\hat{d}_m$ est alors obtenue par :

$$\hat{d}_m = \begin{cases} 1, & \text{si } C_{b_m} \geq 0 \\ 0, & \text{si } C_{b_m} < 0 \end{cases}$$

La structure de cette démodulation CCASK binaire en bande de base par autocorrélation est illustrée dans la figure B.7.

– ***Détection spectrale***[68]
La détection spectrale du signal modulé CCASK binaire repose sur l'analyse spectrale

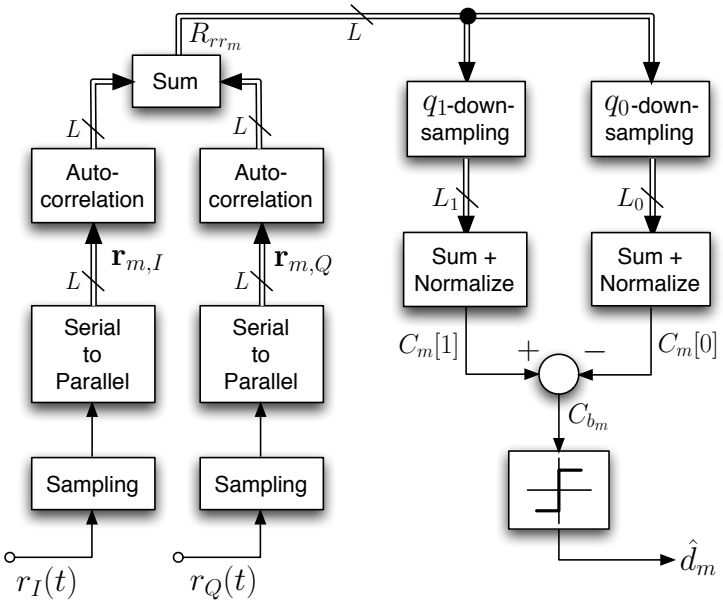

Figure B.7: Structure de démodulation CCASK binaire utilisant la détection par auto-corrélation.

des CCA. Comme indiqué au chapitre 2, le spectre des CCA est en forme de peigne et la position des raies en fréquence dépend de l'ordre de chaque CCA, et par conséquent du symbole transmis. L'amplitude du spectre du signal reçu peut alors être estimée en appliquant une transformée de Fourier discrète à q_v points (q_v-point DFT) ($v \in \{0, 1\}$) :

$$A_m^v[K] = \Big| \sum_{n=1}^{L} r_m[n] e^{-j2\pi \frac{K}{q_v} n} \Big|$$

où $K \in \{1, 2, ..., q_v\}$. La quantité suivante peut alors être obtenue :

$$D_m[v] = \frac{1}{q_v} \sum_{K=1}^{q_v} \Big(A_m^v[K] \Big)^2$$

Selon la répartition des raies du spectre du CCA (propriété spectrale du CCA), une variable de décision concernant le $m^{\text{ième}}$ symbole reçu est donnée par la différence entre $D_m[1]$ et $D_m[0]$:

$$D_{b_m} = D_m[1] - D_m[0]$$

Une estimation du symbole transmis $\hat{d}_m$ est alors obtenue par :

$$\hat{d}_m = \begin{cases} 1, & \text{si } D_{b_m} \geq 0 \\ 0, & \text{si } D_{b_m} < 0 \end{cases}$$

La structure de cette démodulation CCASK binaire en bande de base par détection

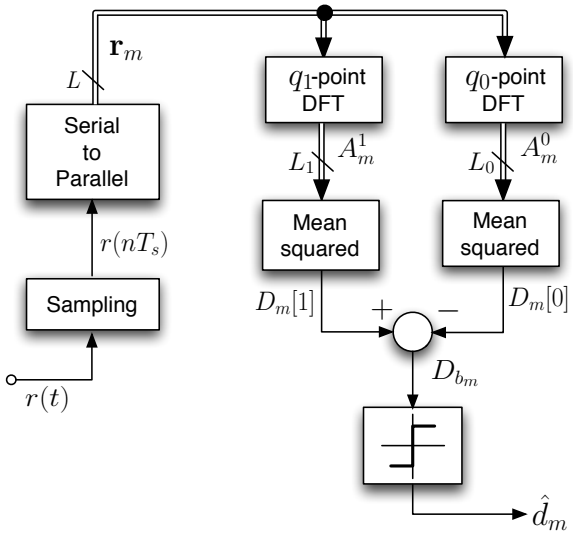

Figure B.8: Structure de démodulation CCASK binaire utilisant la détection par analyse spectrale.

spectrale peut être conçue suivant le schéma de la figure B.8.

– ***Détection statistique***[69]

La détection statistique du signal modulé CCASK binaire est faite en utilisant la quantité p-DMV de chaque symbole reçu. Par décimation des séquences d'un symbole reçu (partie réelle et partie imaginaire de $\mathbf{r}_m$) d'un facteur q_v ($v \in \{0, 1, ..., M-1\}$) avec le décalage $l-1$ ($l \in \{1, 2, ..., q_v\}$), nous obtenons les sous-séquences suivantes $\mathbf{r}_{m_{q_v,l},I} = (r_{m,I}[l],\ r_{m,I}[l+q_v],\ ...,\ r_{m,I}[l+L_v^l q_v])$ et $\mathbf{r}_{m_{q_v,l},Q} = (r_{m,Q}[l],\ r_{m,Q}[l+q_v],\ ...,\ r_{m,Q}[l+L_v^l q_v])$, où $L_v^l = \left\lfloor \frac{L-l}{q_v} \right\rfloor$. Notons la variance de $\mathbf{r}_{m_{q_v,l}}$ et de $\mathbf{r}_{m_{q_v,Q}}$ par $\mathrm{Var}(\mathbf{r}_{m_{q_v,l},I})$ et $\mathrm{Var}(\mathbf{r}_{m_{q_v,l},Q})$. Ainsi, la quantité suivante peut être calculée:

$$V_m[v] = \frac{1}{q_v} \sum_{l=1}^{q_v} \Big(\mathrm{Var}(\mathbf{r}_{m_{q_v,l},I}) + \mathrm{Var}(\mathbf{r}_{m_{q_v,l},Q}) \Big)$$

Selon la propriété statistique du CCA indiquée au chapitre 2, la variable de décision pour l'estimation du $m^{\text{ième}}$ symbole transmis peut être obtenue en effectuant la différence entre $V_m[0]$ et $V_m[1]$:

$$V_{b_m} = V_m[0] - V_m[1]$$

En conséquence, une estimation du symbole transmis $\hat{d}_m$ est alors obtenue par :

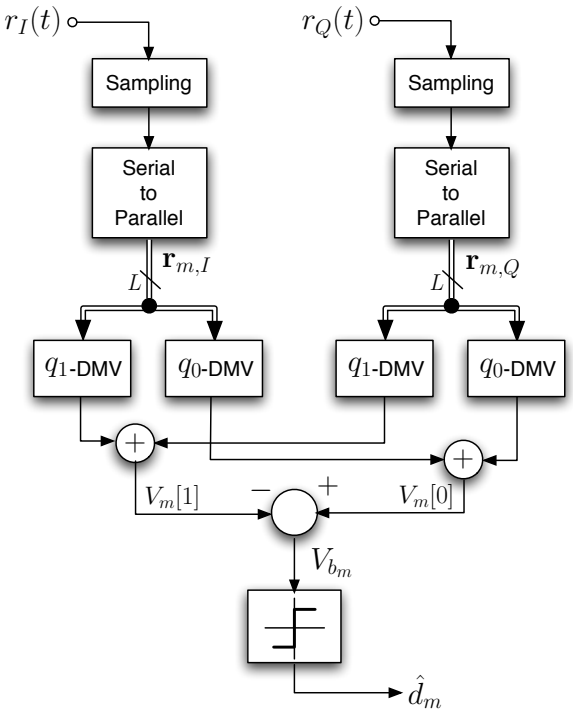

Figure B.9: Structure de démodulation CCASK binaire utilisant la détection par analyse statistique.

$$\hat{d}_m = \begin{cases} 1, & \text{si } V_{b_m} \geq 0 \\ 0, & \text{si } V_{b_m} < 0 \end{cases}$$

La structure de cette démodulation CCASK binaire en bande de base par détection statistique peut être conçue suivant le schéma de la figure B.9.

▶ Evaluation des performances

Les performances du système CCASK utilisant les trois principes de détection précédement présentés, dans le cas d'un canal de bruit additif Gaussien (*additive white Gaussian*

noise, AWGN) ont été étudiées par des analyses théoriques et par des simulations numériques. En outre, la performance dans le cas multi-trajet a été évaluée par simulations numériques dans le modèle de canal à deux trajets.

Le **théorème de Wiener-Khinchine** permet d'établir la relation entre la densité spectrale de puissance d'un signal et sa fonction d'autocorrélation par transformée de Fourier. En outre, le **théorème de Parseval** énonce le rapport entre la variance et l'autocorrélation d'un signal. Nous avons ainsi montré les liens forts entre les trois principes de détection proposés. Ainsi ces trois techniques de démodulation CCASK présentent des performance équivalentes. Bien que ces trois techniques soient différentes en termes de principes et de structures, il a été montré analytiquement et par simulations que les performances pour une canal AWGN sont semblables. Par conséquent, dans ce résumé nous évoquerons seulement les performances de la démodulation CCASK par analyse spectrale.

– Performances pour un canal AWGN

Dans le cadre de cette analyse théorique des performances, nous avons supposé que les séquences CCA-q_i sont de moyenne nulle $\langle \mathbf{x}^{(i)} \rangle = 0$ et $\mathrm{Var}(\mathbf{x}^{(i)}) = \Delta^2$. De plus, les statistiques des échantillons appartenant à la $l^{\text{ième}}$ ($l \in \{1, 2, ..., q_i\}$) zone du CCA-q_i sont données par $\mu_l^{(i)} = \langle \mathbf{x}_{q_i,l}^{(i)} \rangle$ et $\delta_l^{(i)^2} = \mathrm{Var}(\mathbf{x}_{q_i,l}^{(i)})$. Nous définissons aussi les moments statistiques suivants : $\langle \mu^2 \rangle^{(i)} = \frac{1}{q_i} \sum_{l=1}^{q_i} \mu_l^{(i)^2}$, $\langle \delta^2 \rangle^{(i)} = \frac{1}{q_i} \sum_{l=1}^{q_i} \delta_l^{(i)^2}$, $\langle \mu^4 \rangle^{(i)} = \frac{1}{q_i} \sum_{l=1}^{q_i} \mu_l^{(i)^4}$, $\langle \delta^4 \rangle^{(i)} = \frac{1}{q_i} \sum_{l=1}^{q_i} \delta_l^{(i)^4}$ et $\langle \mu^2 \delta^2 \rangle^{(i)} = \frac{1}{q_i} \sum_{l=1}^{q_i} \mu_l^{(i)^2} \delta_l^{(i)^2}$.

L'expression général du taux d'erreurs binaire (*bit error rate*, BER) de la démodulation CCASK par analyse spectrale est alors donnée par :

$$
\begin{aligned}
&\mathrm{BER}_{\mathrm{CCASK}} \\
&= \frac{1}{4} \sum_{i=0}^{1} \mathrm{erfc} \Bigg[\Bigg(\frac{8(L+q_i)}{3L(L-q_i)} \frac{\langle \mu^2 \delta^2 \rangle^{(i)}}{\langle \mu^2 \rangle^{(i)^2}} + \frac{4q_i}{L(L-q_i)} \frac{\langle \delta^4 \rangle^{(i)}}{\langle \mu^2 \rangle^{(i)^2}} + \frac{4(L-q_{1-i})q_i^2}{L(L-q_i)^2 q_{1-i}} \frac{\Delta^4}{\langle \mu^2 \rangle^{(i)^2}} \\
&\qquad + \Big(\frac{8(2L-q_i))}{3L(L-q_i)} \frac{\langle \mu^2 \rangle^{(i)}}{\langle \mu^2 \rangle^{(i)^2}} + \frac{8q_i}{L(L-q_i)} \frac{\langle \delta^2 \rangle^{(i)}}{\langle \mu^2 \rangle^{(i)^2}} + \frac{8(L-q_{1-i})q_i^2}{L(L-q_i)^2 q_{1-i}} \frac{\Delta^2}{\langle \mu^2 \rangle^{(i)^2}} \Big) \sigma^2 \\
&\qquad + \frac{4}{L} \frac{L(q_i+q_{1-i})q_i - 2q_i^2 q_{1-i}}{(L-q_i)^2 q_{1-i}} \frac{\sigma^4}{\langle \mu^2 \rangle^{(i)^2}} \Bigg)^{-\frac{1}{2}} \Bigg]
\end{aligned}
$$

où σ^2 est la densité spectrale de bruit.

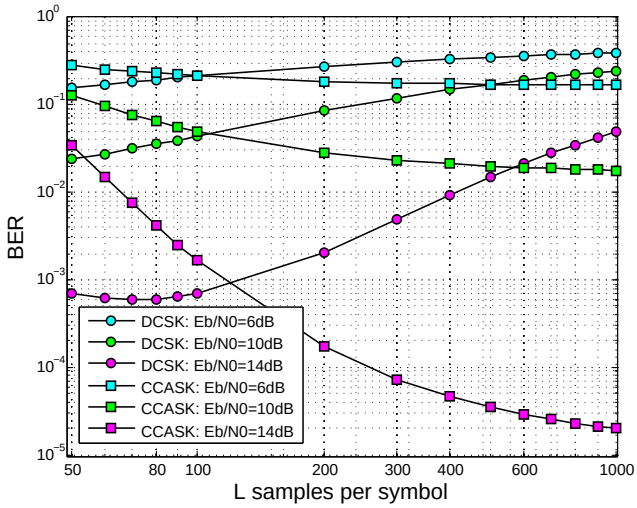

Figure B.10: Performance analytico-numérique de la démodulation CCASK en fonction de L, avec les CCA-29 et CCA-31 améliorés du système (B.16). La performance analytique du DCSK est donnée pour comparaison.

Puisque cette expression générale du BER est fonction de différents moments statistiques des séquences CCA, la performance du système peut être obtenue en calculant numériquement ces moments. En prenant par exemple les statistiques du CCA-31 et du CCA-29 améliorés, les performances de la démodulation CCASK en fonction de L sont illustrées dans la figure B.10. Par comparaison, les performances du système DCSK [48] sont également données. Nous pouvons alors constater de manière globale que le système CCASK proposé est meilleur que les DCSK. Les simulations numériques ont été réalisées en utilisant le CCA-31 et le CCA-29 améliorés du système (B.16) pour moduler "1" et "0" respectivement. Les performances numériques pures du CCASK lorsque $L = 400$ et $L = 1000$ sont illustrées dans la figure B.11. Les performances analytico-numériques ont été calculées dans les mêmes conditions. La comparaison montre une bonne concordance entre les résultats analytico-numériques et purement numériques.

En outre si les valeurs des statistiques des CCA ne sont pas connues, une expression approchée du BER du CCASK peut être obtenue. En effet, en considérant que le nombre des échantillons par symbole est très grand ($L \gg q_0, q_1$), et que les zones des

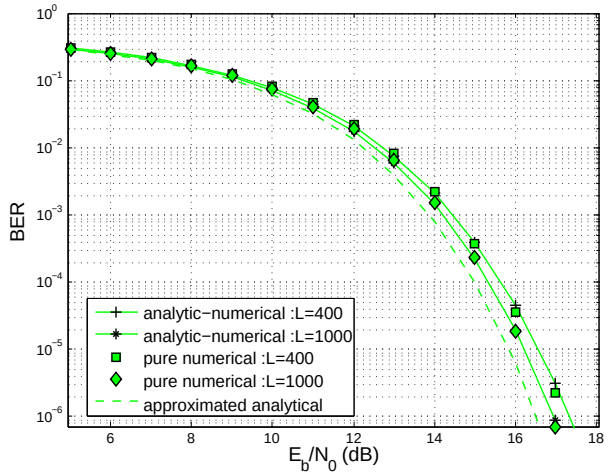

Figure B.11: Performances AWGN du CCASK quand $L = 400$ et $L = 1000$, avec CCA-29 et CCA-31 améliorés.

CCA sont relativement petites, le BER peut être estimé par :

$$\mathrm{BER}_{\mathrm{CCASK}} \approx \frac{1}{4}\sum_{i=0}^{1} \mathrm{erfc}\left[\left(\frac{8}{3}\frac{N_0}{E_b} + \left(q_i + \frac{q_i^2}{q_{1-i}}\right)\frac{N_0^2}{E_b^2}\right)^{-\frac{1}{2}}\right]$$

Cette performance purement analytique approchée pour $q_0 = 29$, $q_1 = 31$ est également illustrée dans la figure B.11.

– Performance pour un canal multi-trajet

Nous avons étudié par simulation le comportement du système CCASK dans le cas d'un canal à deux trajets. Les paramètres choisis sont les suivants : une transmission autour de 2,4 GHz, une largeur de bande $W = 17$ MHz, et un retard de propagation typique de $\tau_d = 75$ ns. La fréquence centrale f_c varie de 2,4 GHz à 2,412 GHz par pas de 3 MHz.

Les résultats des simulations des performances du CCASK (CCA-31 et CCA-29 améliorés) avec $L = 400$ sont illustrés dans la figure B.12. Deux configurations du canal double trajet sont considérées, d'une part lorsque les deux trajets sont de puissance égale et d'autre part lorsque le rapport de puissance des deux trajets est de 10dB.

A travers ces simulations, nous pouvons constater que la dégradation des performances la plus forte est de environ 2 dB pour le CCASK et de 2.5 dB pour le DCSK,

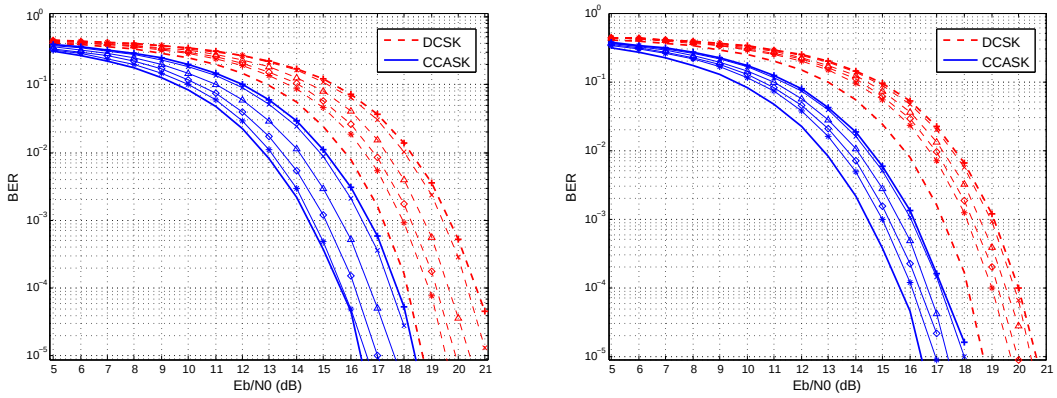

(a) (b)

Figure B.12: Performances du CCASK et du DCSK dans un canal double trajets avec : (a) trajets de gain égal ; (b) trajets de gains différents de 10dB. Les paramètres du canal sont : τ_d=75ns, W=17MHz, et f_c varie : 2,4 GHz (+), 2,403 GHz (△), 2,406 GHz (∗), 2,409 GHz (◊) 2,4012 GHz (×).

dans le cas du canal à deux trajets un gain égal. Ce résultat montre que le système CCASK proposé offre de bonnes performances dans le cas de canaux multi-trajet.

▼ Technique de modulation/démodulation CCAFSK

En appliquant une transformée de Fourier discrète à $2q$ points ($2q$-point DFT) à la séquence CCA-q, q étant impair, nous obtenons:

$$X[K] = \sum_{n=1}^{L} x_n e^{-j2\pi \frac{K}{2q} n}, \qquad K \in [1, 2q]$$

Notons $|X[K]|$ le module du spectre d'indice pair si $K = 2K_1$ ($K_1 \in [1, q]$), et aussi du spectre d'indice impair si $K = 2K_1 - 1$. En raison de la propriété spectrale du CCA, les amplitudes du spectre d'indice pair du CCA-q sont relativement grandes comparées aux amplitudes du spectre d'indice impair.

Une nouvelle séquence $\breve{\mathbf{x}} = (\breve{x}_1,\ \breve{x}_2, ...,\ \breve{x}_L)$ peut étre créée à partir de la séquence initiale $\mathbf{x}$ du signal CCA-q, en changeant simplement le signe d'un élément sur deux de cette dernière :

$$\breve{x}_n\ = (-1)^n x_n = \begin{cases} x_n, & n \text{ est paire} \\ -x_n, & n \text{ est impaire} \end{cases}$$

En appliquant maintenant la transformée de Fourier discrète à $2q$ points ($2q$-point DFT) à la nouvelle séquence $\breve{\mathbf{x}}$, on obtient :

$$\breve{X}[K] = \sum_{n=1}^{L} \breve{x}_n e^{-j2\pi \frac{K}{2q} n}, \qquad K \in \{1, 2, ..., 2q\}$$

Par conséquent, la relation entre la transformée de Fourier discrète à $2q$ points ($2q$-point DFT) de la séquence originale $\mathbf{x}$ et de la séquence modifiée $\breve{\mathbf{x}}$ est donnée par :

$$\breve{X}[K] = \begin{cases} X[K+q], & \text{si } K \in [1, q] \\ X[K-q], & \text{si } K \in [q+1, 2q] \end{cases}$$

où $K \in [1, 2q]$. Les amplitudes du spectre d'indice pair de $\breve{\mathbf{x}}$ correspondent aux amplitudes du spectre d'indice impair de $\mathbf{x}$. Réciproquement, les amplitudes du spectre d'indice impair de $\breve{\mathbf{x}}$ correspondent aux amplitudes du spectre d'indice pair de $\mathbf{x}$.

En conclusion, la séquence originale du signal CCA-q et sa version modifiée sont quasi-orthogonales dans le domaine des fréquences. Le système CCAFSK proposé ici est un système de modulation par séquence chaotique CCA, dont le principe repose sur cette quasi-orthogonalité des séquences. Selon le symbole à transmettre, la séquence CCA-q originale ou la séquence modifiée est envoyée. La démodulation du CCAFSK est naturellement faite par analyse spectrale à l'aide de la transformée de Fourier discrète à $2q$ points ($2q$-point DFT). Si l'on considère plusieurs utilisateurs sur le même canal, des CCA de différentes périodes doivent être choisis pour chacun (avec la contrainte pour les périodes des CCA d'être des nombres premiers entre eux).

▶ Principe de la modulation

Dans le cas du CCAFSK binaire, un seul générateur CCA-q est nécessaire pour produire une séquence CCA originale et obtenir sa séquence modifiée. Rappelons que le signal en bande de base du CCA-q est $x(t) = \sum_n x_n \text{sinc}(Wt - n)$, par conséquent le signal modifié $\breve{x}(t)$ s'écrit :

$$\breve{x}(t) = \sum_n (-1)^n x_n \text{sinc}(Wt - n) = x(t)\tilde{u}(t)$$

où $\breve{x}(n/W) = (-1)^n x_n$ est la valeur de l'échantillon à l'instant n/W, et $\tilde{u}(t)$ est définie par :

$$\tilde{u}(t) = \sum_n (-1)^n \sqcap (t - nT_s)$$

avec $\sqcap(t)$ la fonction rectangle. Les symboles modulés en bande de base sont alors donnés par :

$$s(t) = \sum_{m} \sum_{n=1}^{L} \Big(d_m x_{mL+n} + (1 - d_m) \breve{x}_{mL+n} \Big) \mathrm{sinc}(Wt - (mL + n))$$

où $d_m \in \{0, 1\}$ est le $m^{\text{ième}}$ symbole d'information. Le diagramme de la modulation en bande de base du système CCAFSK binaire est illustré figure B.13.

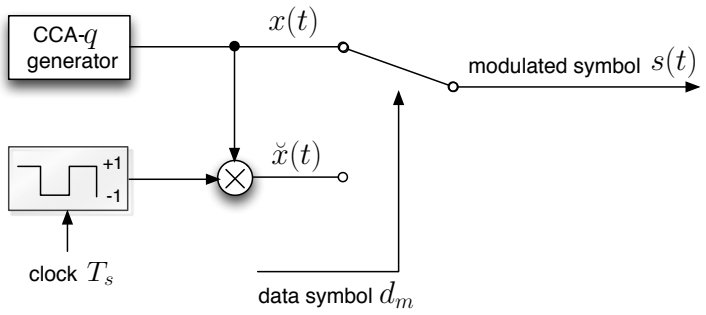

Figure B.13: Structure du modulateur CCAFSK binaire.

► Principe de la démodulation

Considérons le $m^{\text{ième}}$ symbole reçu en bande de base $r(t)$ ($t \in [mT, (m + 1)T]$). La séquence échantillonnée est $\mathbf{r}_m = (r_m[1],\ r_m[2],\ ...,\ r_m[L])$, avec $r_m[n] = r(mT + nT_s)$ ($n \in \{1, 2, ..., L\}$).

En appliquant la transformée de Fourier discrète à $2q$ points ($2q$-point DFT) à la séquence $\mathbf{r}_m$, on détermine les amplitudes du spectre du signal reçu :

$$A_m[K] = \Big| \sum_{n=1}^{L} r_m(n) e^{-j2\pi \frac{K}{2q} n} \Big|$$

où $K \in \{1, 2, ..., 2q\}$. La variable de décision du $m^{\text{ième}}$ symbole reçu peut être déterminée de la manière suivante :

$$B_{b_m} = \frac{1}{q} \sum_{K_1=1}^{q} \Big(A_m^2[2K_1 - 1] - A_m^2[2K_1] \Big)$$

Une estimation du symbole transmis $\hat{d}_m$ est alors obtenue par l'expression suivante :

$$\hat{d}_m = \begin{cases} 1, & \text{si } B_{b_m} \geq 0 \\ 0, & \text{si } B_{b_m} < 0 \end{cases}$$

La structure du démodulateur CCAFSK binaire en bande de base peut être conçue suivant le schéma de la figure B.14.

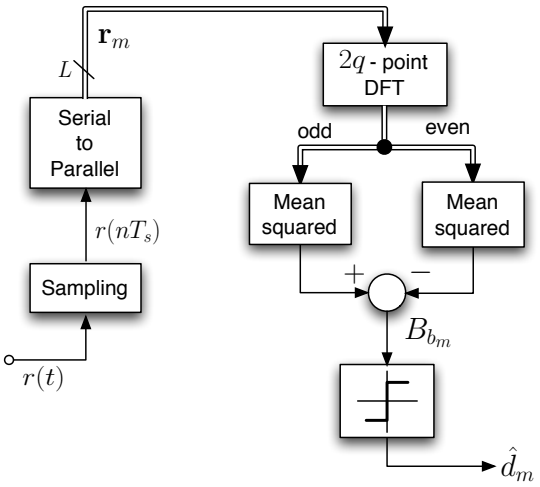

Figure B.14: Structure de démodulateur CCAFSK binaire.

► Evaluation des performances

Les performances du système CCAFSK proposé dans le canal AWGN ont été évaluées par des analyses théoriques et par des simulations numériques. Les performances dans le cas d'un canal double trajet ont été simulées.

– *Performances pour un canal AWGN*

L'expression générale suivante du BER du système CCAFSK a été obtenue :

$$\mathrm{BER}_{\mathrm{CCAFSK}} = \frac{1}{4}\sum_{i=0}^{1}\mathrm{erfc}\left[\left(\frac{2(4L^2+16Lq+15q^2)}{3(L-q)(L+q)^2}\frac{\langle\mu^2\delta^2\rangle}{\langle\mu^2\rangle^2}+\frac{8q}{(L^2-q^2)}\frac{\langle\delta^4\rangle}{\langle\mu^2\rangle^2}\right.\right.$$
$$+\Big(\frac{4(4L^2+4Lq+3q^2)}{3(L-q)(L+q)^2}\frac{\langle\mu^2\rangle}{\langle\mu^2\rangle^2}+\frac{16q}{(L^2-q^2)}\frac{\langle\delta^2\rangle}{\langle\mu^2\rangle^2}\Big)\sigma^2$$
$$\left.\left.+\frac{8q}{(L^2-q^2)}\frac{\sigma^4}{\langle\mu^2\rangle^2}\right)^{-\frac{1}{2}}\right]$$

La figure B.15.(a) représente le BER du système CCAFSK en fonction de L, avec un CCA-29 amélioré. La performance de CCASK est aussi illustrée dans cette figure.

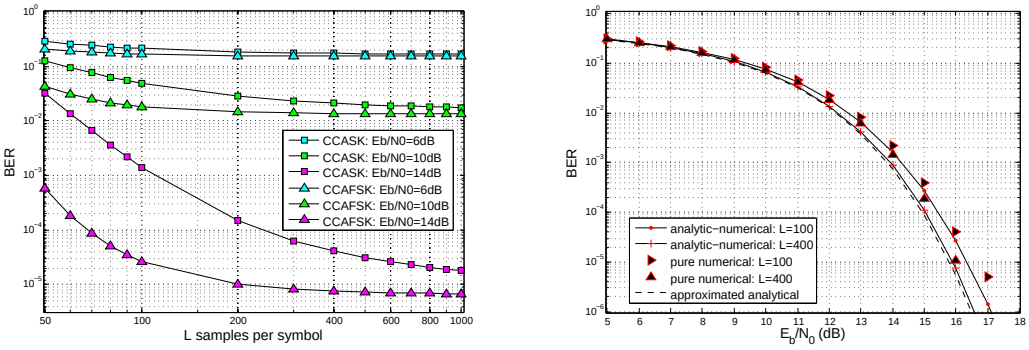

(a) (b)

Figure B.15: (a) Performances analytico-numériques du CCAFSK en fonction de L avec un CCA-29 amélioré. Les performances du CCASK de la figure B.10 sont rappelées pour comparaison. (b) Performances du CCAFSK quand $L = 100$ et $L = 400$.

Ces résultats montrent globalement que le système CCAFSK est meilleur que le système CCASK. Des simulations numériques du système CCAFSK ont été réalisées, avec un CCA-29 amélioré. Ces performances purement numériques quand $L = 100$ et $L = 400$ sont illustrées dans la figure B.15.(b).

Si les valeurs des statistiques du CCA ne sont pas connues, une expression approchée du BER du CCAFSK peut être obtenue. En effet, en considérant que le nombre des échantillons par symbole est très grand ($L \gg q$), et que les zones des CCA sont relativement petites, le BER peut être exprimé par :

$$\mathrm{BER}_{\mathrm{CCAFSK}} \approx \frac{1}{2}\mathrm{erfc}\left[\left(\frac{8}{3}\frac{N_0}{E_b} + 2q\frac{N_0^2}{E_b^2}\right)^{-\frac{1}{2}}\right]$$

Ce BER analytique approché du système CCAFSK avec $q = 29$ est également illustré dans la figure B.15.(b).

– ***Performance pour un canal multi-trajet***

Afin d'évaluer les performances du système CCAFSK dans le cas d'un canal multi-trajet, des simulations numériques ont été effectuées, avec une séquence CCA-29 améliorée du système ($B.16$). Le même modèle de canal à deux trajets que pour l'évaluation du CCASK est utilisé. Le BER du CCAFSK avec $L = 100$ est illustré dans la figure

B.16. L'analyse de ces résultats de simulation indique que le système CCAFSK offre des performances généralement meilleures que CCASK.

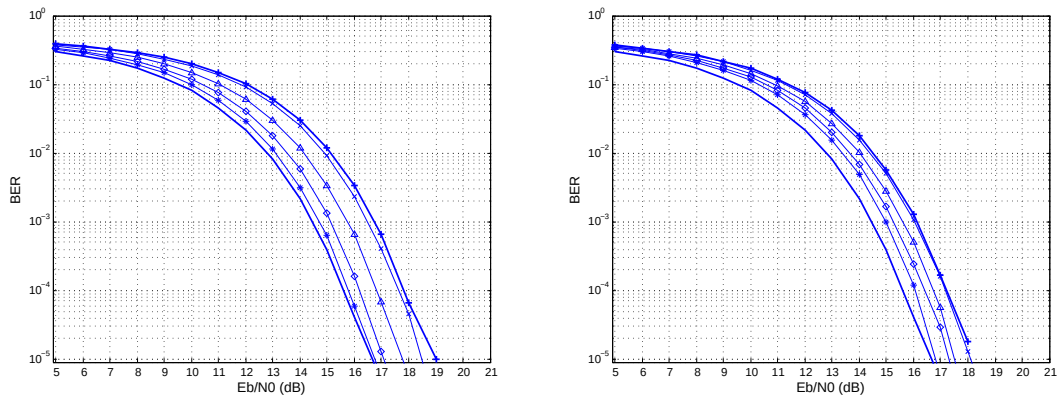

(a) (b)

Figure B.16: Performances du CCAFSK pour canal double trajet avec : (a) trajets de gain égal ; (b) trajets de gains différents de 10dB. Les paramètres du canal sont identiques à ceux de la figure B.12.

▼ Conclusion

Puisque des signaux de CCA peuvent être produits par des circuits électroniques simples, avec un contrôle de leur période par un simple changement des valeurs des paramètres des circuits, les dispositifs émetteurs-récepteurs des systèmes de modulation basés sur les CCA sont considérés comme ayant une très faible complexité.

La technique CCASK montre de bonnes performances pour un canal AWGN en prenant de longues séquences chaotiques pour chaque symbole, c'est-à-dire à faible débit de transmission. Par comparaison avec CCASK, la technique CCAFSK nécessite une durée de symbole beaucoup plus courte pour d'obtenir de bonnes performances. En outre, les deux techniques, CCASK et CCAFSK, ont des performances similaires pour des canaux double trajet. Dans le cas d'un canal multi-trajet, les performances obtenues par les méthodes proposées sont comparables à celles du DCSK. En d'autres termes, ces performance sont bien meilleures que celles des systèmes à bande-étroite.

AUTEUR: YANJUN XU

TITRE: MODULATION AND DETECTION SCHEMES BASED ON CHAOTIC ATTRACTORS PROPERTIES: APPLICATION TO WIDEBAND TRANSMISSIONS

DIRECTEUR DE THESE: DANIELE FOURNIER-PRUNARET, PASCAL CHARGE

LIEU ET DATE DE SOUTENANCE: SALLE DE THESE A L'INSA, 09 JULLIET 2009

RESUME en anglais

In the past twenty years, chaos-based communication systems have been studied, considering the possibility of generating wideband signals by simple electronic circuits, hence low complexity in transceiver.

The aim of this thesis is to study the chaos-based wideband transmission systems relying on the properties of chaotic attractors. Firstly, a dynamical system is selected and studied, allowing to generate the chaotic signals with a periodic component. The analysis of such chaotic cyclic attractors (CCA) shows the specific properties. Then, two CCA-based modulation schemes are proposed, with the simple noncoherent detections realized by observing the specific properties of the received signals. The performance evaluation of CCA-based systems in the additive white Gaussian noise (AWGN) channel shows a better noise performance with long symbol duration, compared to the one of differentially chaos shift keying (DCSK). In addition, they have a comparable multipath performance in the 2.4 GHz ISM environment.

MOTS-CLES: chaos, attractor, wideband communications, chaotic cyclic attractor, Arnold Tongues, noncoherent detection, AWGN, multipath

---

DISCIPLINE ADMINISTRATIVE: SYSTEMES AUTOMATIQUES

INTITULE ET ADRESSE DE L'U.F.R. OU DU LABORATOIRE: LABORATOIRE TOULOUSAIN DE TECHNOLOGIE ET D'INGENIERIE DES SYSTEMES

AUTEUR: YANJUN XU

TITRE: METHODES DE MODULATION ET DE DETECTION BASEES SUR LES PROPRIETES D'ATTRACTEURS CHAOTIQUES : APPLICATION AUX TRANSMISSIONS LARGE-BANDE

DIRECTEUR DE THESE: DANIELE FOURNIER-PRUNARET, PASCAL CHARGE

LIEU ET DATE DE SOUTENANCE: SALLE DE THESE A L'INSA, 09 JULLIET 2009

RESUME en français

Au cours des vingt dernières années, les systèmes de communications basés sur le chaos ont été étudiés, avec pour objectif la possibilité de générer les signaux large-bande par des circuits électroniques simples, permettant une faible complexité des circuits émetteurs-récepteurs.

Cette thèse concerne l'étude de systèmes de transmissions large-bande basés sur le chaos, en utilisant certaines propriétés des attracteurs chaotiques. Tout d'abord, un système dynamique a été choisi et étudié, permettant de générer des signaux chaotiques qui possèdent des composantes périodiques. L'analyse de ces attracteurs chaotiques cycliques (CCA) met en évidence des propriétés spécifiques en lien avec leur période. Ensuite, deux schémas de modulation basés sur les CCAs sont proposés. Les détections non-cohérentes associées sont réalisées par l'observation des propriétés spécifiques des signaux reçus. L'évaluation des performances des systèmes basés sur les CCAs dans le cas d'un canal de bruit additif Gaussien montre des performances meilleures que celles des systèmes dits "differential chaos shift keying (DCSK)", en bas débit de symboles. En outre, les performances dans le cas multi-trajet sont comparables dans la bande de 2,4 GHz.

MOTS-CLES: chaos, attracteur, communications large-bande, attracteur chaotique cyclique, langue d'Arnold, détection non-cohérente, AWGN, multi-trajet

---

DISCIPLINE ADMINISTRATIVE: SYSTEMES AUTOMATIQUES

INTITULE ET ADRESSE DE L'U.F.R. OU DU LABORATOIRE: LABORATOIRE TOULOUSAIN DE TECHNOLOGIE ET D'INGENIERIE DES SYSTEMES